LOW TEMPERATURE POLYMERIC PRECURSOR DERIVED ZINC OXIDE THIN FILMS

Uma Choppali, B.Sc., B. Ed, M.Sc., M.S.

Dissertation Prepared for the Degree of

DOCTOR OF PHILOSOPHY

UNIVERSITY OF NORTH TEXAS

December 2006

APPROVED:

Brian P. Gorman, Major Professor
Richard F. Reidy, Committee Member
Dennis W. Mueller, Committee Member
Mohammad A. Omary, Committee Member
Michael J. Kaufman, Committee Member and Chair of the Department of Material Science and Engineering
Oscar Garcia, Dean of the College of Engineering
Sandra L. Terrel, Dean of the Robert B. Toulouse School of Graduate Studies

Choppali, Uma. Low Temperature Polymeric Precursor Derived Zinc Oxide Thin Films. Doctor of Philosophy (Materials Science and Engineering), December 2006, 204 pp., 8 tables, 72 illustrations, bibliography, 157 titles.

Zinc oxide (ZnO) is a versatile environmentally benign II-VI direct wide band gap semiconductor with several technologically plausible applications such as transparent conducting oxide in flat panel and flexible displays. Hence, ZnO thin films have to be processed below the glass transition temperatures of polymeric substrates used in flexible displays. ZnO thin films were synthesized via aqueous polymeric precursor process by different metallic salt routes using ethylene glycol, glycerol, citric acid, and ethylene diamine tetraacetic acid (EDTA) as chelating agents. ZnO thin films, derived from ethylene glycol based polymeric precursor, exhibit flower-like morphology whereas thin films derived of other precursors illustrate crack free nanocrystalline films. ZnO thin films on sapphire substrates show an increase in preferential orientation along the (002) plane with increase in annealing temperature. The polymeric precursors have also been used in fabricating maskless patterned ZnO thin films in a single step using the commercial Maskless Mesoscale Materials Deposition (M^3D^{TM}) system.

ACKNOWLEDGEMENTS

I would like to express gratitude to my major professor, Dr. Brian P. Gorman, for his guidance and support throughout my doctoral degree program. I would sincerely like to thank Dr. Richard F. Reidy, Dr. Mohammad A. Omary, Dr. Dennis W. Muller, and Dr. Michael Kaufman for serving on my dissertation committee and for their outstanding assistance. I would also like to thank Dr. Nigel Shepherd for invaluable discussions. Special thanks to the office staff of Materials Science and Engineering department at UNT. I would also like to thank my lab-mate, James Meadows for his help and cooperation. Last but not the least, I thank all my colleagues especially Dave, Anantha, Jun, Laxmi, Casey, MingMing, Ravi, and Maia, who have helped me on various occasions of my graduate studies. Great thanks to my husband, Saraju, who has constantly encouraged and mentored me.

TABLE OF CONTENTS

LIST OF TABLES

LIST OF FIGURES

CHAPTER 1

INTRODUCTION

1.1. Motivation

In 2004, Philips unveiled paper-like computer displays made of flexible, low cost plastics [40]. It is projected that the displays will have a major impact economically. These flexible displays have potential to replace computer screens, rigid flat screens, books, newspaper, etc [72, 43]. Moreover, it is anticipated that the flexible displays will be highly beneficial to soldiers on duty. These devices will be designed to be worn on uniform, or folded for portability. For this technology to be economically viable, the displays have to be made of low cost materials or utilizing low cost technology.

ZnO is a II-VI semiconductor with wide band gap and wurtzite structure. Being a direct wide band gap semiconductor (3.3 eV at room temperature) with large exciton binding energy (60 meV), ZnO can be utilized in fabrication of solid state optoelectronic devices operating in near UV region [46, 123]. Moreover, intrinsic ZnO is a n-type semiconductor with maximum optical transparency in visible region of electromagnetic spectrum. Hence, ZnO has the potential to be a transparent conductor as well as the UV emitter for flexible displays. To achieve this objective, ZnO thin films have to be synthesized at temperatures below the glass transition temperatures of plastic substrates.

Low temperature, wet chemical routes offer an exciting possibility for the synthesis of high purity, homogeneous thin films with tailored and predictable properties. The motivation and focus of this dissertation has been to synthesize

ZnO thin films at low temperatures via aqueous polymeric precursor process. Different chelating agents have been utilized to prepare polymeric precursors to ensure uniform distribution of Zn cations and to study the properties of synthesized films. This polymeric precursor method is simple, easy, and cost-effective employing common reagents. The prepared precursors have been spincoated to form ZnO thin films. Spin coating is a low cost, popular technique for producing thin films. This technique is cost effective with scope for substrate size scalability. If low temperature preparation is realized with simple existing process, the applications of ZnO optoelectronics would increase considerably in macroelectronics industries.

1.2. ZnO Thin Films - Processing Techniques

To date, high quality ZnO thin films have been prepared by several thin film deposition techniques, including pulsed laser deposition [64, 68], chemical vapor deposition [85, 42], molecular beam epitaxy [136], sputtering [30, 62, 79], spray pyrolysis [107], metal organic chemical vapor deposition [59], and sol-gel process [22, 81, 45, 18, 34, 149, 2]. However, these deposition techniques can require ultra high vacuum, are expensive, and time-consuming. In the sol-gel process, expensive and water sensitive metal alkoxides, are used as precursors to form sols, which make preparation of sols difficult. However, insolubility of zinc alkoxides in most alcohols poses a major problem for this technique. Working with alkoxides requires special handling as it is a toxic process and quite expensive. Among other established synthesis methods, simple and cost effective routes to synthesize nanocrystalline ZnO thin films by utilization of less

expensive, nontoxic, and environmentally benign precursors are still the key issues.

1.3. Polymeric Precursor Process

The polymeric precursor method or Pechini process [83], named after its inventor Maggio Pechini, is a chemical solution route frequently employed to synthesize polycation oxides. In this technique, aqueous solution of metal salts is dissolved in an aqueous alpha-hydroxycarboxylic acid such as citric acid solution. To this solution, polyhydroxyl alcohol, usually ethylene glycol, is added which is then heated and stirred continuously. During this stage, the ethylene glycol and citric acid undergo polyesterification to form a polymeric solution. Metal cations, added previously, chelate to the polyester formed resulting in uniform distribution of cations [48]. The prepared solution is a rigid network of polyester-type resin, which immobilizes metal ions and reduces the segregation of metal ions. This process enables efficient stoichiometric and particle size control. The polymeric precursor processing route also offers advantages of being simple, low cost utilizing common reagents and synthesis in ambient atmosphere.

1.4. Applications of ZnO

ZnO is a versatile material with diversified technological potentials as transparent electrodes in solar cells [68, 80, 62], catalysts [78, 1], waveguides [88, 31], transparent thin film transistors [29], piezoelectric transducers and actuators [75, 10], surface wave acoustic devices [96, 104, 91], gas sensors [116, 60], photonic crystals with tunable band gaps [17, 33], anti-reflection

coatings [68], varistors [149, 94], and in flat panel displays as a low voltage phosphor. Besides, ZnO has several attractive properties, such as, high chemical stability, good piezoelectric properties, non-toxicity, and bio-compatibility, which have drawn tremendous attention in recent years. Owing to stability in hydrogen plasma, ZnO thin films can be employed in fabrication of hydrogenated amorphous silicon solar cells [57]. ZnO has potential for usage as blue lasers to read compact discs (CDs) and DVDs. ZnO are also of importance for preparing blue light emitting diodes for non-line-of-sight communication receivers for military purposes [23]. ZnO has also created a niche as transparent conducting electrode for CIGS based solar cells due to match of its electrical properties with layers used in solar cells [26].

1.5. Contributions of this Dissertation

A major contribution of this dissertation is the synthesis of low temperature processed ZnO thin films via the aqueous polymeric precursor route. For the fabrication of ZnO thin films, the polymeric precursors are prepared by different routes through the use of ethylene glycol, glycerol, citric acid, and ethylene diamine tetraacetic acid (EDTA), respectively, as chelating agents. In polymeric precursor process, Zn cations chelate to ethereal oxygen of organic chain [48]. EDTA has higher stronger chelation affinity than citric acid [126]. Hence, different chelating agents, with varying affinity for chelation of Zn cations, have been used to study the effect of chelation on morphology of the thin films.

The polymeric precursors were spincoated on functionalized silicon and glass substrates and were annealed at various temperatures from 300°C to

600°C. The resultant films were characterized for degree of crystallization and surface morphology. The thermal decomposition of polymeric precursors was studied by thermogravimetric analysis (TGA) to determine the applicability of the precursor on polymeric substrates. Crystallinity and orientation of grains were studied in depth by X-ray diffraction (XRD). XRD data illustrates the effect of deposition conditions and annealing temperature on growth of ZnO films. Surface morphology of the thin films was evaluated by scanning electron microscopy (SEM) and atomic force microscopy (AFM) to study the microstructure and correlate it to properties of ZnO films. The photoluminescent properties of the thin films were also investigated. Optical and electrical properties of ZnO films were also studied extensively to evaluate the quality of ZnO films to decide their suitability as transparent conductors.

ZnO thin films, derived of ethylene glycol based polymeric precursor, exhibit formations of flower-like morphology. Controlling the reactant concentrations, flower-like morphology of the ZnO structures could be synthesized with excellent reproducibility. It has been observed that number of chelation sites provided by chelating agent determines the morphology of the ZnO film. For glycerol, citric acid, and EDTA based precursors, the number of chelation sites provided is sufficient for formation of crack free smooth ZnO thin films. Epitaxial ZnO thin films grown on lattice matched substrates are favorable for reducing strains and dislocations. ZnO films are commonly grown on (0001) oriented (basal or c-plane) sapphire substrates. ZnO thin films on sapphire substrates were synthesized using citric acid based polymeric precursor as citric

acid provides sufficient chelation sites to synthesize crack free films. X-ray diffraction studies show increase in preferential orientation along the [001] direction with increase in annealing temperature. The polymeric precursors have been utilized in fabricating maskless patterned ZnO thin films in a single step using Maskless Mesoscale Materials Deposition (M^3D)^{TM}. This processing technique enables deposition of array of micropatterns and microlines without using photoresists and lithography.

1.6. Organization of Dissertation

Remaining part of this dissertation is organized as follows: Chapter 2 presents a review of the literature on ZnO thin films and various techniques for processing ZnO thin films. This also describes polymeric precursor method to synthesize oxide thin films. In Chapter 3, processing and characterization of ZnO thin films synthesized using ethylene glycol as chelating agent. Results show that flower-like morphology of ZnO is obtained. Parameters for controlling the morphology has been examined thoroughly are also presented. Results and discussion of ZnO thin films derived from glycerol based polymeric precursors is presented in Chapter 4. Synthesis, processing, and characterization of ZnO thin films derived from citric acid and EDTA, respectively as chelating agents in reaction medium of ethylene glycol is investigated in Chapter 5 and Chapter 6, respectively. Results and discussion presented in Chapter 7 cover comparison of ZnO thin films derived from all precursors synthesized. In Chapter 8, preferred orientation of ZnO thin films along (002) plane when deposited on sapphire substrate is presented. The citric acid based precursor is utilized for conducting

experimental investigation at series of annealing temperatures. The polymeric precursors are used in depositing maskless micropatterns of ZnO. Depositional parameters for reproducing these micropatterns were determined and are presented in Chapter 9. The overall conclusions drawn from this work and future directions of research are discussed in Chapter 10.

CHAPTER 2

LITERATURE SURVEY

2.1. ZnO - Structure and Properties

ZnO is a II-VI compound semiconductor with 55% of ionic bonds due to large differences in electronegativities. It exists as hexagonal wurtzite structure with two lattice parameters *a* = 0.324 nm and *c* = 0. 5207 nm. ZnO belongs to the space group of $P6_3mc$ [123]. The structure is composed of two interpenetrating hexagonal close packed sublattices of oxygen ions displaced by 0.375 along the threefold *c*-axis with respect to Zn ions. In other words, ZnO structure may be described as planes of O^{2-} and Zn^{2+} stacked alternatively along the *c* - *a*xis. Each sublattice has 4 atoms per unit cell. Every Zn cation is tetrahedrally coordinated with 4 O^{2-} at edges of a tetrahedron and vice versa. In other words, Zn^{2+} occupy tetrahedral sites in the hexagonal close packed sublattice of O anions. Schematic

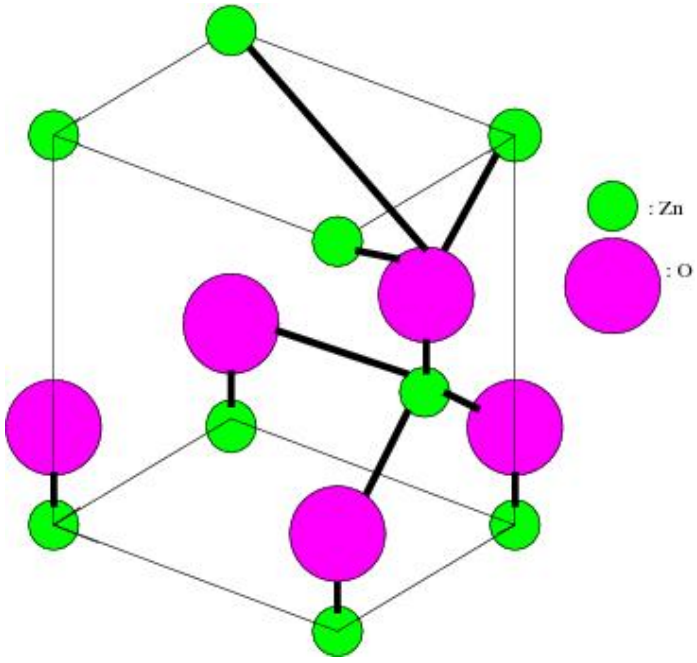

Figure 2.1: Schematic diagram of unit cell of wurtzite ZnO.

diagram of unit cell of wurtzite ZnO is shown in Fig. 2.1.

The tetrahedral coordination in ZnO leads to a lack in inversion symmetry and hence, ZnO exhibits piezoelectricity and pyroelectricity. Owing to the wurtzite structure, ZnO has low symmetry leading to spontaneous polarization along the c-direction. Therefore, ZnO exhibits dielectric, piezoelectric, pyroelectric, acousto-optic, and photoelectrochemical properties also [123, 9].

ZnO has polar surfaces due to the alternate stacking layers of O^{2-} and Zn^{2+} with basal (0001) plane as the common polar surface. Due to the polar surfaces, there exists a normal dipole moment and spontaneous polarization along the *c* axis. Growth and hence, properties of ZnO thin films also depends on this crystallographic polarity. Homoepitaxial ZnO films exhibit different morphology depending on the basal surface when grown on bulk ZnO substrates. ZnO films grown on O-$(000\bar{1})$ basal surface appear smooth with better mechanical properties whereas ZnO films deposited on Zn-(0001) surfaces have rough surface covered with hillocks [69].

Growth habit of crystals depends on relative growth rate of various crystal faces bounding the crystal. This difference in growth rates results in different growth habits. ZnO has three fastest growth directions, namely: <0001>, <0110>, and <2110> [155]. It has been observed that velocities of crystal growth to different directions is $V_{<0001>} > V_{<0110>} > V_{<0001>}$ when growth of <0001> is considered as maximum. Crystal faces with slow growth rate appear whereas crystal face whose growth rate is fast disappears. Hence, the (0001) face

disappears when ZnO crystals are prepared as studied by hydrothermal route [133, 50].

Owing to crystallographic polarity and fastest growth directions, ZnO has displayed a series of nanostructures with different morphologies, such as nanoribbon and combs [153], nanobridges and nanonails [148], thornballs [39], nanorods [38], polyhedral cages [97], nanohelixes, nanosprings, nanorings [145, 143, 142], whiskers [19], nanopins [20], nanoneedles [71, 131], nanowalls [61], etc. A few works have been reported on synthesis of flower-like ZnO nanostructures from aqueous solutions [156, 50, 63, 138, 124, 54, 119].

Being a direct band gap semiconductor, ZnO has many electronic and optoelectronic applications. ZnO with additives like bismuth oxide at grain boundaries have a non-linear I-V characteristics. This makes it suitable for surge suppressing [89] in small current electronic currents [93]. It is also widely used in large current transmission lines due to non-ohmic behavior [93]. ZnO is also suitable for high temperature and high power operation [123].

2.2. ZnO Thin Films - Processing Techniques

ZnO thin films have been deposited on various kinds of substrates, such as glass [157, 99, 82], sapphire [146, 99] , silicon [152], and GaN [99], using different deposition techniques. Some of the widely used techniques have been discussed.

2.2.1. Pulsed Laser Deposition

In pulsed laser deposition method, high power laser pulses (laser fluence = 1 – 1.5 J/cm^2) are used to ablate polycrystalline ZnO target in an oxygen

atmosphere. The ablated species consisting of energetic neutral atoms, ions, electrons, atom clusters, and molten droplets, move away from the target and condense on the substrate placed opposite to target. In this method, stoichiometry of the target is preserved, as the plume is highly directional. For depositing smooth and uniform thin films, the substrates are usually heated in the range of 200°C to 800°C. ZnO thin films, synthesized by pulsed laser deposition, have used excimer lasers such as KrF: λ=248nm [86, 36] and Nd:YAG laser: λ = 355nm [151, 68]. ZnO thin films have been deposited on SiO_2/Si [86], glass [151, 68, 36], $LiAlO_2$ [66, 65] by pulsed laser deposition. Pulsed laser deposition technique requires high vacuum and expensive laser systems. Although the stoichiometry of deposited ZnO film is maintained, a large number of gross particulates also "splash" into the film increasing the surface roughness of the film. Since the plume is highly directional, it is difficult to uniformly deposit films over large substrates. Pulsed laser deposition also requires a homogeneous target for ablation.

Using pulsed laser deposition highly textured and defect free ZnO thin films have been deposited on SiO_2/Si [86]. In [36], preferentially *c*-axis oriented ZnO thin films were deposited on glass substrates. The crystalline quality of the ZnO films increased and electrical resistivity decreased with increase in substrate temperature. The deposited films have a refractive index of 2.008 and band edge at 3.28 eV. ZnO thin films have also been deposited on γ-$LiAlO_2$ substrates by pulsed laser deposition [65]. The deposited films were preferentially oriented when the substrate temperature was set at 550°C.

2.2.2. Metal Organic Chemical Vapor Deposition

Metal Organic Chemical Vapor Deposition (MOCVD) is popular variation of chemical vapor deposition technique. In this method, metal organic precursors are used as starting materials. Typically used precursors for deposition of ZnO thin films are metal alkyls, such as, dimethyl zinc or diethyl zinc [109] as zinc source, and alcohols, such as, isopropanol or tertiary-butanol [4] or oxygen as oxidizer. It has been shown that diethyl zinc is highly reactive with oxygen and is kept in separate injecting chambers.

The substrate is placed in the growth chamber. The precursors undergo chemical reactions and the final product is deposited on the substrate. The quality of synthesized ZnO thin films can be controlled by substrate temperature, partial pressures of precursors, and ratio of partial pressures. The most important advantage of MOCVD process is the use of highly volatile metal organics at low temperatures. All constituents are in gaseous phase allowing precise electronic control of flow rates and their partial pressures. This method is useful in synthesis of large scale, high quality films. MOCVD is suitable for large area deposition, good composition control and film uniformity, and high depositional rates and densities. However, the major drawback of this process is the availability of suitable inexpensive precursors. In MOCVD method, highly reactive precursors are often used as precursors needing utmost safety precautions.

ZnO thin films have been deposited on sapphire substrates by MOCVD. Characterization of the ZnO films illustrate preferential orientation along (002)

plane [4]. Using MOCVD, highly textured ZnO thin films are also deposited on SiO_2/Si [109]. However, these films exhibit electrical resistivity of 10^4 Ω - cm.

2.2.3. Magnetron Sputtering

In this deposition technique, high purity ZnO targets are sputtered, at a particular substrate temperature, to form ZnO thin films using magnetron sputter system. Ar is usually used as sputtering enhancing gas and O_2 as reactive gas. In dc magnetron sputtering system, a gas mixture of Ar+O_2 is used. Sputtering yield rate from ZnO target is controlled by varying rf power. The sputter gas pressure influences energy of depositing atoms and determines the crystallinity, film density, and preferred orientation of the films [79, 35]. This method has advantages of being simple and operating at low temperatures. Another advantage of magnetron sputtering is that ZnO films can be deposited at reduced pressures with uniform coverage on wide range of substrate sizes at high depositional rates. A major disadvantage of magnetron sputtering is poor target utilization due to non-uniform target erosion. Since ZnO thin films are suitable as transparent conducting electrodes in solar cells, sputtering may damage the solar cell on which the deposition is taking place.

After optimizing deposition parameters, the authors achieved crystallites of different width columns with an oriented growth along the [002] directions [35]. In [111], highly transparent polycrystalline ZnO thin films with band gap of 3.28 eV were prepared at an optimized oxygen pressure and substrate temperature of 390°C. It has been found that magnetron sputtering has been effective for doping ZnO thin films.

2.2.4. Spray Pyrolysis

In spray pyrolysis, a solution mixture of zinc acetate and alcohol was used [107, 56], as were $ZnNO_3$ [130] and $ZnCl_2$ [3]. In this technique, the solution is sprayed directly on the substrate heated to desired temperature. Oxygen, nitrogen, or compressed air is used as carrier gas. This carrier gas is used to facilitate atomization of the solution through the deposition nozzle. Studies have shown that the properties of deposited ZnO thin films depend on substrate temperature and gas flow rate [3]. Although this technique is efficient for deposition on large substrates, it has low deposition rate and surface uniformity.

ZnO thin films were deposited on glass substrates at a temperature of 402°C [107]. These films are 85% transmitting in visible region, have high reflectance in IR region and electrical resistivity is 0.15 Ω -m [106]. In [56], ZnO films, deposited on glass substrates, were highly textured along the (002) plane and the depositional properties were optimized [3].

2.2.5. Sol-Gel Process

Solgel method is widely used to obtain various kinds of functional oxide films, including ZnO and doped ZnO thin films with preferred c-axis orientation [82, 22]. In general, two chemical routes are used to synthesize ZnO thin films by sol-gel process: i) the alkoxide route and ii) non-alkoxide process. In alkoxide precursors based process, dimethyl zinc or diethyl zinc are often used which are highly reactive and expensive. For the non-alkoxide route, Zn salts, such as acetates [82], are dissolved in water or alcohol [127]. Monoethanolamine (MEA) is used as a sol stabilizer [34, 127]. The properties and microstructure of sol-gel

derived ZnO thin films are affected by chemical composition, concentration of starting materials, pH of the solution, order, and temperature of reagents. The prepared sol is then spin coated [81] on substrate or dip coated [82, 127, 34]. The as-deposited gel film is then annealed to form ZnO film. This process also allows for doping of ZnO [34, 127]. An advantage of sol-gel route is that on preparing the sol, it can be deposited on substrates for gelling by several simple techniques, such as, spin coating, dip coating, etc. The disadvantage in sol-gel technique is that the properties of ZnO thin films are affected by several parameters that make optimization for high quality films cumbersome. Major disadvantages of the sol-gel process is that alkoxide reagents are expensive and the precursor solution is extremely moisture sensitive.

2.3. Pechini Process

The polymeric precursor method or Pechini process [83], named after its inventor Maggio Pechini, is chemical solution route frequently employed to synthesize polycation oxides. This processing route offers advantages of being simple, low cost utilizing common reagents, and synthesis in ambient atmosphere. A flow chart is shown in Fig. 2.2 for better understanding. In this technique, citric acid or any other alpha hydroxycarboxylic acid and metal salts are dissolved in an aqueous solution. Then ethylene glycol, a polyhydroxyl alcohol, is added which as a reaction medium. On addition of ethylene glycol, citric acid and ethylene glycol react to form a polyester. During this stage, the metal ions are chelated to the polyester to form a polymeric solution with metal cations distributed uniformly [48]. Nitric acid is also added to aid in chelation. The prepared solution is a rigid

network of polyester-type resin with metal ions chelated to resin, which prevents them from segregation. Rigid network reduces the segregation of metal ions enabling stoichiometric and particle size control quite efficiently.

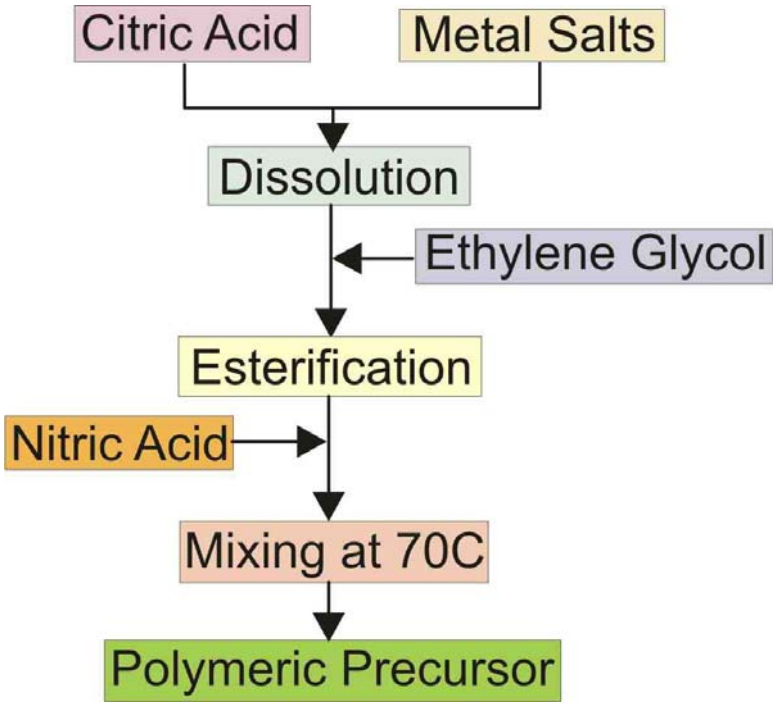

Figure 2.2: Schematic diagram of preparation of polymeric precursor using citric acid as chelating agent and ethylene glycol as esterification agent.

Several groups have synthesized metal oxides using solution of citric acid and ethylene glycol. In this synthesis route, citric acid was used as chelating agent and ethylene glycol as an esterification agent. Using this processing technique, $LiNi_{0.5}Co_{0.5}VO_4$ [112], $BaTiO_3$ [129], $PbZr_xTi_{1-x}O_3$ [95], $Ba_2Ti_9O_{20}$ [150], $Bi_2Ru_2O_7$ [5], $LaCoO_3$ [84] powders were produced. Homogeneous ZnO powders using ethylene glycol and citric acid as reaction medium and chelating agent, respectively [93] also been synthesized. This ethylene glycol mediated polymeric precursor process has yielded either nanoparticles or micrometer sized powders.

Modified Pechini process has also been employed to synthesize polycation oxides using EDTA as chelating agent and ethylene glycol as esterification agent [28]. In this preparation method, EDTA has to be dissolved in ammonium hydroxide to facilitate its dissolution in metal salts solutions. Then ethylene glycol is added to the resultant solution. This solution is then stirred and heated continuously at 80°C to prevent it from precipitation. Nitric acid is added drop wise to the solution to maintain the pH above 5 to avoid irreversible precipitation. EDTA and ethylene glycol react to form polyester. The metal cations chelate to the ethereal oxygen of the polyester [126, 48] to form a polymeric solution. The solution is further heated at 80°C while stirring

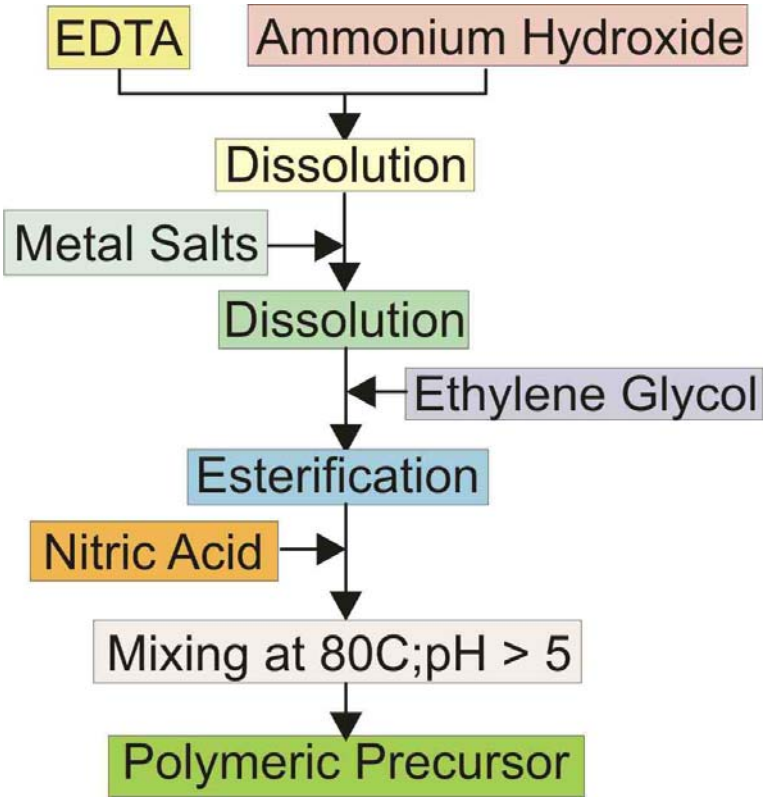

Figure 2.3: Schematic diagram of preparation of polymeric precursor using EDTA as chelating agent and ethylene glycol as esterification agent.

continuously until a clear, precipitate free solution with desired viscosity is reached. A flow chart for preparation of polymeric precursor using EDTA as chelating agent is shown in Fig. 2.3.

Research has been carried out on synthesizing oxides using EDTA as chelating agent in modified Pechini process, such as, $LaAlO_3$ [28], $Eu_2(WO_4)_3$ [14], $BiDy_2Fe_5O_{12}$ [139] and $BaCe_{0.8}Gd_{0.2}O_3$ [126]. It has been proven that EDTA improves distribution of metal cations uniformly in the solution as compared to citric acid [126]. Till date, ZnO thin films or powders have not been synthesized by this or the Pechini method.

2.4. Spin Coating of Polymeric Precursors

Spin coating is a popular technique for producing thin films. It is a cost effective processing technique when compared to other established methods. This method has been a high volume production technique and scalable to all substrate sizes. Spin coating is the preferred method of application of thin uniform film on relatively flat substrates. This method is implemented extensively in microelectronics industry for coating polymer resists for photolithography, coatings of flat panel displays, etc.

Spin coating technique for polymeric precursors, has been developed to deposit oxide thin films [47]. In this technique, a flat substrate is placed on a vacuum chuck. After this, an excess amount of polymeric precursor is applied to the substrate. The substrate is then rotated at high speed to spread the polymer uniformly by centrifugal force. The spin coated film is cured at 70°C to evaporate the solvent and solidify the polymer.

In general, spin coating can be described as four different processes operating simultaneously [24]. First, excess polymeric precursor is added to substrate to ensure complete coverage as shown in Fig. 2.4a. The polymeric precursor has to wet the substrate or have a low contact angle to form uniform thin film. Since the precursors are aqueous based, the substrate surface has to be hydrophilic to achieve uniformity. If the precursor does not wet the substrate, then the surface of the substrate has to be modified using suitable chemistry.

After adding the precursor on the substrate, the substrate is accelerated radially to desired speed of rotation to remove excess solution during the spin up stage. Due to centrifugal force, excess polymer is expelled from the substrate resulting in a thin film (Fig. 2.4b). The substrate rotates at the desired velocity for predetermined amount of time. At this stage, viscous forces of the solution dominate to reduce the film thickness and the polymeric precursor flows uniformly outward (Fig. 2.4c). This is followed by evaporation of the solvent resulting in thinning of film. Since the polymeric precursor has non-volatile solvents, the film has to be cured at 70°C to solidify the polymer (Fig. 2.4d).

Spin coating is simple and cost effective technique. This deposition method has been used successfully to prepare oxide thin films [119, 11, 13, 117]. However, certain issues have to be considered to obtain uniform thin film using polymeric precursors. The precursor has to wet the substrate. Secondly, the substrate has to withstand the sintering temperature needed to pyrolyze the solution. The viscosity of the precursors plays a major role and should be in 1 to 10cP to give thick crack free film. High viscosity of the precursor results in mud

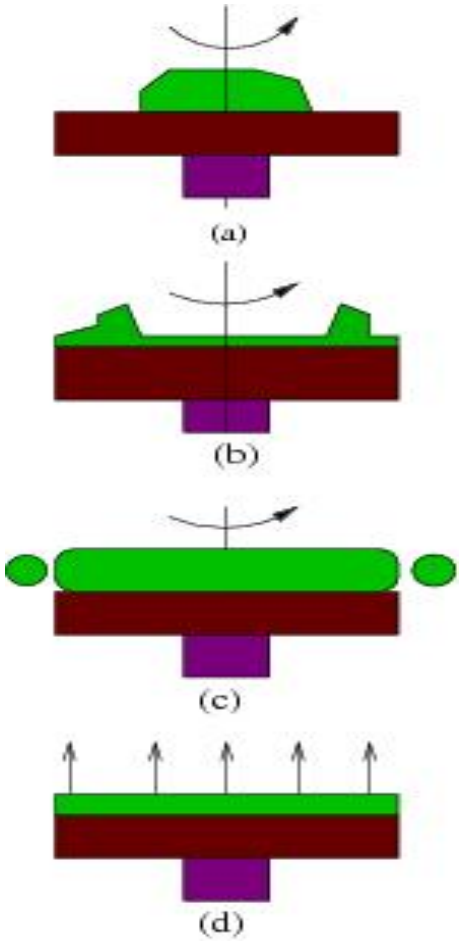

Figure 2.4: Schematic diagram showing processes leading to uniform thin film by spin coating technique.

cracks on pyrolysis which are undesirable in the film. Cracking of the films occurs due to change in volume on pyrolysis. However, cracking can be avoided by reducing the organic content and by increasing the cationic concentration. During pyrolysis of polymer, stress develops in film, which causes shrinkage leading to cracking of films. However, one needs to be careful while increasing cationic concentration for if chelating sites are insufficient, then the cations may precipitate. This will lead to inhomogeneity in microstructure.

CHAPTER 3

CONTROLLING THE MORPHOLOGY OF POLYMERIC PRECURSOR DERIVED ZINC OXIDE NANOSTRUCTURES

The study of possible mechanisms of formation and growth of ZnO nanostructures is crucial as they have potential to find applications in opto-electronic devices. A fundamental understanding of the growth mechanisms is essential to control the morphology precisely and, hence, to improve the quality of the nanostructures. ZnO nanostructures of different morphologies have been synthesized using a low temperature polymeric precursor process. Controlling the Zn cation and nitric acid concentrations, a flower-like morphology of the ZnO nanostructures could be synthesized with excellent reproducibility. In addition to the chemistry, effects of spin coating variables on morphology were also investigated. Results show that morphology of the flowers is controlled by Zn^{2+} ion concentration, whereas spin speed and film thickness is responsible for the size variations. All obtained ZnO structures reveal polycrystalline hexagonal wurtzite structure and strong UV photoluminescence along with lattice defects. Polar surfaces of ZnO promoting multilayer Volmer-Weber growth play a crucial role in the development of these flower-like structures. Possible mechanisms for variations of morphology with synthesis parameters are discussed.

3.1. Introduction

Nanostructures such as wires, rods, belts, and tubes have attracted great scientific interest due to their unique properties and significant potential applications in electronics, photonics, and biochemistry. Organization of these

nanostructures into functional nano-devices such as transistors or waveguides remains an intriguing challenge. Self assembly is an efficient method for synthesizing nanostructures. However, precise control of self assembled nanostructures is essential to establish this technique as a basic and key tool of nanotechnology. Recently, research has been carried out extensively to control the morphology of nanostructures of semiconductors during synthesis [114].

Among II-VI semiconductors, ZnO is a versatile environmentally benign material with several technologically plausible applications. ZnO is a direct wide band gap semiconductor (3.37 eV) with large exciton binding energy (60 meV). It is of interest as a transparent conducting oxide with near UV emission. Owing to these properties, ZnO finds application in low-voltage and short wavelength electro optic devices such as light emitting diodes (LEDs) [132] and UV lasers [76]. ZnO has diversified technological potentials as solar cells [62], catalysts [78, 1], waveguides [88, 31], transparent thin film transistors [29], piezoelectric transducers and actuators [75, 10], surface wave acoustic devices [96, 104, 91], gas sensors [116, 60], and photonic crystals with tunable band gaps [17, 33].

ZnO has displayed a series of nanostructures with different morphologies, such as nanoribbons and combs [153], nanobridges and nanonails [148], thornballs [39], nanorods [38], polyhedral cages [97], nanohelixes, nanosprings, nanorings [145, 143, 142], whiskers [19], nanopins [20], nanoneedles [71, 131], nanowalls [61],etc. However, these morphologies have been deposited by vapor based techniques. Only a few works have been reported on synthesis of flower-like ZnO nanostructures from aqueous solutions. Wang [156] has utilized

ammonia, ammonium salts and thiourea to control morphology and orientation of the tube like, flower like, and tower like nanostructures while preparing them in an aqueous solution. Zhang and his coworkers [50] prepared nanorods of single crystal ZnO clustered into flower-like nanostructures by hydrothermal techniques and controlled the morphology using cetyltrimetylammonium bromide (CTAB) which enhances the growth rate of ZnO by providing adequate active nucleation sites. Zhang [63] decomposed $Zn(OH_4)^{2-}$ or $Zn(NH_3)_4^{2+}$ precursor in an aqueous solution to synthesize flower-like ZnO. Gao and coworkers [138] fabricated flower-like ZnO nanostructures in aqueous solution using hexamethylenetetramine (HMT) and ethylene diamine for controlling morphology. HMT mediates the nucleation and growth of ZnO by controlling the basicity of solution whereas ethylene diamine determines formation of flower-like ZnO nanostructures. Pal [124] synthesized various ZnO nanostructures using hydrothermal processing. They prepared bunches of flower-like nanorods by controlling the pH of the solution and thereby, controlling the nucleation and growth rates of the nanostructures. Du [54] fabricated ZnO flowers in subcritical water solution with CTAB and polyethylene oxide-polypropylene oxide-polyethylene oxide block copolymer of EO17-PO60-EO17 (P103) as surfactants to control nucleation and growth processes. Results of work on flower-like ZnO nanostructures have been briefly summarized in Table 3.1. These works on ZnO flowers consist of clusters of sword like nanorods and most of them have star like or coral (sea urchin) like shape. Ethylene glycol has been used in polymeric precursor solution method for making nanoparticles of complex metal oxides

Table 3.1: Reactants and morphologies obtained in previous work

Authors	Technique	Reactants	Morphology
Wang	Aqueous solution	$Zn(NO_3)_2$. $6H_2O$ + Thiourea + NH_4Cl + H_2O + NH_3	Flowers, Tubes, Towers
Zhang	Hydrothermal	$Zn(Ac)_2$ + CTAB + NaOH	Nanorods clustered to form flowers
Zhang	Aqueous solution	$Zn(Ac)_2$ + NaOH + H_2O $Zn(Ac)_2$ + NH_3 + H_2O	Flowers, snow flakes, short rods, prisms, prickly sphere
Gao	Aqueous solution	$ZnSO_4$ + Ethylenediamine + Hexamethylenetetramine	Flowers, rods
Pal	Hydrothermal	$Zn(Ac)_2$. $2H_2O$ + Ethylenediamine + H_2O + NaOH	Flowers formed of nanorods
Du	Aqueous solution	$ZnCl_2$. $6H_2O$ + CTAB + NAOH + Glycol + P103	Flowers, nanorods
This paper	Polymeric solution	$Zn(NO_3)_2$. $6H_2O$ + Ethylene Glycol + HNO_3 + H_2O	Only Flowers

such as $LiNi_{0.5}Co_{0.5}VO_4$ [112] and perovskites [137]. Till date, ethylene glycol mediated polymeric precursor process has yielded either nanoparticles or micrometer sized powders. In this present paper, we synthesize well defined flower-like ZnO structures composed of 2D nano-sheets by low temperature polymeric precursor process. The morphology, structure and crystallinity of the ZnO flower structures were examined by altering the Zn cation concentration, temperature, preparation time, and spin coating conditions.

3.2. Experimental Methods

All of the chemicals were of analytic-grade and were used as received without further purification. 99% pure zinc nitrate, $Zn(NO_3)_2$ and 99% ethylene

glycol (EG) were obtained from Alfa Aesar. 70% nitric acid (HNO_3), ACS grade potassium hydroxide (KOH) pellets, and citric acid (2-hydroxy-1, 2, 3-propanetricarboxylic acid) were acquired from J. T. Baker, EMD chemical Inc., and Fischer Scientific International Inc., respectively. Deionized and filtered water (resistivity = 18.2MΩ) was also utilized in preparing solutions. Glass microslides (2.54 x 2.54cm^2) were used as substrate. The substrates were thoroughly rinsed ultrasonically in acetone, methanol and deionized water. These were then immersed in 1N potassium hydroxide (KOH) solution to functionalize the substrates with hydroxyls so as to achieve good wetting characteristics. Polymeric precursors for depositing ZnO thin films were prepared using a modified Pechini process [47]. $Zn(NO_3)_2$, ethylene glycol and HNO_3 in varying molar ratios were added to 50 ml of deionized water. The resulting solution was stirred and heated at a constant temperature of 70°C until the final solution was clear, homogeneous, and free from precipitation. The solution was spincoated (CEE Model 100CB, Brewer Science, Inc.) onto prepared substrates at 4000 rpm for 30s, followed by drying at 70°C on a vacuum - chuck hot plate for approximately 1 hour. The films were then annealed for pyrolization of the ethylene glycol and oxide formation at 300°C for 30 min. Similar experiments were also carried out to examine the changes in morphology and growth of flower-like ZnO structures with changes in chemistry. Table 3.2 gives a detailed account of these experiments.

Solutions with lower Zn cation and varying nitric acid concentrations were prepared. Solution was also prepared by changing the sequence of addition of

chemicals at similar chemical concentrations. Solution was also prepared by adding citric acid which acts as chelating agent. The structural and morphological characterization of ZnO structures was examined by field emission scanning electron microscopy, FESEM, (Nova Nanolab 200, FEI Co.), grazing incidence

Table 3.2: Solution numbers, Ratios of Reactants and Morphologies obtained

Solution number	Ratios of Reactants	Morphology	Size (μm)
1	EG/ $Zn(NO_3)_2$/ HNO_3 = 0.7:0.3:0.05	Flower-like	4 – 7
2	EG/ $Zn(NO_3)_2$/ HNO_3 = 0.7:0.3:0.0	Flower-like	6 – 9
3	EG/ $Zn(NO_3)_2$/ HNO_3 = 0.99:0.01:0.1	Sheet	1 – 4
4	EG/ $Zn(NO_3)_2$/ HNO_3 = 0.99:0.01:0.05	Sheet	0.5 – 2
5	EG/ $Zn(NO_3)_2$/ HNO_3 = 0.99:0.01:0.0	Circular Sheet	0.5 – 1.5
6	EG/ $Zn(NO_3)_2$/ HNO_3 = 0.7:0.3:0.1	Flower-like	5 – 7
7	EG/ $Zn(NO_3)_2$/ HNO_3 = 0.7:0.3:0.1	Thin film	-
8	EG/ $Zn(NO_3)_2$/ HNO_3/Citric Acid = 0.7:0.3:0.05:0.3	Thin film	-

X - ray diffraction, GIXRD (Rigaku Ultima III, Cu Kα radiation), transmission electron microscopy, (FEI Tecnai F20ST) and energy dispersive X - ray spectroscopy, EDS (EDAX Inc.). The photoluminescence spectra were acquired with a scanning spectrofluorometer (Photon Technology International) at room temperature with an excitation wavelength of 340 nm using Xenon lamp as an excitation source.

3.3. Results and Discussion

3.3.1. Structure and Morphology

Fig. 3.1 shows an X - ray diffraction spectrum of ZnO layer (solution 1) on glass substrate, annealed at 300°C. The diffraction peaks at 2θ = 31.8°, 34.44°, 36.2°, 47.6°, 56.7°, 62.96°, and 68.04° can be indexed as (100), (002), (101), (102), (110), (103), and (112) planes, respectively. Results show that the

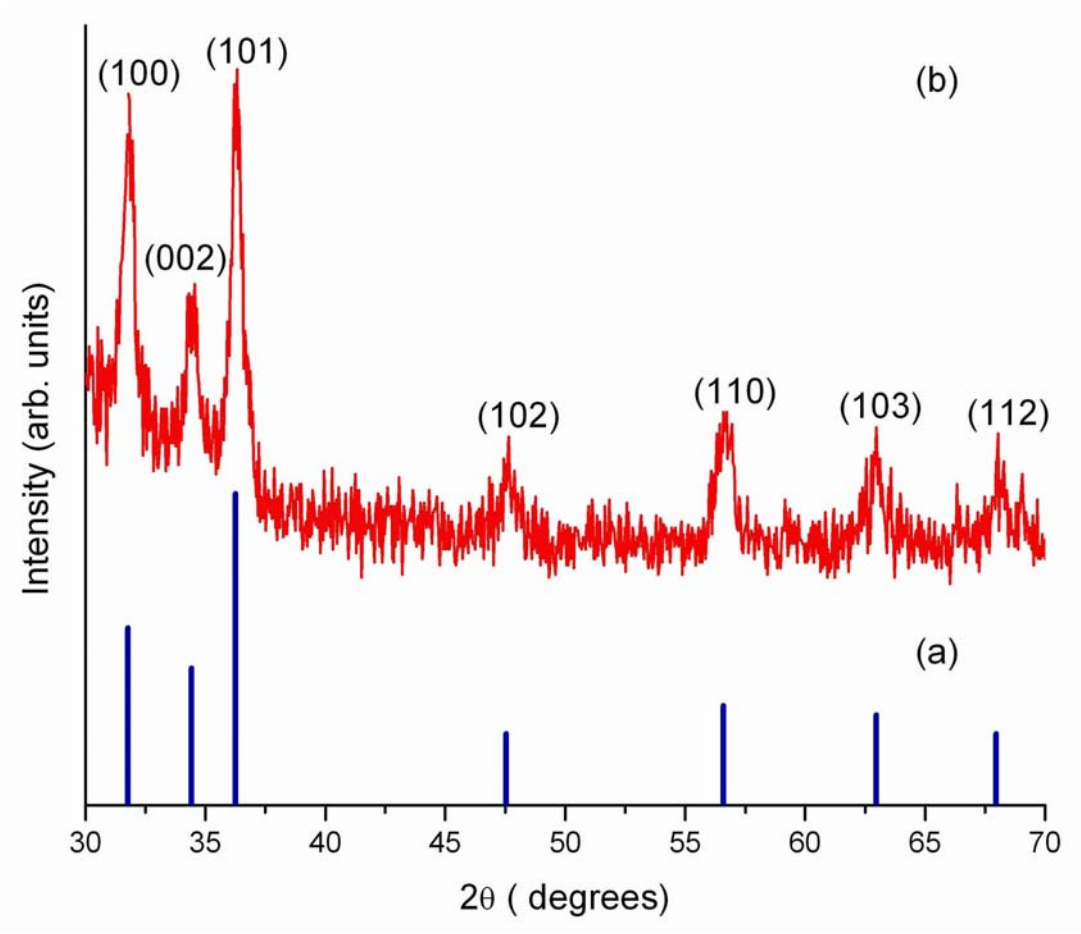

Figure 3.1: XRD spectra of (a) standard ZnO (JCPDS no. 36 - 1451) and (b) flower-like ZnO nanostructures of solution 1.

obtained flower-like ZnO structures possess wurtzite structure (space group $P6_3mc$) and the diffraction peaks can be indexed to hexagonal ZnO (JCPDS No. 36-1451) with cell constants of a = 0.3246 nm and c = 0.5204 nm. No peaks not related to ZnO were formed.

SEM micrographs of flower-like ZnO structures formed using solution 1 on glass substrates are shown in Fig. 3.2. The low magnification image shows that all ZnO flowers are uniformly dispersed throughout the substrate (Fig. 3.2a). Fig. 3.2b and 3.2c show the obtained ZnO flower-like structures at 0° and 70° tilt, respectively. These structures have a well defined hexagonal layered shape. The flowers formed had a layered structure with hollow triangular center. These ZnO flowers are not planar, but are rather hemispherical three-dimensional structures. This fact was confirmed by imaging the sample at 70° tilt. The micrographs also show that the sheet like petals of the flowers self assemble into ZnO structures. Particle size distribution, as shown in Fig. 3.2d, was determined using NIH ImageJ software [125]. It is observed that the diameters of the flower-like ZnO structures are in the range 4-7.5 μm. The mechanism of formation of the ZnO structures is discussed later.

TEM images of the ZnO structures (Fig. 4.3a) show that the structures are polycrystalline with crystallites of approximately 10 nm. The selected area electron diffraction (SAED) pattern obtained indicates that the nanostructures are polycrystalline hexagonal ZnO with wurtzite structure (Fig. 4.3b), consistent with XRD results.

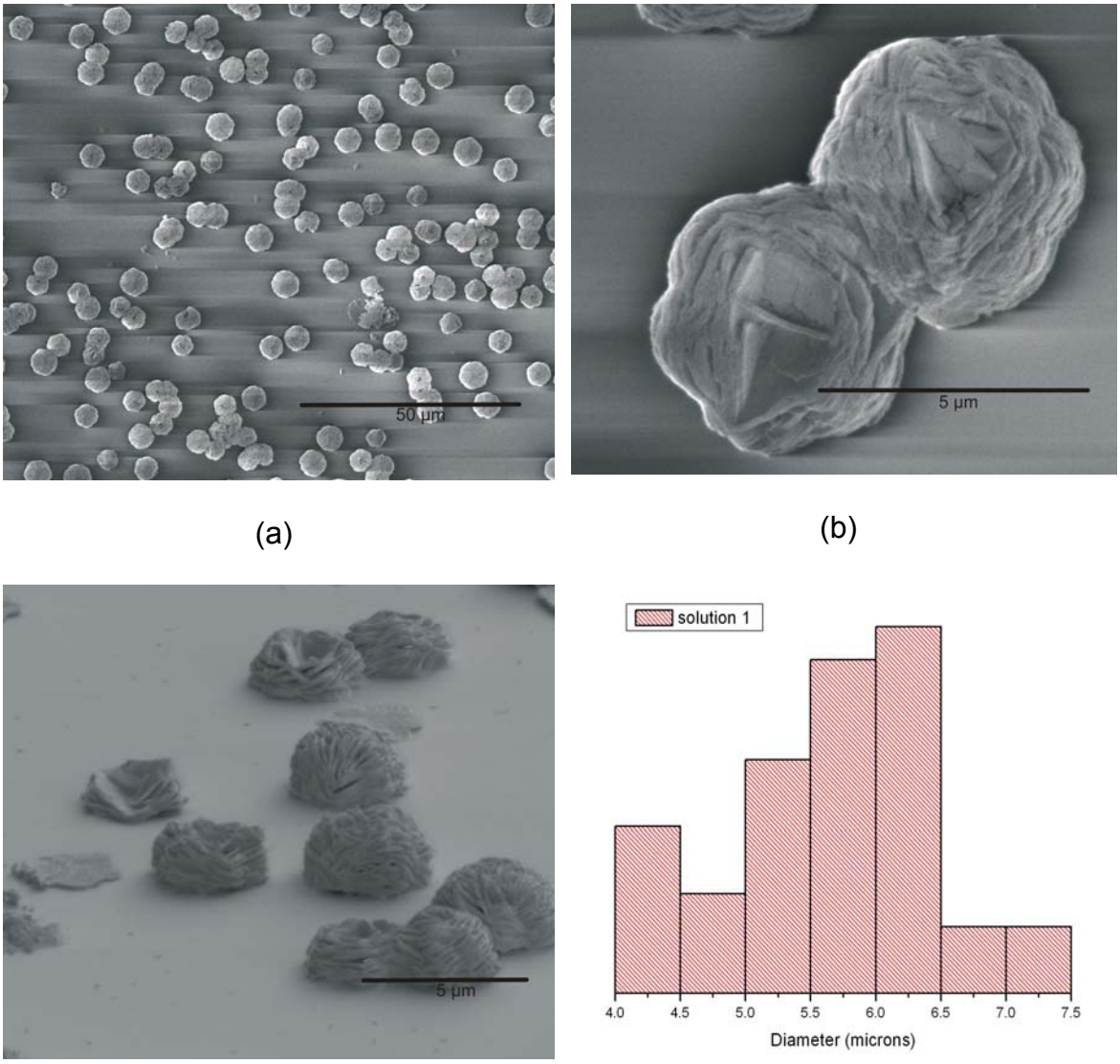

(a) (b)

(c) (d)

Figure 3.2: FESEM micrographs of flower-like ZnO structures on surface modified glass substrates using solution 1 at different magnifications; (a) low, (b) high, (c) 70° tilt respectively, (d) histogram showing the particle size distribution of flowers formed by solution 1.

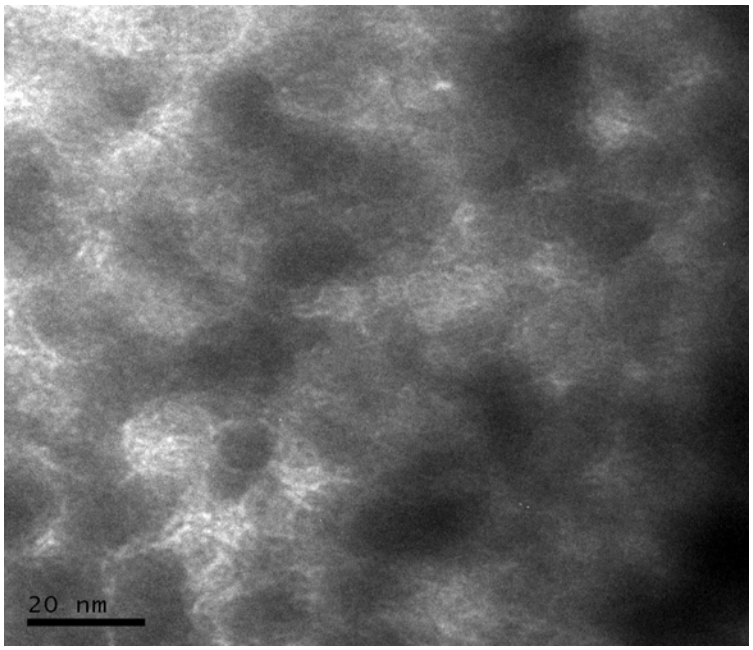

(a)

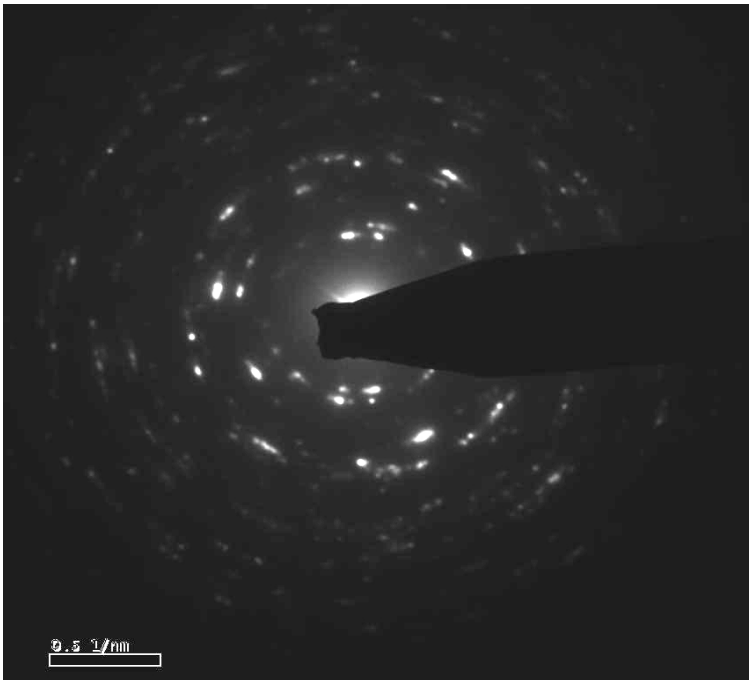

(b)

Figure 3.3: TEM image (a) and (b) electron diffraction pattern of ZnO nanostructures of solution 1 illustrating that polycrystalline hexagonal ZnO.

3.3.2. Effects of Reaction Conditions on Morphology of ZnO Nanostructures

3.3.2.1. $Zn(NO_3)_2$ to EG Ratio

Experiments were subsequently carried out to understand the effect of concentration of $Zn(NO_3)_2$ on the formation of ZnO structures. Solution 4 was prepared with a lower concentration of Zn cations while keeping the HNO_3 concentration constant. An SEM micrograph of solution 4 shows that the size of the structures has reduced considerably (Fig. 3.4a). The well-defined multilayered structure is replaced by an irregular monolayer structure. These structures have diameter of 0.5-2 μm as illustrated by the particle size distribution shown in Fig. 3.4b. Since the amount of ethylene glycol in solution has increased relative to the Zn, there is an increase in chelation sites. The Zn^{2+} cations chelate to the ethylene glycol through the ethereal oxygen of the polymer [48]. As the concentration of Zn^{2+} ions decreases relative to the number of chelation sites, a larger fraction of the Zn^{2+} ions present in solution chelate to ethylene glycol. This results in irregular shaped sheets instead of the layered well-defined six sided flowers as fewer Zn cations are left in the polymeric precursor to directly nucleate on to the substrate.

3.3.2.2. Change in Sequence in Addition of Chemicals

Polymeric precursor solution 6 was prepared by changing the order of addition of chemicals. In this experiment, nitric acid was added to ethylene glycol and was heated for 2 hours to partially polymerize the ethylene glycol. 0.3 moles of $Zn(NO_3)_2$ were subsequently added while stirring continuously. Fig. 3.4c reveals that the flower-like ZnO structures are very well defined multilayered

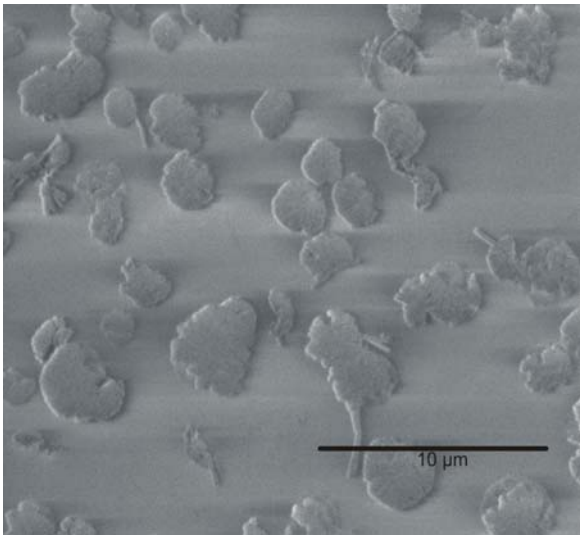

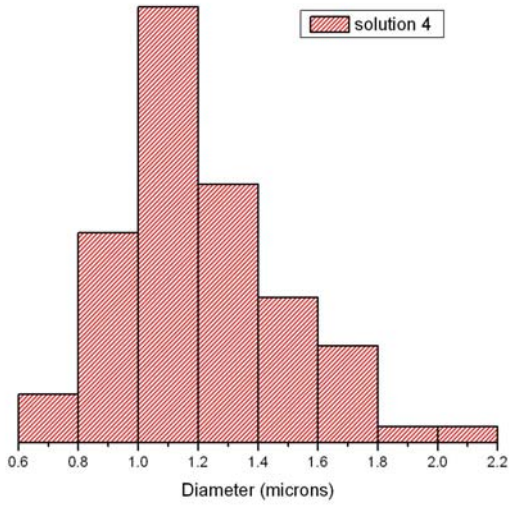

(a) (b)

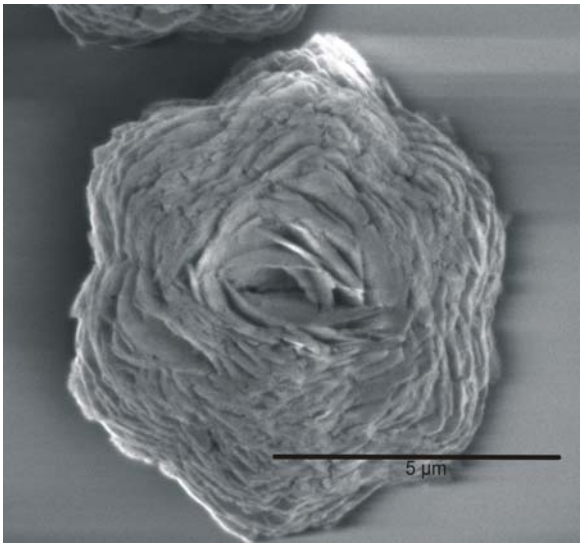

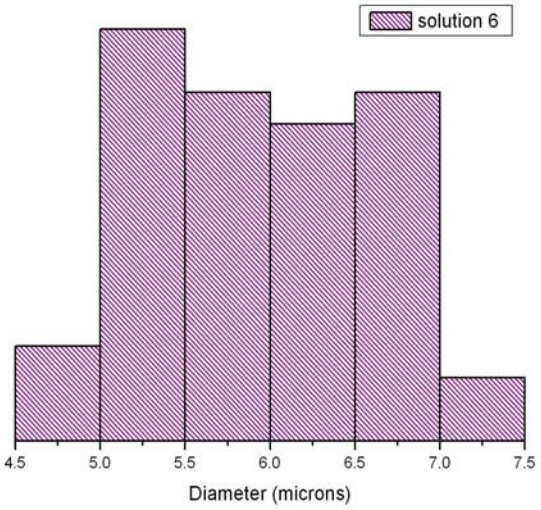

(c) (d)

Figure 3.4: SEM images of ZnO nanostructures formed of (a) solution 4 and (b) solution 6 respectively. Size distribution of these nanostructures is shown in (c) and (d) respectively. These micrographs reveal size and shape variations of nanostructures due to change in Zn cation concentrations.

structures, with diameter of 5-7 μm (Fig. 3.4d). The sizes of these flowers seem to be larger with a narrower size distribution than flowers prepared from solution 1 (Fig. 3.2b and 3.2d). Addition of nitric acid prior to $Zn(NO_3)_2$ polymerizes ethylene glycol and reduces the number of chelation sites considerably and thus, some amount of Zn cations are left unchelated in the polymeric solution. This leads to 5-7 μm monodispersed hexagonal flower-like structures due to nucleation of the unchelated Zn cations on to the substrate.

3.3.2.3. Spin Speed

Experiments were also conducted to study the effect of the spin speed on the formation of ZnO structures. Solution 2 was spincoated at 1000, 2000, and 5000 rpm, respectively. SEM images (Fig. 3.5a and 3.5c) of the films show the creation of flower-like structures when spun at 2000 and 5000 rpm, respectively. It was observed that the diameter of the flower-like structures is 9-12 μm and 6-9 μm for spin speeds 2000 and 5000, respectively (Fig. 3.5b, 3.5d).

However, in case of 1000 rpm, there is formation of dendritic structures. The slow spin speed allows less amount of solution off the substrate and thus results in thicker films. Because of this, more and larger structures are nucleated in close proximity. These larger structures grow and merge to develop dendrites. Fig. 3.6 shows SEM images, which clearly illustrate the formation of dendritic structures at low spin speed.

In order to study the extreme case of very thick films, the solution 2 was coated onto the substrate and was not spun while maintaining other reaction conditions. The samples reveal formation of large dendrites, which can be visual-

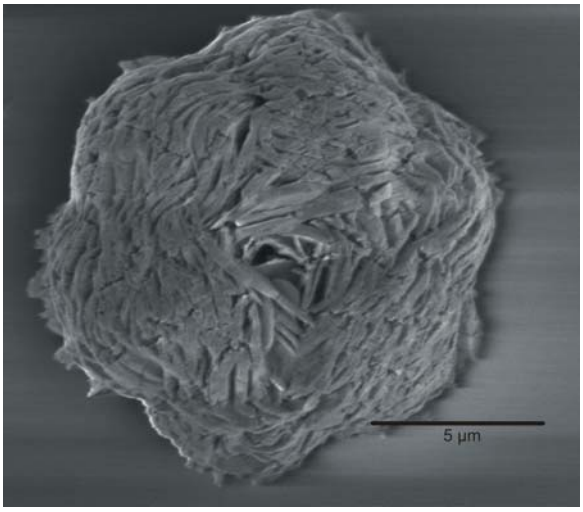

(a)

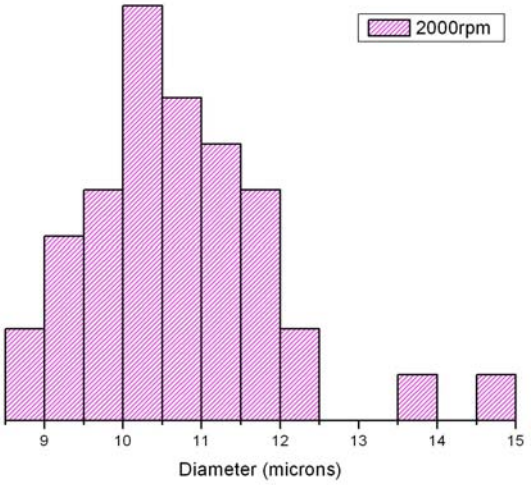

(b)

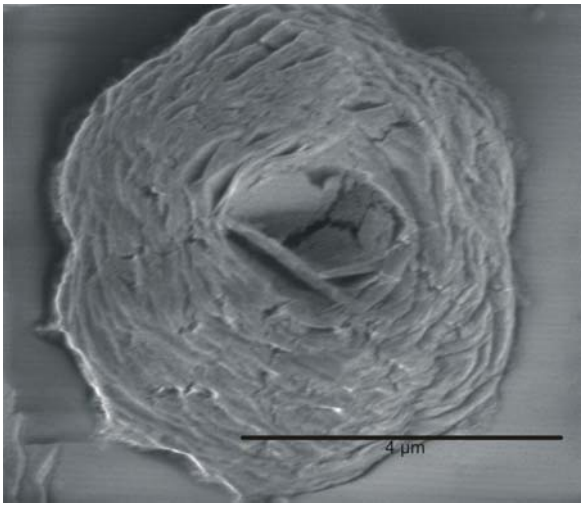

(c)

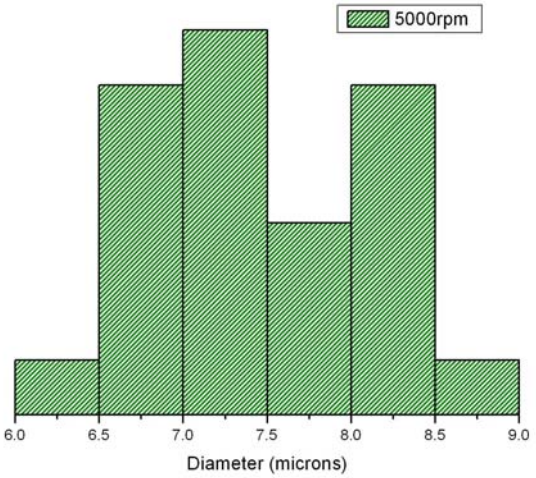

(d)

Figure 3.5: SEM micrographs of flower-like nanostructures of solution 2 spincoated at (a) 2000 rpm and (b) 5000 rpm, respectively. Size distribution of these nanostructures is shown in (c) and (d) respectively. These images illustrate that size control of nanostructures can be achieved by varying spin speed during spin coating process.

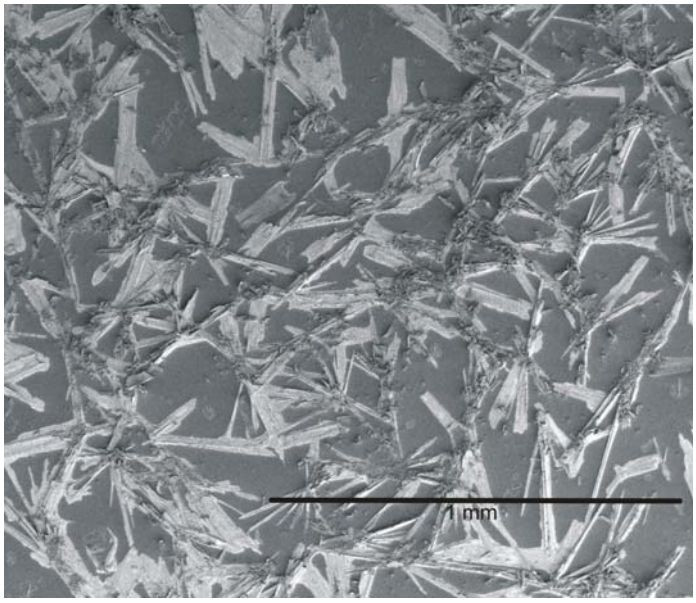

(a)

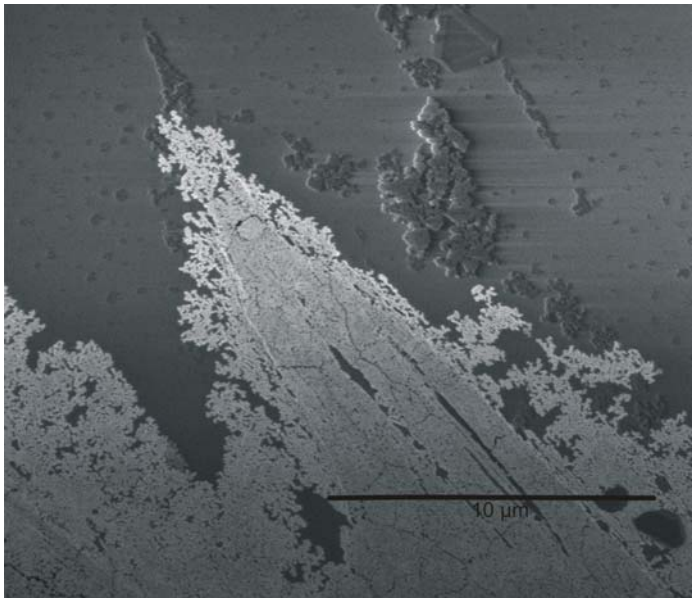

(b)

Figure 3.6: SEM images of solution 2 spincoated at 1000 rpm; (a) low magnification of dendritic structures, (b) tip of a dendrite. These images are being shown to illustrate the fact that low spin speed gives rise to dendritic instead of flower-like structures.

ized with naked eye. Besides the dendrites, SEM images illustrated formation of large ZnO structures. Growth of the dendrite is from the edge towards the center of the sample, which follows the direction of shrinkage due to evaporation of water. On the basis of above facts, it can be deduced that the spin speed during the spin coating of the polymeric solution plays a major role. The sizes of the structure vary depending upon the film thickness; low spin speed gives rise to dendrites whereas high spin speeds help in formation of flower structures. This may be because spinning at high speeds leads to removal of excess solution, but leaving an amount sufficient for the formation of flower-like structures. The mechanism for change in structure size with varying spin speed will be further discussed in subsequent section.

3.3.2.4. Viscosity

Studies have been carried out to study the effect of viscosity of polymeric precursor solutions on the morphology of the ZnO structures. Solution 2 was diluted to varying viscosities using deionized water and was then spincoated onto substrates at constant spin speed of 2000 rpm. On analyzing these thin films under SEM, it was found that the size of the ZnO flowers had reduced while the morphology was similar to the original solution 2. At constant spin speed, more solution is thrown off the substrate, which results in thinner films. Excess solution results in higher nucleation on the substrate and therefore, larger size (10 μm) of structures is formed. The mechanism of formation of flowers will be discussed later in detail.

Solutions 6 were prepared by heating the polymeric solution for different lengths of time and were later spincoated on glass substrates. Different lengths of polymeric solution preparation times also resulted in similar flower-like structures of ZnO as observed using SEM and therefore, have no effect in controlling the morphology of the ZnO flowers.

3.3.2.5. Annealing Temperature

Spincoated thin films of polymeric precursor solution were cured at 70°C and annealed at 200°C or 300°C. The fabricated thin films show no dependence of these annealing temperatures on the morphology of ZnO structures as illustrated by SEM micrographs. However, the shape gets enhanced due to the pyrolysis of the organic substances as shown in Fig. 3.7.

3.3.2.6. Nitric Acid

The effect of varying amounts of nitric acid on formation of ZnO structures was also studied. Solution 7 has been prepared with molar concentration of nitric acid increased compared to solution 1. The concentration of ethylene glycol and $Zn(NO_3)_2$ is maintained constant at 0.7 moles and 0.3 moles, respectively, as in solution 1, while the amount of nitric acid is increased from 0.05 to 0.1 moles. SEM images reveal that formations of thin films of ZnO do not show any presence of flower-like structures (Fig. 3.8a). Although there are more Zn cations, a higher concentration of nitric acid provides sufficient chelation sites for solution 7, inhibiting the formation of ZnO structures from Zn cations remaining in the solution. However, it was observed that the decrease in concentration of nitric

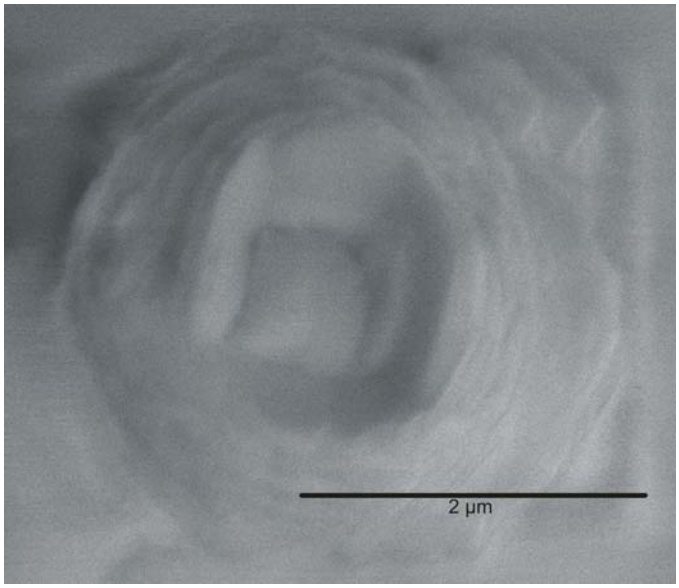

(a)

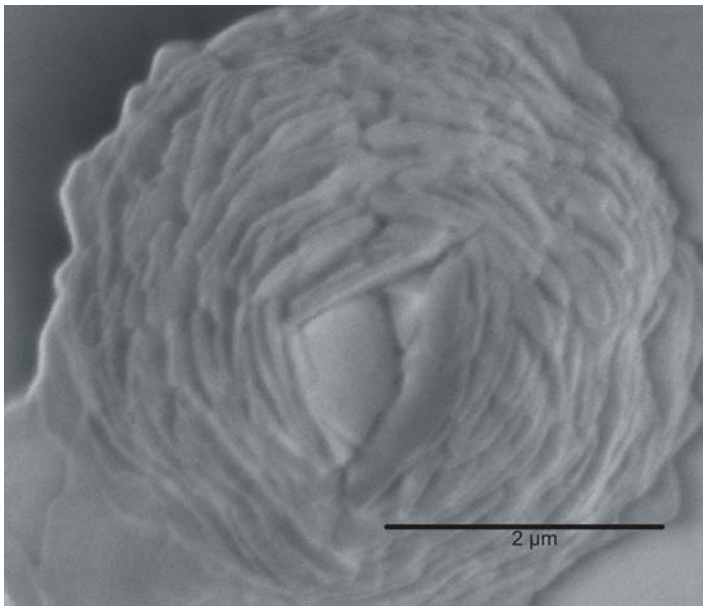

(b)

Figure 3.7: FESEM images of sample of solution 1 annealed at (a) 70°C and (b) 200°C illustrating the clear and sharper shape of nanostructures due to pyrolysis of organic precursors at higher temperatures.

acid leads to formation as well as an increase in the size of the flower-like ZnO structures as shown in Fig. 3.8b and 3.8c.

Addition of nitric acid to ethylene glycol helps in partially polymerizing ethylene glycol and increasing the concentration of chelation sites for Zn cations. When the amount of nitric acid is reduced, the number of chelation sites provided for Zn^{2+} ions also decreases. For higher concentrations of Zn cations, more Zn^{2+} ions remain in solution, which nucleates later directly on the substrate during spin coating as in solutions 1 and 2. This leads to an increase in the diameter of multilayered self assembled flower-like ZnO structures as shown in Fig. 3.8. As discussed earlier, solutions 3, 4, and 5 (lower Zn cation concentration) were prepared by decreasing the amount of nitric acid added to the polymeric solution. SEM images indicate that the shape and size of the flower structures have changed. As the amount of nitric acid decreases the structures' shapes change from irregular sheets to circular sheets. Moreover, the diameter also decreases for solutions 3-5 as shown in Fig. 3.9a, 3.9b, and 3.9c, respectively. These observations are contradictory to the results obtained for solutions 1, 2, and 7 shown in Fig. 3.8. Since the concentration of Zn^{2+} ions is low (0.99 moles of EG to 0.01 Zn^{2+} ions) in solutions 3, 4, and 5, there is an almost chelation of all the available Zn ions. This tends to change the structure morphology from irregular to circular sheets with a progressive decrease in diameter.

On comparing solution 7 and solution 3, we observe that the concentration of EG to HNO_3 is 0.7: 0.1 for solution 7 and 0.99 to 0.1 for solution 3. We postulate that low ratio of EG to HNO_3, as in solution 7, increases the number of

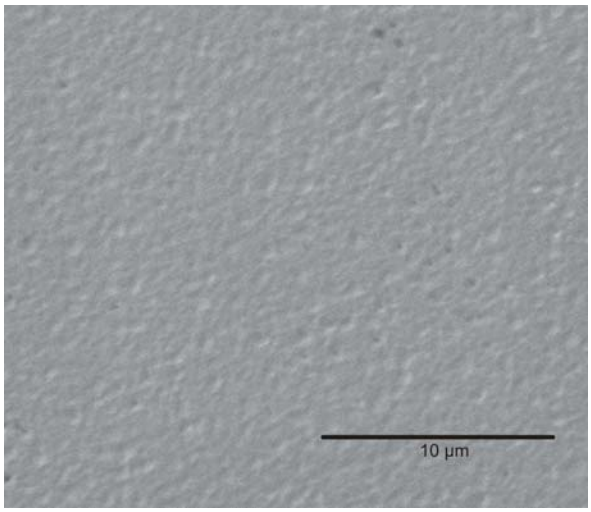

(a)

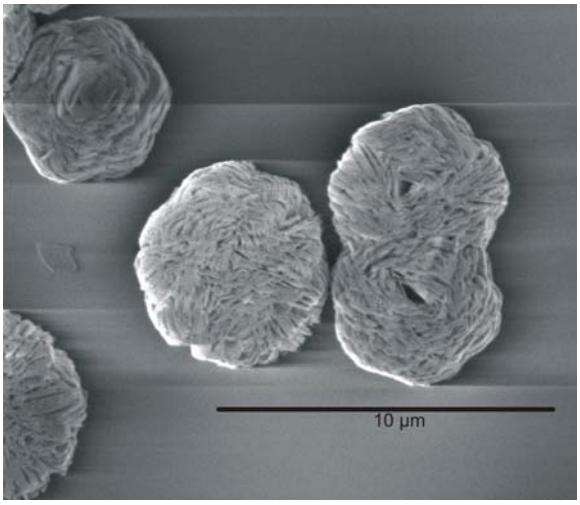

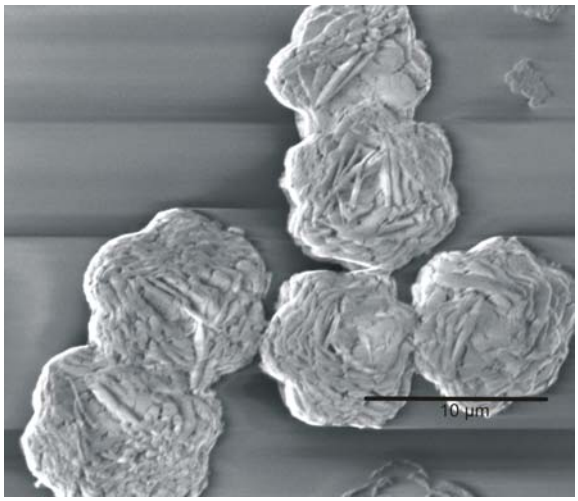

(b) (c)

Figure 3.8: SEM micrographs of solutions (a) 7, (b) 1, and (c) 2, respectively. These solutions were prepared with decreasing amount of nitric acid: (a) 0.1 mole, (b) 0.05 mole and (c) 0 moles. Increase in size of ZnO flower-like structures is observed with decrease in nitric acid.

chelation sites which helps Zn cations to chelate and hence, form ZnO thin films. However, when the ratio is higher as in solution 3, the number of chelation sites

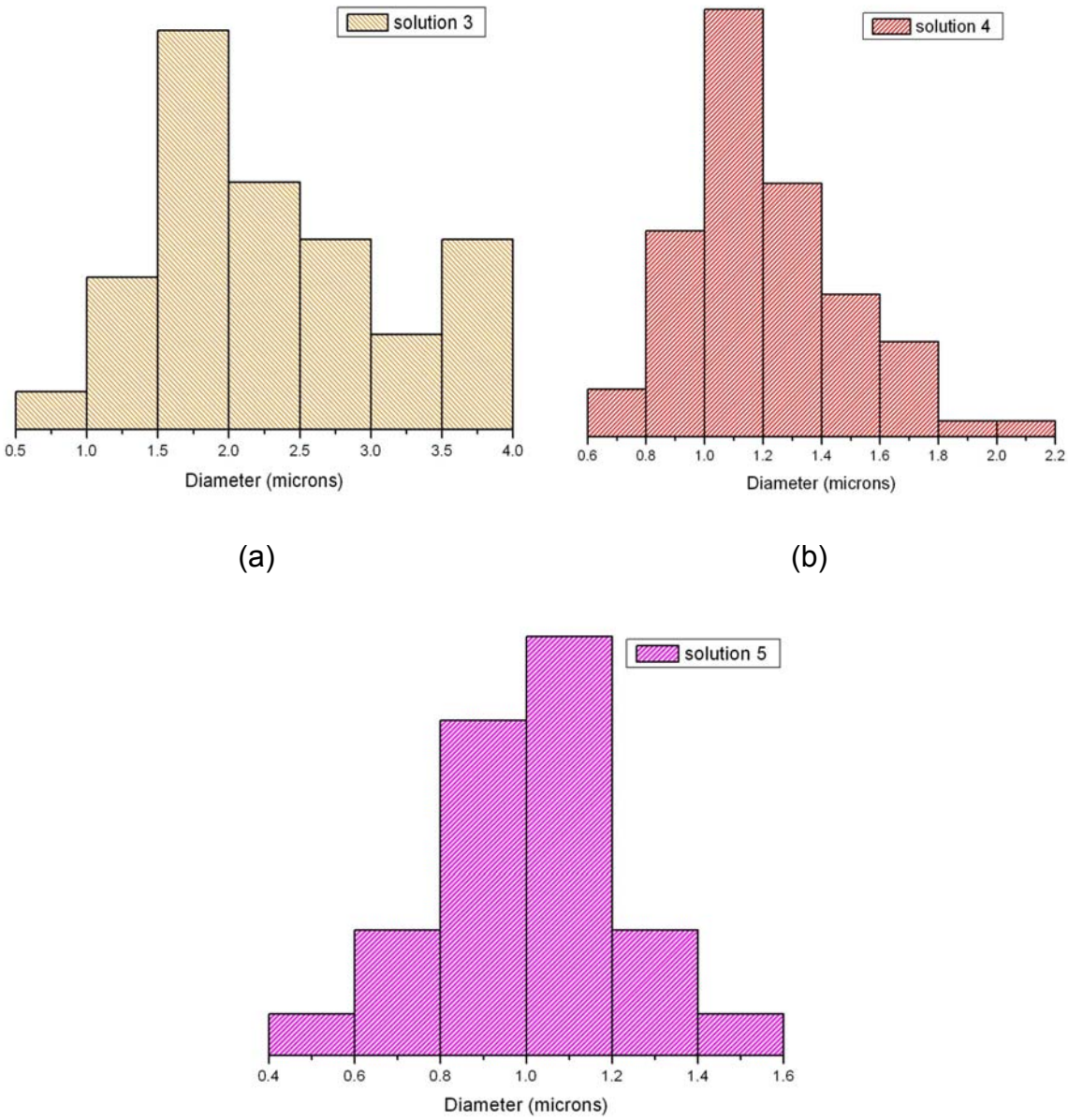

Figure 3.9: Histograms of particle size distribution of nanostructures of solution (a) 3, (b) 4, and (c) 5, respectively. These graphs reveal that the size of nanostructures can be controlled by varying amount of nitric acid added to polymeric precursor solution.

increases which eventually polymerizes EG. This results in reduction of chelation sites for Zn cations leading to formation of irregular structures.

The nature of the chelating agent is also essential to deduce the formation of products. Another chelating agent, citric acid, was used along with ethylene glycol in preparing solution 8. Addition of citric acid to ethylene glycol produces polyester [48]. The citric acid has a stronger affinity for Zn cations, thus more Zn cations get trapped in the polymer leading to good chelation of Zn cations and there are no free cations to nucleate into islands. Hence ZnO thin films (Fig. 3.10) are formed instead of flower-like ZnO structures. However, due to the presence of double bonds in citric acid, the pyrolization temperature for oxide formation is increased and ZnO thin films form at temperatures above 400°C.

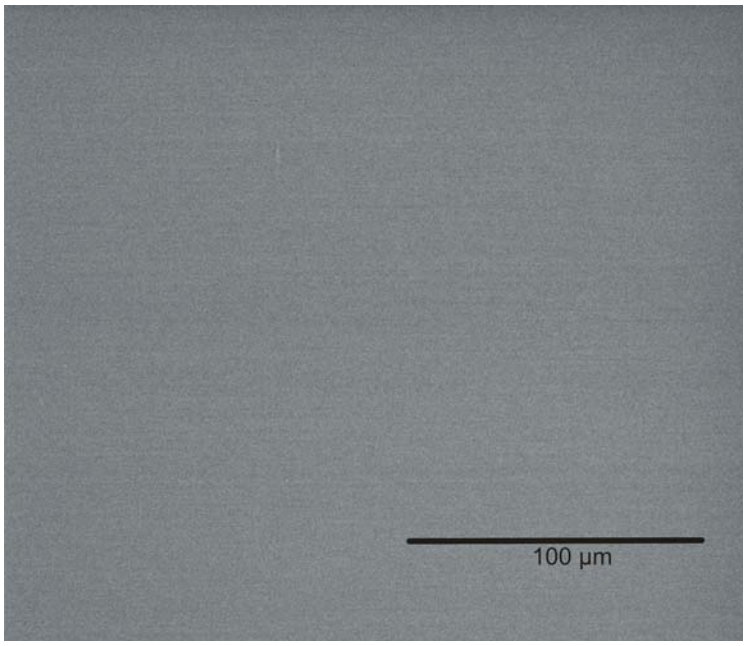

Figure 3.10: SEM micrographs of solution 8 prepared using citric acid as chelating agent. Addition of citric acid to polymeric precursor solution produces thin films of ZnO instead of flower-like nanostructures.

3.3.3. Growth Mechanism

On the basis of experimental results and systematic analysis, the formation of flower-like ZnO structures can be outlined as follows: Firstly, decomposition of $Zn(NO_3)_2$ takes place to form Zn^{2+} ions in solution. Secondly, addition of cold nitric acid oxidizes ethylene glycol to oxalic acid [48]. This is followed by chelation of a fraction of the Zn cations to the oxygen of the carboxyl group of oxalic acid. ZnO is formed by hydrolysis and condensation of the dissolved species in solution, which can be summarized as follows.

$$(CH_2OH)_2 \xrightarrow{HNO_3} (COOH)_2 \xrightarrow{Zn^{2+}} COO - Zn - OOC + Zn^{2+} \quad (1)$$

$$COO\text{-}Zn\text{-}OOC \xrightarrow{\Delta H/O_2} ZnO + 2CO_2 \quad (2)$$

$$Zn^{2+} + 2OH^- \xrightarrow{\Delta H/O_2} Zn(OH)_2 \quad (3)$$

$$Zn(OH)_2 \xrightarrow{\Delta H} ZnO + H_2O \quad (4)$$

Formation of nuclei starts when the polymeric precursor solution is spincoated on the substrate. Self-assembly of ZnO could take place due to either electrostatic interactions [92] or difference in interfacial energy [100] mechanisms. Positively charged colloidal particles get nucleated on negatively charged substrate or vice versa, resulting in the decrease of the surface energy and creation of nucleation sites [90]. Low interfacial energy between the nuclei and substrate also enhances nucleation rate [90]. We postulate that unchelated Zn cations react with hydroxyl ions to form $Zn(OH)_2$ in solution (equation 3). However, there is no evidence of formation of $Zn(OH)_2$ as it is thermally unstable and decomposes at 100°C [74]. We also postulate that $Zn(OH)_2$ (equation 3, 4) adsorbs on the hydroxyl modified substrate. Owing to this, high nucleation rates

are promoted for adsorption of $Zn(OH)_2$ nuclei onto the substrate. The most stable crystal habit is a hexagon elongated along the *c*-axis with a typical basal polar oxygen plane $(000\bar{1})$ and Zn-(0001) plane [73]. Since the basal plane of ZnO is the characteristic polar surface [155], the positively charged Zn-(0001) surface adsorbs at the hydroxyl modified substrate. Due to the surface modification of substrate with OH^- ions, the polymeric precursor wets the substrate, reducing the interfacial energy.

The ZnO structures formed by the polymeric precursor solution grow via the island or Volmer-Weber growth mode [53]. In this growth mode, small clusters of atoms, nucleated on the surface of the substrate, are more strongly bound to one another than to the substrate and subsequently grow into islands, as illustrated by SEM micrographs. When the polymeric solution is dropped onto the functionalized substrate, the adatoms are bound to the hydroxyl ions of the substrate which act as an organic template. As more adatoms approach, they cluster together forming islands. When the clusters acquire critical size, they become stable and form a monolayer island. The critical radius of the monolayer plays a decisive role for nucleation of the second layer. When the critical radii of the monolayer islands is less than the separation between islands, nucleation of a second layer on the islands increases, promoting multilayer growth [58]. However, once a second layer nucleates, it traps most of the adatoms landing on the island. This retards the growth of the first layer. The growth process continues till there are no further nucleation sites on the surface layers. This is prepared show (Fig. 3.2b and 3.2c) both 2D as well as 3D structures developed.

An increase in island density would induce coalescence, thus promoting stacked growth and formation of dendritic structures. Moreover, deposition conditions also have a vital role to play. Lower spinning speeds give thicker precursor films, thus allowing the adatoms to grow until the critical radius is attained which leads to larger islands and hence, larger structures of ZnO.

3.3.4. Photoluminescence

Fig. 3.11 illustrates the room temperature photoluminescence spectrum of the flower-like ZnO structure of solution 1 on glass substrate under photon excitation of 340 nm respectively. A strong and broad UV emission (FWHM = 30 nm) at 392 nm (3.16 eV) dominates the photoluminescence spectra. The energy of photoluminescence agrees with published literature [114, 138]. The UV emission may be attributed to the radiative annihilation of excitons near band edge as ZnO has a high exciton binding energy of 60 meV at room temperature [58, 108]. Besides the strong UV emission peak, there are several weak emission peaks, including a peak with maxima around 470 nm, and a broad peak ranging from 525 to 600 nm, which lies in the yellow-green region. Of the four weak emission peaks, the peak at 468 nm is the strongest. The presence of weak emission peaks around 470 nm has also been observed in a previous work [138] and has been attributed to electron transition from oxygen vacancies to valence band [77, 70]. The origin of this peak is assigned to lattice defects in ZnO [124, 77].

3.4. Conclusions

A polymeric precursor solution based technique was developed to fabrica-

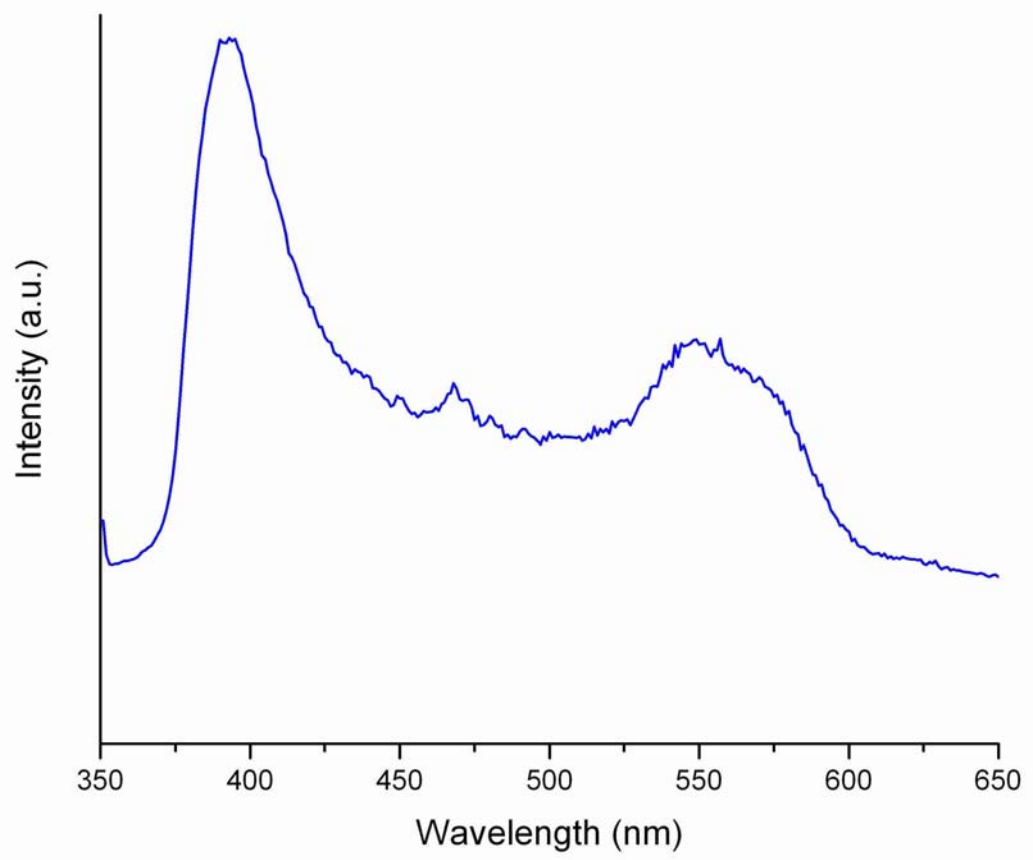

Figure 3.11: Photoluminescence spectrum of flower-like ZnO nanostructures of solution 1 annealed at 300°C under photon excitation of 340 nm at room temperature.

te ZnO nanostructures with hexagonal flower-like morphologies. The flowers synthesized have controlled diameter between 1-10 μm with a multilayered structure. These well-dispersed structures exhibit wurtzite structure with strong UV photoluminescence. Formation of these unique structures is controlled by the Zn cation concentration and the nature of the chelating agent. Factors affecting the size and morphology of the structures, such as, spin speed, temperature, time, and sequence of addition of chemicals, have been thoroughly examined.

Experimental results indicate that the flower-like nanostructures are formed by island growth mode and are controllable by concentration of Zn cations and speed during spin coating process.

CHAPTER 4

NANOCRYSTALLINE ZINC OXIDE THIN FILMS DERIVED USING GLYCEROL AND ETHYLENE GLYCOL AS CHELATING AGENTS IN MODIFIED PECHINI PROCESS

This work presents the preparation of ZnO thin films through the use of polymeric precursors synthesized by two different routes, namely glycerol and ethylene glycol as chelating agents, respectively, in modified Pechini process. The polymeric precursors were spincoated on functionalized silicon and glass substrates and were annealed at various temperatures from 300°C to 600°C. Characterization of the resultant films for degree of crystallization and surface morphology was performed. The thermal decomposition of polymeric precursors was studied by thermogravimetric analysis (TGA). Crystallinity and orientation of grains were studied in depth by X - ray diffraction (XRD). Surface morphology of the thin films was evaluated by scanning electron microscopy (SEM) and atomic force microscopy (AFM). These studies revealed dense, crack free microstucture for films synthesized using glycerol precursor and flower-like structures for ethylene glycol precursor. Room temperature photoluminescent spectra of these films show strong UV emission.

4.1. Introduction

ZnO, a versatile material, has attracted considerable attention due to its potential applications, such as, anti-reflection coatings [68], transparent electrodes in solar cells [68, 80, 62], gas sensors [110], varistors [149, 94], and surface acoustic wave devices [104, 91]. ZnO has a large exciton binding energy

(60 meV) which provides efficient exciton emissions at high temperatures. These properties of ZnO find applications in ultraviolet light emitting diodes, laser devices [76], and in flat panel displays as a low voltage phosphor. A review of properties and applications of ZnO has been published elsewhere [105].

Various techniques, such as pulsed laser deposition [68, 64], chemical vapor deposition [85, 42], magnetron sputtering [30], spray pyrolysis [107], molecular beam epitaxy [136], metal organic chemical vapor deposition [59], etc have been employed to prepare good quality ZnO thin films. Although these processing techniques produce high quality thin films, they are complicated, expensive, and time-consuming. Low temperature, wet chemical routes offer an exciting possibility for the synthesis of high purity, homogeneous thin films with tailored and predictable properties. Sol-gel route has been utilized for preparation of ZnO thin films [34, 18, 81, 2]. However, insolubility of zinc alkoxides in most alcohols poses a major problem for this technique. Working with alkoxides requires special handling as it is a toxic process and quite expensive. Besides, electrical and optical properties of the thin films degrade due to impurities and high density of carrier traps and potential barriers at grain boundaries [81]. Among other established synthesis methods, simple and cost effective routes to synthesize nanocrystalline ZnO thin films by utilization of less expensive, nontoxic, and environmentally benign precursors are still the key issues. The polymeric precursor method, in which a solution of ethylene glycol, citric acid and metal ions is polymerized to form a polyester-type resin, is becoming quite popular because of its simplicity. The metal ions can be immobilized in a rigid

polyester network of polyester-type resin, which can greatly reduce the segregation of a particular metal during the processing.

Pechini process has also been employed to synthesize homogeneous ZnO powders using ethylene glycol and citric acid as reaction medium and chelating agent, respectively [93]. To date, ethylene glycol mediated polymeric precursor process has yielded either nanoparticles or micrometer-sized powders. In this paper, we synthesize nanocrystalline ZnO thin films by low temperature polymeric precursor process by two different routes using glycerol and ethylene glycol as chelating agents, respectively. To our knowledge, this is the first work on synthesizing nanocrystalline ZnO thin films using glycerol as chelating agent by aqueous polymeric precursor process. The prepared polymeric precursors were spincoated on substrates and annealed at different temperatures. Thermal decomposition of the precursors was studied by thermogravimetric analysis (TGA). The synthesized and annealed thin films were characterized by XRD, SEM, and AFM. The photoluminescent properties of the thin films were also investigated.

4.2. Experimental Methods

All chemicals were of analytic-grade and were used as received without further purification. 99% pure zinc nitrate, $Zn(NO_3)_2.xH_2O$, 99% glycerol, and 99% ethylene glycol were obtained from Alfa Aesar. 70% nitric acid (HNO_3) and ACS grade potassium hydroxide (KOH) pellets, were acquired from J. T. Baker and EMD chemical Inc., respectively. Deionized and filtered water (resistivity = 18.2MΩ) was utilized in preparing solutions. Glass microslides and silicon

substrates (2.54 x 2.54cm^2) were thoroughly cleaned ultrasonically in acetone, methanol, and deionized water, followed by surface modification with 1N potassium hydroxide (KOH) solution to achieve good wetting characteristics. Polymeric precursors for depositing ZnO thin films were prepared using modified Pechini process. $Zn(NO_3)_2$, glycerol, and HNO_3 in molar ratios of 0.1: 0.9: 0.1 respectively, were added to 50 ml of deionized water. The resulting solution was stirred continuously and heated at a constant temperature of 70°C until the final solution was clear, homogeneous, and free from precipitation. Solution with similar concentration was prepared with ethylene glycol as chelating agent; details are published elsewhere [119]. Briefly, 0.1, 0.9, and 0.1 moles respectively, of $Zn(NO_3)_2$, ethylene glycol, and HNO_3 were dissolved in deionized water. The resulting solution was stirred continuously and heated at 70°C for approximately 18 hours. The prepared solutions were spincoated (CEE Model 100CB, Brewer Science, Inc.) on surface modified substrates at 4000 rpm for 30s, followed by curing at 70°C on a vacuum - chuck hot plate for approximately 1 hour. The films were then annealed at varied high temperatures for 10 min for pyrolization of the organic precursors and oxide formation.

Thermal decomposition of polymeric precursor of ZnO was studied by thermogravimetric analysis (Perkin Elmer TGA - 7). Structure and morphology of the synthesized ZnO thin films were characterized by X - ray diffraction with CuKα radiation and Bragg – Brentano geometry, (Scintag XDS 2000) and field emission scanning electron microscopy, FESEM, (Nova Nanolab 200, FEI Co.). Digital Instruments Multi-Mode Nanoscope IIIa was also used to study the

surface morphology. AFM imaging was carried out in the tapping mode, at a scanning rate of 1Hz using a silicon cantilever with a spring constant of 20 - 80 N/m. Surface roughness (R_{rms}) was calculated using the equipment's software routine. The photoluminescence spectra were acquired with a scanning spectrofluorometer (Photon Technology International) at room temperature with an excitation wavelength of 340nm using Xenon lamp as an excitation source.

4.3. Results and Discussion

4.3.1. Thermogravimetric Analysis

Fig. 4.1 shows the TGA curves (heating rate = 2°C/min) of ZnO polymeric precursors, prepared using ethylene glycol (Fig. 4.1a) and glycerol (Fig. 4.1b) over the temperature range of 50°C - 600°C. In case of glycerol precursor, as shown in the TGA curves, the weight loss increased up to 550°C as the temperature increased, and beyond that temperature, the weight remained constant. Excess water and polyglycerol are pyrolized and the precursor loses mass till 110°C. Between 110°C and 230°C, another weight loss is observed which is due to pyrolysis of polymeric glycerol. There is a plateau evident from 230°C to 350°C indicating the presence of 3D network of glycerol cross-linked with Zn cations in the precursor solution. Weight loss observed from 350°C to 430°C may be attributed to pyrolysis of polymeric backbone. There is simultaneous formation of ZnO along with the pyrolysis of glycerol backbone. Above 450°C, all of the organic material is removed from the precursor leaving ZnO. Therefore, it is concluded that all of the involved reactions in the weight loss process were finished at 450°C-i.e., the decomposition of all organic products of

the precursor (between 50°C and 400°C) and their combustion (from 400°C to 450°C) along with simultaneous formation of the ZnO structure. For precursor prepared using ethylene glycol, there is weight loss from 50°C to 212°C indicating pyrolysis of excess water and polyethylene glycol. At 212°C, we observe a 15% weight loss due to combustion of organic precursor, ethylene glycol. Beyond this temperature, the weight remained constant implying that all organic materials have been eliminated and there is complete crystallization of ZnO.

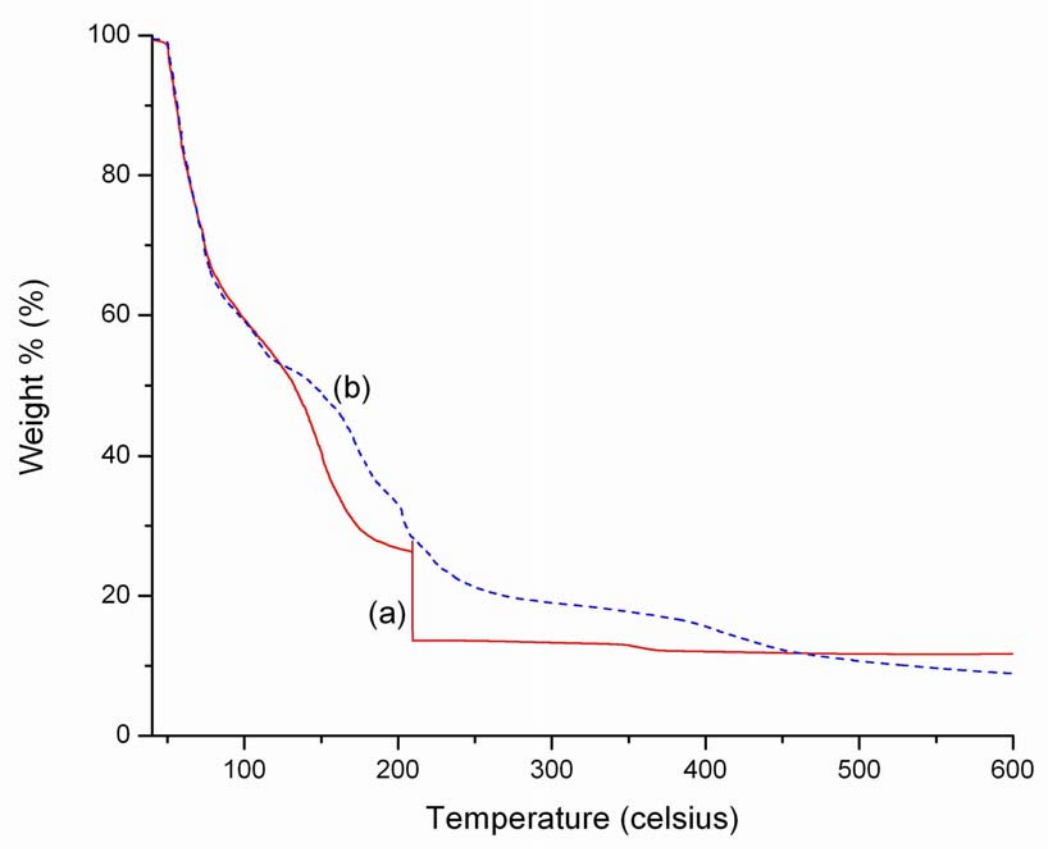

Figure 4.1: TGA curves (heating rate = 2°C/min) of ZnO polymeric precursor prepared using (a) ethylene glycol and (b) glycerol, respectively, as chelating agent.

On comparing the TGA curves, we observe that the TGA curves are similar up to 110°C that may be attributed to removal of excess water from the precursors. Above 110°C, the weight loss in glycerol is lower than ethylene glycol, which occurs due to pyrolysis of polymeric glycerol and polyethylene glycol. There is a sharp change in weight (at 212°C) for ethylene glycol caused due to complete pyrolization of ethylene glycol, after which the weight remains almost constant. However, there is gradual weight loss with increase in temperature up to 450°C in case of glycerol. Hence, TGA curves reveal that pyrolysis of ZnO polymeric precursor is complete at 450°C and 220°C, respectively, for glycerol and ethylene glycol precursors.

4.3.2. X-ray Diffraction

X-ray diffraction of synthesized ZnO thin films were performed in θ - 2θ mode using Bragg - Brentano geometry to determine the crystallinity and orientation and obtained XRD spectra are shown in Fig. 4.2. Each of the polymeric precursors was spincoated on silicon substrates and annealed at 300°C, 450°C, and 600°C respectively. Ethylene glycol based ZnO thin films at 300°C (Fig. 4.2a) show diffraction peaks, which can be indexed as planes of wurtzite structure of ZnO. Peaks not related to ZnO were not observed. Relative intensities of the diffraction peaks reveal that there is no preferred orientation along any particular direction.

For glycerol based polymeric precursor, ZnO thin films annealed at 300°C do not show any diffraction peaks (Fig. 4.2b) due to the presence of organic precursor. Moreover, ZnO is not formed as supported by TGA data. Thin films of

ZnO, annealed at temperatures above 450°C (Fig. 4.2c), possess wurtzite structure with space group $P6_3mc$. The lattice constants *a* and *c* can be calculated using the following equation:

$$\frac{1}{d^2} = \frac{4}{3}\frac{(h^2 + hk + k^2)}{a^2} + \frac{l^2}{c^2} \quad (5)$$

For (100) and (002) diffraction peaks, this equation 5 can be simplified as:

$$a = \sqrt{(\frac{4}{3})}d \quad (6)$$

$$c = 2d \quad (7)$$

The lattice constants calculated using equations 6 and 7 were *a* = 0.3165 nm and *c* = 0.5086nm respectively, which are slightly lower than cell constants of bulk ZnO (JCPDS no. 36 - 1451). The XRD peak positions show a shift to higher diffraction angle illustrating that the films are under compressive strains. On annealing ZnO thin films at 600°C, the diffraction peaks appear shifted to higher diffraction angle than films annealed at 450°C. The calculated lattice constants are *a* = 0.3162 nm and *c* = 0.5079 nm (using eqn.6 and 7). The average crystallite size was calculated using Scherrer's equation:

$$t(nm) = \frac{0.9\lambda}{FWHM \times \cos\theta} \quad (8)$$

where λ is X - ray wavelength of Cukα, (λ = 0.154 nm) and FWHM of (002) diffraction peak width at position 2θ. Using the equation 8, the crystallite sizes for ZnO thin films annealed at 450°C and 600°C were calculated to be 28 nm and 35 nm, respectively.

The XRD spectra illustrates highest intensity for (002) plane than (101)

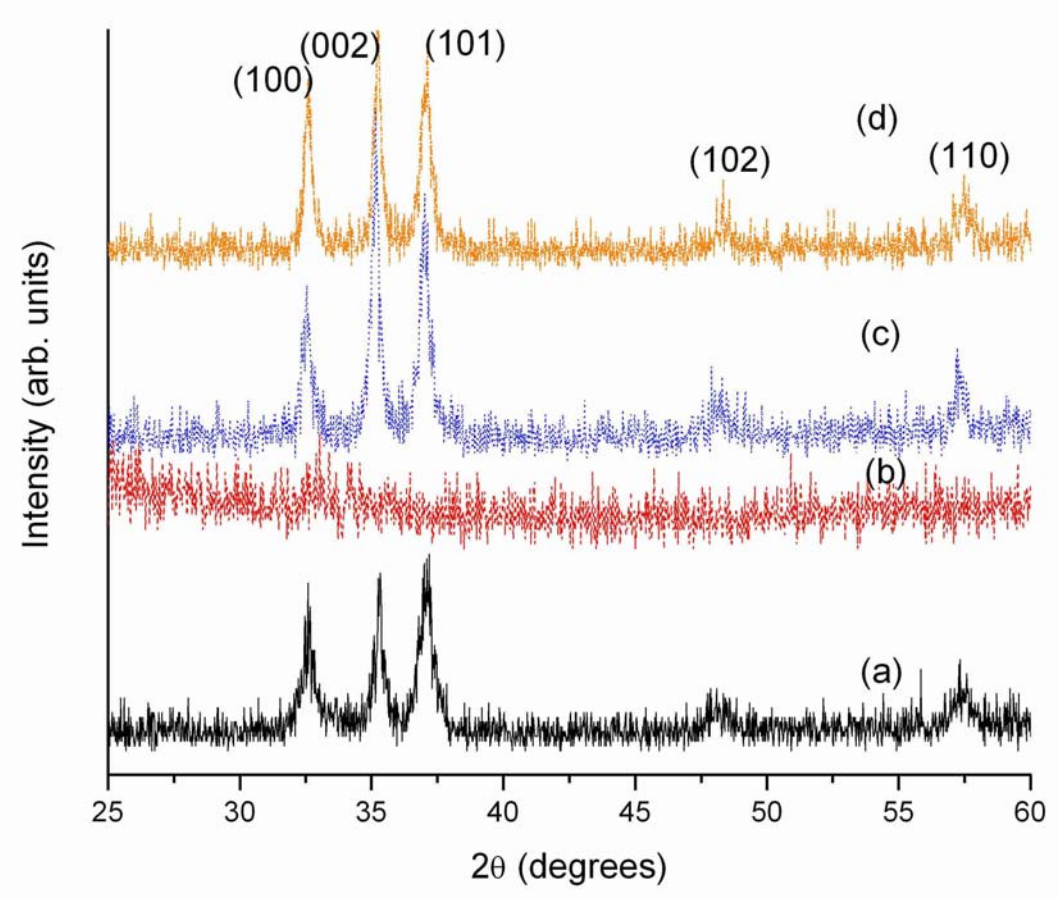

Figure 4.2: XRD spectra of ZnO thin films synthesized by polymeric precursor route using chelating agents - (a) ethylene glycol annealed at 300°C, and glycerol annealed at (b) 300°C, (c) 450°C, and (d) 600°C, respectively. The crystallite sizes calculated using Scherrer's equation, were 28nm and 35nm for glycerol derived films annealed at 450°C and 600°C, respectively.

plane. However, calculations of relative intensities of the three strongest peaks with respect to (101) plane (this plane has highest intensity according to JCPDS) reveal that there is no preferred orientation along [001] direction. No peaks not related to ZnO were detected.

Comparison of XRD spectra illustrates that formation of ZnO occurs at a lower temperature (300°C) for ethylene glycol whereas ZnO diffraction peaks are observed for samples annealed at 450°C and higher for glycerol based polymeric precursor. The spectra reveal that compressive strains is higher in EG than in glycerol thin films. It is also observed that the compressive strains increases with increase in temperatures in glycerol based thin films. We propose that the prepared films are dense to cause compressive strain. This is due to formation of nanometer sized ZnO grains in voids left by polymeric precursors on pyrolysis at annealing temperatures above 450°C. Owing to this, pore coalescence is prevented resulting in compressive strains. This compressive strain may also arise due to difference in coefficients of thermal expansions existing between ZnO thin films and SiO_2/Si. Further detailed studies to determine the cause of the compressive strain and the effect of substrate, defects, and deposition conditions on strain, film thickness, will be studied extensively in future.

4.3.3. Scanning Electron Microscopy

Representative scanning electron micrographs of polymeric precursor derived ZnO thin films using glycerol as chelating agent and annealed at 300°C, 450°C, and 600°C are shown in Fig. 4.3 (a, b, and c). Microstructure studies of samples annealed at 300°C illustrate smooth films probably with no or very fine ZnO particles that are not detected by SEM. On annealing at 450°C, the films have a granular morphology with average grain size of approximately 20 nm. The surfaces of these films appear without cracks, very homogeneous and dense. After annealing at 600°C, the micrographs reveal grain growth with an increase in

average grain size to 60 - 70 nm. Grain growth deteriorates the film surface resulting in high porosity. This may be due to pore coalescence to eliminate pores on sintering. ZnO thin films of ethylene glycol based polymeric precursor were also analyzed by SEM (Fig. 4.3d). Micrographs reveal formation of ZnO flowers, which have hemispherical three-dimensional hexagonal layered shape. The flowers are well dispersed and have an average diameter of 4-7 μm.

Fig. 4.4 show SEM images of FIB cross-section of glycerol based ZnO thin films annealed at 450°C and 600°C, respectively. The micrographs illustrate that the film thickness is approximately 20 nm for 450°C illustrating that the film is one grain thick. On annealing at 600°C, the film thickness increases to 200 nm. From the SEM micrographs, it can be deduced that the film is very porous with spherical particles. The distinct difference in morphology of the thin films of polymeric precursors may be attributed to the chelation of Zn cations to the polymeric backbone. The Zn^{2+} cations chelate to the polymer through its ethereal oxygen [48]. We observe that all the Zn cations chelate to glycerol forming dense, crack free thin films. We postulate that there are insufficient chelation sites for the Zn cations provided by ethylene glycol as compared to glycerol. Hence, some of the Zn ions are left unchelated in the polymeric solution. These unchelated ions nucleate directly on the substrate during spin coating and form ZnO nanostructures on annealing [119]. In case of glycerol, the number of chelation sites provided for Zn ions is adequate leading to chelation of all available cations. Hence, this precursor forms crack free homogeneous ZnO thin films.

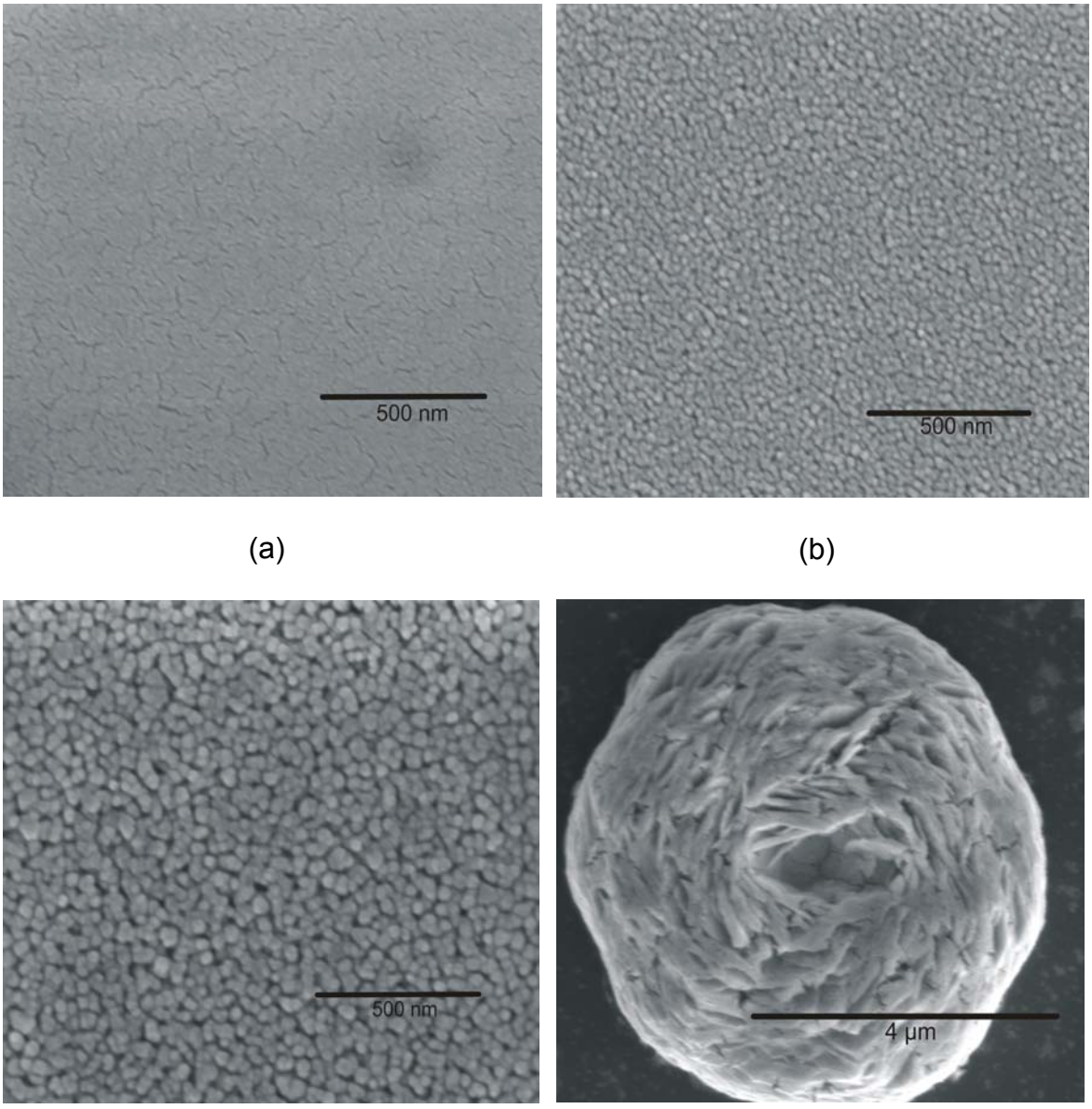

(a) (b)

(c) (d)

Figure 4.3: SEM micrographs of precursor derived ZnO thin films using glycerol as chelating agent and annealed at (a) 300°C, (b) 450°C, (c) 600°C and (d) ZnO nanoflowers prepared using ethylene glycol and annealed at 300°C.

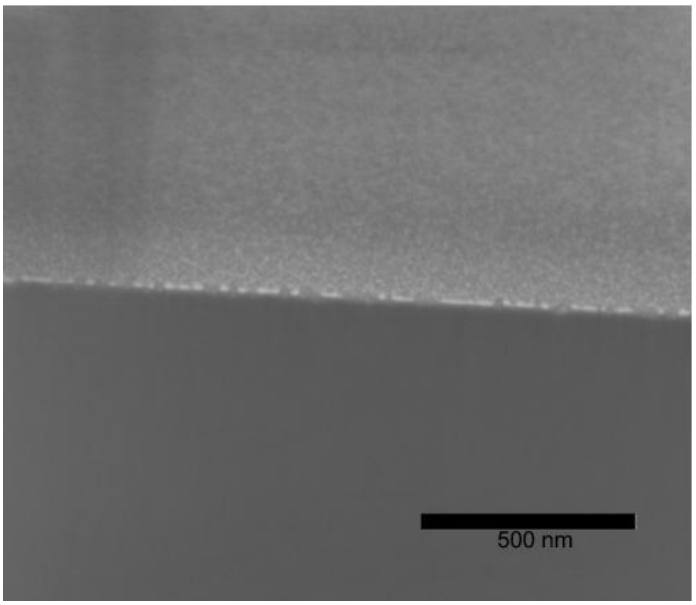

(a)

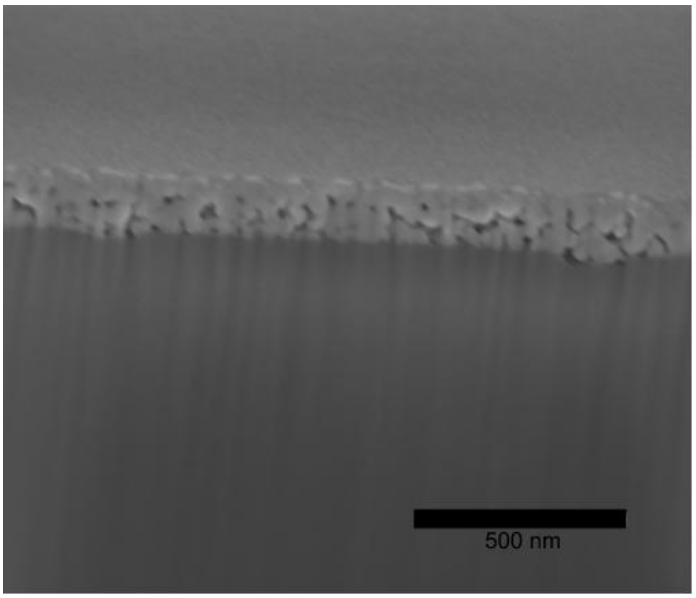

(b)

Figure 4.4: SEM micrographs of FIB cross-section of glycerol precursor derived ZnO thin films annealed at (a) 450°C, and (b) 600°C. The thicknesses were measured to be about 20 nm and 200 nm, for annealing temperatures of 450°C and 600°C, respectively.

4.3.4. Atomic Force Microscopy

Typical AFM micrographs of ZnO thin films prepared by spin coating glycerol based precursor and annealed at 300°C, 450°C, and 600°C are shown in Fig. 4.5(a, b, and c). ZnO thin films synthesized exhibit dense, crack-free microstructure with smooth morphology and small porosity. AFM micrographs revealed differences in the surface morphology of the films annealed at different temperatures. The sample heat treated at 300°C showed a homogeneous surface morphology with very low roughness (root mean square R_{rms}=0.42 nm). There was no evidence of granular structure. When the sample was annealed at 450°C, it displayed a homogeneous nucleation distributed uniformly throughout the thin film with a size distribution approximately 25 – 30 nm. There is an increase in roughness (root mean square R_{rms}=2.188 nm) suggesting that the ZnO film structure is becoming increasingly ordered. On the other hand, the surface morphology changes dramatically at 600°C. At this stage, grain growth occurs along the grain boundaries, leading to coalescence of grains. As a result, there is formation of granular structure with a significant increase of the root mean square roughness, R_{rms}=3.69 nm. AFM image also reveals pores located at the boundaries of the grains.

4.3.5. Photoluminescence

In representative photoluminescence (PL) spectra of ZnO thin films (Fig. 4.6), the glycerol based ZnO thin films showed only UV emission attributed to free - exciton recombination or to the radiative annihilation of excitons near band edge as ZnO has a high exciton binding energy of 60meV at room temperature.

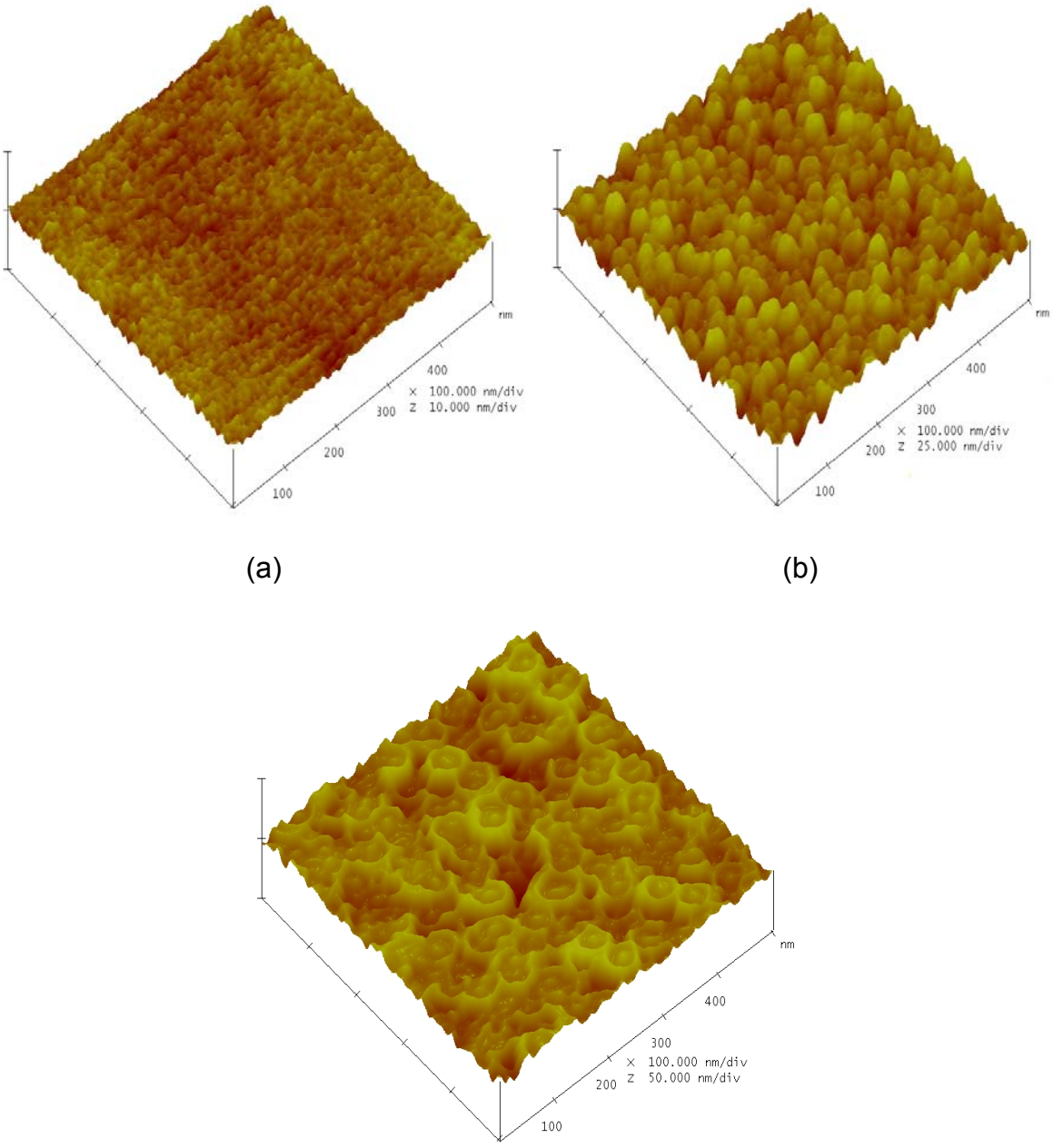

(a) (b)

(c)

Figure 4.5: AFM images of ZnO thin films prepared by spin coating glycerol polymeric precursor and annealed at: (a) 300°C, (b) 450°C, and (c) 600°C, respectively.

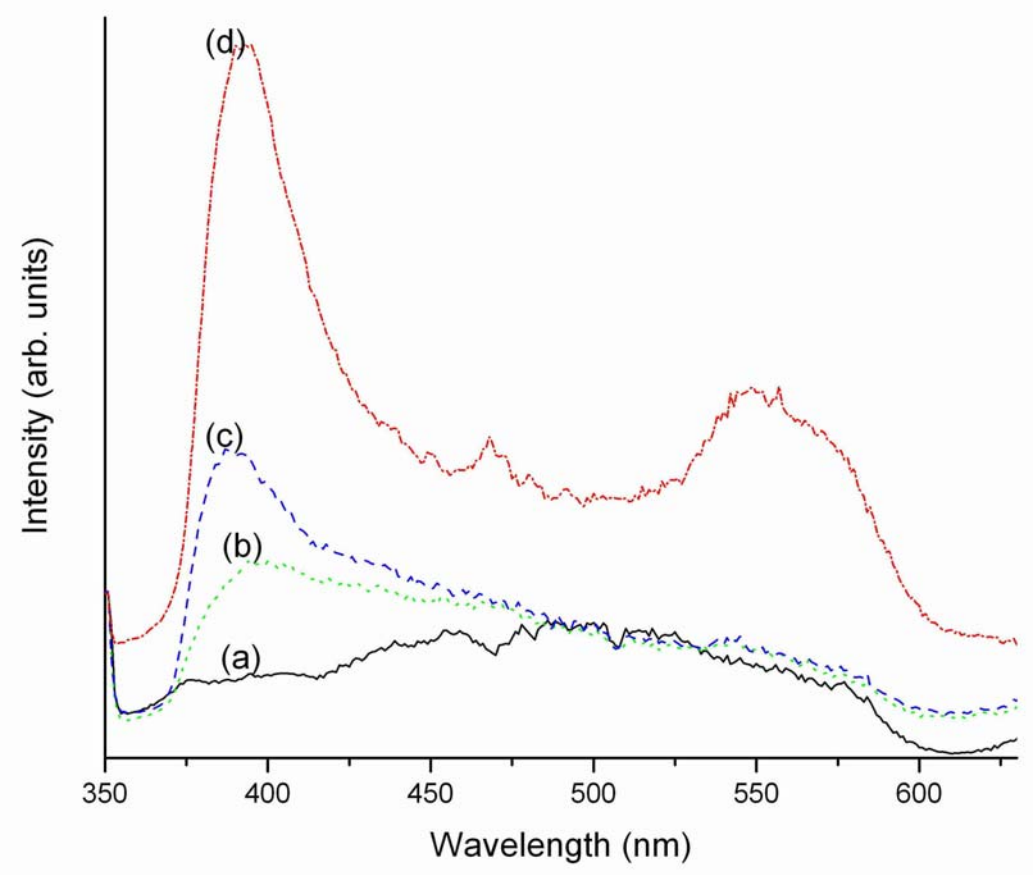

Figure 4.6: Room temperature photoluminescence of ZnO thin films prepared from glycerol and annealed at (a) 300°C, (b) 450°C, (c) 600°C, and (d) ethylene glycol annealed at 300°C.

PL spectrum of sample prepared at 300°C (Fig. 4.6a) does not show any emission due to presence of organic precursors in the films. Samples annealed at 450°C and 600°C (Fig. 4.6b and Fig. 4.6c) show UV emission at 395 nm and 387 nm, respectively. Blue shift in photoluminescent peak is usually attributed to quantum confinement of small particles. However, the SEM data illustrate that there is grain growth with higher annealing temperatures. Hence, the blue shift in UV emission may be due to strain in films as revealed by XRD data. It is also observed that the intensity of PL peak increases with an increase in annealing

temperature. This increase in intensity may be attributed to increase in grain size with temperature. There is absence of visible green emission for samples annealed at higher temperatures revealing the high quality of films synthesized.

Fig. 4.6d illustrates the room temperature photoluminescence spectrum of the flower – like ZnO structure of under photon excitation of 340 nm. A strong and broad UV emission at 392 nm dominates the photoluminescence spectra. Besides the strong UV emission peak, there is a broad peak ranging from 525 to 600 nm which lies in the yellow green region. The broad emission peak may be due to the overlap of yellow and green emission peaks. The origin of this peak is assigned in other studies to lattice defects in ZnO [70].

4.4. Conclusions

Nanocrystalline ZnO thin films have been synthesized by modified polymeric precursor method using glycerol and ethylene glycol as chelating agents, respectively. Till date, ZnO thin films have not been synthesized by this method. The thin films were annealed at various temperatures, namely 300°C to 600°C. Thermal decomposition of synthesized polymeric precursors were analyzed by TGA. XRD data for ethylene glycol based thin films show that ZnO prepared has wurtzite structure even when annealed at 300°C and higher temperatures. In case of glycerol based thin films, no XRD data was obtained for samples annealed at 300°C suggesting that formation of ZnO occurs at higher temperature. Samples annealed at 450°C and above, showed characteristic peaks pertaining to wurtzite ZnO structure. There is a shift of diffraction peaks to higher angles implying existence of compressive strains. SEM micrographs

illustrate that the glycerol based thin films are smooth, dense, and have crack free microstructures. The images also reveal increase in grain size with annealing temperature which can be attributed to grain growth. However, in case of ethylene glycol based ZnO thin films, hexagonal flower - like structures are observed. These flowers have a multilayered structure with an average diameter of 4-7 μm. From AFM studies on glycerol based thin films, it has been observed that an increase in annealing temperature improved film crystallinity but also led to an increase in roughness due to grain growth. Room temperature photoluminescence exhibit strong UV emission for glycerol based thin films. The thin films display a tendency to increase grain size and hence the intensity of the UV emission with increase in annealing temperature. However, ZnO flowers formed of ethylene glycol precursor show broad visible green emission along with sharp strong UV emission.

CHAPTER 5

SYNTHESIS AND CHARACTERIZATION OF NANOCRYSTALLINE ZINC OXIDE THIN FILMS BY CITRATE PRECURSOR ROUTE

Nanocrystalline zinc oxide (ZnO) thin films have been deposited by spin coating polymeric precursor solution synthesized by a modified Pechini process using ethylene glycol as reaction medium and citric acid as chelating agent for Zn cations. The polymeric precursors were spincoated on glass and silicon substrates and annealed from 300°C to 600°C. The resultant films were characterized for degree of crystallization and surface morphology. The thermal decomposition of polymeric precursor was studied by thermogravimetric analysis (TGA). The average crystallite size, orientation, and strain were studied in depth by X - ray diffraction (XRD). XRD results illustrate that there is an increase in texturing of grains perpendicular to the substrate and compressive strain with increase in annealing temperature. Morphology of the thin films was evaluated by scanning electron microscopy (SEM) and atomic force microscopy (AFM). SEM and AFM micrographs illustrate that the films are crack free and composed of well-dispersed homogeneous microstructures. Room temperature photoluminescence spectra of these films show strong UV emission around 392 nm with an increase in intensity with annealing temperature.

5.1. Introduction

Zinc oxide (ZnO) is a II-VI n-type semiconductor with a wide direct band gap of 3.3eV. Besides the wide band gap, ZnO has several attractive properties, such as, large exciton binding energy (60meV at room temperature), high

chemical stability, good piezoelectric properties, non-toxicity and bio-compatibility, which have drawn tremendous attention in recent years [105]. Owing to stability in hydrogen plasma, ZnO thin films can be employed in fabrication of hydrogenated amorphous silicon solar cells [57]. These thin films can also be utilized for developing semiconductor gas sensors [110]. ZnO thin films also have potential for practical applications, notably in short wavelength optical devices especially in ultraviolet-blue emission devices [76].

To date, high quality ZnO thin films have been prepared by several thin film deposition techniques, including pulsed laser deposition [64, 68], chemical vapor deposition [85, 42], molecular beam epitaxy [136], sputtering [30, 62, 79], spray pyrolysis [107], and sol-gel process [22, 81, 45, 18, 34, 149]. However, these deposition techniques can require ultra high vacuum, expense and are time - consuming. In the sol - gel process, expensive and toxic metal alkoxides reacting with humidity, are used as precursors to form sols, which makes preparation of sols difficult.

An approach for the chemical synthesis of thin films, based on a method developed by Pechini [83], has been extensively used for several polycation oxides and perovskites [37]. This polymeric precursor method is simple, easy and cost - effective employing common reagents. In this technique, aqueous solution containing metal salts and alpha-hydroxycarboxylic acid such as citric acid is prepared. Then a polyhydroxyl alcohol, usually ethylene glycol, followed by nitric acid, is added to the aqueous solution. The solution is constantly heated and stirred. On heating the solution, citric acid and ethylene glycol undergo

polyesterification. The metal cations chelate to the polyester to form a polymeric solution with metal cations distributed uniformly [48]. Nitric acid enhances oxidation of the polyester and provides sufficient number of chelation sites to the metal cations. Polymeric precursor method offers many advantages, such as, good stoichiometry, precise size control, working in ambient atmosphere with aqueous solutions. Since this method has been utilized to successfully synthesize oxide thin films [7, 52], this paper aims to report fabrication of nanocrystalline ZnO thin films and its morphological characterization. The prepared polymeric precursor was spincoated on to substrates and annealed to different temperatures. Thermal decomposition of the precursor was studied by thermogravimetric analysis (TGA). The synthesized and annealed thin films were characterized by XRD, SEM, and AFM. The photoluminescence properties of the thin films were also investigated.

5.2. Experimental Methods

99% pure zinc nitrate, $Zn(NO_3)_2.xH_2O$ and 99% ethylene glycol (EG) were acquired from Alfa Aesar. 70% nitric acid (HNO_3), ACS grade potassium hydroxide (KOH) pellets, and citric acid (2-hydroxy-1, 2, 3-propanetricarboxylic acid), were acquired from J. T. Baker, EMD chemical Inc., and Fischer Scientific International Inc., respectively. These chemicals were used as received without further purification. Deionized and filtered water (resistivity = 18.2MΩ) was used in preparing solutions. Glass microslides and silicon substrates (2.54 x 2.54cm^2) were thoroughly cleaned ultrasonically in acetone, methanol and deionized

water, followed by surface modification with 1N potassium hydroxide (KOH) solution to achieve good wetting characteristics.

Polymeric precursors for depositing ZnO thin films were prepared using Pechini process. 0.1 moles of citric acid was dissolved in 50 ml of deionized water. To this aqueous solution, $Zn(NO_3)_2$, ethylene glycol, and HNO_3, in molar ratios of 0.1: 0.9: 0.1, respectively, were added. The resulting solution was stirred continuously and heated at a constant temperature of 70°C until the final solution was clear and homogeneous. The solution was spincoated (CEE Model 100CB, Brewer Science, Inc.) onto cleaned and surface modified substrates at 4000 rpm for 30s. After deposition, the layer was dried at 70°C on a hot plate for an hour to remove residual water. The films were then annealed at different temperatures in an ambient furnace for pyrolysis of organic precursors and oxide formation.

Thermogravimetric analysis of polymeric precursor of ZnO was obtained (Perkin Elmer TGA - 7) at a ramp rate of 1°C/min. X-ray diffraction (XRD) patterns were obtained using a CuKα radiation source to determine the structure of the films in the θ-2θ scan mode, recorded on a Scintag XDS 2000 X-ray diffractometer. Interplanar spacing *d* of the ZnO films is calculated using the Bragg equation. The lattice constant *a* is calculated using the following equation: $a = \sqrt{(4/3)}d$ for (100) diffraction peak of ZnO. Similarly, the lattice constant *c* for hexagonal ZnO is related to interplanar spacing *d* for (002) planes by $c = 2d$. The average crystallite size was calculated from Scherrer equation,

$$t(nm) = \frac{0.9\lambda}{FWHM \times \cos\theta} \tag{9}$$

where λ is X - ray wavelength of Cukα, (λ = 0.154 nm) and FWHM of (002) diffraction peak at position 2θ. Film strain ε_Z along the *c* axis is then given by [79]

$$\varepsilon_Z = (c - c_o)/c_o \times 100\% \quad (10)$$

where c_o, the strain-free lattice parameter measured from ZnO powder, is equal to 0.5204nm. According to the above equation, the strain can be positive (tensile) or negative (compressive). Preferential orientation can be quantified by texture coefficients defined by [98],

$$T(hkl) = \frac{I(hkl)/I_r(hkl)}{1/n\Sigma(I(hkl)/I_r(hkl))} \quad (11)$$

where n is the number of (hkl) diffraction peaks, I(hkl), and I_r(hkl) are integrated intensities of these peaks in samples with preferential and random orientation, respectively. Morphology of the synthesized ZnO thin films were characterized by field emission scanning electron microscopy, FESEM, (Nova Nanolab 200, FEI Co.) and atomic force microscopy, AFM, (Digital Instruments Multi-Mode Nanoscope IIIa). The photoluminescence spectra were acquired with a scanning spectrofluorometer (Photon Technology International) at room temperature with an excitation wavelength of 340nm using Xenon lamp as an excitation source.

5.3. Results and Discussion

5.3.1. Thermogravimetric Analysis

Fig. 5.1 shows the thermogravimetric analysis (TGA) curve of the synthesized ZnO polymeric precursor. The TGA analysis indicated a major weight loss (40%) between 50°C and 200°C, which corresponds to the evaporation of water and pyrolization of excess polyethylene glycol (PEG). A

plateau is evident from 200°C to 250°C, indicating that the entire PEG has been pyrolized, leaving cross-linked network of citric acid and ethylene glycol with Zn cations in the film. This is followed by a weight loss (25%) between 250°C and 450°C, due to the combustion of citric acid. There is formation of ZnO during the pyrolysis of the organic precursors. After 450°C, no obvious weight loss was observed and complete crystallization of ZnO took place.

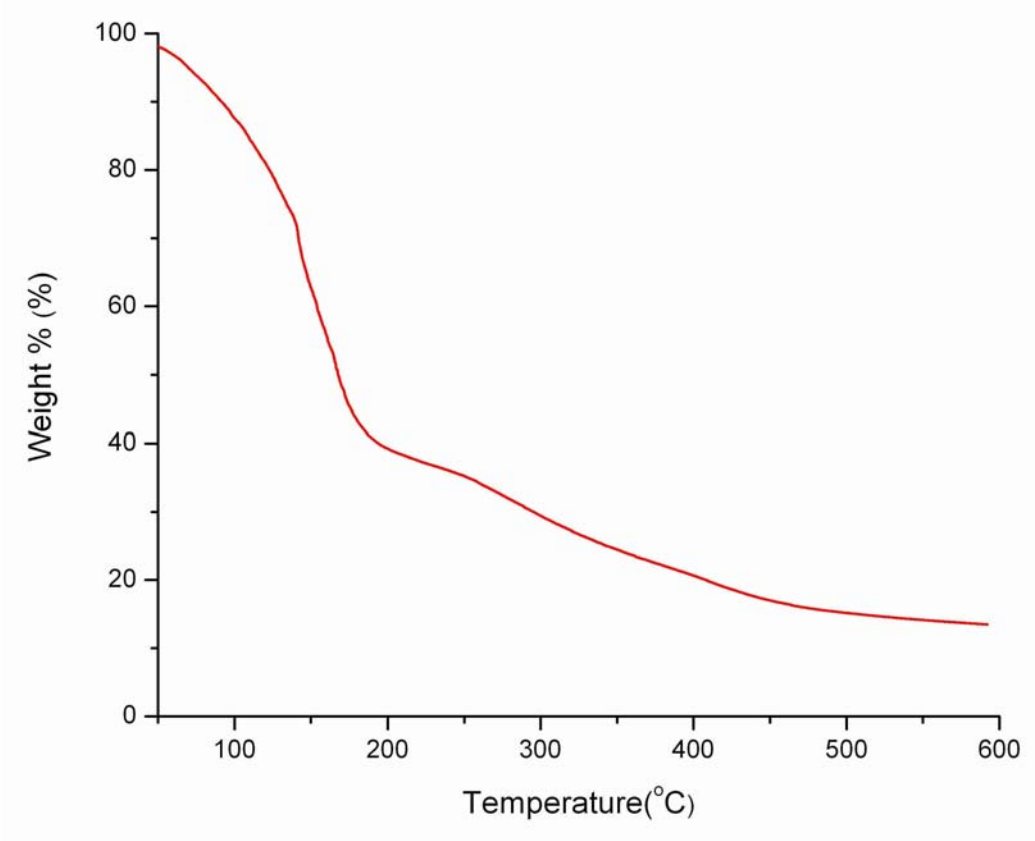

Figure 5.1: TGA curve (heating rate = 1°C/min) of ZnO polymeric precursor prepared using ethylene glycol and citric acid as a reaction medium and chelating agent respectively.

5.3.2. X-ray Diffraction

XRD was performed in the θ-2θ scan mode to determine the crystallite size, orientation, and average strain of ZnO grains. The XRD spectra of the ZnO thin films deposited on silicon substrates and annealed at 300°C, 450°C, and 600°C are shown in Fig. 5.2.

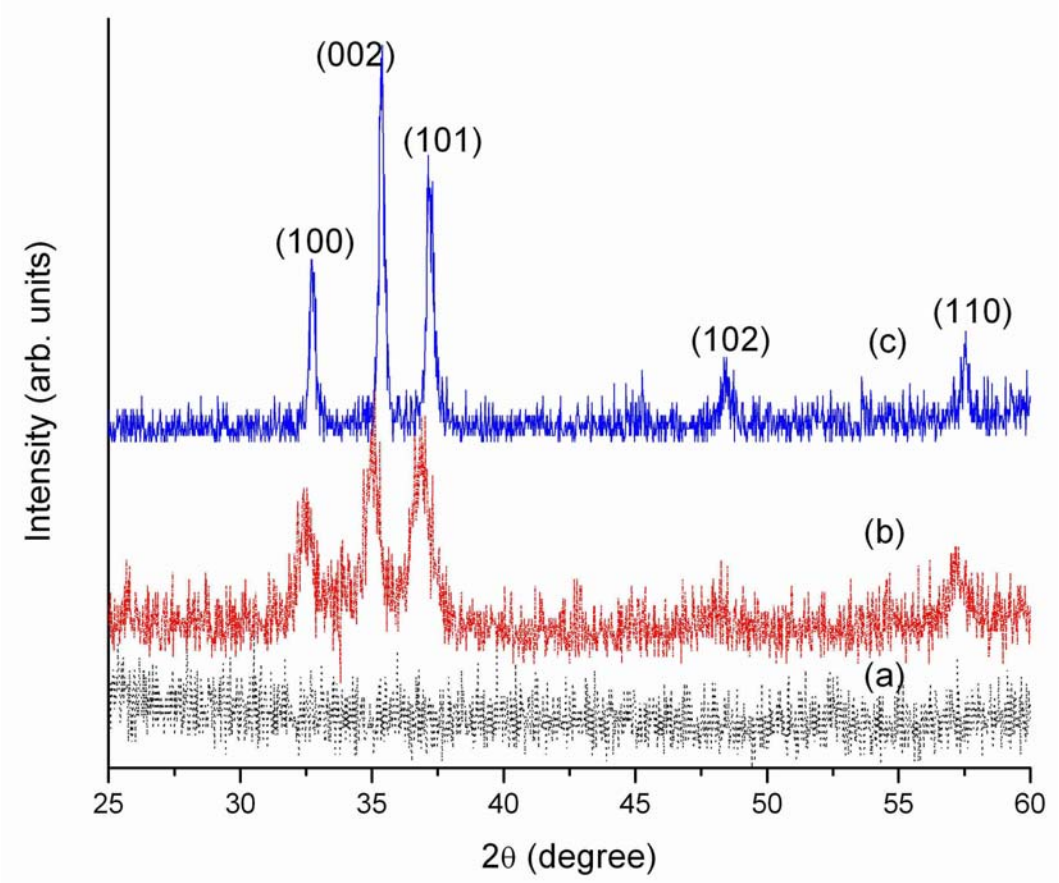

Figure 5.2: XRD spectra of ZnO thin films synthesized by spin coating citrate polymeric precursor, followed by curing at 70°C, and finally annealed at different temperatures (a) 300°C, (b) 450°C, and (c) 600°C for 1 hour. The crystallite size calculated, using Scherrer's equation, were 20nm and 35nm for 450°C and 600°C, respectively.

All the diffraction peaks can be indexed to the pure hexagonal phase of ZnO [space group: $P6_3mc$] which are in good agreement with the reported data (JCPDS, 36-1451). No peaks were observed which cannot be assigned to ZnO. At the temperature of 300°C, diffraction peaks are not observed in the XRD spectrum (Fig. 5.2a) due to the presence of organic precursors. Moreover, ZnO is not formed at this temperature, which is also supported by the TGA data. When the annealing temperature was increased to 450°C (Fig. 5.2b), diffraction peaks at 2θ = 32.47°, 34.99°, 36.89°, and 57.2°, corresponding to (100), (002), (101) and (110) planes, are observed. The cell constants were calculated to be *a* = 0.3182 nm and *c* = 0.5125 nm compared with *c* = 0.5204 nm. ZnO crystals tend to grow along the *c*-axis perpendicular to the substrate. These basal ZnO planes give rise to a dominant (002) diffraction peak around 34.44°. Hence, this peak position is considered to calculate crystallite size and average crystallite size was determined to be 19.5 nm (using equation 9). The (002) peak of the ZnO film annealed at 450°C is quite broad (FWHM = 0.445°) and shifted by 0.55° to higher 2θ angle. At annealing temperature of 600°C (Fig. 5.2c), the diffraction peaks occur at 2θ = 32.69°, 35.39°, 37.17°, and 57.57°, corresponding to (100), (002), (101), and (110) planes along with appearance of peak at 48.49° related to (102) plane. On calculation of cell constants for 600°C, it was found that these have decreased to *a* = 0.316 nm and *c* = 0.507 nm. We observe that on annealing to 600°C, the widths of the diffraction peaks of the film has narrowed (FWHM = 0.28° for (002) peak) indicating that grain growth has occurred. The crystallite

size was calculated to be 31 nm (using equation 9). Moreover, there is a significant shift of 0.95° in peak positions to higher 2θ angles.

For the samples annealed at 450°C and 600°C, the intensities of three main diffraction peaks are used for calculating the texture coefficients using equation 11. When annealed at 450°C, the texture coefficients are obtained as T(100) = 0.8, T(002) = 1.522, and T(101) = 0.674. For samples annealed at 600°C, the texture coefficients calculated are as follows: T(100) = 0.663, T(002) = 1.729, and T(101) = 0.6. We observe that the texture coefficient are quite similar for (101) plane and has slightly decreased for (100). However, there is marked preferential crystallite orientation along the (002) as texture coefficient is greater than 1 (T(hkl) = 1 for randomly oriented crystallites).

The strain in ZnO thin films on annealing was calculated using equation 10. Films annealed at 450°C and 600°C showed compressive strains of -1.57% and -2.66%, respectively. It is observed that the average compressive strain increases with increase in annealing temperature. This strain may be due to intrinsic strain because of lattice mismatch existing between ZnO thin films and SiO_2/Si and a difference in coefficients of thermal expansions of ZnO and silicon. However, on annealing to 600°C, the interfacial strain between the film and substrate should become negligible due to relaxation. This indicates that the compressive strain observed may be due to thermal mismatch strain in ZnO thin films and SiO_2/Si substrates on cooling as ZnO has a higher coefficient of thermal expansion than both SiO_2 and Si [16]. During annealing at temperatures above 450°C, the combustion of polymeric precursors leaves voids in the film

that are rapidly filled with nanometer sized ZnO grains. The presence of these grains prevents pore coalescence, which also results in compressive strains.

5.3.3. Scanning Electron Microscopy

Fig. 5.3 shows SEM micrographs of ZnO thin films annealed at 300°C, 450°C, and 600°C. As can be observed, samples annealed at 300*o*C show a very smooth surface with only the presence of organic precursors. Moreover, XRD and TGA results also confirm that there is no ZnO formation at 300°C (Fig. 5.3a). The sample annealed at 450°C (Fig. 5.3b) presents a surface without cracks, is very homogeneous and is relatively dense (not many pores are observed) with a microstructure having an average grain size of 20nm. On annealing the sample at 600°C (Fig. 5.3c), SEM micrographs illustrate that the films are smooth and dense with uniform and well - developed grains of order of 30 nm size. The films appear to have few pores with no cracks or voids. The measured average grain sizes are 20nm and 35nm, respectively for samples annealed at 450°C and 600°C, which, matches and reconfirms the value of crystallite size calculated using Scherrer's method (equation 9). It is proposed that large compressive strains provide a driving force for grain growth during annealing [79]. Hence, the compressive strains observed in ZnO thin film deposited on SiO_2/Si energetically favors grain boundary crystallization on annealing resulting in faceted grains as seen in Fig. 5.3c.

5.3.4. Atomic Force Microscopy

Representative AFM micrographs of ZnO thin films prepared by spin coating and annealed at 300°C, 450°C, and 600°C are shown in Fig. 5.4. ZnO

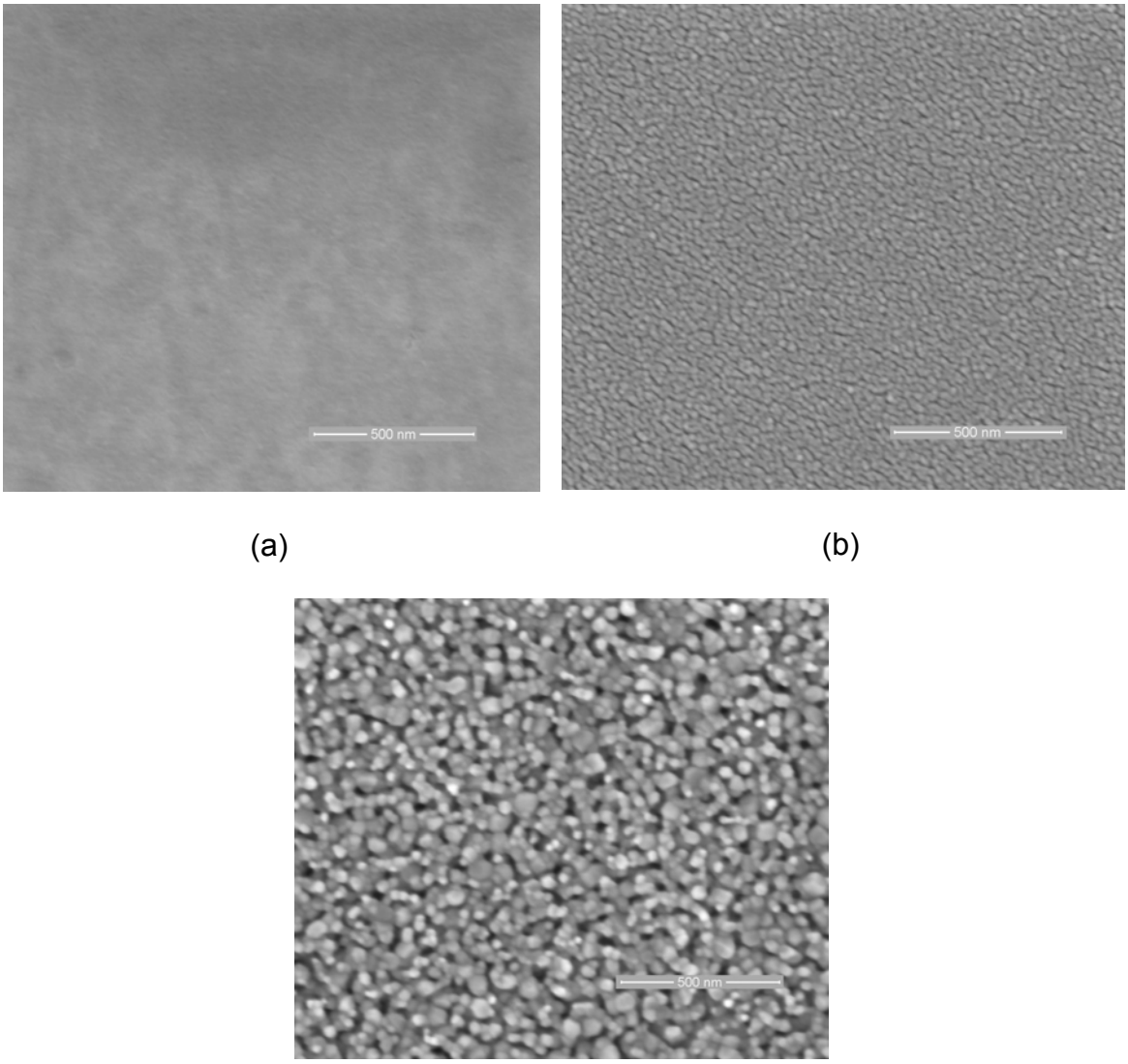

(a) (b)

(c)

Figure 5.3: SEM micrographs of ZnO thin films prepared from polymeric precursor using ethylene glycol and citric acid and annealed at: (a) 300°C, (b) 450°C, and (c) 600°C.

thin films obtained by polymeric precursor method using citric acid as a chelating agent, exhibited a dense and crack-free microstructure. The morphology of the thin films appears to be smooth with small porosity. A more detailed observation

of AFM images revealed a difference in the surface morphology of the films prepared at different annealing temperatures. The micrographs show a considerable variation in the surface morphology between the samples annealed in the range 300°C to 600°C. The sample annealed at 300°C (Fig. 5.4a) showed a surface morphology with very low surface roughness (root mean square = 0.877 nm) and no evidence of a granular structure. The sample annealed at 450°C displayed a homogeneous granular structure distributed uniformly throughout the thin film (Fig. 5.4b). There is an increase in roughness (root mean square = 1.919 nm) suggesting that the ZnO film structure is becoming increasingly ordered. When heat-treated at 600°C (Fig. 5.4c), the average grain size and the surface roughness of the films increases to 70 – 90 nm and 8.737 nm, respectively. The particles are mono-dispersed with spherical morphology and uniformly distributed on the substrate.

5.3.5. Photoluminescence

Room temperature photoluminescence (PL) spectra of ZnO thin films annealed at 300°C, 450°C, and 600°C under photon excitation of 340nm are shown in Fig. 5.5. The samples show strong and sharp UV emission attributed to free exciton recombination [108, 70]. ZnO thin films annealed at 300°C (Fig. 5.5a) did not show any UV emission. Samples annealed at 450°C and 600°C showed UV emission at 393 nm (Fig. 5.5b and c), respectively. This shift in band gap can be attributed to compressive strains in the films [128]. Moreover, the intensity of PL peak increases with increase in annealing temperature between 450°C to 600°C. This increase in intensity may be attributed to an increase in

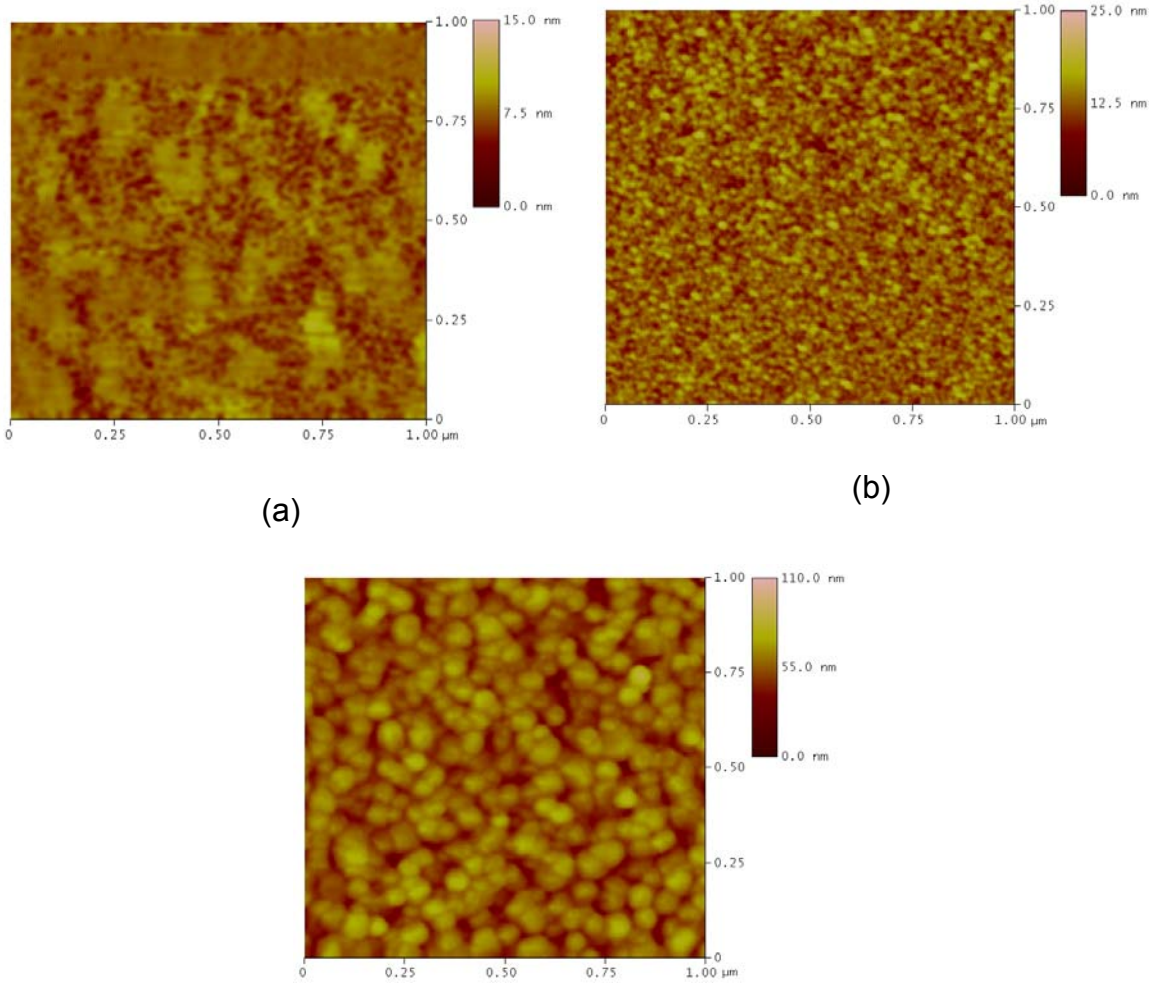

(a)

(b)

(c)

Figure 5.4: AFM images of ZnO thin films annealed at: (a) 300°C, (b) 450°C, and (c) 600°C showing grain growth on increase in annealing temperature.

grain size and crystallinity with temperature.

5.4. Conclusions

Nanocrystalline ZnO thin films have been synthesized by simple polymeric precursor method using ethylene glycol as reaction medium and citric acid as chelating agent. The thin films were annealed from 300°C to 600°C. Samples

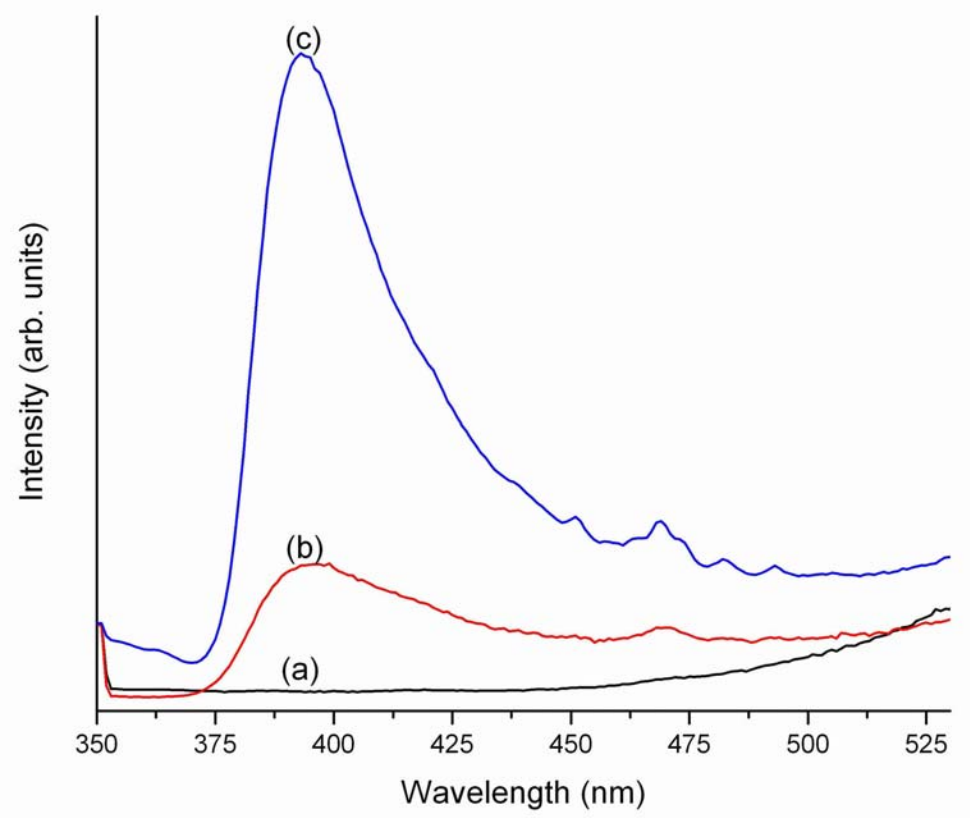

Figure 5.5: Room temperature photoluminescence spectra of ZnO thin films prepared by polymeric precursor method using ethylene glycol and citric acid as reaction medium and chelating agent respectively. The thin films were annealed at (a) 300°C, (b) 450°C, and (c) 600°C, respectively.

annealed at 300°C did not show any diffraction peaks suggesting that ZnO did not form. This is confirmed by TGA results. Samples annealed at temperatures of 450°C and above, illustrate wurtzite structure with crystallite size increasing with annealing temperatures between 450° to 600°C. XRD spectra show an increase in preferential orientation of grains along the (002) plane with increase in annealing temperature. The thin films exhibit compressive strains of -1.57% and

-2.66% for annealing temperatures of 450° and 600°C, respectively. This strain may be attributed to thermal mismatch in ZnO films and SiO_2/Si substrate as well as dense, basal oriented nano-grained films leading to grain growth along grain boundaries. SEM and AFM micrographs illustrate smooth, crack free microstructures with small pores. Room temperature photoluminescence spectra show strong UV emission, which is blue-shifted with increase in annealing temperature probably due to compressive strain in the films. We also observe that the intensity of the UV emission increases with increase in annealing temperature, which may be attributed to an increase in grain size and crystallinity. Studies to determine the specific cause of the strain in films (that is, effects of substrates, deposition conditions, etc) and to determine its effect on photoluminescence will be studied in future.

CHAPTER 6

POLYMERIC PRECURSOR DERIVED NANOCRYSTALLINE ZINC OXIDE THIN FILMS USING EDTA AS CHELATING AGENT

Nanocrystalline zinc oxide (ZnO) thin films have been deposited by spin coating polymeric precursor solution synthesized by a modified Pechini process. ZnO thin films were successfully synthesized by polymeric precursor route using ethylene glycol as reaction medium and ethylene diamine tetraacetic acid (EDTA) as chelating agent for Zn cations. The polymeric precursors were spincoated on glass and silicon substrates and were annealed from 300°C to 600°C. The thermal decomposition of polymeric precursor was studied by thermogravimetric analysis (TGA). The average crystallite size, orientation, and strain were studied in depth by X - ray diffraction (XRD). XRD results illustrate that there is strong preferred orientation of grains along (002) plane. Compressive strains exist in films, which increases on increasing annealing temperature. Surface morphology of the thin films was evaluated by scanning electron microscopy (SEM) and atomic force microscopy (AFM). FIB cross-sectional view of the samples illustrate that the films are dense. Transmission spectra reveal that ZnO thin films annealed at 450°C and 600°C, respectively, are highly transparent with band edge at 372 nm and 376 nm, respectively. Room temperature photoluminescent spectra of these films show strong UV emission around 380 nm.

6.1. Introduction

Zinc oxide (ZnO) is a II-VI n-type semiconductor with a wide direct band

gap of 3.3eV. ZnO has several attractive properties, such as, large exciton binding energy (60meV at room temperature), high chemical stability, good piezoelectric properties, non-toxicity and bio-compatibility, which have drawn tremendous attention in recent years.

Among various techniques employed to prepare ZnO thin films, sol - gel route has been widely used [22, 98, 18, 149, 45, 2, 81, 93]. However, in the sol - gel process, metal alkoxides are used as starting material to undergo hydrolysis and polymerization reactions for preparing sol. These materials are expensive, toxic, and insoluble in most alcohols, which make synthesis of stable sols quite tedious and difficult. Zinc acetate is inexpensive but zinc acetate dissolved in alcohols do not form gels completely on addition of water [81].

A simpler and less toxic approach for the chemical synthesis of ZnO thin films can be implemented using a aqueous polymeric precursor method. This method, developed by Pechini [83], has been used to synthesize several polycation oxides and perovskites [37, 7] using citric acid as chelating agent and ethylene glycol as reactive medium. This polymeric precursor method is a simple, easy and cost - effective process employing common reagents. Research has also been carried out using modified Pechini process in which citric acid has been replaced by ethylene diamine tetraacetic acid (EDTA) as chelating agent [126, 28]. It has been show that EDTA improves distribution of metal cations uniformly in the solution and hence influences the structure of films [126]. To our knowledge, this is the first work on synthesizing nanocrystalline ZnO thin films using EDTA as chelating agent by aqueous polymeric precursor process.

In this paper, nanocrystalline ZnO thin films are prepared by a modified Pechini process. The complexing agent used is ethylene diamine tetraacetic acid (EDTA) so as to increase the extent of chelation of Zn cations in the solutions. The prepared polymeric precursor was spincoated onto surface modified substrates and annealed to different temperatures. Thermal evolution of the ZnO was studied by thermogravimetric analysis (TGA). The annealed thin films were characterized by XRD, SEM, and AFM. The transmission and photoluminescence properties of the thin films were also investigated.

6.2. Experimental Methods

Polymeric precursors for depositing ZnO thin films were prepared using modified Pechini process. The starting materials were zinc nitrate, $Zn(NO_3)_2.xH_2O$ (99%, Alfa Aesar), ethylene glycol (EG)(99%, Alfa Aesar), ethylene diamine tetraacetic acid (EDTA) (99%, Acros), ammonium hydroxide, NH_4OH (29%, Fisher Scientific Inc.), and nitric acid, HNO_3 (70%, J. T. Baker). $Zn(NO_3)_2$ was dissolved in deionized water and was standardized thermogravimetrically to calculate amount of cation content. Ethylene glycol and EDTA were used as complexation agents for this synthesis. First, 2.0 moles of EDTA was dissolved in ammonium hydroxide to facilitate its dissolution in deionized water. To this, 0.1 moles of zinc nitrate, dissolved in deionized and filtered water (resistivity = 18.2MΩ), was added to the solution, followed by 0.9 moles of ethylene glycol. The resulting solution, with pH = 9, was then stirred and heated continuously at 80°C. After heating for an hour, 0.1 moles of nitric acid was added drop wise to the solution. Addition of nitric acid promotes

polymerization, and hence enhances number of chelating sites for Zn cations [48]. Solution pH has to be maintained above 5 to prevent irreversible precipitation. The amount of EDTA was determined by the molar ratio of EDTA to Zn cations [126]. The solution was further heated at 70°C while stirring continuously (for approximately 9 hours) until a clear, precipitate free solution with desired viscosity was reached.

Glass microslides and silicon (2.54 x 2.54cm^2) were used as substrates. The substrates were thoroughly rinsed ultrasonically in acetone, methanol, and deionized water followed by an immersion in 1N potassium hydroxide (KOH, EMD chemical Inc.) solution to functionalize the substrates with hydroxyls so as to achieve good wetting characteristics. The polymeric precursor was spincoated at 4000 rpm for 30s, on surface modified substrates, followed by curing at 70°C on a hot plate for 1 hour. The films were then annealed at different temperatures in an ambient box furnace for pyrolysis of polymeric precursor followed by formation of ZnO.

Thermogravimetric analysis (TGA) was used to monitor the decomposition and pyrolysis of the precursor at a heating rate of 1°C/min under nitrogen atmosphere. X-ray diffraction patterns were obtained on a Scintag XDS 2000 model using CuKα radiation (40 kV and 30 mA) in θ-2θ mode in the interval of 25° to 60° and integration time of 1 s. Interplanar spacing *d* of the EDTA derived ZnO thin films is calculated using Bragg equation. Since ZnO has hexagonal structure, the lattice constants *a* and *c* can be calculated from (100) and (002) diffraction peaks, respectively using the following equation:

$$\frac{1}{d^2} = \frac{4}{3}\frac{(h^2 + hk + k^2)}{a^2} + \frac{l^2}{c^2} \quad (12)$$

The average crystallite size was calculated using Scherrer's equation [8]:

$$t(nm) = \frac{0.9\lambda}{FWHM \times \cos\theta} \quad (13)$$

where λ is X - ray wavelength of Cukα (λ = 0.154 nm) and FWHM of (002) diffraction peak width at position 2θ. Film strain ε_Z along the c axis is [79]:

$$\varepsilon_Z = (c - c_o)/c_o \times 100\% \quad (14)$$

where c_o, the strain-free lattice parameter measured from ZnO powder, and equal to 0.5204 nm. Surface morphology of the synthesized ZnO thin films were characterized by field emission scanning electron microscopy, FESEM, (Nova Nanolab 200, FEI Co.) and atomic force microscopy, AFM, (Digital Instruments Multi-Mode Nanoscope IIIa), respectively. Variable angle spectroscopic ellipsometer (VASE, J.A.Woollam Inc.) was used in transmission mode to characterize optical properties of annealed films of ZnO on glass substrates. Scanning spectrofluorometer (Photon Technology International) was used to acquire photoluminescence spectra at room temperature with an excitation wavelength of 320 nm using Xenon lamp as an excitation source.

6.3. Results and Discussion

6.3.1. Thermal Evolution

Fig. 6.1 shows the thermogravimetric analysis (TGA) curve of the synthesized ZnO polymeric precursor. The TGA analysis indicated a major weight loss (30%) between 30°C and 150°C, which corresponds to the evaporation of absorbed water and pyrolization of excess polyethylene glycol

(PEG). A slight plateau is evident from 150°C to 205°C, suggesting that there is cross-linked network of EDTA and ethylene glycol with Zn cations in the film. This is followed by another weight loss (20%) between 205°C and 255°C, which we believe is due to pyrolization of PEG. There is further weight loss (15%) up to 400°C illustrating that part of the organic precursors of the rigid network have been removed and beyond 400°C, the weight decreases progressively which makes it difficult to speculate the temperature of formation of ZnO.

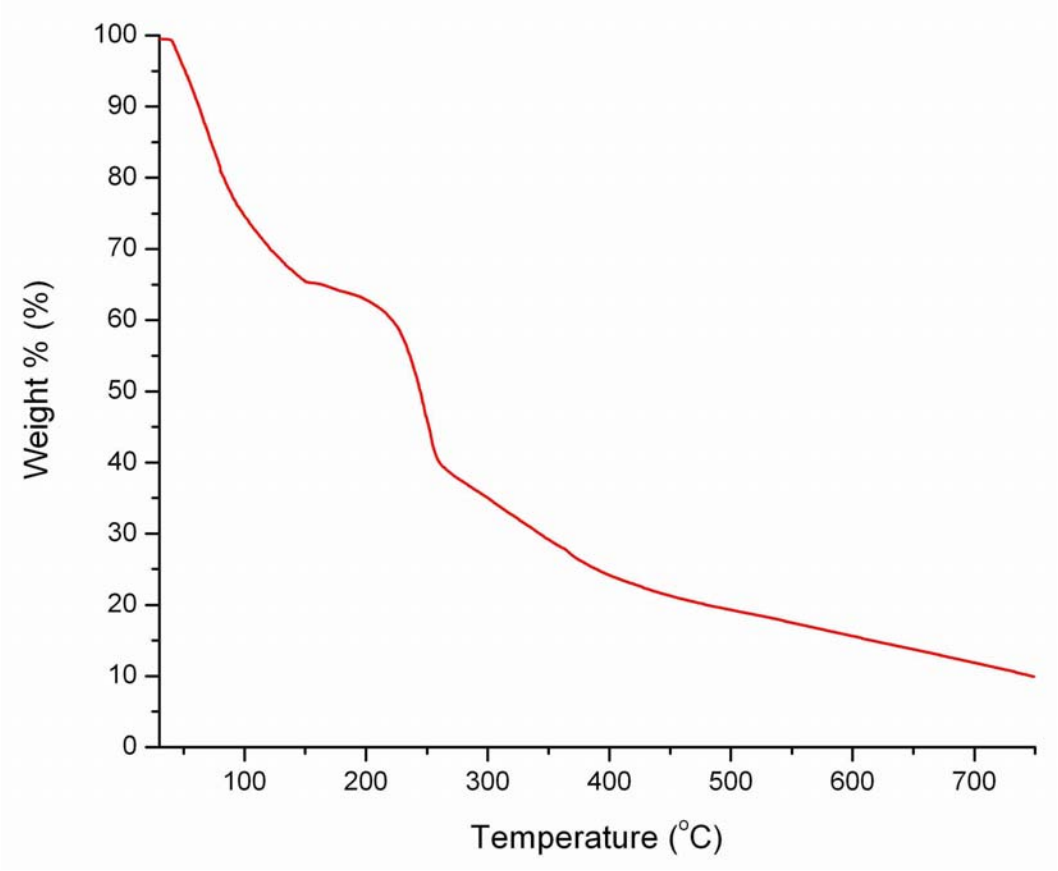

Figure 6.1: TGA curve of ZnO polymeric precursor prepared using ethylene glycol and EDTA as chelating agent.

6.3.2. Microstructure of ZnO Thin Films

SEM micrographs of ZnO thin films prepared by spin coating polymeric

precursor using EDTA as chelating agent and annealed at 300°C, 450°C, and 600°C are displayed in Fig. 6.2. Sample annealed at 300°C (Fig. 6.2a) shows smooth surface with presence of organic precursors. Moreover, TGA results also confirm that there is no ZnO formation at 450°C. The sample annealed at 450°C (Fig. 6.2b) presents a microstructure without cracks and few pores. The micrograph illustrates homogeneous granular structure with highly faceted grains. SEM image of samples annealed at 600°C (Fig. 6.2c) illustrates that the films are dense with homogeneous and well - developed spherical grains. The films appear to have no cracks or voids but with few pores. Thickness of ZnO thin films annealed at 450°C and 600°C was obtained from FIB cross-sectional SEM micrographs. Films annealed at 450°C were about 25 nm thick (Fig. 6.3a) whereas those annealed at 600°C were 130 nm thick (Fig. 6.3b) and are dense.

AFM micrographs of ZnO thin films annealed at 300°C, 450°C, and 600°C are shown in Fig. 6.4. The sample annealed at 300°C (Fig. 6.4a) showed surface morphology with very low surface roughness (mean roughness, R_a = 1.989 nm, root mean square, R_{rms}=2.592 nm) and porous structure related to organic precursors. The sample annealed at 450°C displayed a homogeneous granular structure with an average grain size of 60 - 70 nm and distributed uniformly throughout the thin film (Fig. 6.4b). There is an increase in roughness (R_a = 10.98 nm, R_{rms}=14.07 nm) suggesting that the ZnO film structure is becoming increasingly ordered. When heat - treated at 600°C (Fig. 6.4c), these films exhibit dense and crack-free microstructure. The morphology of the thin films appears to be smooth with small porosity. The average grain size and the surface roughness

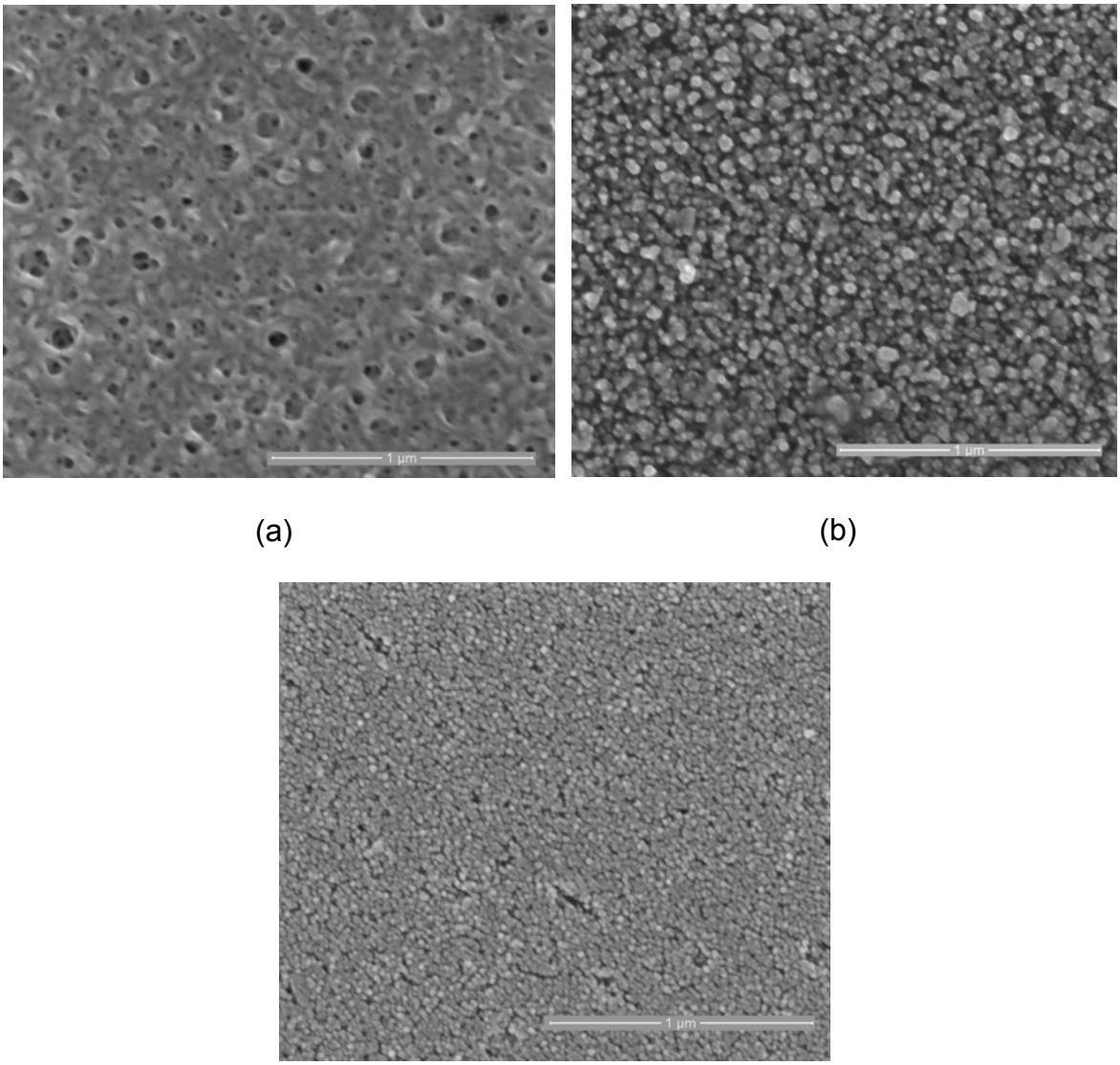

(a) (b)

(c)

Figure 6.2: SEM micrographs of ZnO thin films prepared by spin coating polymeric precursor prepared using ethylene glycol and EDTA on silicon substrates and annealed at: (a) 300°C, (b) 450°C, and (c) 600°C.

of the films decrease to 25 - 30 nm and 3.59 nm (R_a = 2.78 nm, R_{rms}= 3.59 nm), respectively. The particles are mono-dispersed with spherical morphology and well distributed on the substrate. Decrease in average grain size suggests that

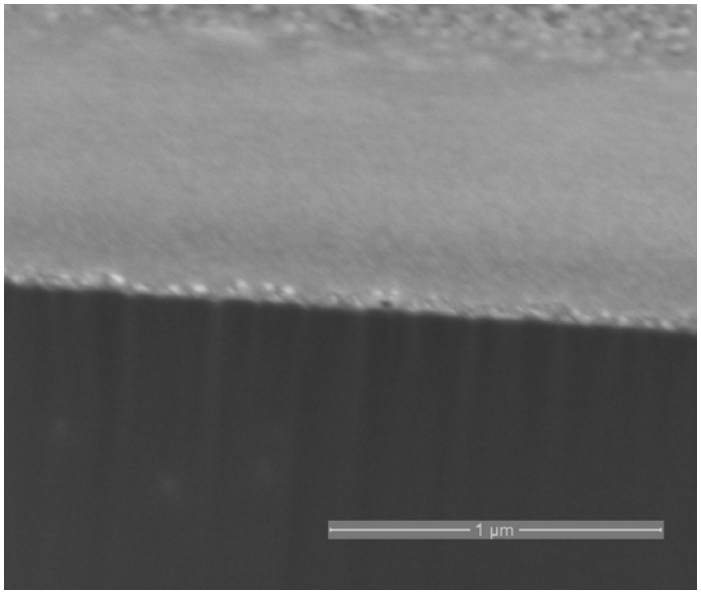

(a)

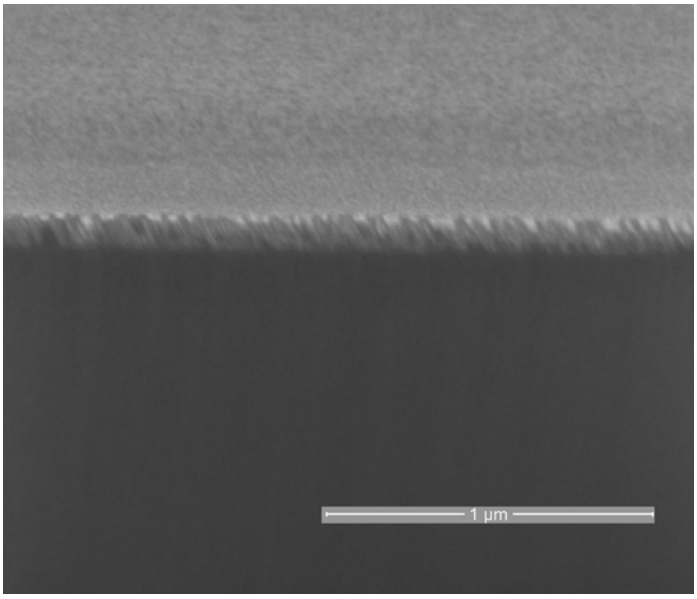

(b)

Figure 6.3: Cross sectional SEM micrographs of polymeric precursor derived ZnO thin films annealed at: (a) 450°C and (b) 600°C. The thicknesses were measured to be about 25 nm and 130 nm, for annealing temperatures of 450°C and 600°C, respectively.

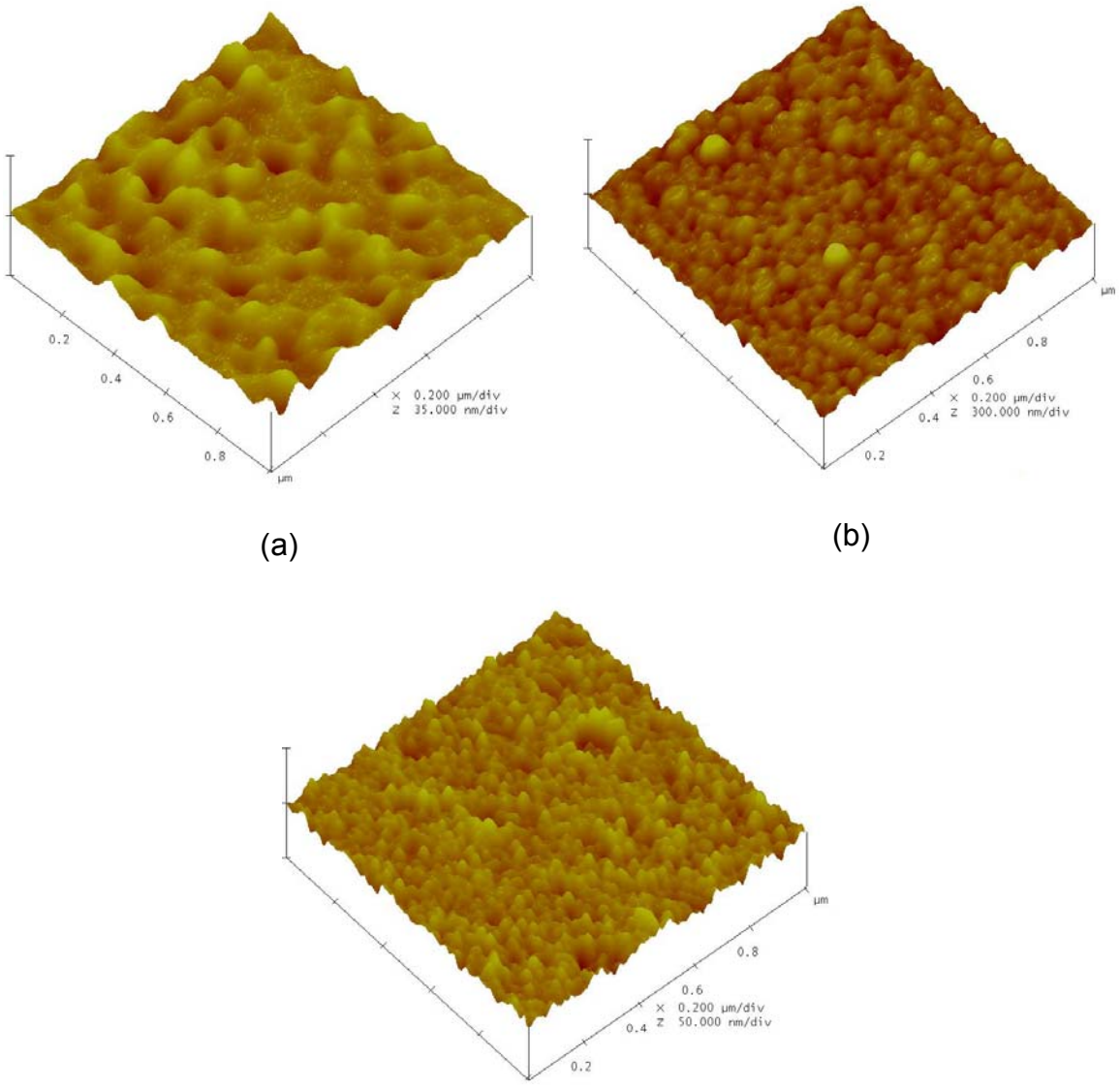

(a) (b)

(c)

Figure 6.4: AFM images of ZnO thin films annealed at: (a) 300°C, (b) 450°C, and (c) 600°C.

ZnO forms at 600°C and the morphology seen at 450°C is due to organic matter present. AFM images reveal that the majority of pores are located at the grain boundaries with a few isolated pores located within the grains.

6.3.3. Crystallographic Orientation of ZnO Thin Films

XRD spectra were acquired in the θ - 2θ scan mode to determine the crystallite size, orientation, and average strain of ZnO thin films deposited on silicon substrates and annealed at 300°C, 450°C, and 600°C as shown in Fig. 6.5. At the temperature of 300°C, a peak related to silicon (002) plane is observed which is background corrected; diffraction peaks related to ZnO are not observed in the XRD spectrum (Fig. 6.5a). When the annealing temperature was increased to 450°C, diffraction peaks at 2θ = 34.9° corresponding to (002) plane

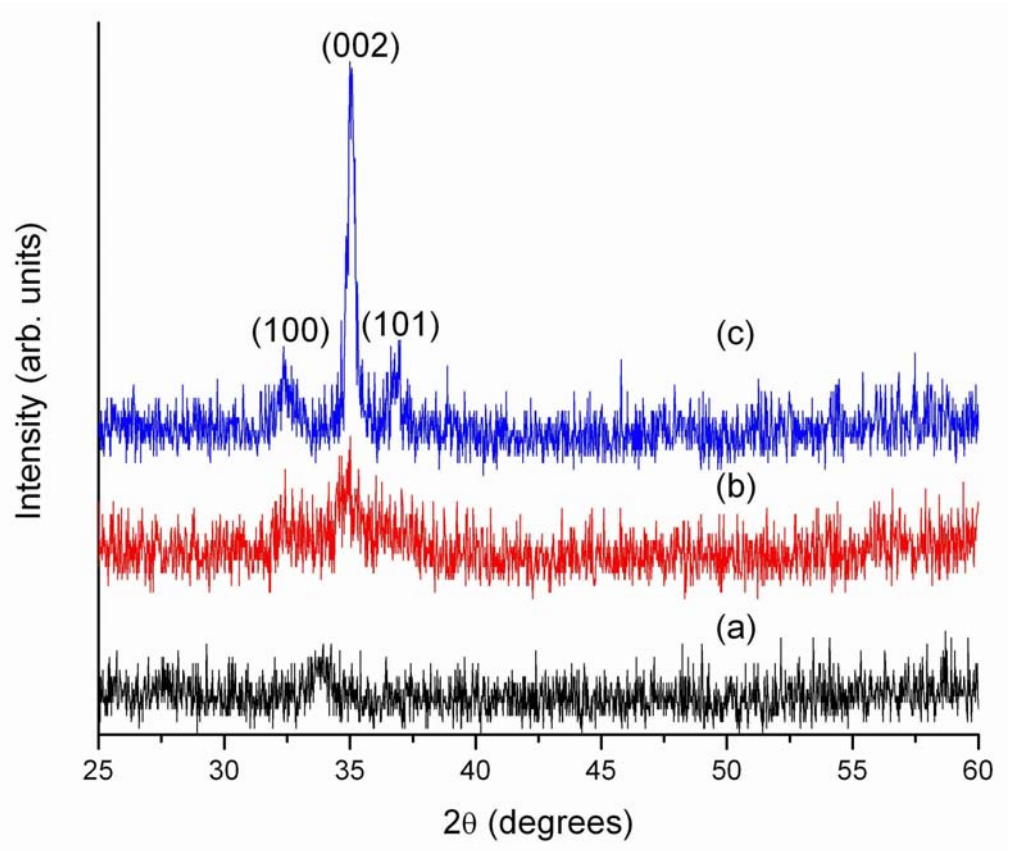

Figure 6.5: XRD spectra of ZnO thin films synthesized by spin coating EDTA derived polymeric precursor, followed by curing at 70°C, and finally annealed at different temperatures: (a) 300°C, (b) 450°C, and (c) 600°C for 1 hour.

is observed (Fig. 6.5b). On annealing the sample at a temperature of 600°C, the diffraction peaks occur at 2θ = 32.43°, 34.98°, 36.78°, corresponding to (100), (002), and (101) planes (Fig. 6.5c). The spectrum illustrates a strong preferred orientation along the (002) plane on annealing at 600°C. The width of the (002) diffraction peak has narrowed (FWHM = 0.31°). Appearance of two new diffraction peaks and a narrow FWHM for highly intense (002) peak indicates that grain growth has occurred. The cell constants were calculated to be *a* = 0.3185 nm and *c* = 0.5126 nm. The crystallite size was calculated to be 26.76 nm (using equation 13). Also, there is a significant shift of 0.54° in peak positions to higher 2θ angles.

6.3.4. Strain in ZnO Thin Films

The strain in ZnO thin films, deposited on silicon substrates and annealed, was calculated using equation 14. Films annealed at 450°C and 600°C showed compressive strains of -1.28% and -1.5%, respectively. It is observed that the average compressive strain increases with increase in annealing temperature.

During annealing at temperatures above 450°C, the pyrolysis of polymeric precursors leave voids in the film, which are rapidly filled with nanometer, sized ZnO grains formed. Presence of these grains prevents pore coalescence, which results in compressive strains. We also propose that the prepared films may be highly dense to cause compressive strain. This compressive strain may also arise due to difference in coefficients of thermal expansions existing between ZnO thin films and SiO_2/Si. Moreover, the thickness of the ZnO film (as determined by FIB cross-sections) is less than that of the substrate (Fig. 6.3).

This leads to stress free substrate and strains are borne by the films [128]. Further detailed studies to determine the cause of the compressive strain and the effect of substrate, defects, and deposition conditions on strain, film thickness, will be studied extensively in future.

6.3.5. Optical Properties of ZnO Films

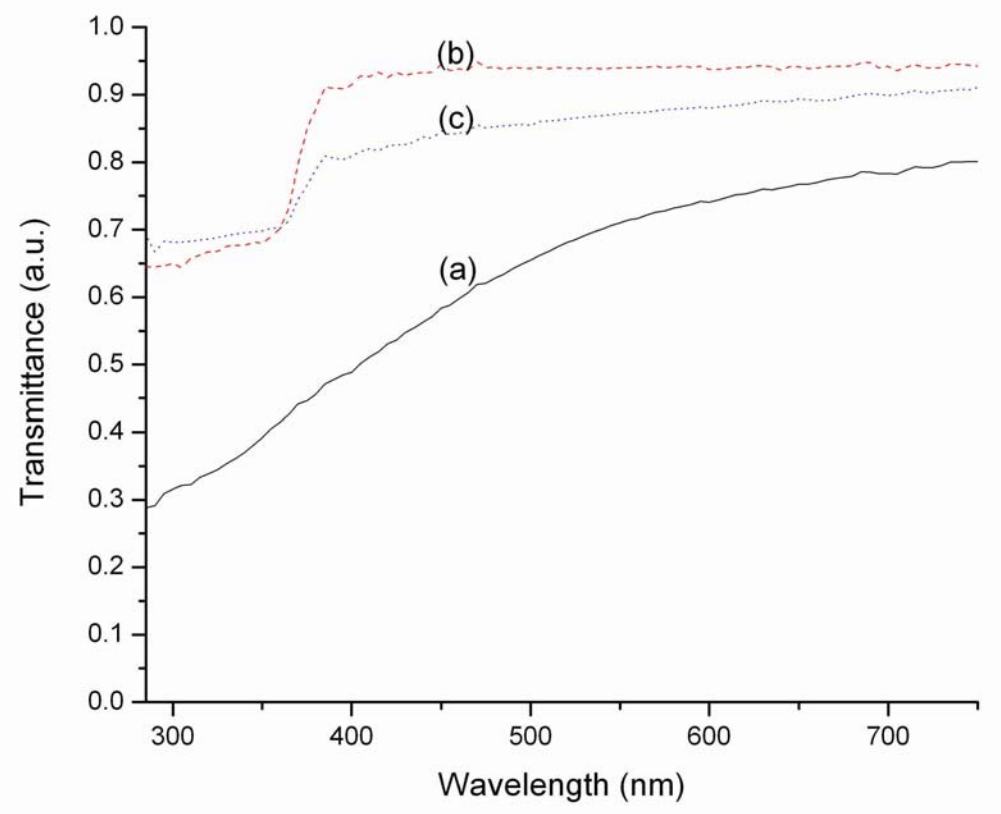

Figure 6.6: Transmission spectra of ZnO thin films annealed at (a) 300°C, (b) 450°C, and (c) 600°C, respectively. These films were prepared by polymeric precursor method using ethylene glycol and EDTA as reaction medium and chelating agent respectively.

Fig. 6.6 shows spectral dependencies of transmission in the wavelength range 260 – 750 nm for the annealed ZnO thin films. The film annealed at 300°C

(Fig. 6.6a) does not show absorption edge for the whole range suggesting that formation of ZnO did not take place. Films annealed at 450°C and 600°C (Fig. 6.6b and c) exhibit a weak transmission in the UV region, which increases sharply in visible region due to onset of absorption edge of ZnO. For 450°C annealed films, the film is 95% transparent whereas the film annealed at 600°C exhibits 85% transparency with band edge at 376nm.

Room temperature photoluminescence (PL) spectra of ZnO thin films annealed at 300°C, 450°C, and 600°C under photon excitation of 320nm are shown in Fig. 6.7. The samples show UV emission attributed to free - exciton recombination [108, 70]. ZnO thin film annealed at 300°C (Fig. 6.7a) did not show any UV emission. Samples annealed at 450°C and 600°C showed UV emission at 380 and 385 nm (Fig. 6.7b and c), respectively showing red-shifted on annealing which may be attributed to increase in compressive strains.

6.4. Conclusions

Nanocrystalline ZnO thin films have been synthesized by modified polymeric precursor method using ethylene glycol and EDTA as reaction medium and chelating agent, respectively. To our knowledge, ZnO thin films have not been synthesized employing this method previously. The thin films were annealed from 300°C to 600°C. Samples annealed at 300°C did not show any diffraction peaks suggesting that ZnO did not form which is also confirmed by TGA results. Samples annealed at temperatures of 450°C and above, illustrate wurtzite structure. XRD spectra show a sharp increase in preferential orientation of grains along the (002) plane with increase in annealing temperature. The thin

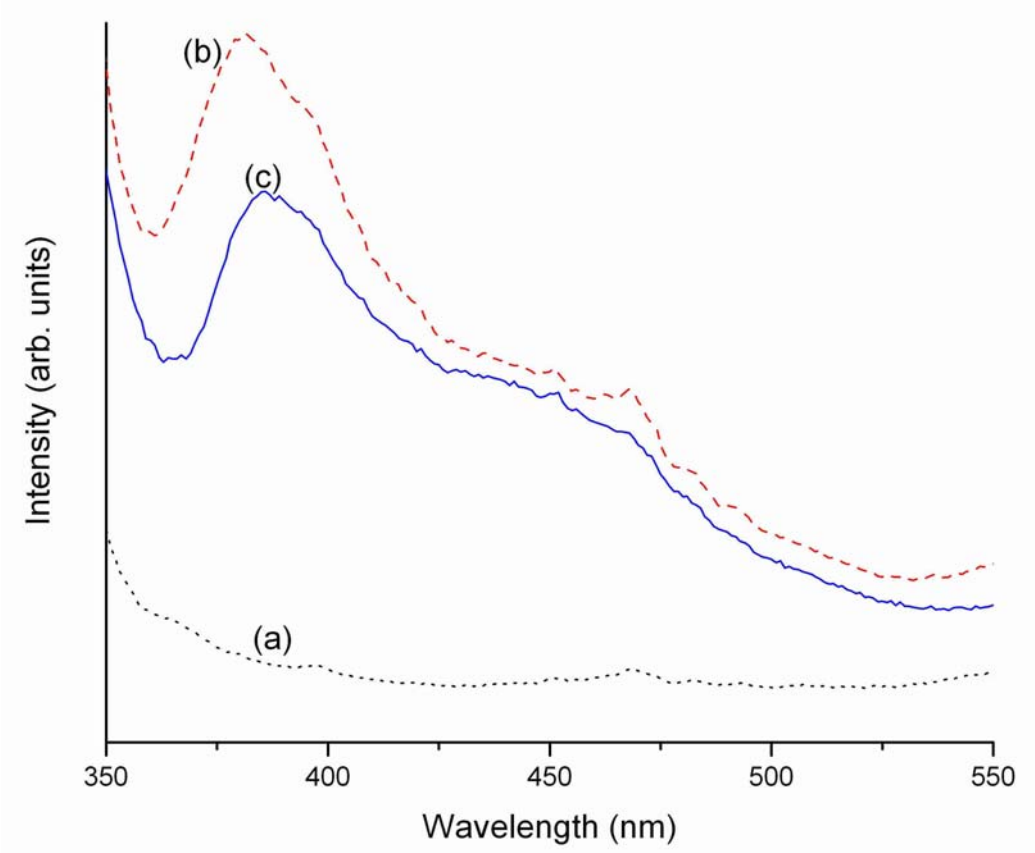

Figure 6.7: Room temperature photoluminescence spectra of ZnO thin films prepared by polymeric precursor method using ethylene glycol and EDTA as chelating agents. The thin films were annealed at (a) 300°C, (b) 450°C, and (c) 600°C, respectively. The films were excited with 320 nm wavelengths using Xenon lamp.

films exhibit compressive strains of -1.28% and -1.5% for annealing temperatures of 450°C and 600°C, respectively. Pyrolysis of organic precursors and simultaneous formation of ZnO grains within the polymeric network leads to obstruction of pore coalescence. These processes may contribute to compressive strains in the films. Compressive strains can be attributed to thermal

mismatch in ZnO films and SiO_2/Si substrate as well as dense, basal oriented nano-grained films. SEM and AFM micrographs illustrate smooth, crack free microstructures with small pores. These images reveal that the grain size decreases with increase in annealing temperatures probably due to new grain growth on annealing. UV-Vis spectra obtained in transmission mode illustrate that the films, annealed at 450°C and 600°C, are highly transparent in the visible region and have a band edge at about 372 nm and 376 nm, respectively. Room temperature photoluminescence spectra show UV emission in the films. We also observe that the intensity of the UV emission decreases with increase in annealing temperature, which may be attributed to decrease in grain size. We have successfully synthesized highly transparent nanocrystalline ZnO thin films using EDTA as chelating agent in modified Pechini process.

CHAPTER 7

POLYMERIC PRECURSOR DERIVED ZINC OXIDE THIN FILMS - A COMPARATIVE VIEW

Nanocrystalline zinc oxide (ZnO) thin films have been deposited by spin coating polymeric precursor solution synthesized by modified Pechini process. ZnO thin films were successfully synthesized by polymeric precursor route using ethylene glycol, glycerol, citric acid, and ethylene diamine tetraacetic acid (EDTA) as chelating agents for Zn cations. The polymeric precursors were spincoated on glass and silicon substrates and were annealed from 300°C to 600°C. The thermal decomposition of polymeric precursor was studied by thermogravimetric analysis (TGA). TGA data shows that ethylene glycol has the lowest whereas EDTA has the highest pyrolytic temperature. The crystallite orientation and strain were studied in depth by X - ray diffraction (XRD). XRD results show formation of wurtzite ZnO using ethylene glycol at 300°C whereas diffraction peaks of ZnO are formed above 450°C for other precursors. XRD results also illustrate that there is strong preferred orientation of grains along (002) plane for films derived of EDTA based polymeric precursor. Compressive strains exist in these films, which increases on increasing annealing temperature. Surface morphology of the thin films was evaluated by scanning electron microscopy (SEM) and atomic force microscopy (AFM). SEM micrographs of ZnO films illustrate formation of flower-like morphology for ethylene glycol derived polymeric precursor at 300°C. ZnO films, derived of glycerol, citric acid, and EDTA based precursors, are nanocrystalline, dense, and crack-free when

annealed at 450°C. The films also show grain growth with increase in annealing temperature. FIB cross-sectional view of these samples annealed at 600°C illustrate that the films have high density. Transmission spectra reveal that ZnO thin films annealed at 450°C and 600°C, respectively, are highly transparent with a steep absorption edge.

7.1. Introduction

Zinc oxide (ZnO) is a II-VI semiconductor with a wide direct band gap of 3.3 eV. ZnO has large exciton binding energy (60 meV at room temperature). As a transparent conducting oxide and wide band gap with near UV emission, ZnO has niche applications in light emitting diodes [132] and UV lasers [76]. ZnO is also chemical stable and unreacting even in hydrogen plasma. Hence, ZnO thin films can be employed in fabrication of hydrogenated amorphous silicon solar cells [57]. Due to its structure, ZnO also has good piezoelectric properties, which have drawn tremendous attention in recent years.

ZnO thin films have been synthesized by various techniques of which sol - gel method has been widely used [22, 98, 18, 149, 45, 2, 81, 93]. This technique is relatively simple but has few disadvantages. In sol-gel process, sols are prepared using metal alkoxides as starting material. However, these materials are expensive, toxic, and insoluble in most alcohols making their synthesis difficult. Sols have also been prepared using zinc acetate but they do not gel completely in water [81].

ZnO thin films have been prepared by aqueous polymeric precursor method. This is a simple and less toxic method, which has been developed by

Pechini [83]. This method has been used extensively for preparation of several polycation oxides and perovskites [37, 7, 150, 13, 122] employing common reagents. In this technique, metal salts are dissolved in aqueous solution of alpha-hydroxycarboxylic acid such as citric acid. To this solution, polyhydroxyl alcohol, usually ethylene glycol, is added to form polyester. The metal cations chelate to the polyester to distribute the cations uniformly [48]. This process has many advantages such as, good stoichiometry, cost effectiveness, and precise particle size control. This method employs aqueous solutions and can be prepared in ambient atmosphere. Research has also been carried out in synthesizing polymeric precursors using EDTA as chelating agent [126, 28, 121] as EDTA improves the chelation of metal cations to the polymers.

In this paper, properties of nanocrystalline ZnO thin films prepared by Pechini process using ethylene glycol, glycerol, citric acid, and EDTA are compared. The prepared polymeric precursor was spincoated on surface modified substrates and annealed to different temperatures. Thermal decomposition of the ZnO polymeric precursors were studied by thermogravimetric analysis (TGA). The annealed thin films were characterized by XRD, SEM, and AFM. The optical and electrical properties as a function of annealing temperature of the thin films were also investigated.

7.2. Experimental Methods

All chemicals of analytic - grade were used as received without further purification. 99% pure zinc nitrate, $Zn(NO_3)_2.xH_2O$ was obtained from Alfa Aesar. Ethylene glycol (99%), glycerol (99%), citric acid (2-hydroxy-1, 2, 3

propanetricarboxylic acid), and ethylene diamine tetraacetic acid (EDTA, 99%) used as chelating agents, were obtained from Alfa Aesar, Fischer Scientific International Inc., and Acros, respectively. Nitric acid (70%) was acquired from J. T. Baker. Polymeric precursors were synthesized by four different chemical routes following modified Pechini process and are briefly summarized in Table 7.1. In these techniques, zinc nitrate was standardized thermogravimetrically for exact calculation of cation content in solutions. Then calculated amounts of zinc nitrate, as mentioned in Table 7.1, was dissolved in deionized and filtered water (resistivity = 18.2MΩ). Measured amount of chelating agent was then added to the solution. In cases of citric acid and EDTA, these chelating agents were dissolved in deionized water and ammonium hydroxide, respectively, which were then added to zinc nitrate solution. This was followed by addition of nitric acid to polymerize the solution and to create chelation sites. To the solutions of citric acid and EDTA, ethylene glycol was also added to the solution to act as reacting medium. The solution was stirred continuously and heated at 70°C until the resultant solution was clear, homogeneous, and precipitate free.

Table 7.1: Preparation of polymeric precursors

Polymeric Precursor	Reactants	Ratio of Reactants
Ethylene glycol	$Zn(NO_3)_2$/EG/HNO_3	0.1:0.9:0.1
Glycerol	$Zn(NO_3)_2$/Glycerol/HNO_3	0.1:0.9:0.1
Citric acid	$Zn(NO_3)_2$/EG/HNO_3/Citric acid	0.1:0.9:0.1:0.1
EDTA	$Zn(NO_3)_2$/EDTA/EG/HNO_3	0.1:0.2:0.9:0.1

Glass microslides and silicon substrates (2.54 x 2.54cm^2) were thoroughly cleaned ultrasonically in acetone, methanol and deionized water, followed by surface modification with 1N potassium hydroxide (EMD chemical Inc.) solution to achieve good wetting characteristics. The prepared solutions were spincoated (CEE Model 100CB, Brewer Science, Inc.) on surface modified substrates at 4000 rpm for 30s, followed by curing at 70°C on a hot plate for approximately 1 hour. The films were then annealed at varied high temperatures for 10 min for pyrolysis of the organic precursors and formation of ZnO.

Thermal decomposition of polymeric precursor of ZnO was studied by thermogravimetric analysis (Perkin Elmer TGA - 7). Structure and crystallinity of the synthesized ZnO thin films were characterized by X - ray diffraction with CuKα radiation in Bragg – Brentano geometry (Scintag XDS 2000). Morphology of the deposited ZnO films were analyzed by field emission scanning electron microscopy, FESEM, (Nova Nanolab 200, FEI Co.) and atomic force microscopy, AFM, (Digital Instruments Multi-Mode Nanoscope IIIa). AFM imaging was carried out in the tapping mode, at a scanning rate of 1Hz using a silicon cantilever with a spring constant of 20 - 80 N/m. Surface roughness (R_{rms}) was calculated using the equipment's software routine. Transmission spectra of ZnO films, as a function of annealing temperatures, were obtained using variable angle spectroscopic ellipsometer (VASE, J.A.Woollam Inc.). Two probe electrical resistivity measurements (Model 6430 sub-femto sourcemeter, Keithley Instruments) were conducted using sputter coated Au electrodes on the annealed thin films.

7.3. Results and Discussion

7.3.1. Thermal Evolution

Fig. 7.1 and 7.2 show the TGA curves (heating rate = 2°C/min) of ZnO polymeric precursors, prepared using ethylene glycol (Fig. 7.1a), glycerol (Fig. 7.1b), citric acid (Fig. 7.2a), and EDTA (Fig. 7.2b), respectively, as chelating agents over the temperature range of 50 - 750°C. For precursor prepared using ethylene glycol (Fig. 7.1a), there is weight loss from 50 to 212°C indicating pyrolysis of excess water and polyethylene glycol. At 212°C, we observe a significant sharp 15% weight loss due to combustion of organic precursor, ethylene glycol. Above 212°C, the weight remained constant implying that all organic materials have been eliminated and there is complete crystallization of ZnO.

In case of glycerol precursor (Fig. 7.1b) the weight loss increased up to 550°C as the temperature increased, and beyond that temperature, the weight remained constant. Excess water and polyglycerol are pyrolized and the precursor loses mass till 110°C. Between 110°C and 230°C, another weight loss is observed which is due to pyrolysis of polymeric glycerol. There is a plateau evident from 230°C to 350°C indicating the presence of 3D network of glycerol cross-linked with Zn cations in the precursor solution. From 350°C to 430°C, there is slight weight loss, which may be attributed to pyrolysis of polymeric backbone. There is simultaneous formation of ZnO along with the pyrolysis of glycerol backbone. Above 450°C, all of the organic material is removed from the precursor leaving ZnO. Therefore, it is concluded that all of the involved reactions

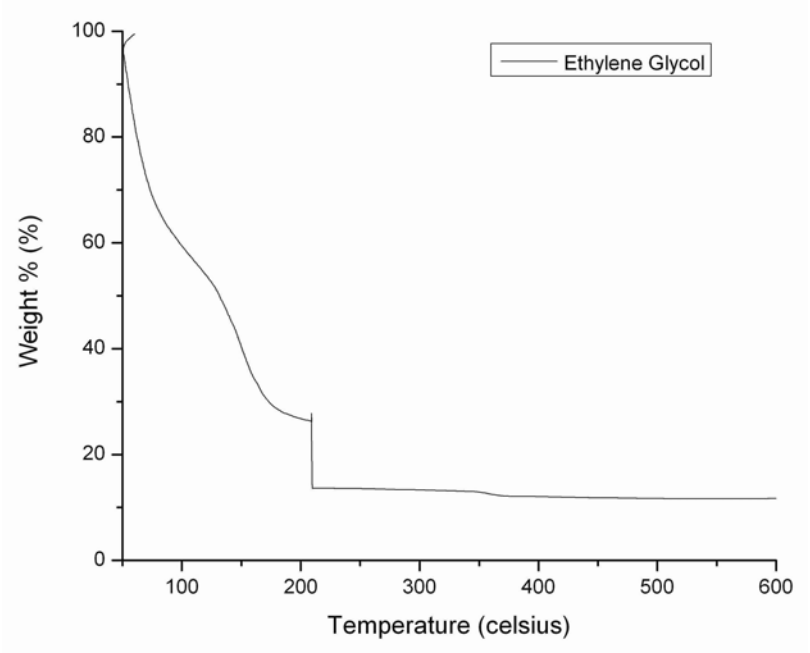

(a)

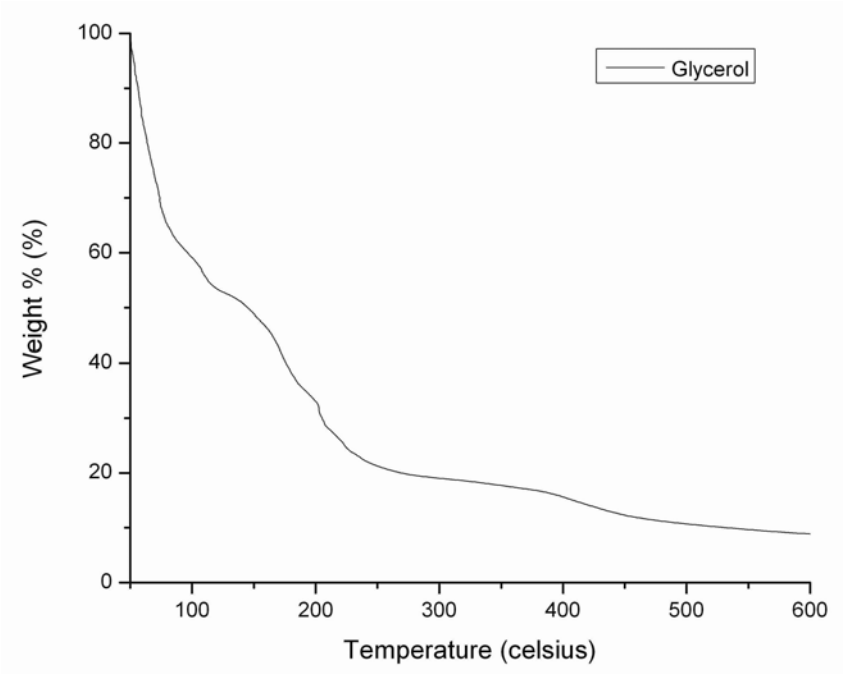

(b)

Figure 7.1: TGA curves of ZnO polymeric precursor prepared using (a) ethylene glycol and (b) glycerol, respectively, as chelating agents.

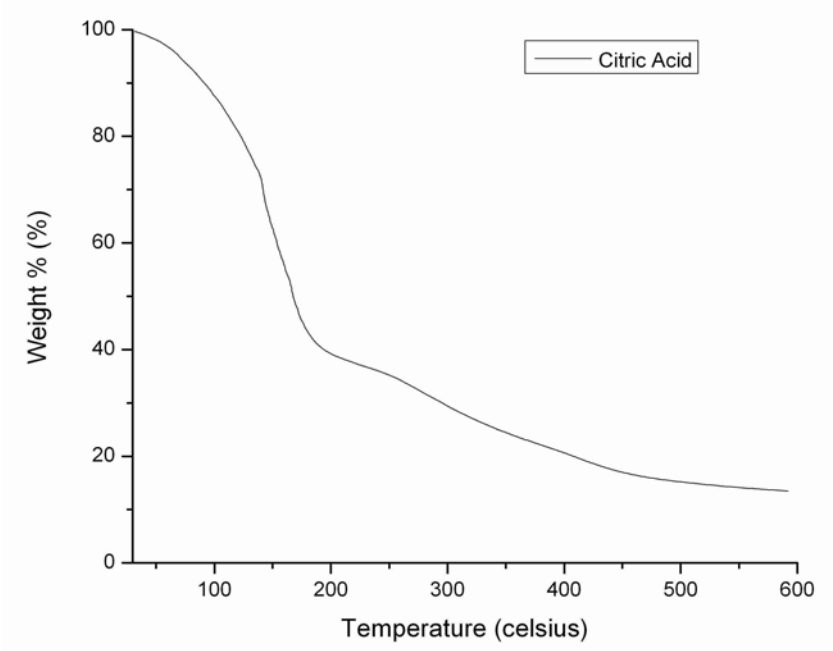

(a)

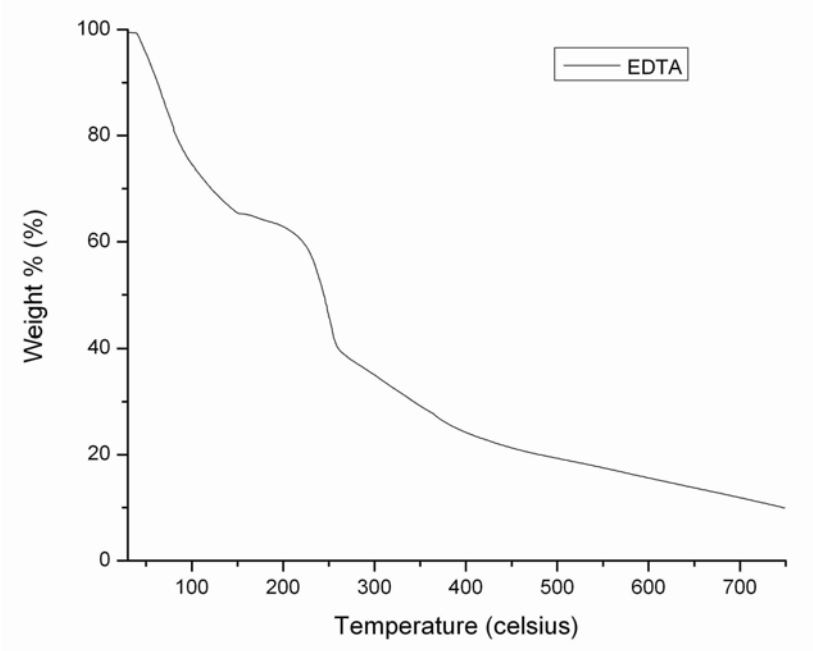

(b)

Figure 7.2: TGA curves of ZnO polymeric precursor prepared using (a) citric acid and (b) EDTA, respectively, as chelating agents.

in the weight-loss process were finished at 450°C along with simultaneous formation of the ZnO structure. Finally, the ZnO crystallization process was complete at 600°C.

In case of citric acid precursor (Fig. 7.2a), the TGA analysis indicates a weight loss (40%) between 50 and 190°C, corresponding to the evaporation of excess water and pyrolysis of polyethylene glycol. Presence of plateau from 190°C to 250°C implies 3D networking and cross-linking of ethylene glycol and citric acid with Zn ions. A weight loss (25%) between 250 and 450°C is observed due to the removal of organic precursors and their combustion. There may be formation of ZnO during the combustion of the organic precursors. After 450°C, no obvious weight loss was observed and complete crystallization of ZnO must have taken place.

The TGA analysis for EDTA polymeric precursor (Fig. 7.2b) indicated a major weight loss (30%) between 30°C and 150°C, which corresponds to the evaporation of absorbed water and pyrolization of excess polyethylene glycol (PEG). A slight plateau is evident from 150°C to 205°C, indicating that the entire PEG has been pyrolized, leaving cross-linked network of EDTA and ethylene glycol with Zn cations in the film. This is followed by another weight loss (20%) between 205°C and 255°C, which is probably due to pyrolization of EDTA. There is further weight loss (15%) upto 400°C illustrating that all of the organic precursors have been removed, giving way to formation of oxide. Beyond 400°C, the weight decreases progressively while complete crystallization of ZnO takes place.

From the above TGA analysis of different precursors, it can be deduced that the ethylene glycol based precursor has the lowest temperature of decomposition. This precursor will be highly suitable for low temperature processing for application in flexible displays. Precursor solutions from glycerol, citric acid, and EDTA do not display a sharp transition like ethylene glycol but have a gradual decrease in weight loss. TGA analysis of citric acid and EDTA show that they will decompose completely at temperatures above 450°C and 600°C, respectively. These chelating agents have carboxylic acid groups that require higher energy to break the double bonds. Hence, these precursors cannot be used for low temperature processing. Glycerol does not have any double bonds. However, the amount of organics to be removed increases when compared to ethylene glycol. Therefore decomposition temperature of glycerol is higher than ethylene glycol.

7.3.2. Microstructure of ZnO Thin Films

ZnO thin films of ethylene glycol based polymeric precursor were analyzed by SEM (Fig. 7.3a). Micrographs reveal formation of hexagonal ZnO flowers. These flower structures have hemispherical three-dimensional multilayered shape. The flowers are well dispersed and have an average diameter of 4-7 μm. These flowers grow by island or Volmer-Weber growth mode [119].

SEM and AFM micrographs of polymeric precursor derived ZnO thin films using glycerol, citric acid, and EDTA, respectively, as chelating agent and annealed at 300°C are shown in Fig. 7.3(a - c) and Fig. 7.4(a - c). Microstructural studies of these samples illustrate smooth films without any evidence of granular

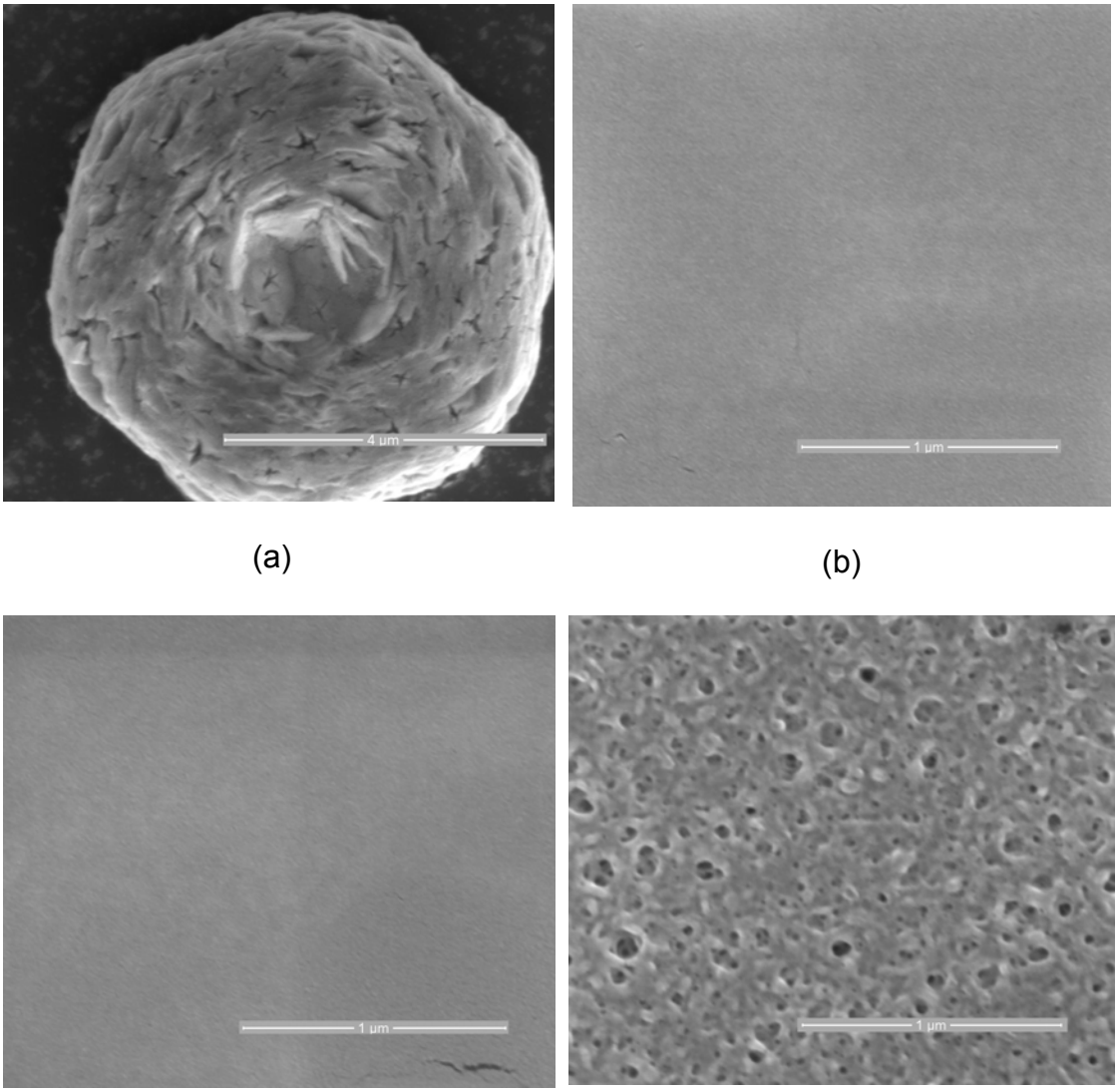

Figure 7.3: SEM micrographs of ZnO thin films prepared using (a) ethylene glycol, (b) glycerol, (c) citric acid, and (d) EDTA, respectively, as chelating agents and annealed at 300°C.

structure. These films probably have no ZnO particles. The glycerol (Fig. 7.4a) and citric acid (Fig. 7.4b) sample showed a homogeneous surface morphology

with very low roughness. The prepared EDTA sample (Fig. 7.4c) showed a porous structure due to presence of organic precursors.

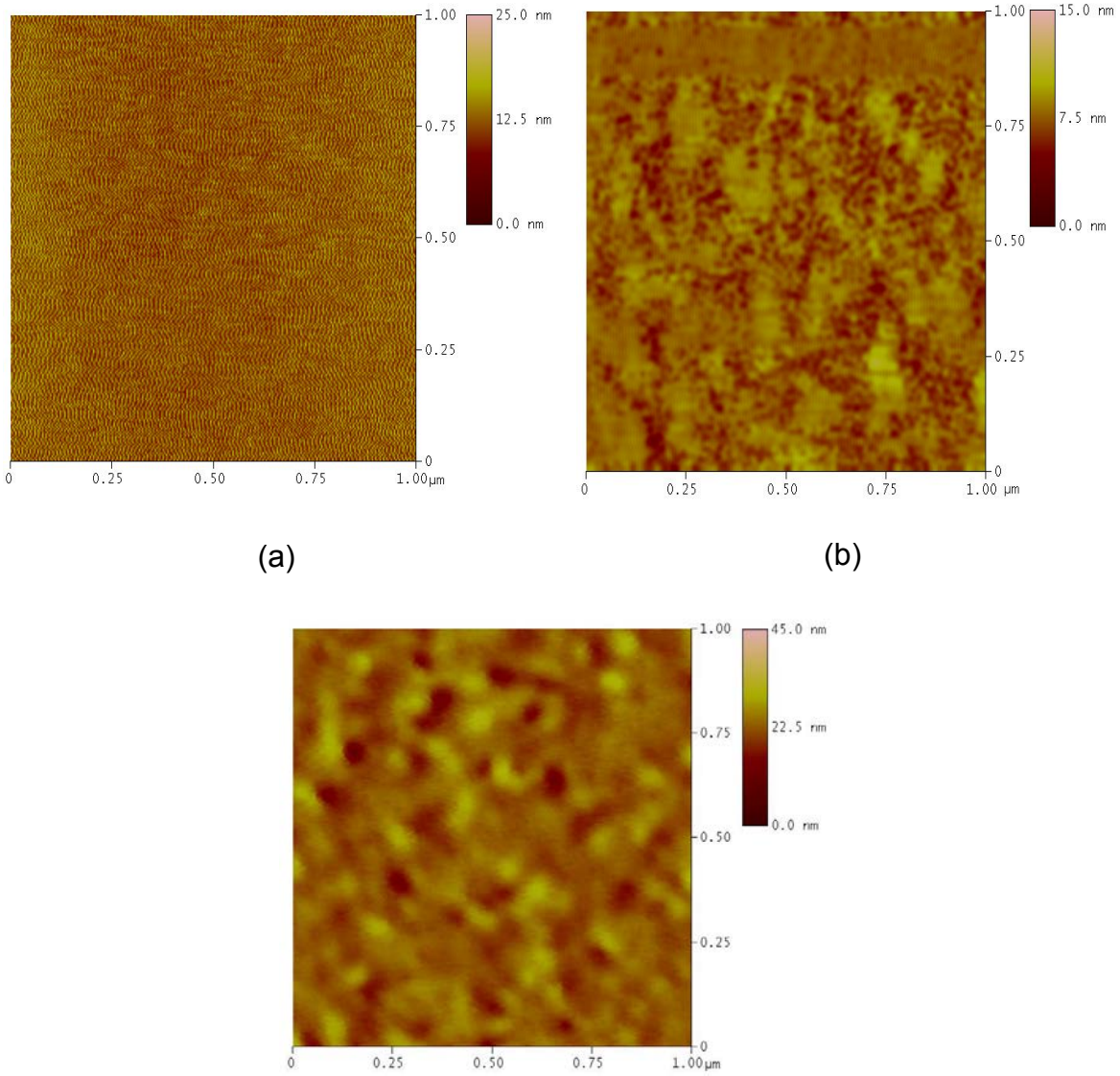

(a) (b)

(c)

Figure 7.4: AFM micrographs of ZnO thin films prepared using (a) glycerol, (b) citric acid, and (c) EDTA, respectively, as chelating agents and annealed at 300°C.

Fig. 7.5(a - c) and 7.6(a - c) illustrate micrographs taken of samples fabricated using precursors of glycerol, citric acid and EDTA, respectively, as chelating agents and annealed at 450°C. The glycerol-based films have spherical granular morphology with average grain size of approximately 20 - 30 nm (Fig. 7.5a). The surface of these films appears very homogeneous and dense without cracks. AFM images (Fig. 7.6a) displayed grains distributed uniformly throughout the thin film with a size distribution approximately 20 - 25nm and rise in surface roughness (root mean square, R_{rms}=2.188 nm). For citric acid based films, SEM micrographs of samples (Fig. 7.5b) annealed at 450°C also illustrate homogeneous surface morphology without presence of cracks and average grain size of 20nm. There is an increase in roughness (R_{rms}=1.919 nm) (Fig. 7.6b). SEM image of EDTA sample annealed at 450°C (Fig. 7.5c) demonstrates a uniformly distributed granular microstructure with highly faceted grains of 30 - 40 nm size throughout the thin film (Fig. 7.6c). The presence of large grains causes an increase in surface roughness (R_{rms}=14.07 nm).

On annealing at 600°C, SEM (Fig. 7.7a) and AFM (Fig. 7.8a) micrographs of glycerol based thin films reveal grain sizes of 30 - 40 nm with root mean square roughness, R_{rms} = 3.69 nm. The films illustrate grain growth with an increase in annealing temperature and have huge pores located at the boundaries of the grains. SEM and AFM images show that the grain growth occurs along the grain boundaries leading to coalescence of grains. This process deteriorates the film surface resulting in high porosity. Citric acid based thin films illustrate grain size of 50 – 60 nm (Fig. 7.7b) with root mean square roughness

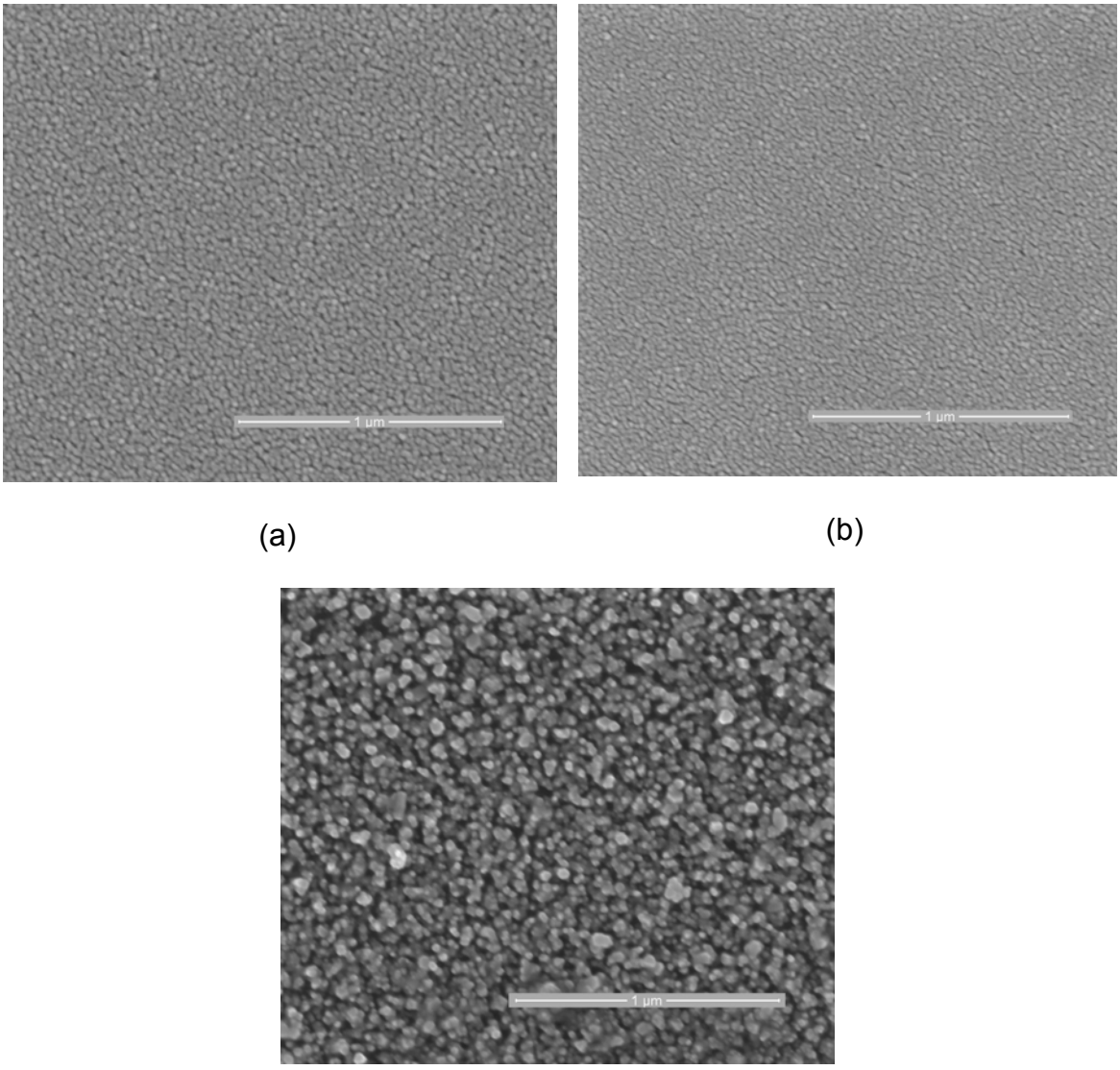

(a) (b)

(c)

Figure 7.5: SEM micrographs of ZnO thin films prepared using (a) glycerol, (b) citric acid, and (c) EDTA, respectively, as chelating agents and annealed at 450°C.

R_{rms} = 8.737 nm (Fig. 7.8b). The films have mono-dispersed and well-distributed spherical grains. When EDTA based thin films were annealed at 600°C (Fig. 7.7c), SEM and AFM images exhibit complete coating of the substrate with

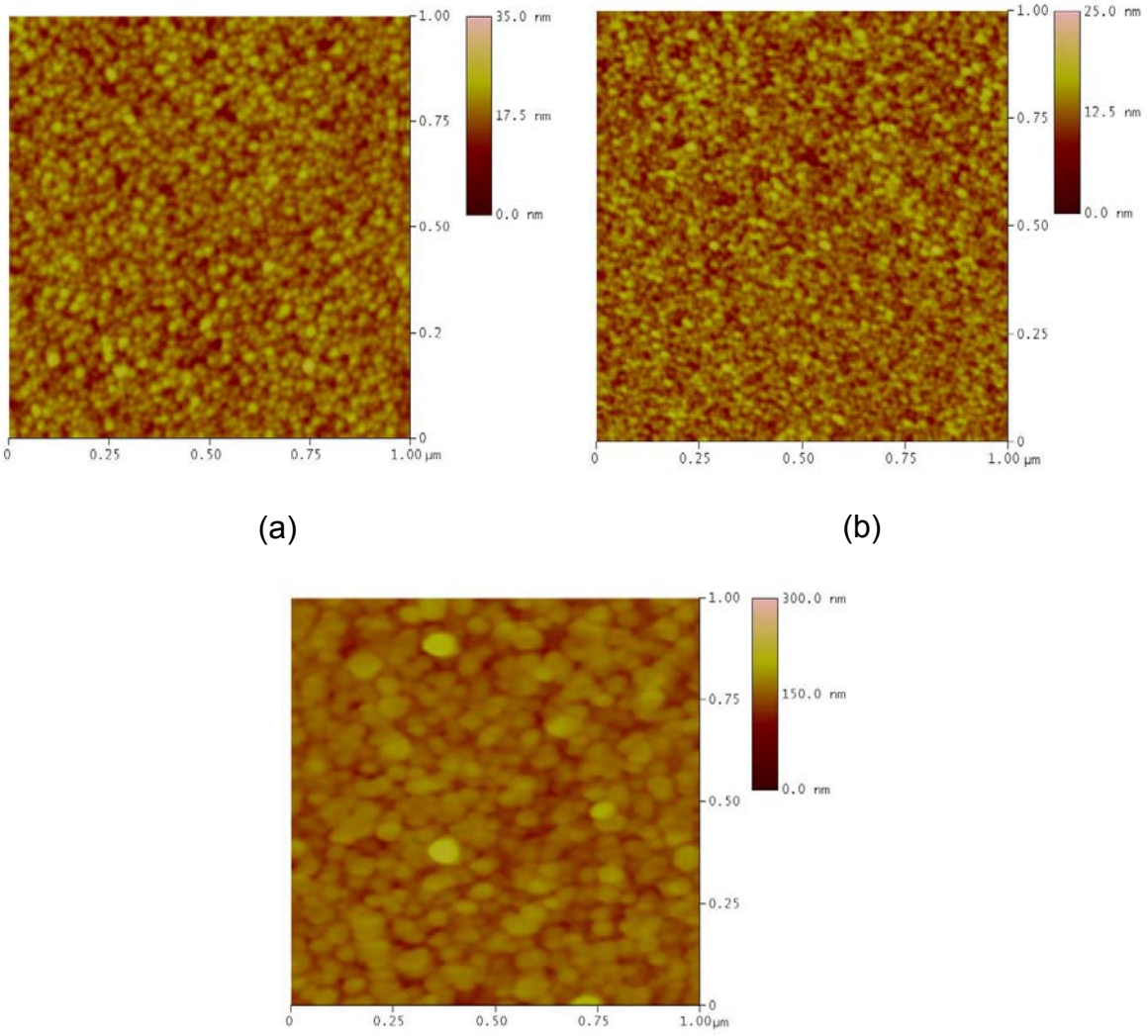

Figure 7.6: AFM micrographs of ZnO thin films prepared using (a) glycerol, (b) citric acid, and (c) EDTA, respectively, as chelating agents and annealed at 450°C.

and crack-free microstructure (Fig. 7.8c). The morphology of the thin films appears to be smooth with small porosity. The average grain size and the surface roughness of the films decrease to 20 – 25 nm and R_{rms} = 3.59 nm, respectively. Decrease in average grain size suggests that ZnO actually forms at

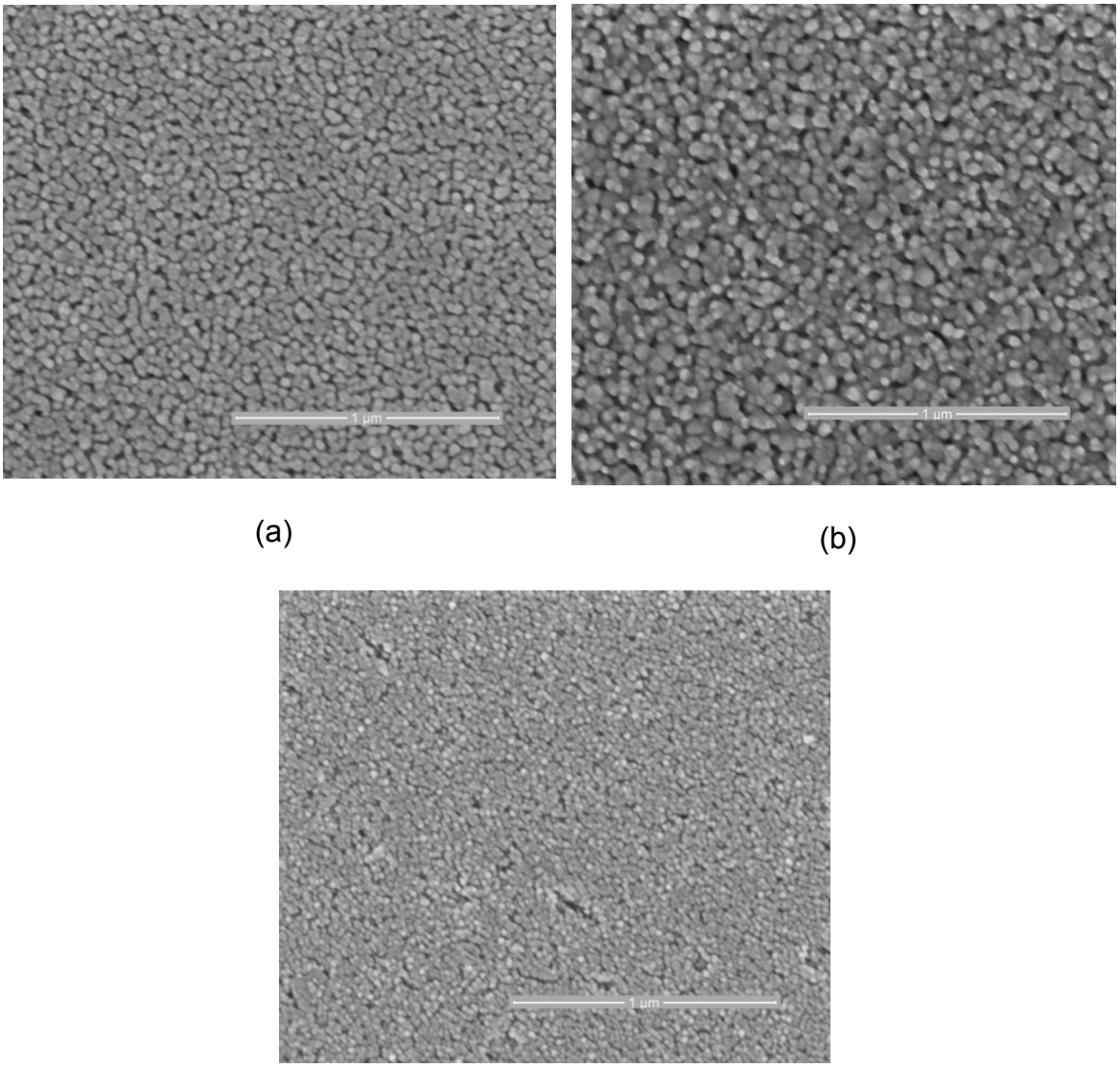

(a) (b)

(c)

Figure 7.7: SEM micrographs of ZnO thin films prepared using (a) glycerol, (b) citric acid, and (c) EDTA, respectively, as chelating agents and annealed at 600°C.

600°C and the granular morphology observed for 450°C annealed samples may belong to the organic matrix.

Microstructure of ZnO thin films annealed at 600°C was also analyzed by

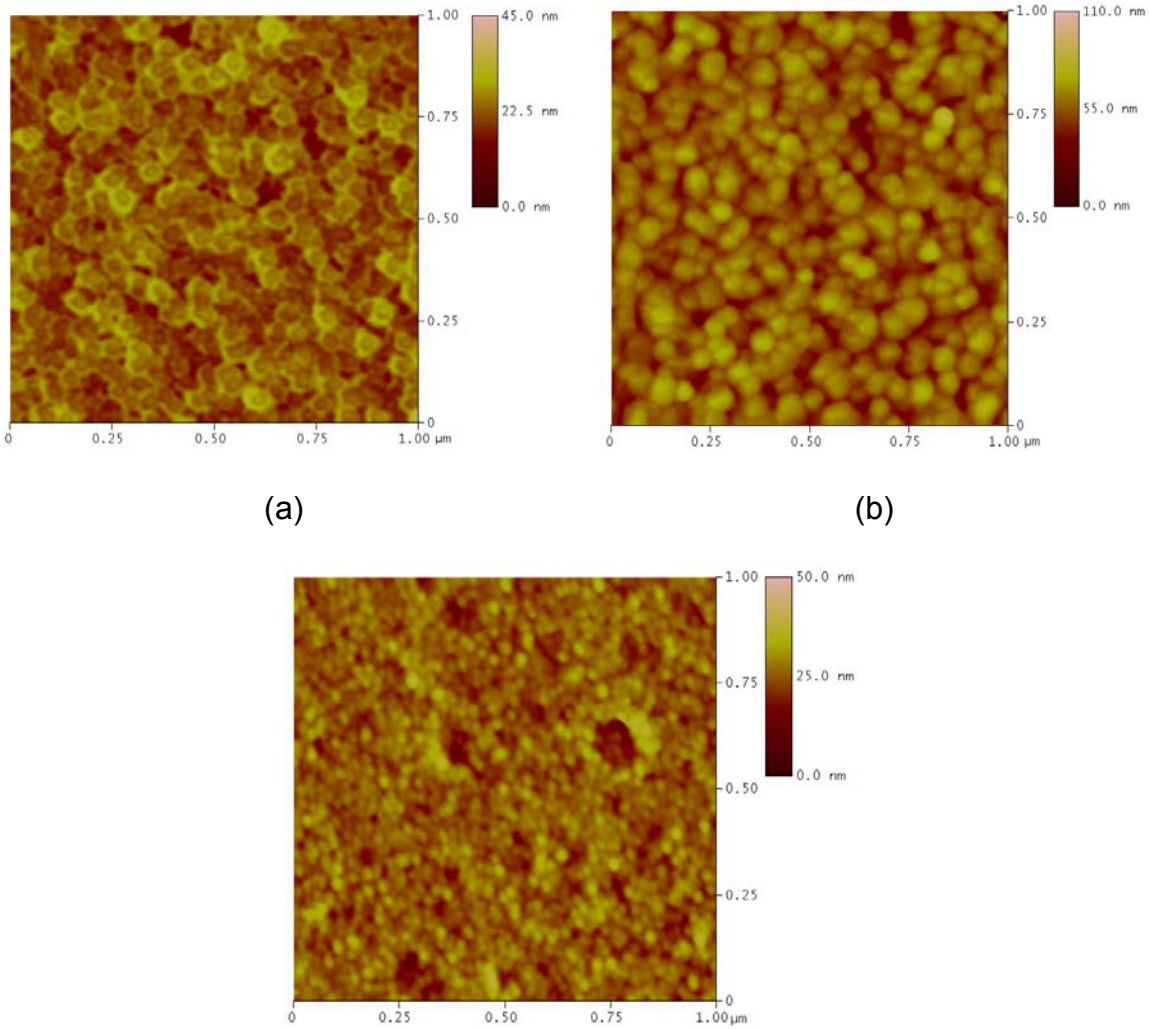

(a) (b)

(c)

Figure 7.8: AFM micrographs of ZnO thin films prepared using (a) glycerol, (b) citric acid, and (c) EDTA, respectively, as chelating agents and annealed at 600°C.

observing FIB cross-sectional SEM micrographs. SEM micrographs of glycerol-derived films illustrate highly porous and 200 nm thick films with spherical particles (Fig. 7.9a). FIB cross-sectional SEM micrographs of citric acid derived ZnO thin film illustrate that the films are porous and are 160 nm thick. However,

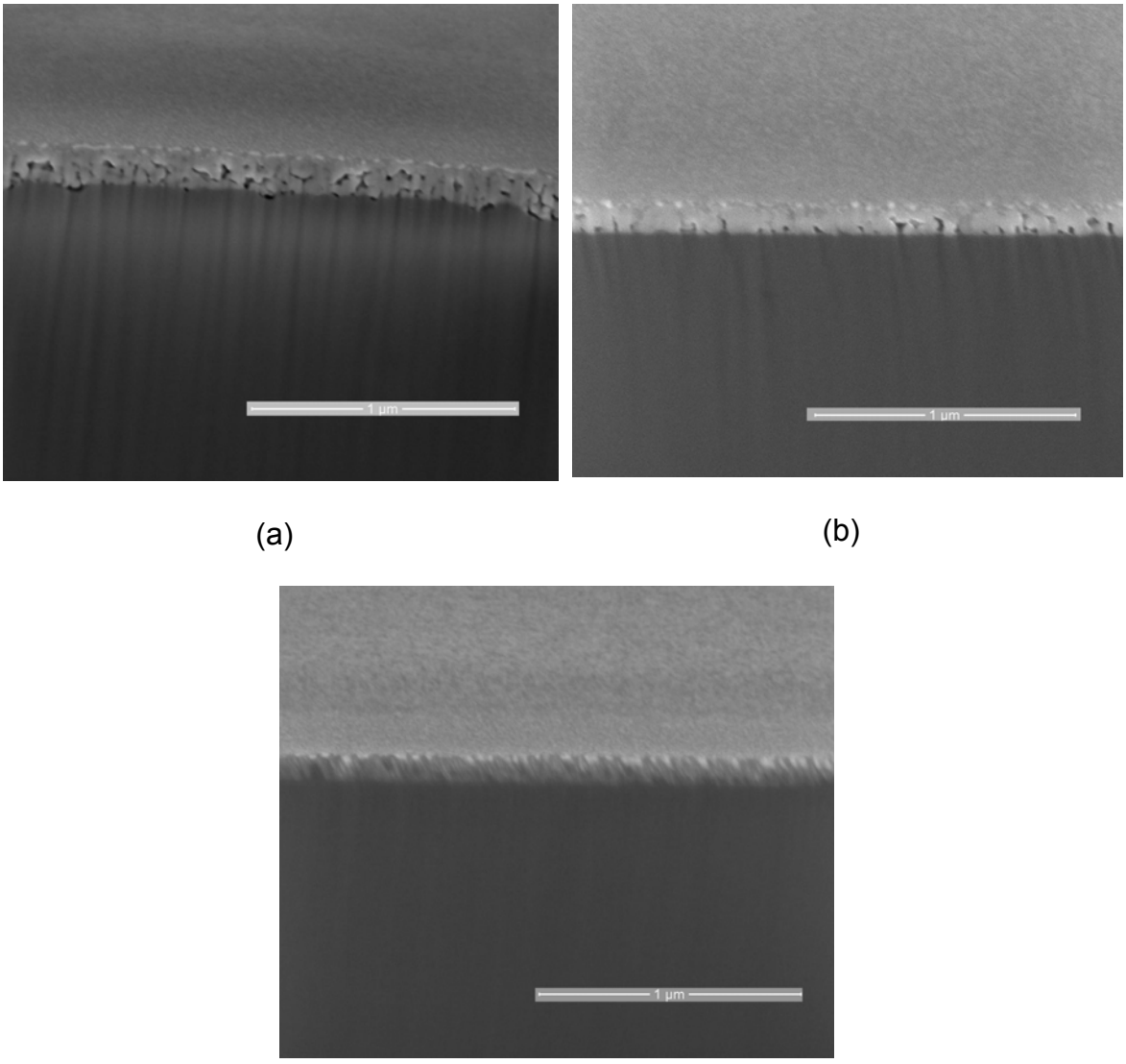

(a) (b)

(c)

Figure 7.9: SEM micrographs of ZnO thin films prepared using (a) glycerol, (b) citric acid, and (c) EDTA, respectively, as chelating agents and annealed at 600°C.

the particles do not appear as spherical as glycerol based ZnO thin film. ZnO thin film prepared from EDTA precursor exhibits dense columnar grains and uniform thickness of 130 nm.

The distinct difference in morphology of the thin films of polymeric precursors may be attributed to the chelation of Zn cations to the polymeric backbone. The Zn^{2+} cations chelate to the polymer through its ethereal oxygen [48]. We postulate that there are insufficient chelation sites for the Zn cations provided by ethylene glycol. Hence, some of the Zn ions are left unchelated in the polymeric solution. These unchelated ions nucleate directly on the substrate during spin coating and form ZnO nanostructures on annealing [119]. In case of glycerol, citric acid, and EDTA, we observe that all the Zn cations chelate to the polymers, forming dense, crack free thin films. The number of chelation sites provided by these chelating agents for Zn ions is adequate forming crack free homogeneous ZnO thin films.

7.3.3. Crystallographic Orientation of ZnO Thin Films

X-ray diffraction of synthesized ZnO thin films were performed in θ - 2θ mode using Bragg - Brentano geometry to determine the crystallinity and orientation. Each of the polymeric precursors were spincoated on silicon substrates and annealed at 300°C, 450°C, and 600°C, respectively, and obtained XRD spectra are shown in Fig. 7.10, 7.11, and 7.12.

Ethylene glycol based ZnO thin films at 300°C (Fig. 7.10a) show diffraction peaks which can be indexed as (100), (002), (101), (102) and (110) planes of wurtzite structure of ZnO. Peaks not related to ZnO were not found. Relative intensities of the diffraction peaks reveal that there is no preferred orientation along any particular direction. For chelating agents, like glycerol, citric acid and EDTA, based polymeric precursors, ZnO thin films annealed at 300°C do not

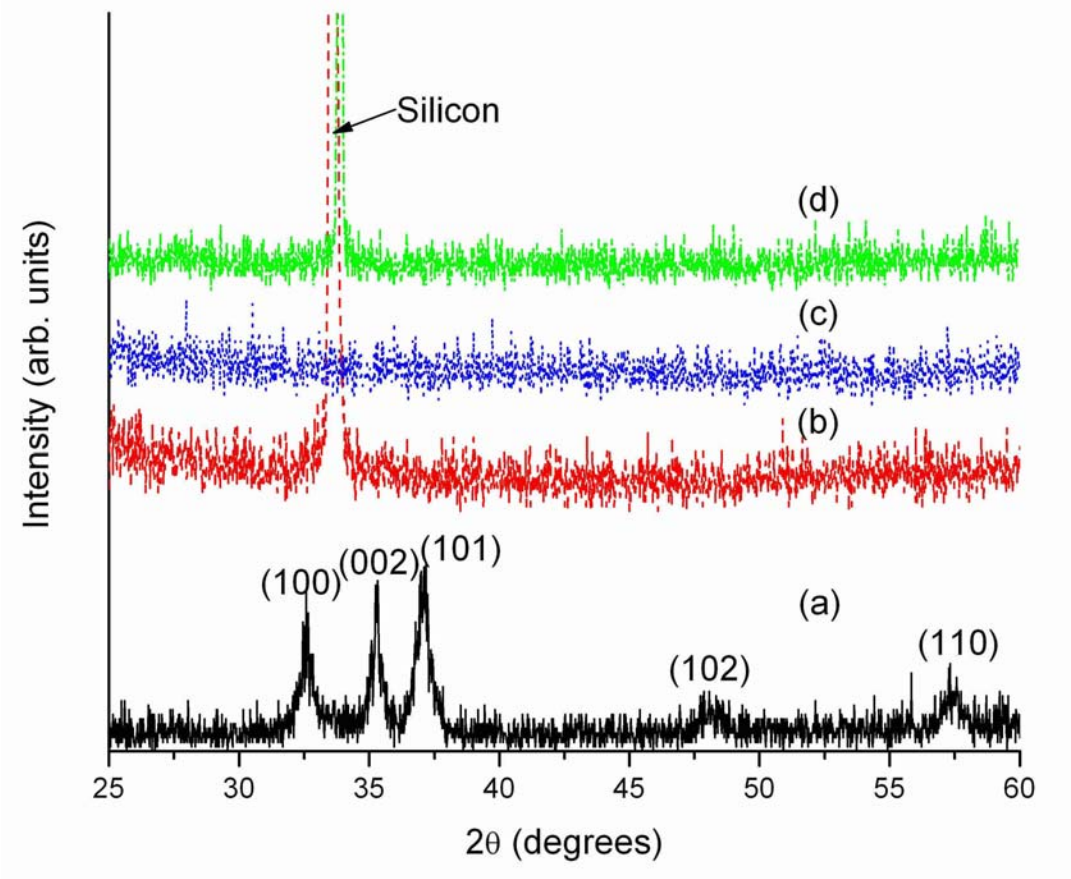

Figure 7.10: XRD spectra of ZnO thin films synthesized by polymeric precursor route using chelating agents - (a) ethylene glycol (b) glycerol, (c) citric acid, and (d) EDTA, respectively at 300°C.

show any diffraction peaks (Fig. 7.10) because of the presence of organic precursors. These spectra also reveal that ZnO is not formed at 300°C.

Thin films of ZnO, annealed at 450°C (Fig. 7.11), possess wurtzite structure with space group $P6_3mc$. The glycerol derived ZnO thin films (Fig. 7.11a) exhibits three strongest diffraction peaks at 2θ = 32.52°, 35.12°, and 36.98° which can be indexed as (100), (002), and (101) planes, respectively. These XRD peak positions show a shift to higher diffraction angle. The lattice

constants calculated were a = 0.3177 nm and *c* = 0.5106 nm, respectively. These cell constants are slightly lower than cell constants of bulk ZnO (JCPDS no. 36 - 1451). For ZnO thin films derived from citric acid based precursors (Fig. 7.11b), the diffraction peaks corresponding to (100), (002), and (101) planes are observed at 2θ = 32.40°, 35.01°, and 36.87°. The cell constants were calculated to be *a* = 0.3188 nm and *c* = 0.5122 nm. However, ZnO thin films derived of EDTA precursor exhibits only one discernible diffraction peak at 2θ = 34.9° corresponding to (002) plane while the (100) and (101) peaks appear as

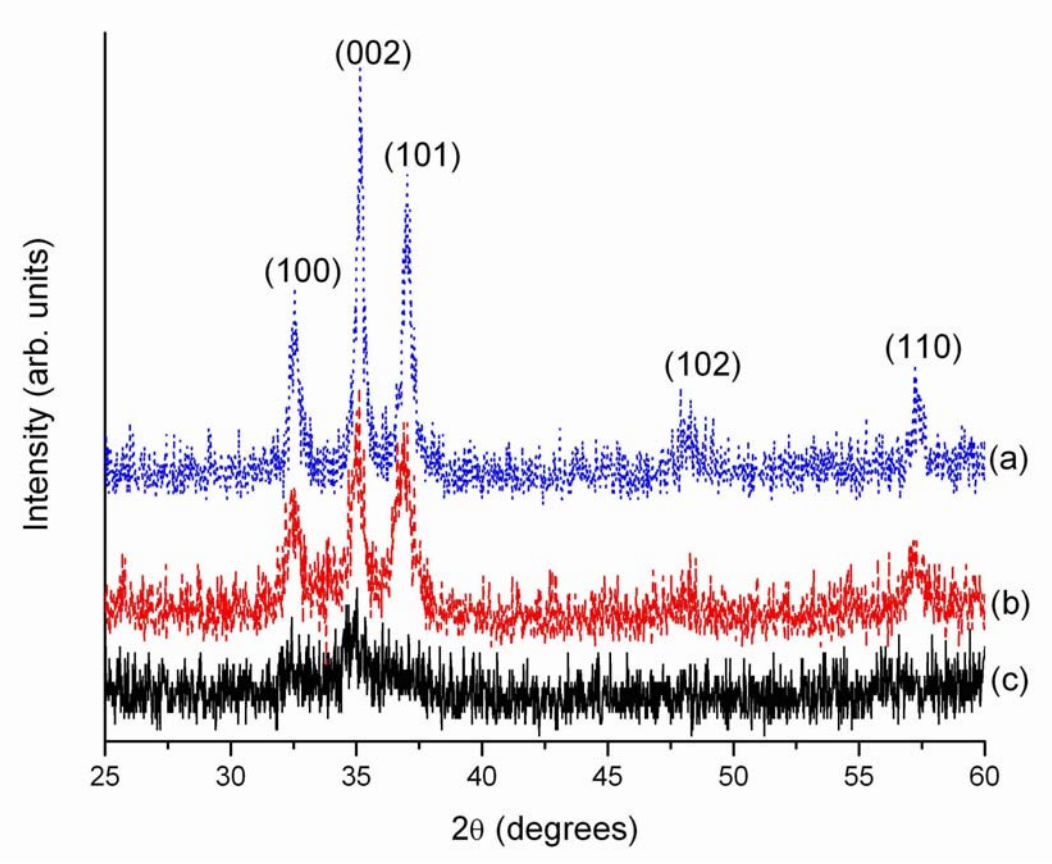

Figure 7.11: XRD spectra of ZnO thin films synthesized by polymeric precursor route using chelating agents - (a) glycerol (b) citric acid, and (c) EDTA, respectively at 450°C.

shoulders when annealed at 450°C (Fig. 7.11c). The cell constants were calculated to be a = 0.3221 nm and c = 0.5137 nm. We also observe that the peaks corresponding to (102) and (110) planes, as seen in case of glycerol and citric acid, do not appear in EDTA based ZnO films.

On annealing at 600°C, glycerol derived ZnO thin films exhibit three strong diffraction peaks at 2θ = 32.54°, 35.2°, and 37.06° (Fig. 7.12a) along with two peaks at 48.268°, and 57.398° which can be indexed as (102) and (110) planes.

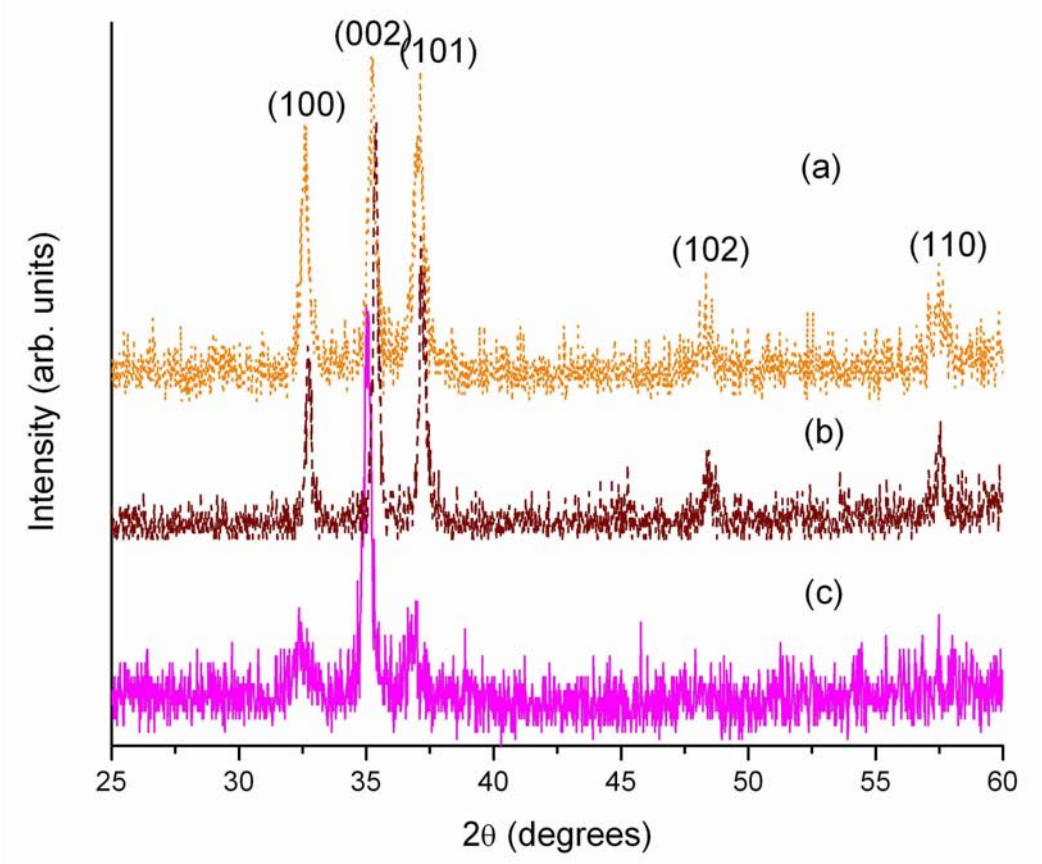

Figure 7.12: XRD spectra of ZnO thin films synthesized by polymeric precursor route using chelating agents - (a) glycerol (b) citric acid, and (c) EDTA, respectively at 600°C.

All these peak positions appear shifted to higher diffraction angle than films annealed at 450°C. The calculated lattice constants are a = 0.31747 nm and c = 0.5095 nm. ZnO thin films derived from citric acid precursor exhibit the diffraction peaks at 2θ = 32.69°, 35.34°, 37.15°, 48.34° and 57.17°, corresponding to (100), (002), (101), (102) and (110) planes (Fig. 7.12b). On calculation of cell constants for 600°C, it was found that these have decreased to a = 0.3159 nm and c = 0.50758 nm. On annealing the ZnO thin film derived from EDTA precursor solution at a temperature of 600°C, the diffraction peaks occur at 2θ = 32.44°, 35.02°, 36.94°, corresponding to (100), (002), and (101) planes (Fig. 7.12c). The spectrum illustrates a strong preferred orientation along the (002) plane on annealing to 600°C. The cell constants were calculated to be a = 0.31844 nm and c = 0.5120 nm. In addition, there is a significant shift of 0.54° in peak positions to higher 2θ angles.

Texturing was determined by finding the ratio of intensities of (002) and (101) planes using the following equation:

$$T(002) = \frac{I(002)}{I(101)} \tag{15}$$

where I(002) and I(101) are intensities of diffraction peaks in samples annealed at different temperatures, respectively. On calculating the texture coefficient (shown in Table 7.2), we found that there is preferred orientation in all ZnO thin films. We also note that this preferred orientation decreases with increase in annealing temperature in case of glycerol based films suggesting grain growth along other planes. EDTA based ZnO films show a preferred orientation along

the (002) plane.

7.3.4. Strain in ZnO Thin Films

Deposition of thin films on substrate of the leads to strain in the film due to lattice mismatch or difference in coefficient of thermal expansion. Synthesis of ZnO thin films on silicon substrates leads to strain in the films. Film strain ε_Z along the c axis [79] is given by,

$$\varepsilon_Z = (c - c_o)/c_o \times 100\% \quad (16)$$

where c_o = 0.5204 nm, the strain-free lattice parameter measured from ZnO powder.

Strain in ZnO thin films prepared using glycerol precursor was calculated using equation 16. These films exhibited compressive strains of -1.89% and -2.09% when annealed at 450°C and 600°C, respectively. ZnO thin films derived from citric acid precursor and annealed at 450°C and 600°C showed compressive strains of -1.58% and -2.46%, respectively whereas the strain in EDTA derived ZnO thin films annealed at 450°C and 600°C showed compressive strains of -1.28% and -1.61%, respectively.

Strain and crystallite size are also calculated from Williamson-Hall plot. In a Williamson-Hall Plot, the effect of microstrain and broadening due to crystallite size can separated. From this plot, we can determine strain from the slope of the graph and calculate crystallite size from the intercept using the following [8]:

$$FWHM \times \cos\theta = 0.9\lambda/t + 2\Delta d/d \sin\theta \quad (17)$$

where θ is the peak position and FWHM is the integral breadth for the peak position. Using equation 17, a linear plot of FWHM*cosθ and sinθ is drawn. We

calculated a compressive strain of -0.16% and -0.66% for glycerol derived ZnO thin films annealed at 450°C and 600°C, respectively. This was calculated using software installed in XRD. This is a very reliable method for calculating strain. However, there was huge error in the linear plot, which got incorporated in the strain calculations also.

7.3.5. Optical Properties of ZnO Films

Fig. 7.13a show transmission spectra of ZnO thin films annealed at 300°C and derived from glycerol, citric acid, and EDTA precursors, respectively. These films do not show absorption edge suggesting that formation of ZnO did not take place.

Films annealed at 450°C (Fig. 7.13b) are transparent in the visible region; however, EDTA derived thin films has highest transparency (95%), followed by glycerol based film (90%). The film derived from citric acid precursor exhibits 85% transparency. We also observe that EDTA transmits 65% light even in UV region due to presence of organic precursors. Glycerol and citric acid precursors derived thin films exhibit a weak transmission in the UV region, which increases sharply in visible region due to onset of fundamental absorption of ZnO. The band edge of ZnO films derived from glycerol, citric acid, and EDTA was found at 370 nm and 374 nm, respectively. Band edge at lower wavelength for glycerol-based films may be due to smaller crystallite size.

Transmission spectra of glycerol, citric acid, and EDTA based thin films annealed at 600°C is shown in Fig. 7.14. We observe that the citric acid film is more transparent in the visible region (transparency is 90%) whereas glycerol

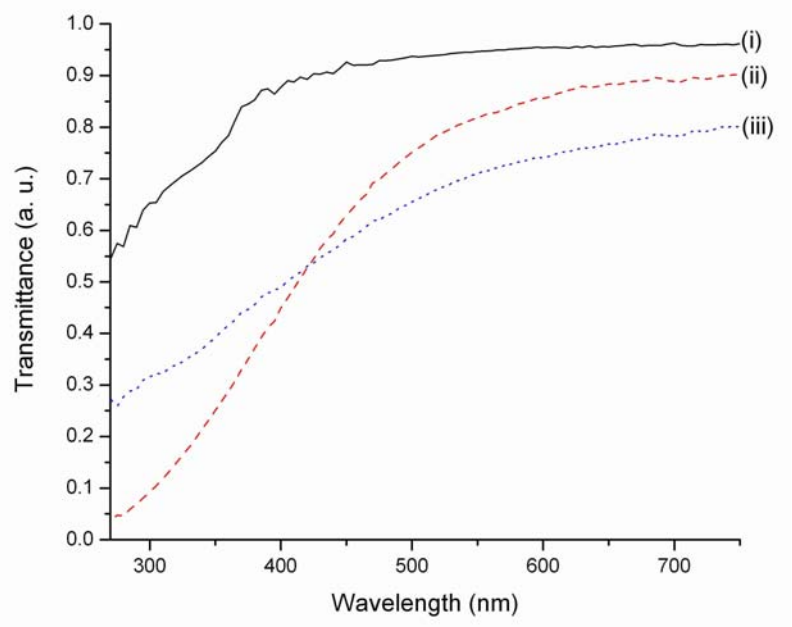

(a)

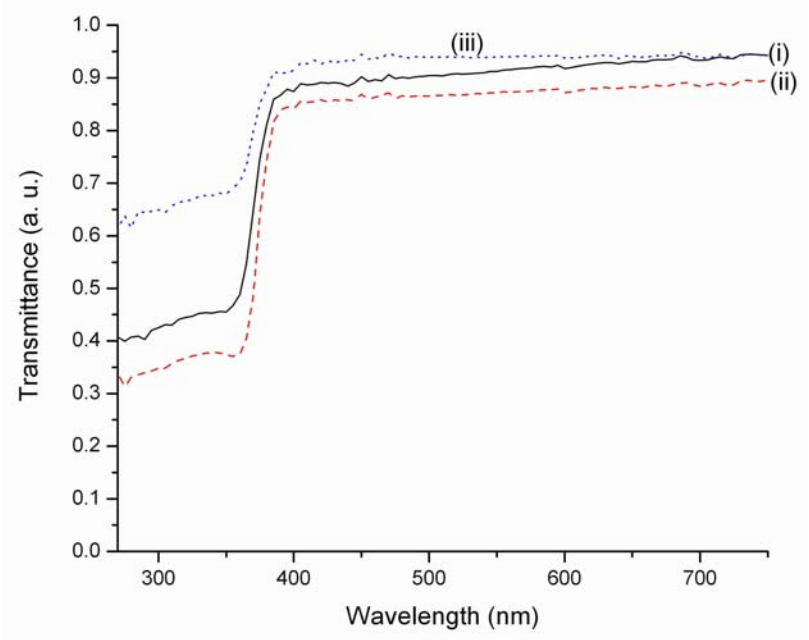

(b)

Figure 7.13: Transmission spectra of ZnO thin films prepared using (i) glycerol, (ii) citric acid, and (iii) EDTA, respectively, as chelating agents and annealed at (a) 300°C and (b) 450°C, respectively.

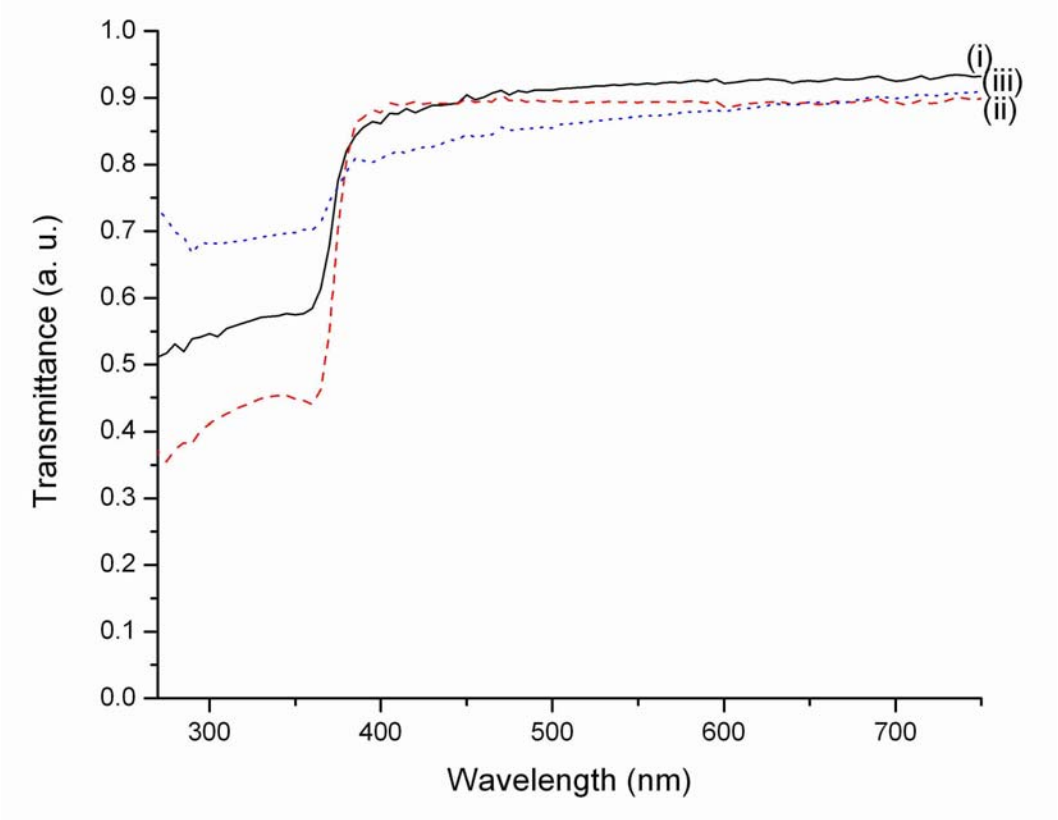

Figure 7.14: Transmission spectra of ZnO thin films prepared using (i) glycerol, (ii) citric acid, and (iii) EDTA, respectively, as chelating agents and annealed at 600°C.

based film does not show any change. However, there is a decrease (from 90% to 85%) in transparency of EDTA derived film. The band edge was found to be at 376 nm for all three precursors. There is a shift in onset of absorption edge with increase in annealing temperature. We observe that the optical absorption edge shifts by 2-6 nm to longer wavelengths. Moreover, the absorption edge also becomes steeper for all three precursors. These changes can be attributed to oxygen absorption by the film as they were annealed in ambient atmosphere. This leads to improvement in stoichiometry of the synthesized ZnO film [25].

Although we observe a change in transparency with annealing temperature, these are superior quality films as they are 85-90% transparent and can be utilized as transparent conducting electrodes.

7.4. Electrical Resistivity

Direct current electrical resistivity of the ZnO thin films on surface modified glass substrates, derived from polymeric precursors, was measured at room temperature through the film parallel to the substrate. We calculated electrical resistivity of polymeric precursor derived films annealed at 450°C (Fig. 7.15i) and 600°C (Fig. 7.15ii). I-V characteristics of these films annealed at 450°C (Fig. 7.15i) and 600°C (Fig. 7.15ii) show a linear plot suggesting ZnO behaves as an ohmic conductor. We observe that all films annealed at 450°C have resistivity values in same range of 10 - 14 Ω-m as these samples have similar thickness in the range of 20-25 nm. When annealed at 600°C, we notice a significant change in resistivity. There is two orders of increase in resistivity for glycerol (297 Ω-m) and EDTA derived ZnO films (515 Ω-m) whereas studies have resulted in increase of 9 orders in resistance [25].

Conductivity in undoped ZnO thin films is due to defects, such as, zinc interstitials or oxygen vacancies. On annealing at high temperatures, say 600°C, these defects are removed as a result of reaction of oxygen with ZnO. This, in turn, reduces the density of charge carriers and hence, increases in resistivity [25]. Electrical resistivity decreases with increase in crystalline orientation and reduction of grain boundaries [22]. However, in this work, we observe that when the preferred orientation increases, electrical resistivity also increases. So resisti-

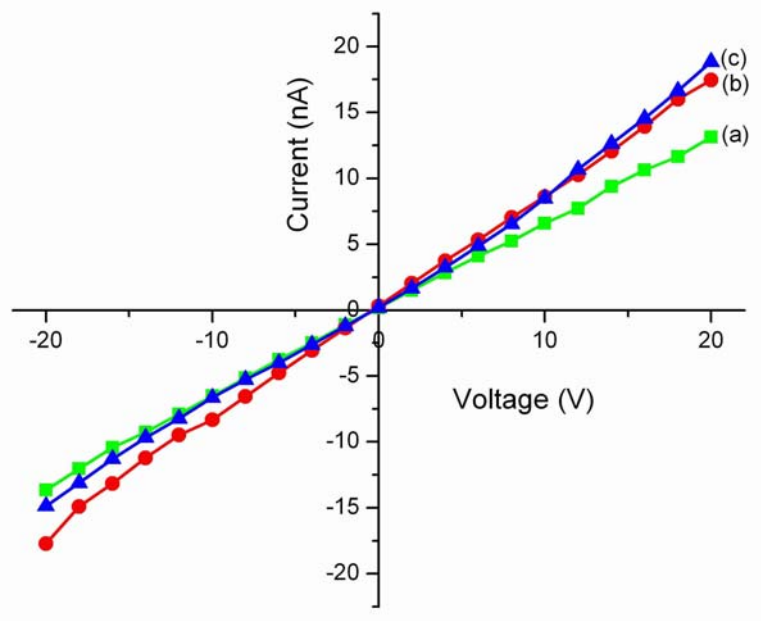

(i)

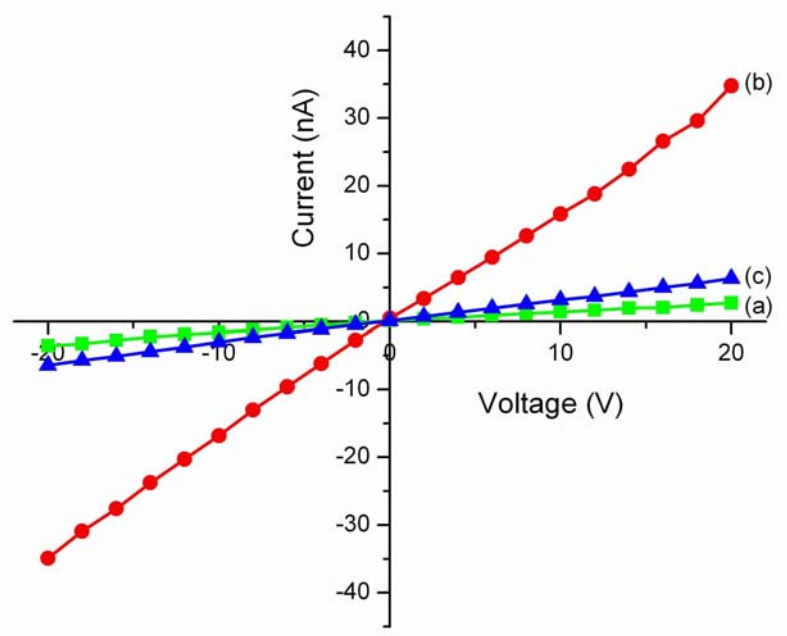

(ii)

Figure 7.15: I-V characteristics of ZnO thin films prepared using (a) glycerol, (b) citric acid, and (c) EDTA, respectively, as chelating agents and annealed at (i) 450°C and (ii) 600°C, respectively.

vity is affected by other phenomena.

The change in electrical resistivity on annealing ZnO films may be attributed to chemisorption of oxygen at the grain boundaries [106]. Since the charge carrier concentration is low in undoped ZnO, the oxygen chemisorption acts as surface acceptor on ZnO film surface and depletes the electrons. It has also been suggested [113] that presence of carbon in ZnO films may lead to chemisorption of oxygen. This may result in CO_2^- or Zn-C-O complex on the surface, which may act as traps of charge carriers. This explanation well describes the resistivity behavior of EDTA derived ZnO thin films. TGA data shows a gradual decrease in weight even at 600°C suggesting presence of organic precursors. Hence, the EDTA derived ZnO thin films when annealed at 600°C shows the highest electrical resistivity due to maximum trapping of electrons.

Based on the experimental data on electrical resistivity, we can conclude that citric acid derived ZnO films are better as conducting electrodes. The high resistivity values may be decreased slightly by increasing the thickness of the films and significantly by annealing in vacuum. Further studies will be carried on the effect of vacuum annealing on electrical resistivity of the polymeric precursor derived ZnO films.

7.5. Conclusions

Nanocrystalline zinc oxide (ZnO) thin films have been deposited by spin coating polymeric precursor solution synthesized by modified Pechini process. ZnO thin films were successfully synthesized by polymeric precursor route using

ethylene glycol, glycerol, citric acid, and ethylene diamine tetraacetic acid (EDTA) as chelating agents for Zn cations. The polymeric precursors were spincoated on glass and silicon substrates and were annealed from 300°C to 600°C. The prepared polymeric precursors and ZnO thin films were analyzed in-depth. All experimental results for ZnO films, derived from glycerol, citric acid, and EDTA based precursors, have been summarized in Table 7.2.

TGA data of the polymeric precursors show that ethylene glycol has the lowest whereas EDTA has the highest pyrolytic temperature. There is a sharp weight loss at around 200°C in case of ethylene glycol based precursor but a gradual decrease is seen even at 600°C for EDTA derived precursors. Surface morphology of the thin films was evaluated by scanning electron microscopy (SEM) and atomic force microscopy (AFM). SEM micrographs of ZnO films illustrate formation of flower-like morphology for ethylene glycol derived polymeric precursor at 300°C whereas there is no formation of ZnO when derived of glycerol, citric acid and EDTA based precursors. ZnO films, derived of glycerol, citric acid, and EDTA based precursors, are nanocrystalline, dense, and crack-free when annealed at 450°C. On annealing at 600°C, the glycerol and citric acid based films show an increase in grain size with increase in annealing temperature. FIB cross-sectional view of these samples annealed at 600°C illustrate that the films have high density.

The average orientation and strain were studied in depth by X - ray diffraction (XRD). XRD results show formation of wurtzite ZnO using ethylene

Table 7.2: Properties of ZnO thin films derived from polymeric precursors

Characte-rization Technique	Property	Annealing Temperature	Polymeric Precursors		
			Glycerol	Citric acid	EDTA
AFM	Grain Size (nm)	450°C	20-30	20-25	30-40
		600°C	30-40	50-60	20-25
	R_{rms} (nm)	450°C	2.19	1.92	14.07
		600°C	3.69	8.74	3.59
FIB	Thickness (nm)	600°C	200	160	130
XRD	Strain (%)	450°C	-1.89	-1.58	-1.28
		600°C	-2.09	-2.46	-1.61
	Texture Coefficient	450°C	1.01	0.83	–
		600°C	0.84	1.19	3.0
UV-Vis	Band edge (nm)	450°C	370	374	374
		600°C	376	376	376
	Transpare-ncy%	600°C	90	90	85
I-V	Electrical Resistivity (Ωm)	450°C	14.2	11.8	10.2
		600°C	297	32	515

glycol at 300°C whereas diffraction peaks of ZnO are observed above 450°C for other precursors. XRD results also illustrate that there is strong preferred orientation of grains along (002) plane for films derived of glycerol polymeric precursor at 450°C. At 600°C, the preferred orientation becomes more pronounced in citric acid and EDTA based ZnO films. XRD data also illustrates existence of compressive strains in these films that increases on increasing annealing temperature. However, EDTA derived ZnO films have relatively less strain as compared to glycerol and citric acid based ZnO films.

Transmission spectra reveal that ZnO thin films do not show absorption edge when annealed at 300°C. On annealing above 450°C, the ZnO films are highly transparent with optical absorption edge shifting to longer wavelengths with increase in annealing temperature. The absorption edge becomes steeper and the transparency also increases.

Electrical resistivity of ZnO films derived from glycerol, citric acid, and EDTA based precursors, annealed at 450°C, is 10-14 Ω-m. When annealed at 600°C, there is a significant increase in resistivity for all precursor derived ZnO films. However, EDTA based films show maximum and citric acid based films show minimum electrical resistivity when annealed at 600°C. This rise in resistivity may be attribute to oxygen chemisorption when annealed at high temperatures in air.

Based on these observations, we can conclude that ethylene glycol based precursor has a low pyrolytic temperature, which is suitable for deposition on polymeric substrates. However, these films form flower-like morphology instead

of smooth crack-free films. So the suitable option would be glycerol based precursors for applications on polymeric substrates. However, these glycerol derived films have a very high electrical resistivity when annealed at 600°C in air. Hence, ZnO films derived from citric acid precursors are ideal as transparent conductors due to relatively low electrical resistivity (31.63 Ω-m) and high transparency (90%) in the visible region. Further research has to be carried out for decreasing the resistivity of glycerol based ZnO films by adding suitable dopants or annealing in vacuum.

CHAPTER 8

SYNTHESIS OF TEXTURED ZINC OXIDE THIN FILMS USING POLYMERIC PRECURSOR PROCESSING

Zinc oxide (ZnO) thin films have been deposited by spin coating polymeric precursor solution synthesized by polymeric precursor route using ethylene glycol as reaction medium and citric acid as chelating agent for Zn cations. The polymeric precursors were spin coated on sapphire substrates and annealed from 400°C to 1000°C. Surface morphology of the thin films was evaluated by field emission scanning electron microscopy (FESEM). FIB cross-sectional view of the samples illustrate that the films are dense. The grain size and thickness of the films increase with an increase in annealing temperature. Crystallinity of the ZnO films was studied by X-ray diffraction (XRD). XRD results illustrate that preferred orientation of grains along (002) plane increase with an increase in annealing temperature and become very pronounced above 800°C. In-plane XRD scans of sample annealed at 1000°C illustrate a strong diffraction peak along [100] suggesting strong preferentially oriented ZnO film. Transmission spectra reveal that the films are 60 - 70% transparent for annealing temperatures 400°C to 900°C. The sample annealed at 1000°C has 45% optical transparency in the visible region. Moreover, it is observed that onset of absorption edge of ZnO thin films remains constant with increase in annealing temperature. Room temperature photoluminescence studies reveal that the PL spectra for temperatures 700°C to 900°C is asymmetric with emission due to coupling of free excitons and longitudinal optical (LO) phonon replicas whereas the spectra of

samples annealed at 400°C and 1000°C, respectively, are symmetric with emission due to annihilation of free excitons. It is observed that the intensity of the PL peaks increases with increase in annealing temperatures due to improvement in crystallinity and increase in grain size of the films.

8.1. Introduction

ZnO thin films are technologically important materials due to innumerable interesting properties exhibited by this material. As a material with band gap of 3.3 eV at room temperature, ZnO is ideal in short-wavelength light emitting or receiving semiconductor devices. These thin films also have potential for electronic device applications requiring transparency in the visible region, high temperature operation, or radiation hardness. Various forms of ZnO, such as, polycrystalline thin films, nanowires, etc have been synthesized based on requirement of application. Epitaxial ZnO thin films are beneficial for developing ultraviolet-blue light emitting diode (LED) and laser diode.

Epitaxial ZnO thin films have been synthesized employing techniques such as pulsed laser deposition [140, 55, 32], molecular beam epitaxy [115, 103, 51, 44, 144] and magnetron sputtering [67]. In all these works, epitaxial ZnO thin films were prepared on *c*-sapphire substrate as it possesses hexagonal symmetry and is cost-effective as a substrate. Film growth was carried at substrate temperature of 700-800°C [67]. However, differences in lattice parameters and thermal expansion between ZnO and sapphire cause difficulties in heteroepitaxy of ZnO thin film on sapphire. The lattice mismatch between ZnO and *c*-sapphire is 18% leading to high dislocation density. Research has also

been carried out to synthesize (002) oriented ZnO thin films by sol-gel process on silica glass substrates [22, 82] and on sapphire by chemical solution deposition [12].

In this paper, we deposit ZnO thin films on sapphire substrates by Pechini process. The polymeric precursor was prepared using citric acid as chelating agent and ethylene glycol as reactive medium, respectively. The prepared polymeric precursors were spincoated on sapphire substrates and were annealed at different temperatures to study the effect of annealing temperature on texturing of films. Surface morphology and crystallinity of the ZnO films were characterized by FESEM and XRD. The transmission and photoluminescence properties of the thin films were also investigated. A detailed study of the effects of annealing temperature on crystallinity, preferential orientation, and microstructure has been carried out.

8.2. Experimental Methods

ZnO thin films were grown on *c*-plane sapphire substrates using polymeric precursor process. Polymeric precursor using citric acid as chelating agent was prepared by following procedure prescribed in [48]. 99% pure zinc nitrate, $Zn(NO_3)_2.xH_2O$ and 99% ethylene glycol (EG) were acquired from Alfa Aesar. 70% nitric acid (HNO_3), ACS grade potassium hydroxide (KOH) pellets, and citric acid (2-hydroxy-1, 2, 3-propanetricarboxylic acid), were acquired from J. T. Baker, EMD chemical Inc., and Fischer Scientific International Inc., respectively. All these chemicals were of analytic - grade and were used as received without further purification. Deionized and filtered water (resistivity = 18.2MΩ) was used

in preparing solutions. *C*-plane sapphire substrates were acquired from Crystal Systems, Inc.

Polymeric precursors for depositing ZnO thin films were prepared using Pechini process. In this process, 0.1 moles of citric acid was dissolved in 50 ml of deionized water. Then 0.1 moles of $Zn(NO_3)_2$ and 0.9 moles of ethylene glycol were added to the aqueous solution. To this solution, 0.1 moles of HNO_3 was added followed by deionized water. The resulting solution was stirred continuously and heated at a constant temperature of 70°C till the final solution was clear, homogeneous, and free from precipitation. The sapphire substrates were cleaned by heating them in furnace at 1000°C for 1 hour. The solution was spincoated (CEE Model 100CB, Brewer Science, Inc.) onto the cleaned substrates at 4000 rpm for 30s. After deposition, the layer was cured at 70°C on a hot plate for approximately 1 hour to remove residual water. The films were then annealed in an ambient furnace for pyrolization of the ethylene glycol and citric acid and oxide formation at different temperatures. The deposition conditions were the same for all samples. A thicker sample was also prepared by spin coating five layers of polymeric precursors followed by curing at 70°C, pre-firing at 300°C after each spin coat, and finally annealing at 800°C. Similarly, another thicker sample was also prepared by spin coating five layers of polymeric precursors with each coating followed by curing at 70°C and pre-firing at 300°C. After two consecutive pre-firing, the film was annealed at 1000°C for 10 minutes. In other words, the ZnO thin film was annealed twice at 1000°C.

X-ray diffraction patterns were obtained on a Rigaku Ultima III model using CuKα radiation (40 kV and 44 mA) in θ-2θ mode in the interval of 25° to 65°. Surface morphology of the ZnO thin films on sapphire were characterized by field emission scanning electron microscopy, FESEM (Nova Nanolab 200, FEI Co.). Variable angle spectroscopic ellipsometer (VASE, J. A. Woollam, Inc.,) was used in transmission mode to determine optical transparency of annealed films of ZnO on sapphire substrates. Scanning spectrofluorometer (Photon Technology International) was used to acquire photoluminescence spectra at room temperature with an excitation wavelength of 340nm using Xenon lamp as an excitation source.

8.3. Results and Discussion

8.3.1. X-ray Diffraction

Fig. 8.1 shows the X-ray diffraction spectra of ZnO thin films on sapphire substrates and annealed at temperatures from 400°C to 1000°C, and 5 layers thick ZnO films annealed at 800°C and twice at 1000°C, respectively. After annealing at 400°C, (100), (002) and (101) diffraction peaks were observed in the XRD pattern (Fig. 8.1a) with no preferential orientation compared to JCPDS. Preferential orientation is calculated from ratio intensities of (002) and (101) planes. Results show that the obtained ZnO thin films possess wurtzite structure (space group $P6_3mc$) and the diffraction peaks can be indexed to hexagonal ZnO (JCPDS No. 36-1451). When the firing temperature was increased to 700°C (Fig. 8.1b), the intensity of (100) and (101) peaks also increased along with (002) peak intensity. This illustrates that there is homogeneous growth in thin film with no

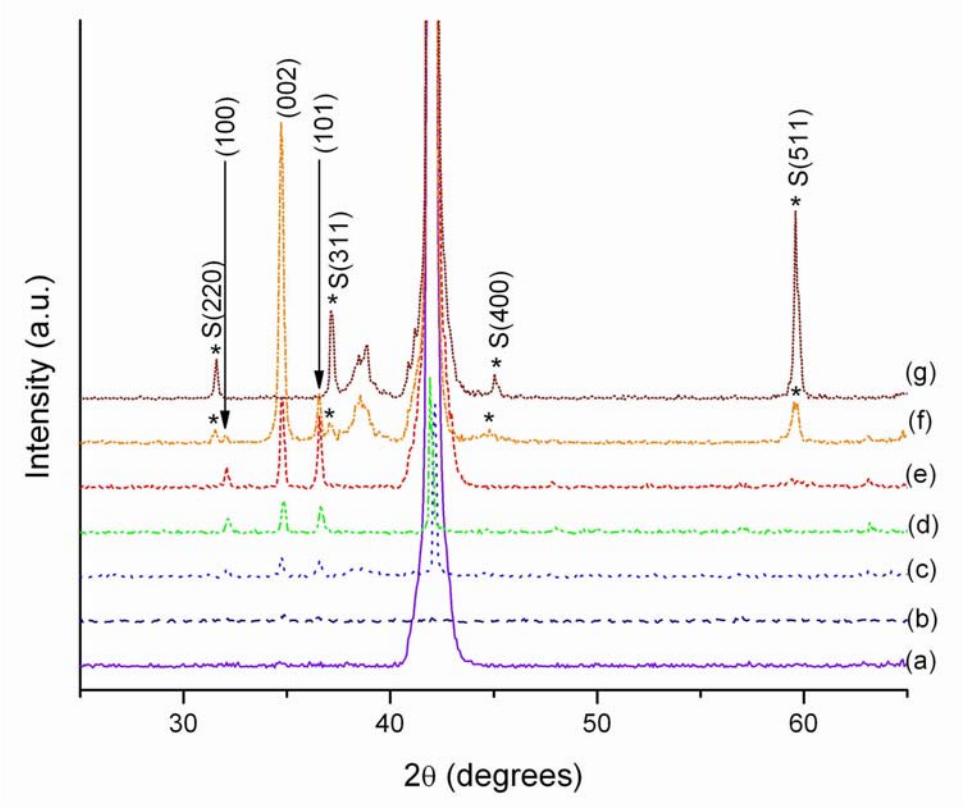

Figure 8.1: X-ray diffraction spectra of polymeric precursor derived ZnO thin films on sapphire substrates and annealed at (a) 400°C, (b) 700°C, (c) 800°C, (d) 5 layers thick sample annealed at 800°C, (e) 900°C, (f) 1000°C, and (g) 5 layers thick film of ZnO annealed twice at 1000°C. Diffraction peaks of spinel $ZnAl_2O_4$ are marked as "*S".

preferential orientation and growth. At 800°C, the intensity of (100), (002), and (101) peaks increases (Fig. 8.1c). Moreover, (002) peak has 4.6% higher intensity than (101) showing preferential orientation. This trend still continues for thicker samples annealed at 800°C (Fig. 8.1d). At the annealing temperature of 900°C, the intensity of (002) increases significantly than (101) and (100) peaks. Three new peaks of ZnO appear corresponding to (102), (110), and (103) planes

(Fig. 8.1e). On annealing at 1000°C, there is marked preferential orientation along the (002) plane of ZnO (Fig. 8.1f). Low intense ZnO peaks corresponding to (100), (101), and (103) planes also exist. Besides, additional peaks appear which do not belong to ZnO. These diffraction peaks can be indexed to zinc aluminate, $ZnAl_2O_4$ (JCPDS No. 05-0669) [141]. The diffraction peaks at 2θ = 31.52°, 37.04°, 44.8°, 59.68°, and 64.8° can be indexed as (220), (311), (400), (511), and (440) planes, respectively. The thick sample, twice annealed at 1000°C, exhibits diffraction peaks, as shown in Fig. 8.1g, corresponding only to spinel $ZnAl_2O_4$. No peaks corresponding to ZnO were formed. The diffraction peak (2θ) positions of ZnO and $ZnAl_2O_4$ samples annealed at 1000°C and their standard JCPDS positions are tabulated in Table 8.1. The diffraction spectra illustrates that there is complete conversion of ZnO thin film on sapphire to $ZnAl_2O_4$ due to solid state reaction on annealing twice at 1000°C. $ZnAl_2O_4$ also shows preferred orientation along the [111].

Preferential orientation in ZnO films can be quantified by calculating texture coefficients defined by [98],

$$T(hkl) = \frac{I(hkl)/I_r(hkl)}{1/n\Sigma(I(hkl)/I_r(hkl))} \quad (18)$$

where n is the number of (hkl) diffraction peaks, I(hkl), and I_r(hkl) are intensities of these peaks in samples with preferential and random orientation, respectively. It is assumed that T(hkl) = 1 for randomly oriented crystallites. Preferential orientation is exhibited if the value of texture coefficient is greater than 1.

Table 8.1: JCPDS and experimental data of diffraction peak positions of ZnO and spinel $ZnAl_2O_4$ at 1000°C.

ZnO			$ZnAl_2O_4$			
(hkl)	JCPDS 2θ	Experimental 2θ at 1000°C	(hkl)	JCPDS 2θ	Experimental 2θ	
					1000°C	Twice annealed at 1000°C
(100)	31.77	32.16	(220)	31.236	31.52	31.6
(002)	34.42	34.72	(311)	36.835	37.04	37.12
(101)	36.25	36.56	(400)	44.807	44.8	45.04
(102)	47.54	–	(331)	49.068	–	–
(110)	56.6	–	(422)	55.656	–	–
(103)	62.96	63.2	(511)	59.342	59.59	59.6
(112)	67.96	–	(440)	65.233	64.8	–

For the samples annealed above 800°C, the intensities of three main diffraction peaks of ZnO, i.e., (100), (002), and (101) planes are used for calculating the texture coefficients using equation 18. When annealed at 800°C, the texture coefficients are obtained as T(100) = 0.679, T(002) = 1.619, and T(101) = 0.702. For samples annealed at 900°C, the texture coefficients calculated are as follows: T(100) = 0.394, T(002) = 1.878, and T(101) = 0.727. Texture coefficients for sample annealed at 1000°C were calculated as: T(100) = 0.046, T(002) = 2.737, and T(101) = 0.215. There is distinct preferential crystallite orientation along the (002) plane. We also observe that the texture

coefficients are less than 1 for (100) and (101) planes and these decrease further with increase in annealing temperatures.

Texturing can also be determined by finding the ratio of intensities of (002) and (101) planes using the following equation:

$$T(002) = \frac{I(002)}{I(101)} \tag{19}$$

where I(002) and I(101) are intensities of diffraction peaks in samples annealed at different temperatures, respectively. We observed that the texturing increased with increase in annealing temperature, which is also displayed in Fig. 8.2. The plot illustrates a gradual increase in texturing for temperature range 400°C to 900°C. On annealing to 1000°C, there is a drastic increase and most of the grains of ZnO films are preferentially oriented along the (002) plane but also converted to spinel. Hence, from the diffraction spectra, we can conclude that ZnO thin films annealed above 800°C exhibit distinct preferential orientation.

Although sapphire is used as substrate for epitaxial ZnO films, there is 18% lattice mismatch between the film and the substrate leading to strain in the ZnO films. We have calculated strains in our films from the XRD spectra using Williamson-Hall Plot for each annealing temperature. In a Williamson-Hall Plot, the effect of microstrain and broadening due to crystallite size can be separated. FWHM is calculated as [8],

$$FWHM \times \cos\theta = \frac{0.9\lambda}{t} + 2\frac{\Delta d}{d}\sin\theta \tag{20}$$

where θ is the peak position and FWHM is the integral breadth for the peak position. Using equation 20, a linear plot of FWHM*cosθ and sinθ is drawn. The

values of 2θ and FWHM are shown in Table 8.2. We can then determine strain, Δd/d, from the slope of the graph and calculate crystallite size, t, from the intercept.

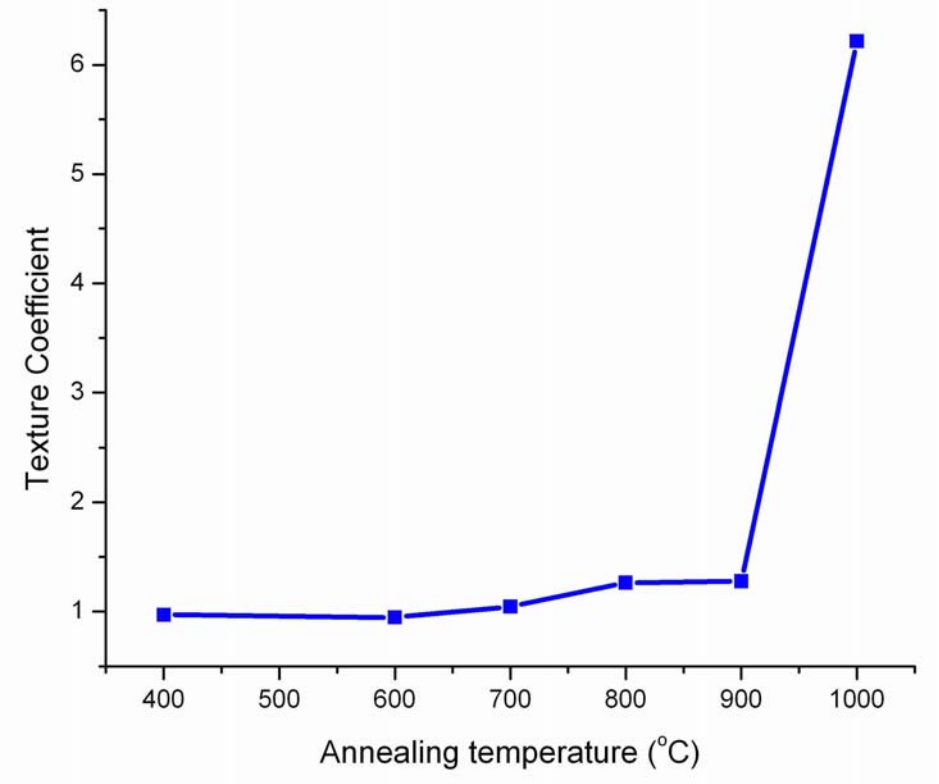

Figure 8.2: Change in preferential orientation with annealing temperature. This plot illustrates that texturing of ZnO films along (002) plane increases with increase in annealing temperature.

Table 8.2 shows that there is no particular trend in change in values of 2θ and FWHM. For each annealing temperature, we analyzed Williamson-Hall plots, which was plotted using (100), (002), and (101), to calculate strain. However, we did not get a linear plot. Therefore, we did not use Williamson-Hall plots, as it was error prone.

Table 8.2: 2θ and FWHM of diffraction spectra of ZnO thin films at different annealing temperatures.

Annealing Temperature (°C)	2θ			FWHM (degrees)		
	(100)	(002)	(101)	(100)	(002)	(101)
400	32.06 (±0.482)	34.77 (±0.716)	36.73 (±0.565)	0.36	0.66	0.79
700	32.26 (±0.057)	34.686 (±0.067)	36.53 (±0.078)	0.45	0.36	0.56
800	32.11 (±0.041)	34.75 (±0.012)	36.59 (±0.002)	0.18	0.13	0.19
900	32.06 (±0.59)	34.75 (±0.03)	36.55 (±0.085)	0.15	0.16	0.15
1000	32.16 (±0.59)	34.73 (±0.026)	36.56 (±0.59)	0.11	0.20	0.14

We calculated strain in films along the *c*-axis, as shown in Table 8.3, using the following equation [79]:

$$\varepsilon_Z = (c - c_o)/c_o \times 100\% \quad (21)$$

where c_o is 0.5204 nm, the strain-free lattice parameter measured from ZnO powder.

We observe that samples annealed at 400°C show compressive strain of -0.92% that may be due to initial film shrinkage occurring on pyrolization of

Table 8.3: Calculation of strain in ZnO films at different annealing temperatures.

Annealing Temperature (°C)	2θ (degrees)	d-spacing (nm)	C (nm)	Strain, ε_Z = $(c–c_o)/ c_o*100\%$
400	34.77(±0.716)	0.2578	0.5156	-0.92
700	34.68(±0.067)	0.2584	0.5168	-0.69
800	34.75(±0.012)	0.2579	0.5158	-0.88
900	34.75(±0.003)	0.2580	0.5160	-0.85
1000	34.72(±0.026)	0.2581	0.5162	-0.81

organic precursors. However, on annealing at 700°C, there is huge change in strain values and the value of strain changes to -0.69%. This indicates that there is grain growth leading to decrease in compressive strains. Compressive strain increases to -0.88% on annealing at 800°C which may be due to difference in coefficients of thermal expansion between the ZnO films and the sapphire substrates. It has been reported that thermal expansion coefficients of ZnO and sapphire along *a*-axis are 6 – 8 x 10^{-6}/K [16] and 6.3 x 10^{-6}/K [101], respectively. Moreover, there is significant grain growth and texturing at this temperature, which also contributes to the compressive strains. Thereafter, there is incremental decrease in compressive strain on annealing above 900°C. This suggests that the grain growth progressively increases causing decrease in compressive strains in the film. Moreover, the decrease in strain when annealed above 900°C may be attributed to formation of new phase, $ZnAl_2O_4$. XRD spectrum also shows that a new phase, $ZnAl_2O_4$ forms at 1000°C. The formation

of spinel structure, as a buffer layer, at the interface of sapphire substrate and ZnO film helps in reduction of compressive strain. A plot of the various changes in strain with annealing temperature is shown in Fig. 8.3. All the samples exhibit compressive strains, which differs from that observed in [99] where a tensile strain of 0.1% is reported for ZnO film on sapphire substrate.

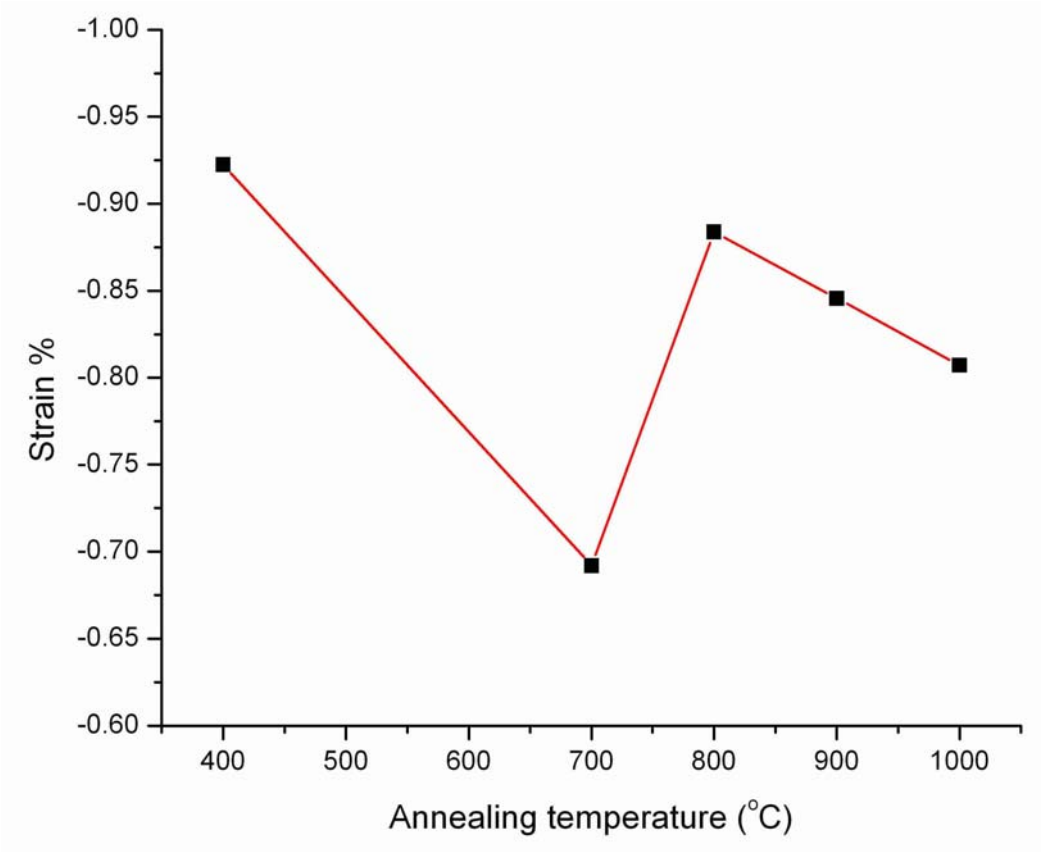

Figure 8.3: Change in strain observed in ZnO films along *c*-axis with annealing temperature. This plot illustrates that strain in ZnO films is compressive which changes with increase in annealing temperature.

On calculating the crystallite size using Scherrer's equation, we find that there is an increase in crystallite size with increase in annealing temperature.

The crystallite size increases from 14 nm to 29 nm when annealing temperature increases from 400°C to 700°C. There is a significant increase in crystallite size (240 nm) when annealed at 800°C after which the crystallite size decreases as shown in Fig. 8.10. We have also shown the crystallite sizes, for each annealing temperature, as determined by FESEM to have a comparative view. There is discrepancy between the values calculated by Scherrer's equation and those measured from FESEM micrographs. This may be due to strain in films, which

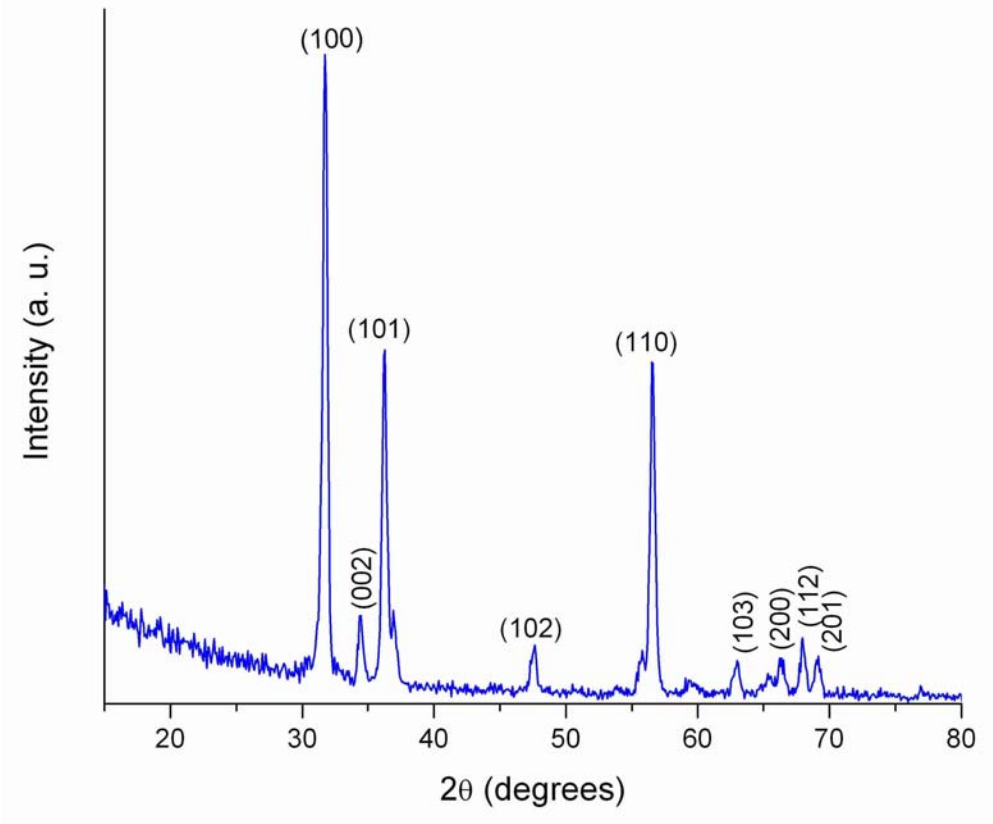

Figure 8.4: In-plane X-ray diffraction spectra of polymeric precursor derived ZnO thin films on sapphire substrate and annealed at 1000°C. The spectra shows a strong [100] diffraction peak in this in-plane scan.

has not been taken in account while calculating crystallite sizes.

In-plane ($2\theta_\chi/\phi$) measurements of the ZnO thin annealed at 1000°C and 5 layers thick film annealed twice at 1000°*C* were carried out. The measurement of in-plane scans is achieved by rotating the detector in equatorial direction. In other words, the detector collects data for in-plane measurements perpendicular to the sample surface. Fig. 8.4 shows in-plane XRD scan obtained for ZnO thin film on sapphire and annealed at 1000°C. The spectrum shows a strong (100) diffraction peak in-plane. This also confirms that there is preferential orientation along [001] and all grains are along the basal planes of the ZnO thin film. Thick ZnO film annealed twice at 1000°C was also characterized by in-plane ($2\theta_\chi/\phi$) scans. The diffraction spectrum (Fig. 8.5) shows that there is preferred orientation along [110]. There are no peaks related to ZnO confirming the formation of spinel $ZnAl_2O_4$.

From the XRD spectra, we can conclude that there is rise in intensity of peaks with an increase in annealing temperature suggesting improvement in crystallinity of ZnO. Preferred orientation in ZnO thin films along (002) increase as annealing temperature increases. Moreover, there is noticeable increase in preferred orientation along (002) plane at 800°C which differs from that reported in [12] where texturing was observed only at 850°C and on annealing for extended period of time. Texturing increased significantly when annealed at 1000°C with $ZnAl_2O_4$ formation also. This suggests that spinel formation starts on annealing at 1000°C. When the sample is annealed twice at 1000°C, there is reaction between ZnO and Al_2O_3 (sapphire substrate) resulting in formation of

$ZnAl_2O_4$. Hence, we need to anneal no higher than 900°C for obtaining preferentially oriented ZnO thin films. When ZnO and Al_2O_3 powders were mixed together and annealed at 700°C XRD data showed diffraction peaks

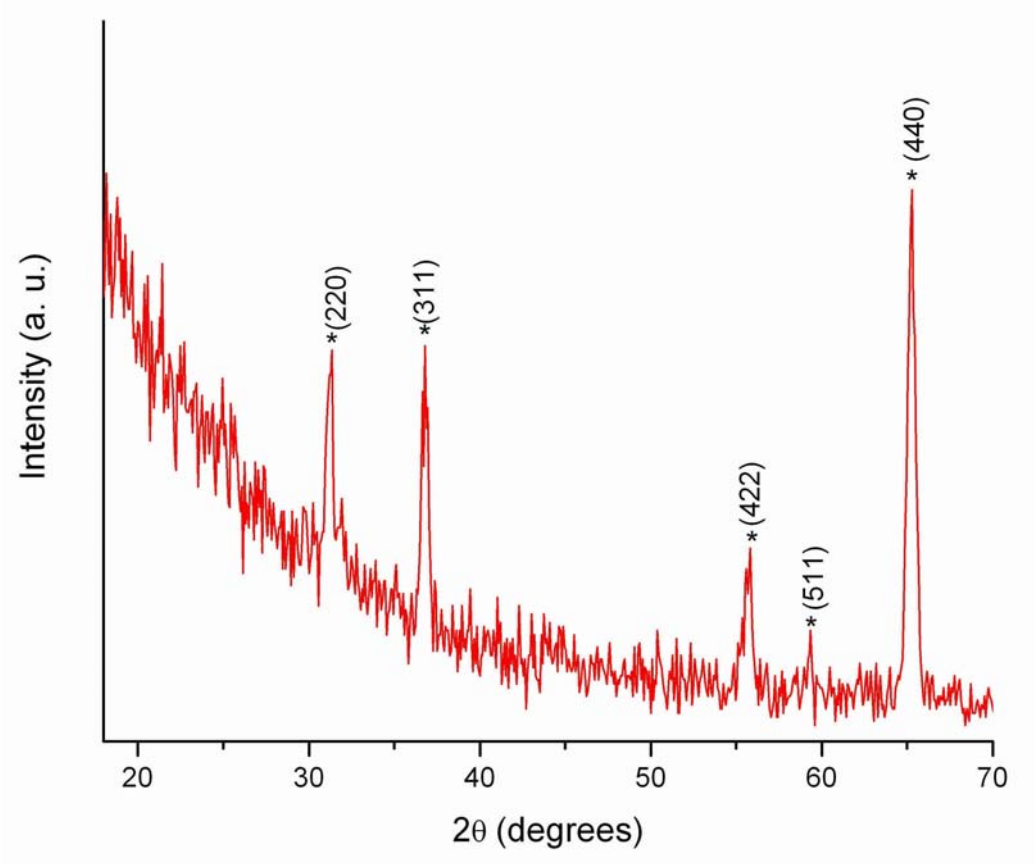

Figure 8.5: In-plane X-ray diffraction spectra of polymeric precursor derived 300 nm thick ZnO film on sapphire substrate and annealed twice at 1000°C. The spectra shows a strong [110] diffraction peak in-plane XRD scan.

corresponding to spinel $ZnAl_2O_4$ [12]. Hence, it is suggested that ZnO film and sapphire substrate begin to react at 700°C. Therefore, further studies on the lattice matching and extent of reaction between the ZnO film and sapphire substrate by HRTEM are under way.

8.3.2. Scanning Electron Microscopy

Annealing temperature is an important factor to grow high-quality epitaxial films. Effect of annealing temperature on surface morphology of ZnO thin films were observed by FESEM. Fig. 8.6, 8.7, 8.8 show micrographs of ZnO thin films spincoated on sapphire substrates and annealed at temperatures from 400°C to 1000°C, respectively. The sample annealed twice at 1000°C was also characterized by FESEM (Fig. 8.8b). These micrographs illustrate that there is an increase in grain size with increase in annealing temperature. Samples annealed at 400°C (Fig. 8.6a) reveal smooth crack free polycrystalline film with grain size of 15 nm. When annealed at 700°C, the grain size of ZnO films increases to 30 nm at 700°C. The films have a dense spherical microstructure with no cracks (Fig. 8.6b). The shape of microstructure changes drastically when annealed at 800°C. At 800°C (Fig. 8.7a), the grains are faceted, have polyhedral shapes and the size varies between 40-65 nm. As the annealing temperature is increased to 900°C (Fig. 8.7b), all the grains are highly faceted and their size range varies from 70-95 nm. SEM micrographs also illustrate that the ZnO films are formed of a layer of these faceted grains exhibiting island formation. All these grains are connected together to form a porous layer through which the sapphire substrate is visible. As demonstrated in [12], epitaxial ZnO films were formed when annealed at 900°C by the presence of 120° faceted grains shown in Fig. 8.7b. When annealed at 1000°C (Fig. 8.8a), there is abnormal grain growth leading to a huge variation in grain size and shape. Almost all the grains are faceted with size of some grains increasing drastically to 150-350 nm. These larger grains

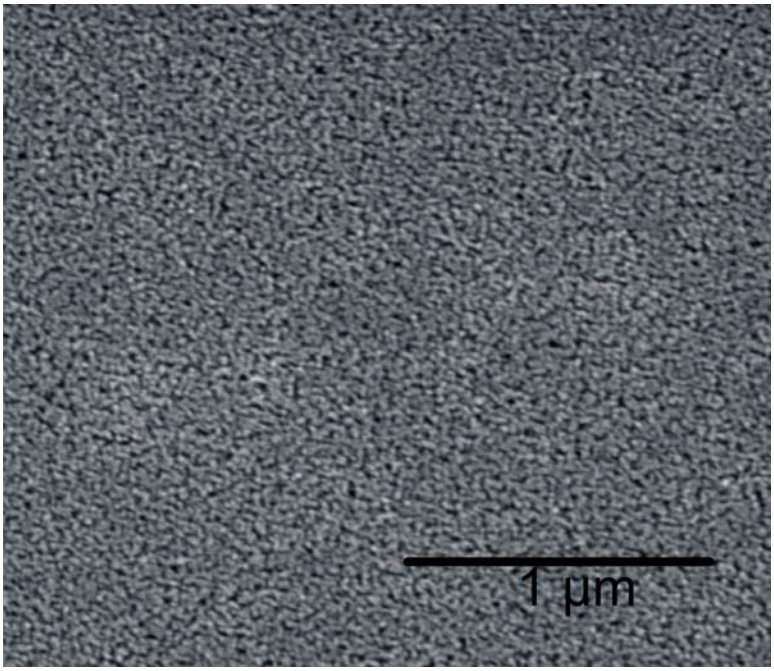

(a)

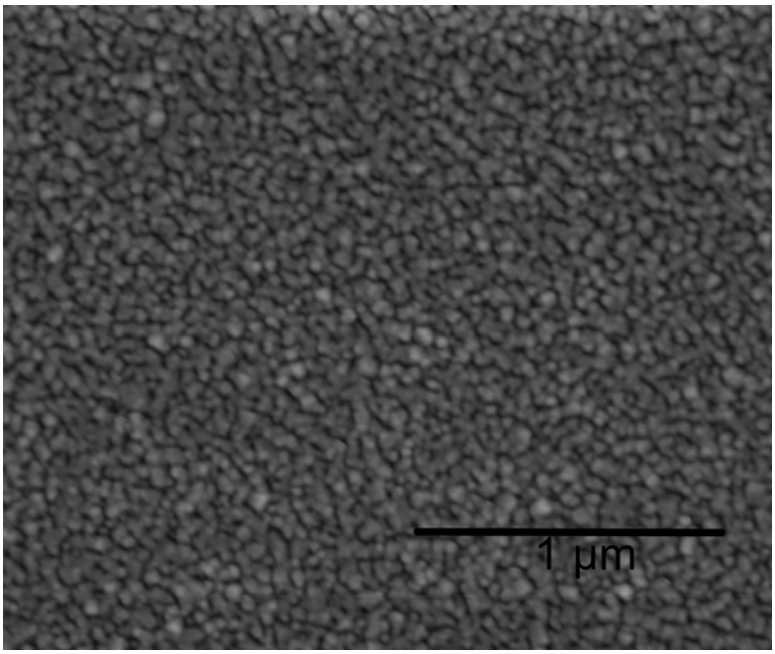

(b)

Figure 8.6: SEM micrographs of precursor derived ZnO thin films on sapphire substrate and annealed at (a) 400°C and (b) 700°C.

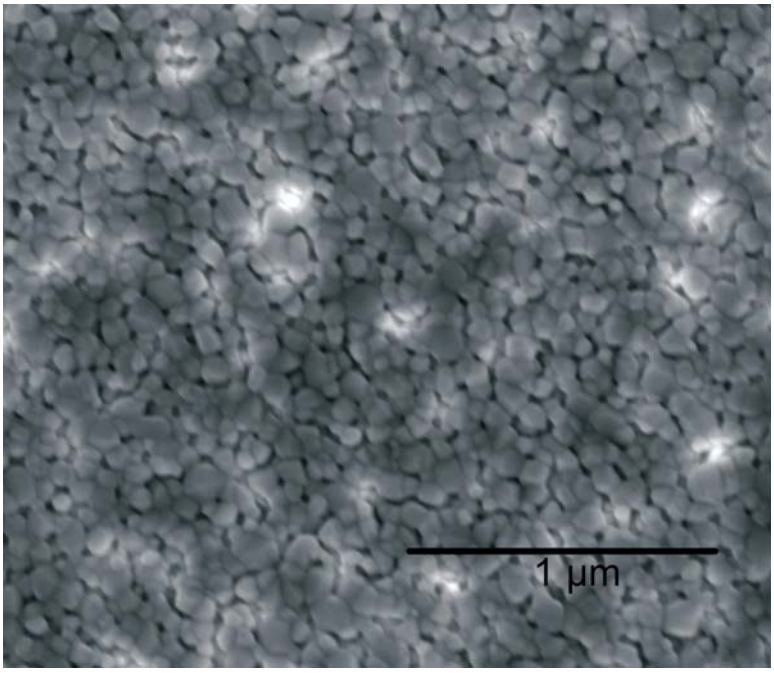

(a)

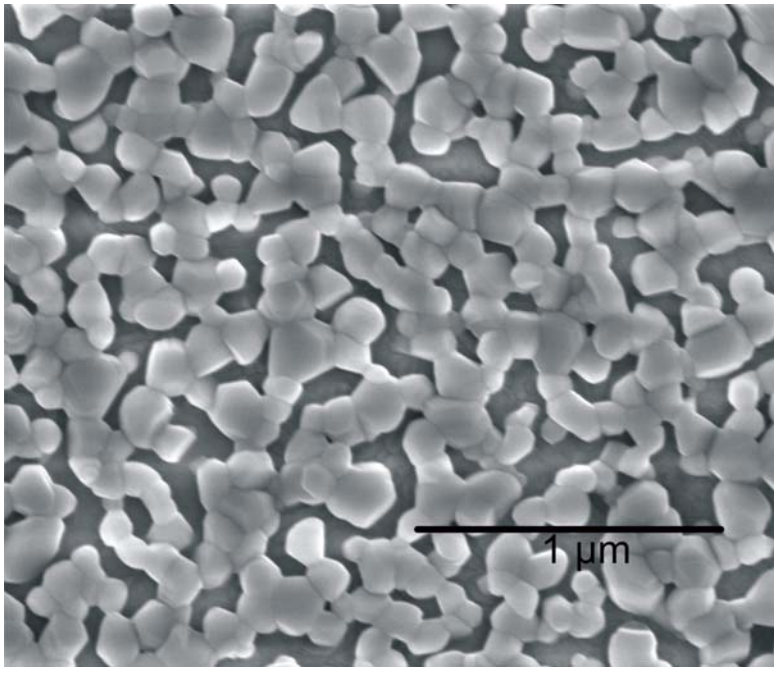

(b)

Figure 8.7: SEM micrographs of precursor derived ZnO thin films on sapphire substrate and annealed at (a) 800°C and (b) 900°C.

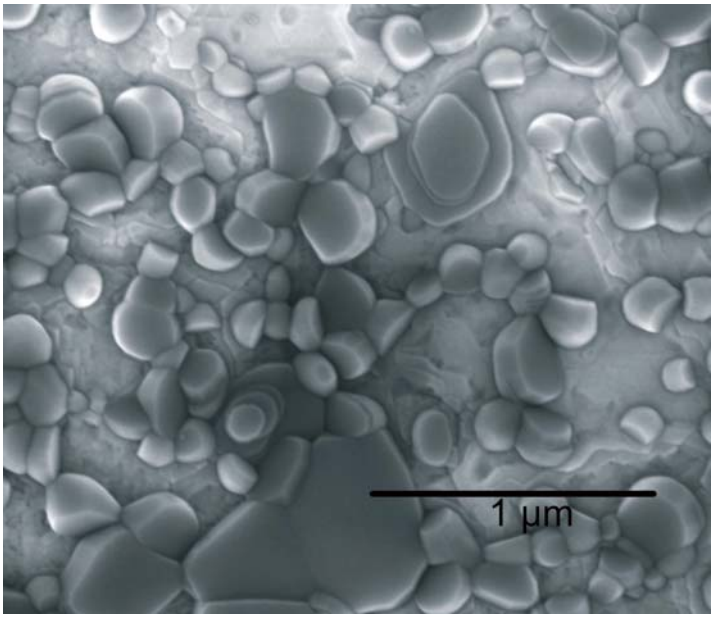

(a)

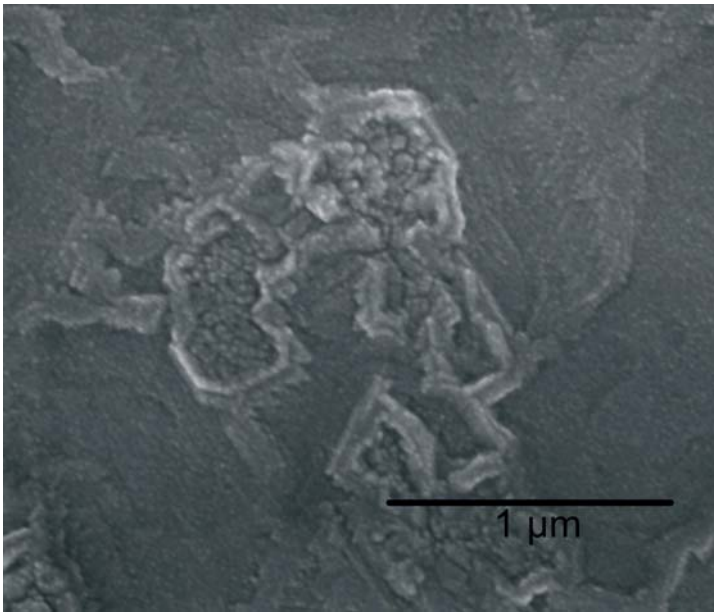

(b)

Figure 8.8: SEM micrographs of precursor derived ZnO thin films on sapphire substrate and annealed at (a) 1000°C and (b) thicker layer of ZnO annealed twice at 1000°C.

have special orientation; they appear flat on the substrate and initiate abnormal grain growth, which results in a multilayered hexagonal structure. The smaller grains, of 60-90 nm, appear to be hemispherical with faceted circumference. SEM micrographs of 5 layer thick ZnO film, which was twice annealed at 1000°C, reveal a distinct change in microstructure. The films do not appear granular as in previous cases but is a relatively smooth uniform film with few lines forming random shapes. Similar surface morphology has also been observed in previous work [154]. Change in grain size of ZnO thin films on sapphire substrate with annealing temperature is shown in Fig. 8.10. The error in measurement was determined using standard differential error analysis.

FIB cross-section micrographs of ZnO thin films annealed at different temperatures are shown in Fig. 8.9. As can be seen, the films annealed at 400°C (Fig. 8.9a) have grains arranged randomly with film thicknesses of 70 nm. The film annealed at 800°C illustrates a highly dense columnar film with coalescence of all grains (Fig. 8.9b). Thickness of this film has been measured, using FEI Co. software, to be 140 nm. Significant grain growth occurs at this temperature to minimize surface and strain energies, which in turn, depend on crystallographic orientations of the grains. In order to achieve this, the grains orient in such a manner so as to reduce energies at the surface but also within the volume leading to columnar film [147]. The sample of 5 layer thick ZnO film annealed twice at 1000°C was also characterized by FIB cross-section. The cross-sectional micrographs reveal variation of thickness from 200-400 nm. These films show two distinct layers. We can conclude that the thickness as well as density

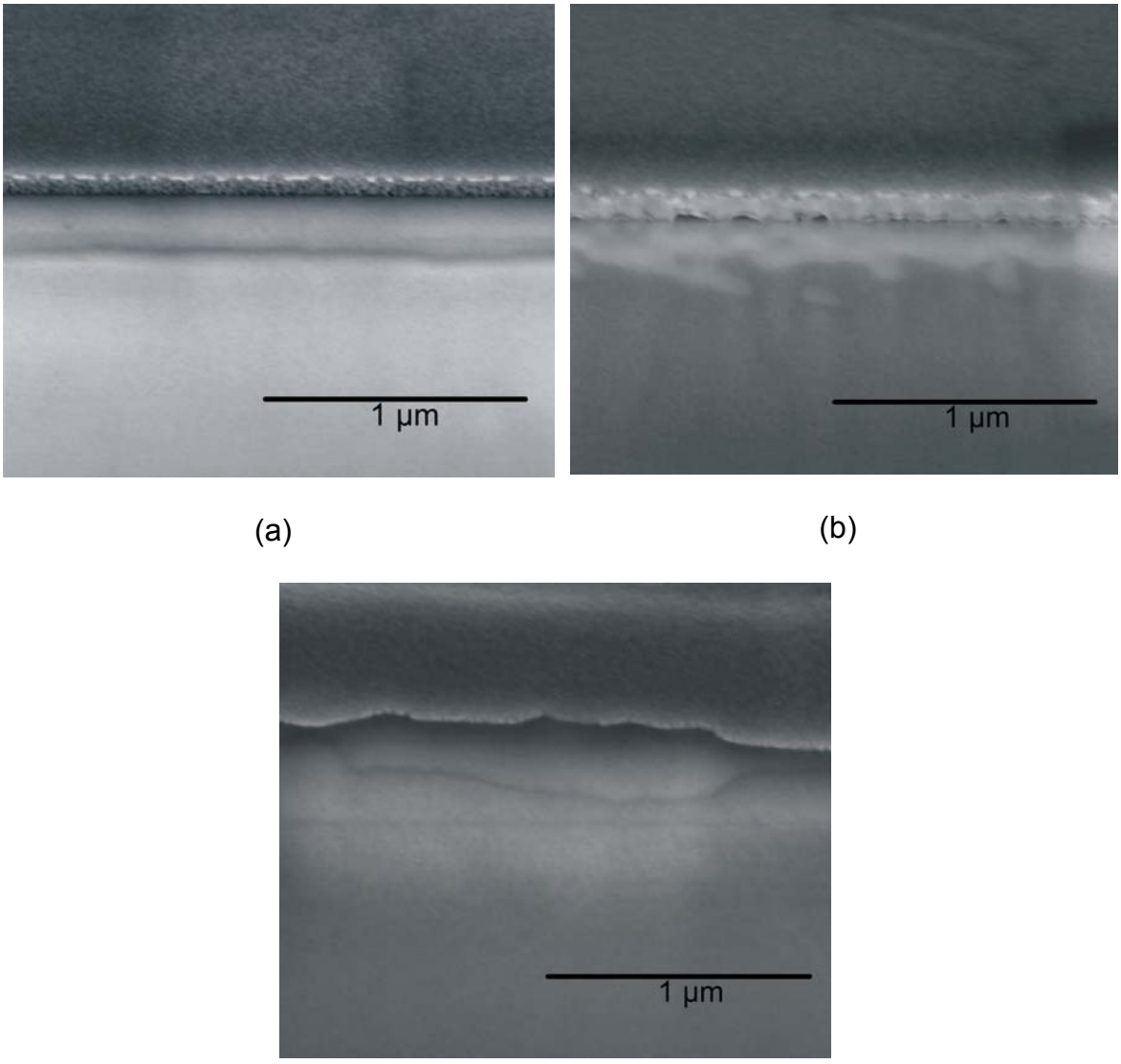

(a) (b)

(c)

Figure 8.9: SEM micrographs of FIB cross-section of precursor derived ZnO thin films on sapphire substrate and annealed at (a) 400°C, (b) 800°C, and (c) 5 layers of ZnO annealed twice at 1000°C.

of ZnO films increases with increase in annealing temperature.

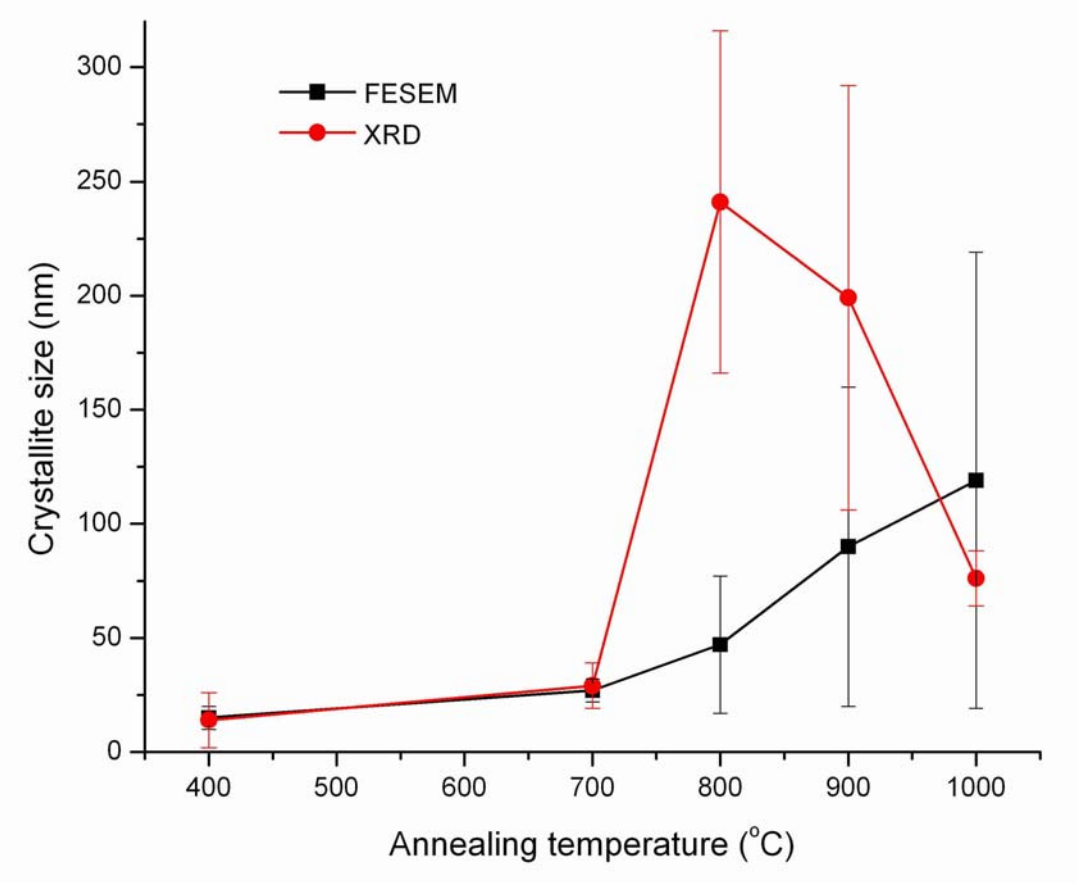

Figure 8.10: Change in grain size of the ZnO thin films with annealing temperature as measured by FESEM and calculated using Scherrer's equation.

8.3.3. Optical Properties of ZnO Thin Films

8.3.3.1. Transmission Measurements

UV-Vis transmission spectra in the wavelength range 260 - 800 nm of ZnO thin films on sapphire substrate prepared at different annealing temperatures is shown in Fig. 8.11. All the films exhibit transmittance in the visible region. It is seen that the transmittance increases from 65% to 80% with increase in annealing temperature from 400°C to 700°C. Thereafter the transmittance remains constant for samples annealed at 900°C and 5 layers thick ZnO film

annealed at 800°C. ZnO thin film annealed at 1000°C shows a decrease in transmittance in the visible region. On annealing 5 layers thick ZnO film twice at 1000°C, the sample does not exhibit any band edge corresponding to ZnO. This fact confirms the XRD result that shows formation of $ZnAl_2O_4$. Except for the 5 layer thick ZnO film annealed twice at 1000°C, all samples illustrate sharply decreasing transmittance in the UV region because of the onset of absorption. All these samples have band edge at 376 nm except for samples annealed at 800°C

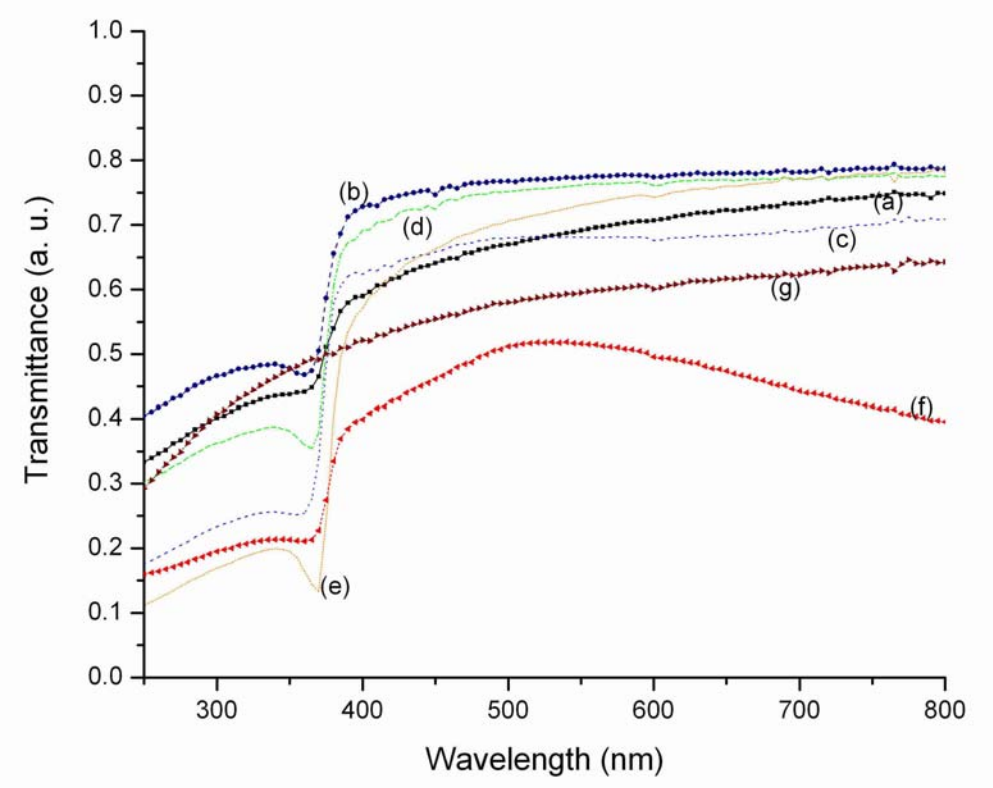

Figure 8.11: UV-Vis transmission spectra of ZnO thin films at different annealing temperatures: (a) 400°C, (b) 700°C, (c) 800°C, (d) 5 layers thick sample annealed at 800°C, (e) 900°C, (f) 1000°C, and (g) 5 layers thick sample twice annealed at 1000°C.

and 900°C, respectively. The sample annealed at 800°C has a band edge at 374 nm whereas the sample annealed at 900°C has band edge at 378.5 nm. The shift in wavelength for sample annealed at 900°C may be attributed to change in crystallite size. We also observe that the slope of the band edge becomes relatively sharp as the annealing temperature increases from 400°C to 1000°C. The band edge of all ZnO thin films has been tabulated in Table 8.4.

8.3.3.2. Photoluminescence

Fig. 8.12 illustrates the room temperature photoluminescence spectra of ZnO thin films on sapphire substrates under photon excitation of 340 nm. A strong and broad UV emission dominates the photoluminescence spectra, the energy of which agrees with published literature [114, 138]. This near band edge emission is sharp and asymmetric with a tail on the lower energy side for samples annealed at temperatures 700°C to 900°C. The UV emission may be attributed to the radiative annihilation of excitons near band edge as ZnO has exciton binding energy of 60 meV at room temperature [58, 108].

We observe that ZnO film annealed at 400°C has UV emission at 376 nm (3.3 eV) (Fig. 8.12a) which corresponds to the absorption onset of bulk ZnO. The ZnO film annealed at 700°C (Fig. 8.12b) shows a broad UV emission peak with intensity weaker than that of 400°C. A Gaussian fit to this spectrum (Fig. 8.13a) illustrates that the spectrum has two overlapping UV emission peaks at 380 nm and 400.5 nm. Similarly, the films annealed at 800°C, both single and five layered films (Fig. 8.12c and d), show a broad peak due to two overlapping UV

emission peaks (Fig. 8.13b and c). Gaussian fits to these spectra illustrate that the peak positions are at 380 nm and 403 nm for 800°C and at 383.5 nm and

Table 8.4: Photoluminescence peak positions and band edge of ZnO thin films on sapphire annealed at different temperatures.

Annealing temperature (°C)	Wavelength (nm)	
	PL spectra	Transmission spectra
400	376	376
700	380, 400.5	376
800	380, 403	374
800 (5 layers)	383.5, 400	376
900	380	378
1000	377	376
1000 (5 layers)	–	–

400 nm for 5 layers thick film annealed at 800°C. The ratio of the intensities of the two peaks reveals that the peak around 380 nm is more intense for all three samples under consideration. Due to increase in thickness of five layered film, there is an increase in intensity for ZnO films when annealed at same temperature, 800°C. In these spectra, there is a shift in position of photoluminescent peaks to higher wavelengths, which may be due to the compressive strain in the films owing to thermal expansion mismatch and grain growth. On annealing at 900°C, the ZnO film exhibits only one highly intense UV

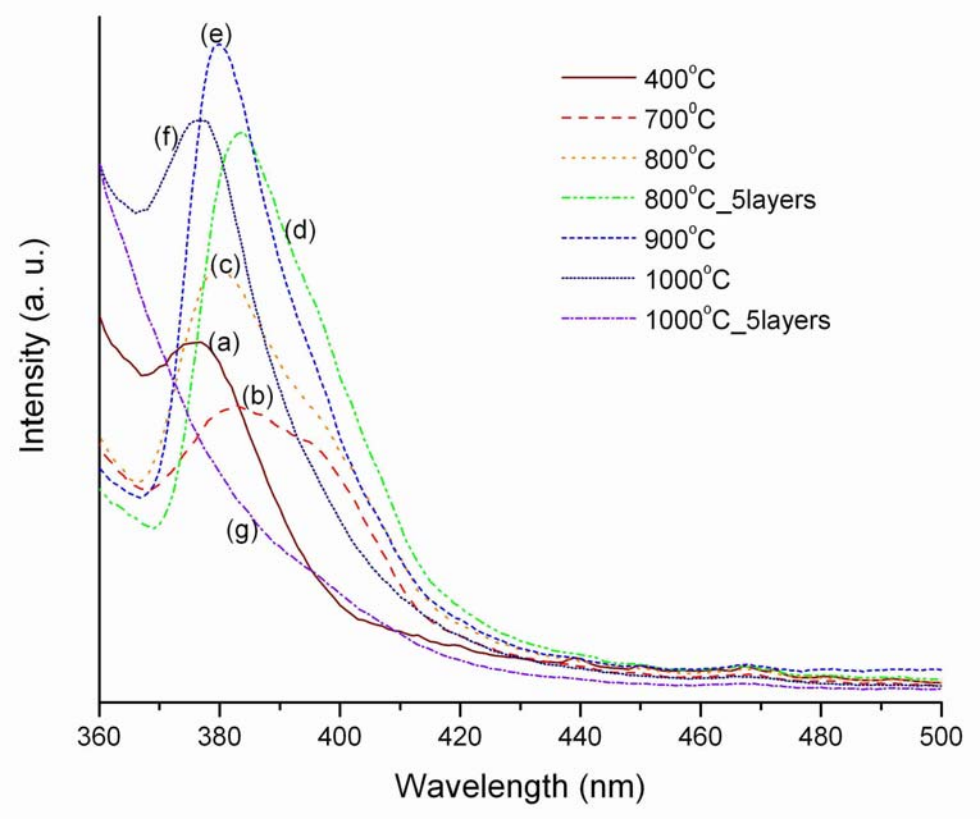

Figure 8.12: Room temperature photoluminescence spectra of ZnO thin films spincoated on sapphire substrates at different annealing temperatures: 400°C - 1000°C.

emission peak at 380 nm (Fig. 8.12e). ZnO film annealed at 1000°C has UV photoluminescent peak at 377 nm (Fig. 8.12f). This shift in peak to lower wavelength can be attributed to decrease in strain in films due to formation of spinel phase. Thicker ZnO film annealed twice at 1000°C does not show any emission confirming that ZnO is not present in the film (Fig. 8.12g). There is no deep level emission, which is usually present in the blue-green region. This suggests that the prepared ZnO thin films are of high crystallinity. From this photoluminescent data, we can illustrate that the intensity of the UV emission

peak increases with increase in grain size and the position of the peak shifts with change in strain in the ZnO films.

It has been found that the room temperature photoluminescence of ZnO thin films has been dominated by free exciton longitudinal optical (LO) phonon replica emissions [134]. In other words, there is simultaneous emission of photons and phonons during the annihilation process of free excitons [134]. In this work, we find that the sample annealed at 400°C has emission at 3.3 eV (376 nm) corresponding to room temperature free exciton peak position [27]. As the annealing temperature is increased to 700°C, there is a slight peak shift to lower energy (3.269 eV) coinciding exactly with the emission of 1LO phonon replica of free excitons. The Gaussian fit to these spectra reveals overlap of 2 peaks (Fig. 8.13). These peaks originate from the emission of free exciton phonon replicas. For samples annealed at 800°C, the most intense peak is at 1LO energy and intensities of higher order of phonon replicas become weaker. On increasing the annealing temperature to 900°C, photoluminescent spectra illustrates a decrease in intensity of the peak at 400 nm. The photoluminescent peak has an asymmetric shape due to the contribution to emission of these higher order phonon replicas. In [134], intensities of LO phonon emission decreased with increase in data collection temperature. We observe a similar trend for room temperature photoluminescence for ZnO thin films on sapphire annealed at different temperatures. Moreover, we observe that the PL peak of 1000°C annealed samples is symmetric in shape suggesting that there is no phonon-assisted emission, which may be due to presence of spinel phase.

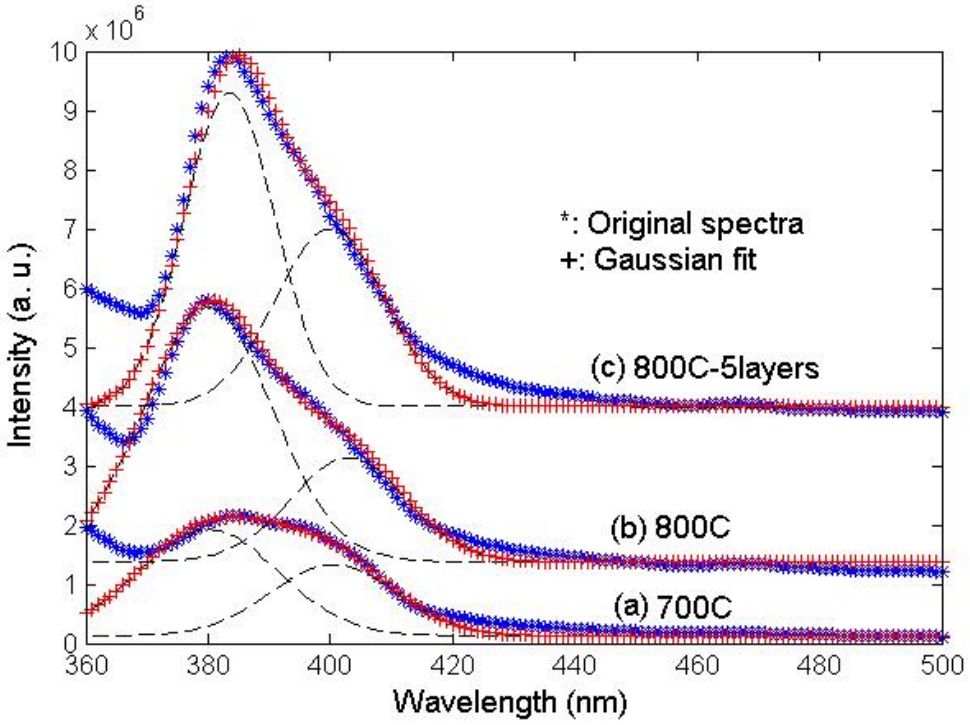

Figure 8.13: Gaussian fit to room temperature photoluminescence spectra of annealed ZnO thin films on sapphire substrates at temperatures: (a) 700°C, (b) 800°C, and (c) 5 layers thick film annealed at 800°C. The *(blue) curve is the original spectra and the +(red) curve is the Gaussian fit. The spectra have been shifted vertically for clarity.

Hence, the LO phonon exciton coupling between temperatures of 700°C to 900°C confirms superior quality of ZnO formed.

8.4. Conclusions

ZnO thin films have been synthesized by spin coating polymeric precursor method on sapphire substrates. The polymeric precursor was prepared using citric acid and ethylene glycol as chelating agent and reaction medium, respectively. The thin films were annealed at various temperatures, namely

400°C to 1000°C. XRD data for ZnO thin films show that the synthesized films have wurtzite structure when annealed at 400°C and higher temperatures. Diffraction spectra illustrates that there is preferred orientation along (002) plane. With increase in annealing temperature, the texturing along (002) also becomes highly pronounced with the maximum at 1000°C. It is also observed that on annealing at 1000°C, there is formation of spinel $ZnAl_2O_4$. When a five layered ZnO thin film was annealed twice at 1000°C, there is complete transformation of ZnO to $ZnAl_2O_4$ due to solid state reaction between the ZnO film and Al_2O_3 substrate. SEM micrographs illustrate that the ZnO based thin films are smooth, dense, and have crack - free microstructures. The images also reveal increase in grain size with annealing temperature, which can be attributed to grain growth. It has been observed that an increase in annealing temperature improved film crystallinity and changed shape of grains from spherical to faceted grains. Transmission spectra illustrates that the ZnO films have high transparency (70%) in the range 500 - 800 nm. The band edge has been determined to be at 376 nm that remains almost constant for different annealing temperatures. Room temperature photoluminescent studies reveal that the photoluminescence is mostly due to coupling between free excitons and longitudinal optical (LO) phonon replicas. The spectra illustrates that the photoluminescent peak is located at free exciton-1LO energy and its intensity increases with increase in annealing temperature. This may be attributed to an increase in crystallinity and preferential orientation of the ZnO film. The peaks due to (LO) phonon replicas are noticeable at annealing temperatures of 700°C to 900°C. However, the

intensities of emission of the higher order phonon replicas decrease with an increase in annealing temperature giving an asymmetrical shape to PL peak. PL peak position for 400°C and 1000°C annealed samples, respectively, appear at lower wavelengths than for samples of 700°C to 900°C. This may be due to smaller crystallite size or due to presence of spinel phase.

CHAPTER 9

MASKLESS DEPOSITION OF ZINC OXIDE FILMS

Maskless Mesoscale Materials Deposition (M^3D^{TM}) is a new direct write technique, which is versatile enough to deposit all kinds of precursors and colloidal suspensions. It is a simple and convenient process for rapid prototyping of structures and components. This maskless deposition method operates in air and at room temperature. In this study, glycerol based polymeric precursor was used for depositing ZnO thin films on surface modified glass substrates. The parameters for deposition using M^3D^{TM} were thoroughly examined and optimized.

9.1. Introduction

ZnO is II-VI wide band gap semiconductor with important technological applications in the areas of transparent conducting electrodes in solar cells, and in flat panel displays as a low voltage phosphor [68, 80, 62]. ZnO has a large exciton binding energy (60 meV) which provides efficient exciton emissions at high temperatures. These properties of ZnO have applications in ultraviolet light emitting diodes and laser devices [76]. ZnO is also used in synthesis of planar waveguides [87].

In [87], the authors used photolithography and wet chemical etching methods to fabricate Er-doped ZnO planar waveguide structures. These methods are expensive, highly inconvenient and can be averted by direct write technologies [21]. The direct write methods are technologically important for fabricating mesoscale components, such as resistors, etc, directly on the substrates producing prototypes without the use of masks. Different direct write

processes, such as, laser direct writing [118, 49, 15] and ink-jet printing [135] can deposit desirable patterns in a single step. Maskless Mesoscale Materials Deposition (M^3D^{TM}), being commercialized by Optomec Inc., and is also a method that can be developed into a high volume component manufacturing technique [41].

Maskless Mesoscale Materials Deposition (M^3D^{TM}) is an aerosol-based technology for deposition of various materials with particle sizes less than 0.5 μm. To date, barium titanate, metallic contacts like Au, Ag, Cu and Pt [102], and biological materials [41] on various substrates have been deposited using this process. In this method, patterns of sub-micron sized aerosol droplets of molecular precursors and colloidal suspensions are deposited with ease. The desired patterns are drawn using CAD software, which can be conveniently converted into CAM tool-paths. This enables rapid prototyping of components. In this direct write technology, the precursors or colloidal dispersions are atomized pneumatically or ultrasonically. The atomized particles are guided and deposited onto substrate surfaces through use of carrier gas.

In this paper, patterned ZnO films have been deposited by M^3D^{TM} technology. A specific goal of this work was to deposit continuous ZnO lines using a pneumatic configuration. Parameters affecting the quality of deposition of polymeric precursor aerosols, such as, rate of atomization, carrier gas flow rates, viscosity of precursors, were optimized. An attempt was made to measure the electrical resistivity of the deposited patterns.

9.2. Experimental Methods

All chemicals were of analytic - grade and were used as received without further purification. 99% pure zinc nitrate, $Zn(NO_3)_2.xH_2O$ and 99% glycerol were obtained from Alfa Aesar. 70% nitric acid (HNO_3) and ACS grade potassium hydroxide (KOH) pellets, were acquired from J. T. Baker and EMD chemical Inc., respectively. Deionized and filtered water (resistivity = 18.2MΩ) was utilized in preparing solution. Glass microslides were ultrasonically cleaned in acetone, methanol and deionized water. The cleaned substrates were immersed in a 1N potassium hydroxide (KOH) solution to make the surface hydrophilic and to improve wetting characteristics.

Polymeric precursors for depositing ZnO films were prepared using modified Pechini process. In this process, 0.1 moles $Zn(NO_3)_2$, 0.9 moles glycerol, and 0.1 moles of HNO_3, were added together. To this solution, deionized water was added and the resulting solution was heated at a constant temperature of 70°C while stirring continuously. The final solution synthesized was clear, homogeneous, and precipitate free. The prepared solutions were utilized in depositing maskless patterns using Maskless Mesoscale Materials Deposition (M^3D^{TM}, Optomec Inc.,) on surface modified glass substrates, followed by curing at 70°C on a hot plate for 1 hour. The films were then annealed at 600°C for 10 min in an ambient furnace for pyrolization of the organic precursors and ZnO formation.

In this work, M^3D^{TM} deposition system has been used to make patterns of ZnO using glycerol based polymeric precursors. Fig. 9.1 shows the schematic

diagram of the M^{3}D^{TM} deposition system in a pneumatic configuration. It shows an overview of general processes used to aerosolize polymeric precursors. The polymeric precursor is kept in a glass atomization container. Compressed nitrogen gas is expanded through the atomizer nozzle to produce a high-velocity jet. The velocity of the compressed nitrogen gas, also referred as the atomizer flow rate, is controlled by a unit called the process control module. Due to the Bernoulli effect, the precursor is drawn into the atomizer nozzle. The high velocity

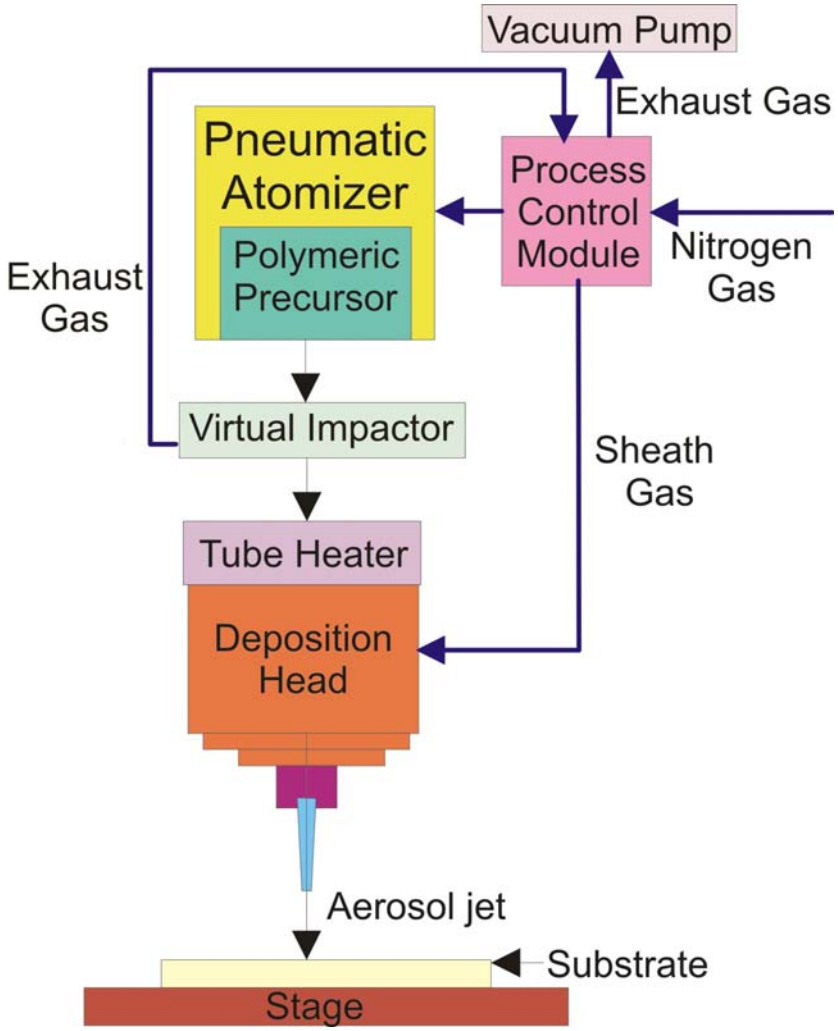

Figure 9.1: Schematic diagram of Maskless Mesoscale Materials Deposition system, M^{3}D^{TM}, in pneumatic configuration.

gas stream then atomizes the precursor and the resulting droplets are suspended in gas flow. After exiting the atomizer nozzle, this gas flow collides with the sidewalls of the atomization container to eliminate large droplets while smaller droplets are carried towards the deposition head.

On atomizing the precursors, the aerosol is transported to virtual impactor by nitrogen carrier gas. In the virtual impactor, excess carrier gas is removed. In pneumatic atomization, there is a size distribution of atomized droplets. The virtual impactor helps in limiting the size variations and eliminates the droplets, which are below the minimum value. This excess gas flowing out of the virtual impactor is referred as impact exhaust flow and is also controlled by the process control module. The difference between the atomizer and impact exhaust flow is actually the material injected into the deposition head.

The aerosol is then carried to the deposition head. Another line of nitrogen gas, also controlled by the process control module, forms an annular ring around the aerosol material. This sheath gas focuses the atomized flow and guides it through the deposition head. The aerosol is then deposited on surface modified glass substrates. The prepared samples were later heat treated for pyrolization of organic material and formation of ZnO.

After annealing the samples at 600°C, the ZnO films were analyzed by optical microscopy (Nikon Digital Optical Microscope), field emission scanning electron microscopy (FESEM, Nova Nanolab 200, FEI Co.) and two probe resistivity measurements across the deposited line (Model 6430 sub-femto

sourcemeter, Keithley Instruments). Prior to FESEM, the patterned samples were coated with a 10 nm gold film.

9.3. Results and Discussion

9.3.1. Effects of Deposition Conditions

9.3.1.1. Viscosity

Experiments were carried out to study the effect of viscosity of polymeric precursors on the direct writing of patterns on substrates. Solutions utilized in preparing glycerol derived spincoated ZnO thin films [120] were used for direct writing of patterns as shown in Fig. 9.2. Fig. 9.3a and 9.3b show the patterns made using glycerol based polymeric precursors of 5 cP and 1 cP viscous solutions under similar deposition conditions. SEM micrographs of these samples reveal that continuous lines with uniform thickness are obtained with 5 cP viscous solution whereas a broken line consisting of spherical droplets is formed from the 1 cP viscous solution. The width of the deposited continuous line was measured to be 200 μm. We observe that for less viscous solution, there is over-spray of the solution.

9.3.1.2. Write Speed

Glycerol based polymeric precursor of 1cP viscosity was used to write lines at different speeds with a M^3D^{TM} system. The lines were deposited on surface modified glass substrates at sheath gas flow rate of 60 cc/min, impact exhaust flow rate of 500 cc/min, and atomizer flow rate of 1000 cc/min. The deposited samples were cured at 70°C and annealed at 600°C. The lines were generated at different writing speeds, such as 1 mm/s (Fig. 9.4a), 5 mm/s (Fig.

9.4b), 10 mm/s (Fig. 9.5a), and 20 mm/s (Fig. 9.5b). It is observed that the write speeds affect the shape of lines drawn at similar deposition conditions. At write speed of 1 mm/s, the lines are of uniform width and as the write speed increases to 5 mm/s, the width of these lines decreases. On further increase in writing speed, the width decreases further. The shape of the line deposited also differs

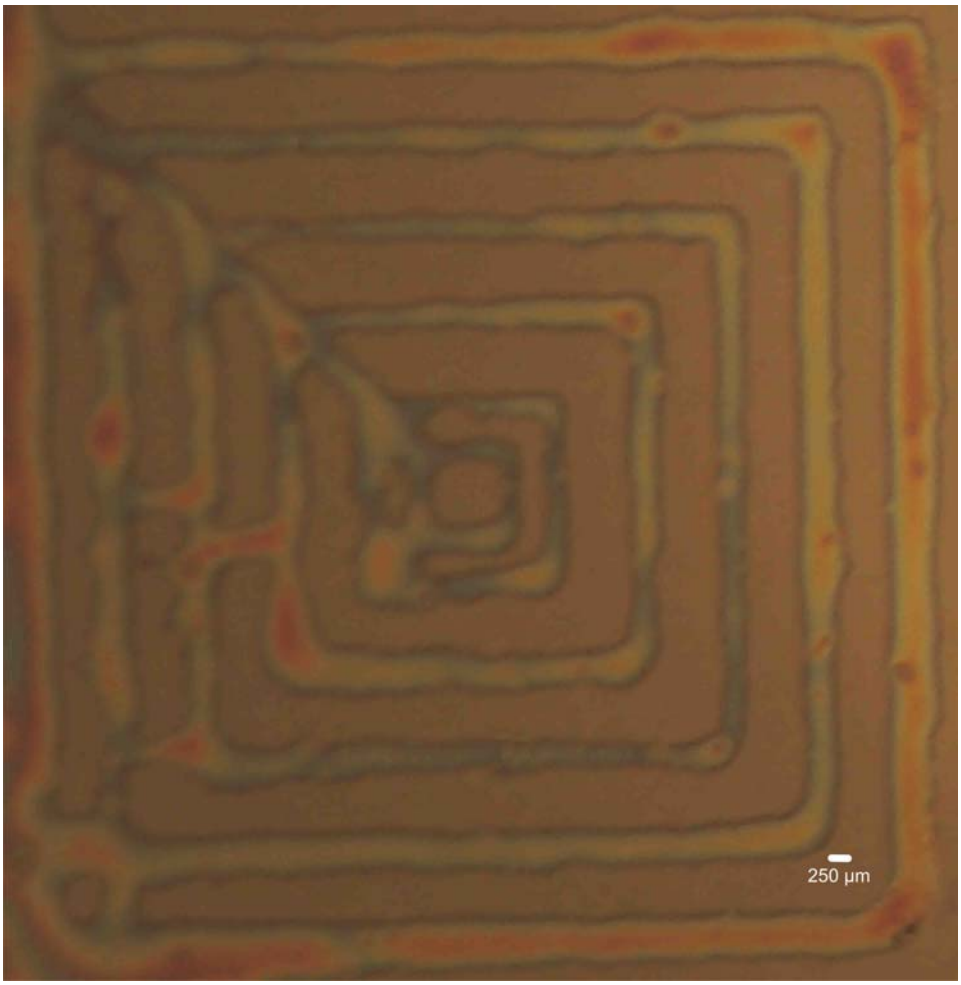

Figure 9.2: A complex square pattern of ZnO deposited on surface modified glass substrate using Maskless Mesoscale Materials Deposition (M^3D^{TM}) technology.

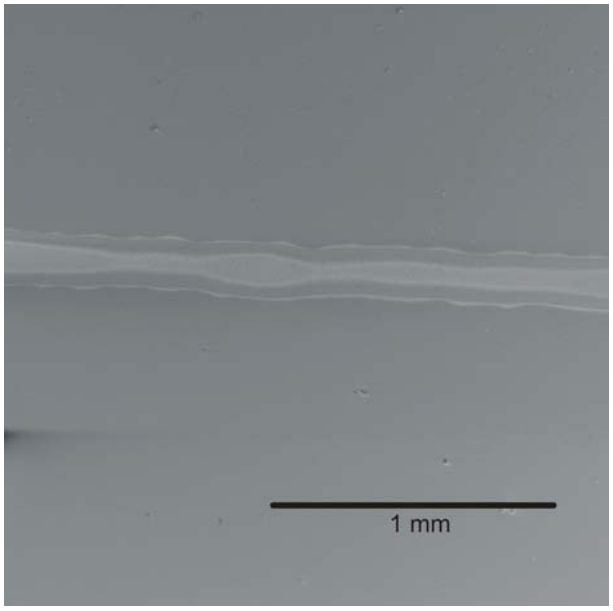

(a)

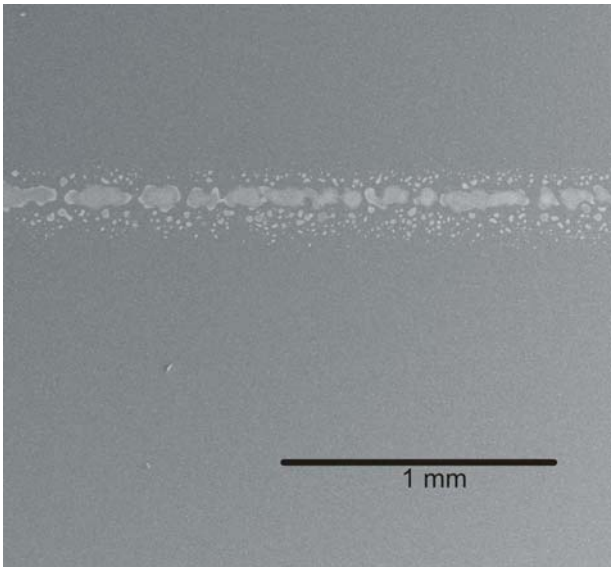

(b)

Figure 9.3: SEM micrographs of directly written line in a M^3D^{TM} system using polymeric precursors of different viscosity; (a) 5 cP and (b) 1 cP. These images are being shown to illustrate the fact that highly viscous precursors deposit continuous lines compared to less viscous ones.

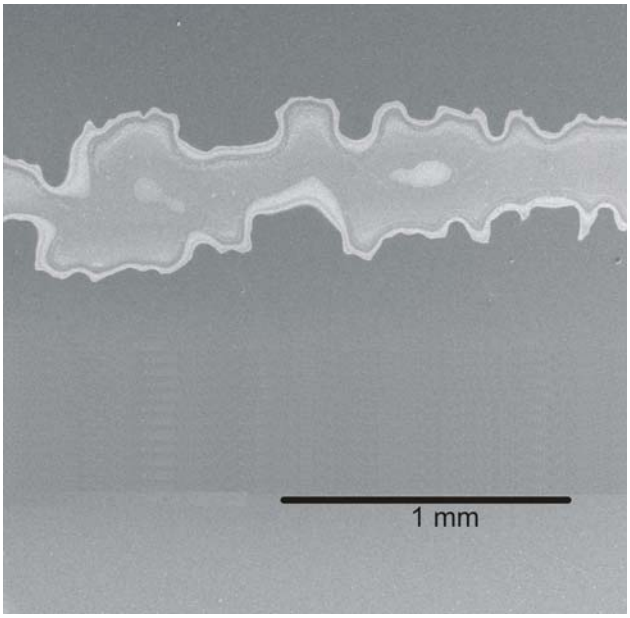

(a)

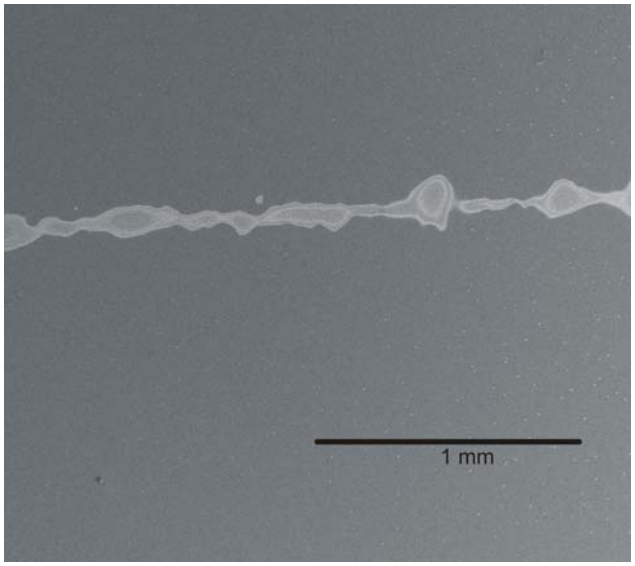

(b)

Figure 9.4: SEM micrographs of microlines written directly using M^3D^{TM} system using 1 cP viscous glycerol based polymeric precursor at different writing speeds; (a) 1 mm/s and (b) 5 mm/s. These images illustrate that continuous lines are more likely at lower write speeds.

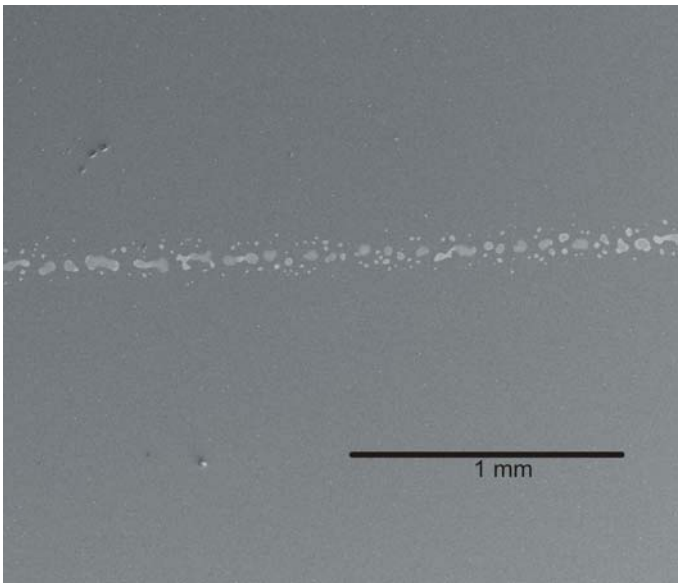

(a)

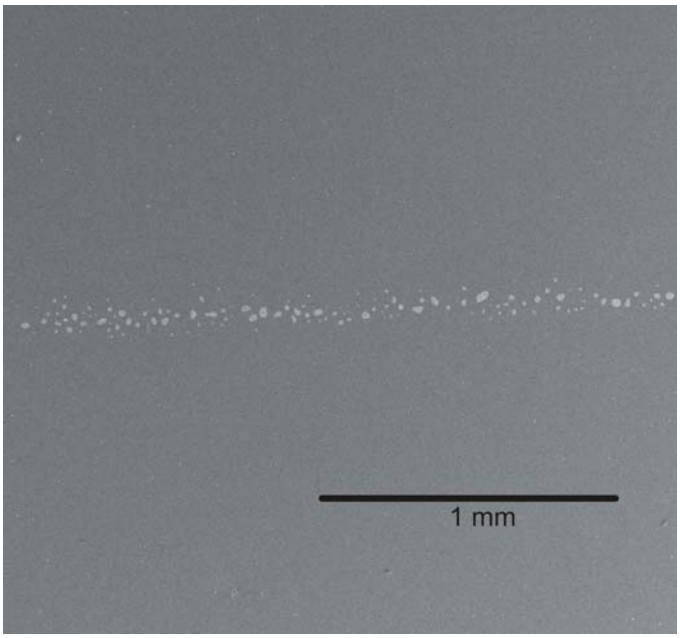

(b)

Figure 9.5: SEM micrographs of microlines written directly using M^3D^{TM} system using 1 cP viscous glycerol based polymeric precursor at different writing speeds; (a) 10 mm/s and (b) 20 mm/s. These images illustrate that as write speed increases the lines consist of droplets.

with writing speed. We observe that with increase in write speed, the lines appear broken and formed of droplets. The shape of these droplets becomes circular and smaller as the speed increases to 20 mm/s. When the write speed is slow, there is more deposition of aerosol and hence, the lines are wider. Moreover, there is sufficient time for the atomized particles to deposit and flow together uniformly. As the write speed increases, the amount of atomized material being deposited on a spot decreases. This results in a non-uniform deposition and flow of the aerosol. Hence, at the write speed of 20 mm/s, the lines deposited are broken with small circular droplets of atomized material.

9.3.1.3. Substrate Condition

Polymeric precursors for synthesizing ZnO films were used to direct write patterns on surface modified glass substrates using M^3D^{TM} technology. The glass substrates were immersed in a 1N KOH solution to functionalize them and to improve their hydrophilicity and wetting characteristics. The deposited lines were subsequently annealed and characterized by FESEM.

SEM micrographs shown in Fig. 9.6 (a and b) illustrate that the directly written straight lines are of uniform width (200 μm) when deposited on surface modified glass substrates. In comparison, the lines, deposited on a heated (at 70°C) surface modified substrate, are not straight, and are of non – uniform width. A closer examination of the micrographs (Fig. 9.6b) reveals that the initial deposition of the aerosol is uniform which may be due to the aerosol getting heated while nucleating on the substrate. After being in contact with the hot substrate, there may be evaporation of the residual water from the deposited

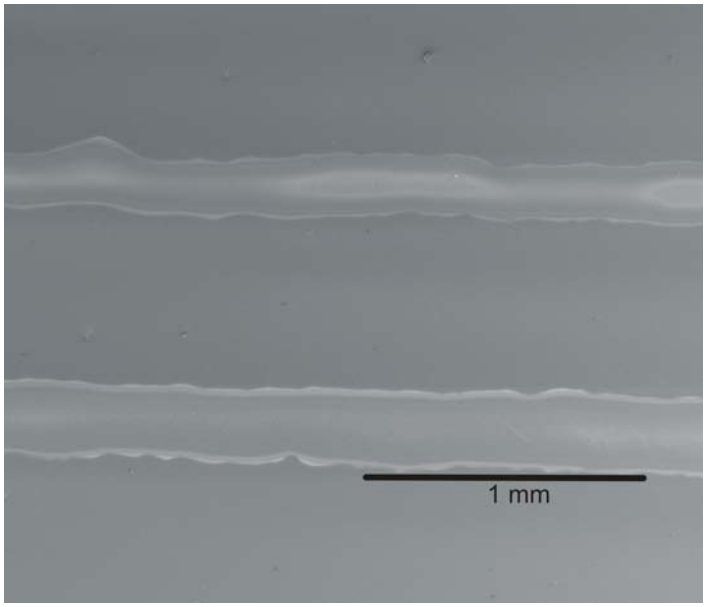

(a)

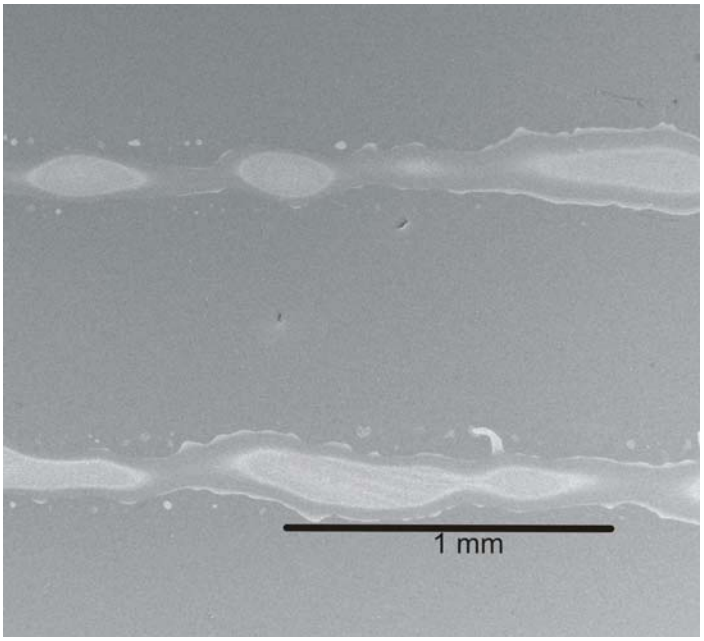

(b)

Figure 9.6: SEM micrographs of directly written line in a M^3D^{TM} system using polymeric precursors of 5cP viscosity on surface modified substrates; (a) without curing and (b) with curing at 70°C while depositing.

aerosol. This evaporation causes the material to dry out faster leading to shrinkage along the width. Hence, we conclude that the patterns, with uniform widths, have to be deposited on surface modified substrate without curing at 70°C while writing.

9.3.1.4. Flow Rates

Lines were also written by varying the atomizer flow rate while keeping other deposition conditions constant. Glycerol based polymeric precursor of 5 cP viscosity was used to write patterns on surface modified glass substrates. The sheath gas flow rate and the impact exhaust flow rates were maintained at 60 cc/min and 500 cc/min, respectively. Fig. 9.7 illustrates the change in line width and shape with change in atomizer flow rates when written at a speed of 2 mm/s.

To begin atomization, the atomizer flow rate has to be higher than the impact exhaust flow rate. When an atomizer flow rate of 600 cc/min was chosen, there was no deposition due to inadequate atomization of the polymeric precursor. SEM micrographs of the samples illustrate a change in line width and shape with change in atomizer flow rate. The lines drawn at 700 cc/min of atomizer flow rate are narrow but not of uniform width (Fig. 9.7a). Moreover, the lines are not continuous at places. When the atomizer flow rate is set to 800 cc/min, there is a significant improvement in deposition (Fig. 9.7b). The lines are continuous but are not of uniform width. There is also some over-spray. At 900 cc/min flow rate of atomizer (Fig. 9.7c), the over spray of the aerosol decreases considerably and the average width of the lines is 195 μm. Uniform lines of 237 μm wide are deposited at 1000 cc/min. However, there is a lot of over spray (Fig.

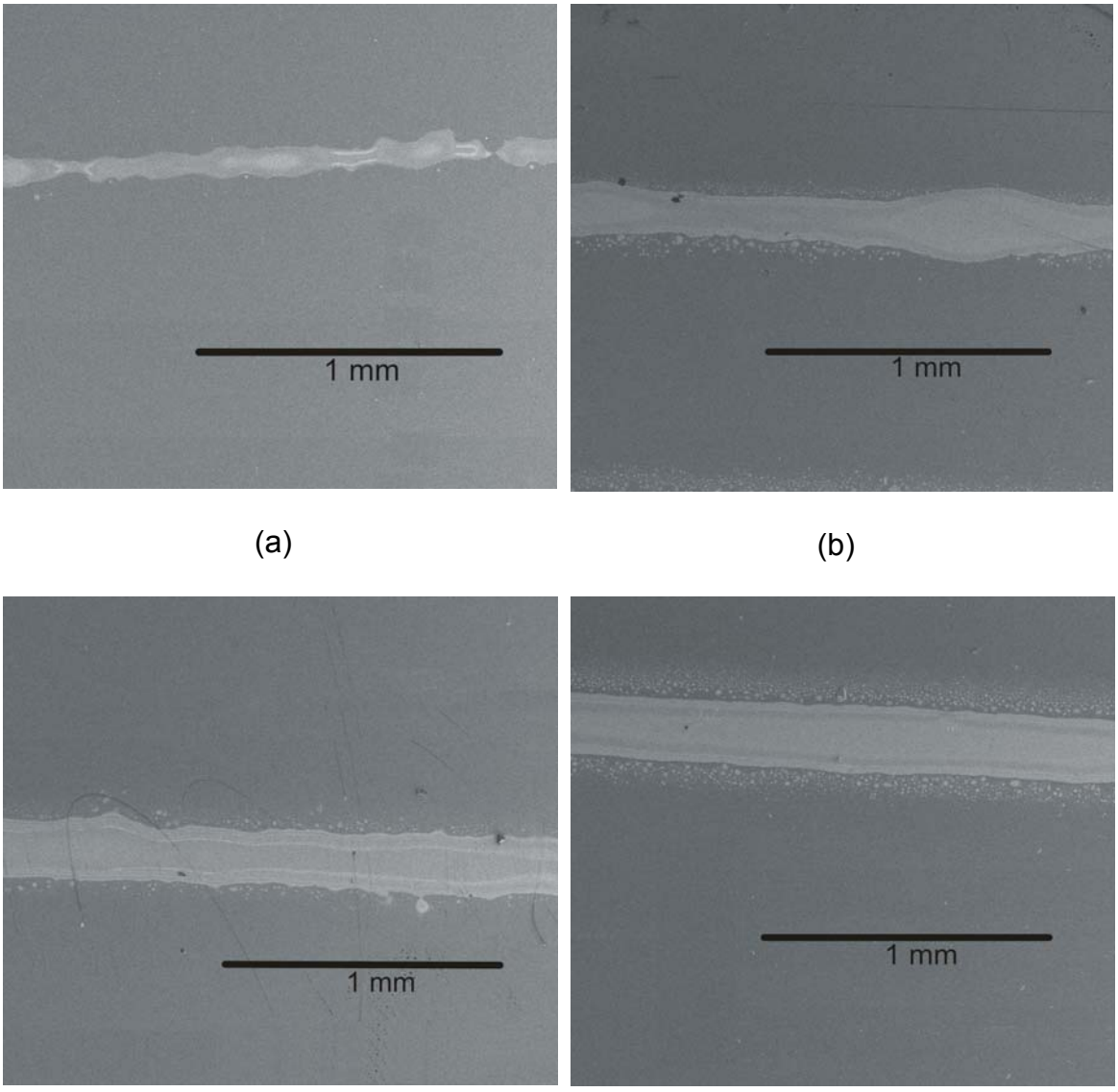

Figure 9.7: SEM micrographs of directly written line in a M^3D^{TM} system at atomizer flow rates; (a) 700 cc/min, (b) 800 cc/min, (c) 900 cc/min, and (d) 1000 cc/min. These were made using polymeric precursors of 5cP viscosity on surface modified substrates at a write speed of 2 mm/s. The sheath gas flow rate and the impact exhaust flow rates were maintained at 60 cc/min and 500 cc/min, respectively.

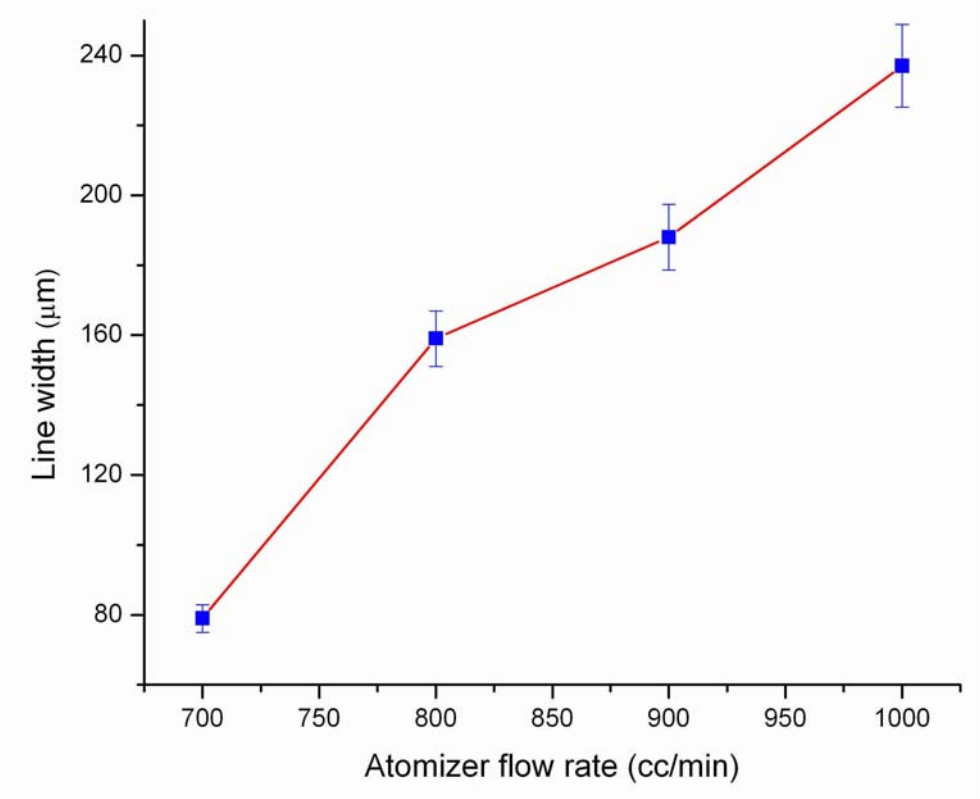

Figure 9.8: Change in line width of directly written lines with atomizer flow rate.

9.7d). From the micrographs, we observe that there is increase in line width with increase in atomizer flow rate as plotted in Fig. 9.8.

Lines were also drawn by varying the impact exhaust flow rate while keeping other conditions constant. In this study, 5 cP viscous glycerol based polymeric precursor was used for atomization. The sheath gas flow rate and atomizer flow rates were maintained at 70 cc/min and 900 cc/min respectively. The patterns were directly written at a speed of 2 mm/s. Fig. 9.9 illustrates the change in line width and shape with change in impact exhaust flow rates.

SEM micrographs of the samples illustrate changes in the type of line

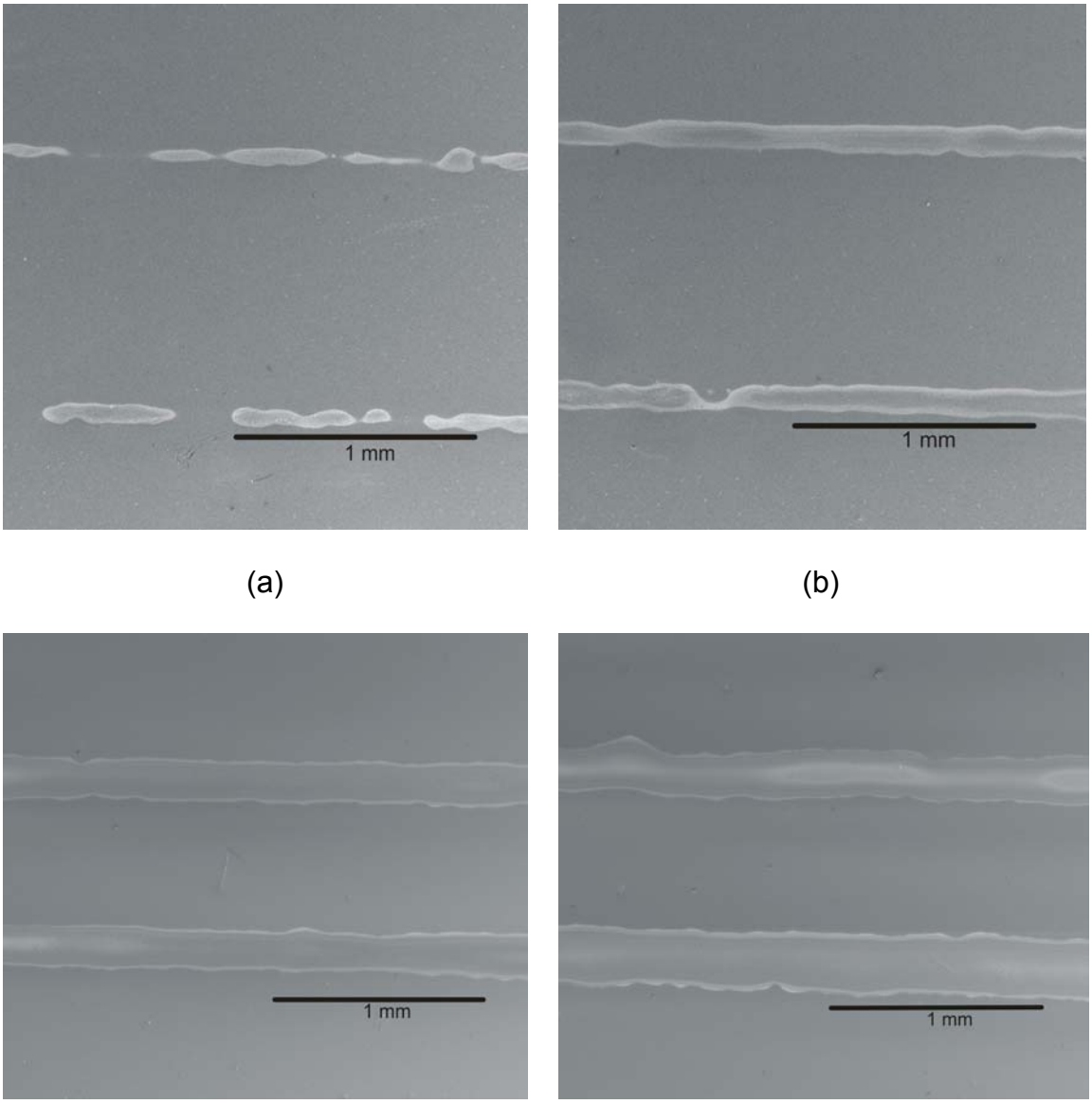

(a) (b)

(c) (d)

Figure 9.9: SEM micrographs of directly written lines in a M^3D^{TM} system at impact exhaust gas flow rates; (a) 300 cc/min, (b) 400 cc/min, (c) 500 cc/min, and (d) 600cc/min using 5cP solution on surface modified substrates at a write speed of 2 mm/s. The sheath gas flow rate and atomizer flow rates were maintained at 70 cc/min and 900 cc/min respectively.

drawn as the impact exhaust flow rates change. The lines drawn at 300 cc/min of impact exhaust flow rate are narrow (80 μm) and discontinuous (Fig. 9.9a). At 400 cc/min lines are not broken but their width varies (Fig. 9.9b); average line width was determined to be 120 μm. There is a significant improvement in deposition (Fig. 9.9c) at 500 cc/min flow rate of impact exhaust. The lines are of uniform width (210 μm). The same trend continues when the impact exhaust flow rate is set at 600 cc/min (width = 260 μm) (Fig. 9.9d). From the micrographs, we observe that there is an increase in line widths with the increase in impact exhaust flow rates which is also shown in Fig. 9.10. Moreover, the deposition also improves and the lines obtained after annealing are uniformly drawn with no cracking.

On being atomized, the aerosol is carried by nitrogen gas to the virtual impactor (Fig. 9.1). In here, the excess gas is stripped off to reduce the aerosol flow rate and concentrate the material. When we fixed the impact exhaust flow at 500 cc/min and varied the atomizer flow rates from 700 cc/min to 1000 cc/min, the difference in these flow rates is increased. Hence, more aerosol material is available to deposit leading to wider lines. Since less of carrier gas is being removed, there is an increase in the over spray or spread in deposition of aerosol. In the second study, we had varied the impact exhaust flow rate at fixed atomizer flow rate of 900 cc/min. In this case, we observed that as the difference in impact exhaust and atomizer flow rates decreased, the lines appear to be uniformly wide. This is due to a reduction in excess carrier gas. Therefore, the material entering the deposition head consists mostly of the atomized particles

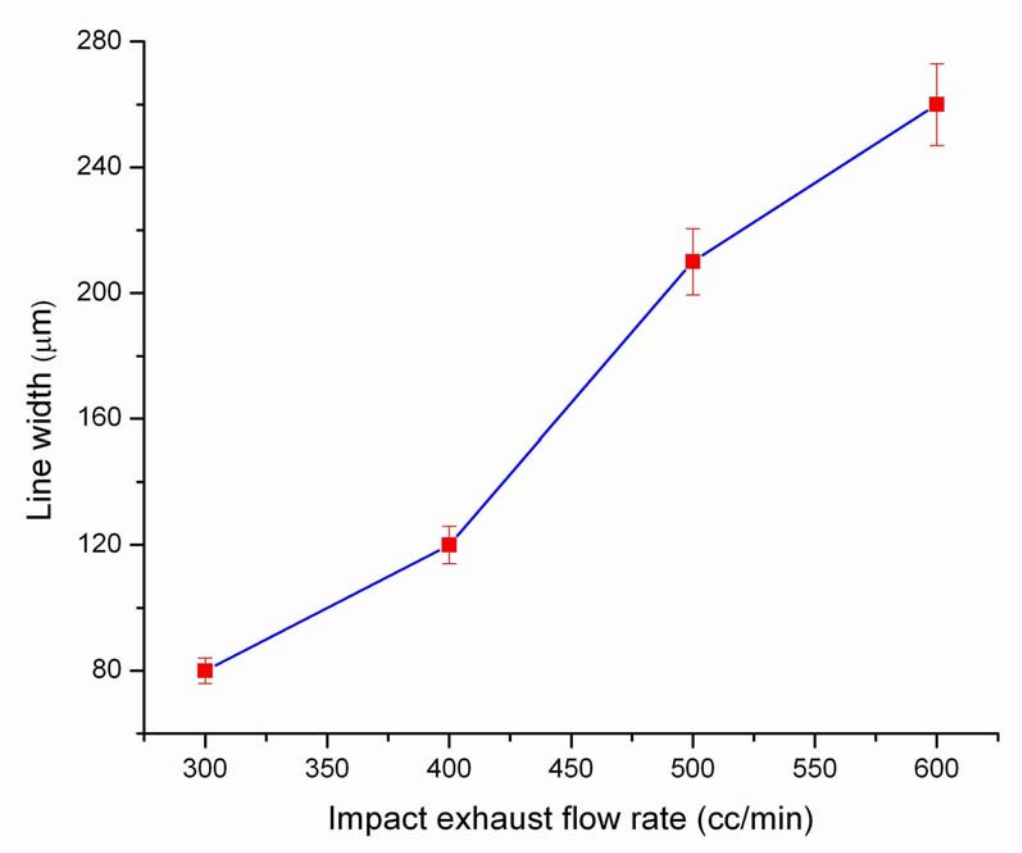

Figure 9.10: Change in line width of directly written lines with increase in impact exhaust gas flow rates at constant sheath gas flow rate and atomizer flow rates at 70 cc/min and 900 cc/min respectively.

which results in wide uniform lines.

Sheath gas is used in M^3D^{TM} to provide an annular flow of nitrogen gas around the aerosol jet. We carried out experiments to study changes in written lines with sheath gas flow rates (Fig. 9.11). In this study, we chose impact exhaust flow rate and atomizer flow rate as 500 cc/min and 900 cc/min, respectively. The line patterns of 5 cP solution were written at 2 mm/s. We find that there is no difference in line widths or shape with change in sheath gas flow

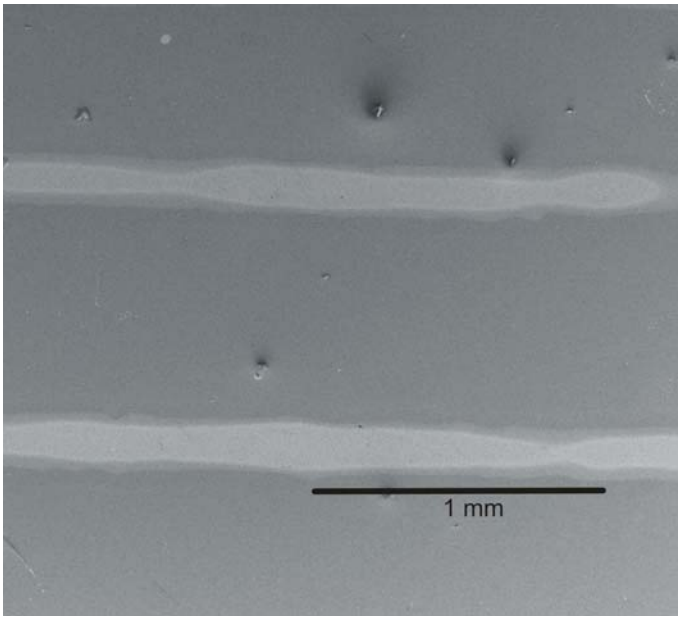

(a)

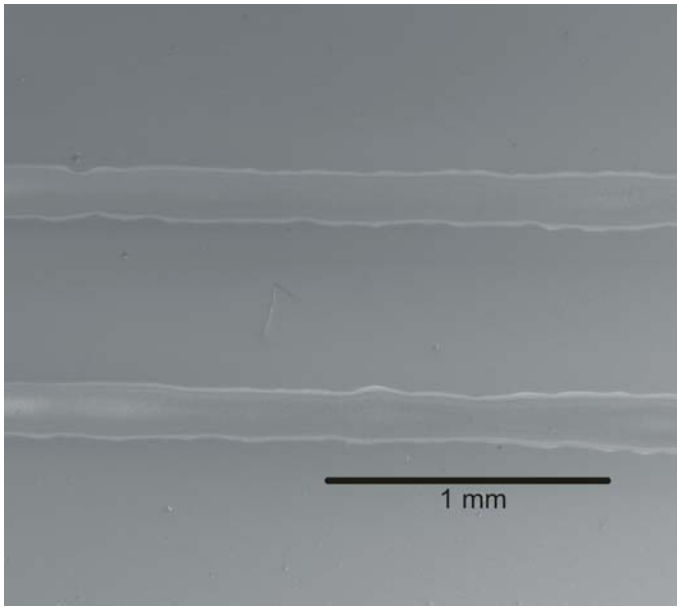

(b)

Figure 9.11: SEM micrographs of ZnO lines directly written with impact exhaust and atomizer flow rates of 500 cc/min and 900 cc/min, respectively and varying sheath gas; (a) 50 cc/min and (b) 70 cc/min.

rates. The lines are 195 μm wide and are uniform.

9.3.2. Electrical Resistivity

As the first step towards the determination of material properties of ZnO lines deposited by M^3D^{TM} and annealed at 550°C, electrical resistivity was calculated from measured resistances of a series of parallel lines of approximately 25 mm length and geometrical data determined by optical microscopy. The average resistivity of the ZnO lines was measured to be $9x10^3$ Ω-m at room temperature. In [6], silver lines were deposited using MAPLE direct-write technique and the electrical resistivity was measured. They report resistivity 1000 times higher than the bulk Ag value. The measured resistance also scaled with respect to cross-section and length as expected. Despite the poor conductivity of the ZnO lines, these initial results demonstrate that patterned ZnO films can be fabricated using M^3D^{TM} technology. By varying the annealing temperatures [25], improvements in conductivity of ZnO patterns produced by M^3D^{TM} process may be achieved.

9.4. Conclusions

Maskless Mesoscale Materials Deposition (M^3D^{TM}) is a new versatile direct write technique to deposit molecular precursors and colloidal suspensions. A glycerol-based polymeric precursor was used for depositing ZnO thin films on surface of modified glass substrates. The parameters for deposition were examined and optimized and various types of patterns have been deposited successfully.

We conclude that to directly write continuous line of uniform width, we

need to use solutions of 5 cP or higher while using pneumatic atomization. For viscosity 5 cP, solutions can be atomized by ultrasonic atomization. However, we have concentrated our attention only on optimization of deposition parameters for pneumatic atomization. The lines need to be written at a speed 2 mm/s on a surface modified glass substrate. The atomization of polymeric precursors has to be adequate to achieve deposition. The atomizer and impact exhaust flow rates have to be chosen appropriately so as to avoid excess stripping of the carrier gas and also to avoid over spray of the aerosol. We deduce that for glycerol based polymeric precursors, lines 200 μm wide can be written continuously at a speed of 2 mm/s for a solution of 5 cP using atomizer, impact exhaust and sheath gas flow rates as 900 cc/min, 500 cc/min, and 60 cc/min, respectively. The electrical resistivity of these lines was estimated to be $9x10^3$ Ω-m at room temperature. Further studies need to be undertaken to accurately measure the resistivity values of ZnO lines.

CHAPTER 10

CONCLUSIONS AND FUTURE WORK

ZnO thin films have been prepared by aqueous polymeric precursor process. During the course of this investigation, polymeric precursors have been synthesized using different chelating agents such as ethylene glycol, glycerol, citric acid, and ethylene diamine tetraacetic acid (EDTA). These chelating agents have varying affinity to chelation of Zn cations, which affects the properties of ZnO films. These polymeric precursors were spincoated on various substrates like glass, silicon, and sapphire. Studies showed different morphologies formed using different polymeric precursors. Flower-like ZnO morphology were obtained using ethylene glycol based precursor whereas spherical morphologies was observed for other precursors. Reactant concentrations, spin coating conditions and viscosity were varied to observe changes in flower-like morphology of the ZnO structures. TGA data of the polymeric precursors show that ethylene glycol has the lowest whereas EDTA has the highest pyrolytic temperature. We observed that ethylene glycol based precursor has a low pyrolytic temperature, which is suitable for deposition on polymeric substrates. However, these films form flower-like morphology instead of smooth crack-free films. So the most suitable option would be glycerol-based precursors for applications on polymeric substrates. However, electrical resistivity of glycerol derived films is high (298 Ω-m) when annealed at 600°C in air whereas ZnO films of citric acid based precursors have relatively low electrical resistivity (31.63 Ω-m) and high

transparency (90%) in the visible region making them suitable as transparent conductors.

Epitaxial ZnO thin films grown on (0001) oriented (basal or c-plane) sapphire substrates using citric acid based polymeric precursor. XRD data for ZnO thin films show that the synthesized films have wurtzite structure. The effect of annealing temperatures on the ZnO films on sapphire was analyzed. XRD spectra illustrates that there is texturing along (002) plane. With an increase in annealing temperature, the texturing becomes highly pronounced with the maximum at 1000°C. Spinel $ZnAl_2O_4$ also formed when ZnO films were annealed at 1000°C due to solid-state reaction between the ZnO film and Al_2O_3 substrate. SEM micrographs reveal an increase in grain size with annealing temperature, which can be attributed to grain growth. An increase in annealing temperature improved film crystallinity and grains changed shape from spherical to highly faceted.

The polymeric precursors have been utilized in fabricating maskless patterned ZnO thin films in a single step using Maskless Mesoscale Materials Deposition (M^3D^{TM}) in pneumatic atomization. This processing technique enabled us to deposit complex patterns and lines without using photoresists and lithography. Parameters were optimized for proper aerosolization for pneumatic atomization. Electrical resistivities of directly written continuous lines of uniform width were also used calculated. The electrical resistivity of these lines was calculated to $9x10^3$ Ω-m at room temperature. Further studies need to be undertaken to decipher the enormous resistivity values of ZnO lines.

In the future, research has to be carried out for decreasing the resistivity of glycerol-based ZnO films by adding suitable dopants or annealing in vacuum. Transmission electron microscopic studies will be undertaken to study the effct of annealing on Al diffusion into the ZnO films on sapphire substrates. Strain due to lattice mismatch between ZnO film and sapphire substrate will also be analyzed by HRTEM. Ultrasonic atomization (M^3D^{TM}) will be used for depositing patterns of ZnO films.

BIBLIOGRAPHY

[1] A. Akyol and M. Bayramoglu, “Photocatalytic degradation of Remazol Red F3B using ZnO catalyst”, *J. Hazard. Mater.* 124 (2005), 241.

[2] A. Chatterjee, C. H. Shen, A. Ganguly, L. C. Chen, C. W. Hsu, J. Y. Hwang and K. H. Chen, “Strong room-temperature UV emission of nanocrystalline ZnO films derived from a polymeric solution”, *Chem. Phys. Lett*. 391 (2004), 278.

[3] A. El Hichou, M. Addou, J. Ebothé and M. Troyon, “Influence of deposition temperature (T_s), air flow rate (f) and precursors on cathodoluminescence properties of ZnO thin films prepared by spray pyrolysis”, *J. Lumin*. 113 (2005), 183.

[4] A. El-Yadouni, A. Boudrioua, J.C. Loulergue, Vincent Sallet and R. Triboulet, “Growth and optical characterization of ZnO thin films deposited on sapphire substrate by MOCVD technique”, *Opt. Mater*. 27 (2005), 1391.

[5] A. Kahoul, P. Nkeng, A. Hammouche, F. Naamoune and G. Poillerat, “A Sol–Gel Route for the Synthesis of $Bi_2Ru_2O_7$ Pyrochlore Oxide for Oxygen Reaction in Alkaline Medium”, *J. Solid State Chem*. 161 (2001), 379.

[6] A. Piqué, D.B. Chrisey, R.C.Y. Auyeung, J. Fitz-Gerald, H.D. Wu, R.A. McGill, S. Lakeou, P.K. Wu, V. Nguyen and M. Duignan, “A novel laser transfer process for direct writing of electronic and sensor materials”, *Appl. Phys. A: Mater. Sci. Process*. 69 (1999), S279.

[7] A. Z. Simões, A. Ries, C. S. Riccardi, A. H. Gonzalez, M. A. Zaghete, B. D. Stojanovic, M. Cilense and J. A. Varela, “Potassium niobate thin films prepared through polymeric precursor method”, *Mater. Lett.* 58 (2004), 2537.

[8] B. D. Cullity and S. R. Stock, *Elements of X-Ray Diffraction*, 3 ed., Prentice Hall, Inc., 2001.

[9] B. Hadimioglu, B. T. Khuri-Yakub, L. C. Goddard, C. F. Quate, *Multilayer ZnO Acoustic Transducers*, IEEE Conference on Ultrasonics Symposium (1986), 361.

[10] B. Hadimioglu, L. J. La Comb, Jr., D. R. Wright, B. T. Khuri-Yakub, and C. F. Quate, "High efficiency, multiple layer ZnO acoustic transducers at millimeter-wave frequencies", *Appl. Phys. Lett*. 50 (1987), 1642.

[11] B. P. Gorman, *Processing and Characterization of thin film solid oxide fuel cell structures*, *Ph.D. thesis*, Univ. of Missouri-Rolla, 2003.

[12] B. Wessler, F. F. Lange, W. Mader, "Textured ZnO thin films on (0001) sapphire produced by chemical solution deposition", *J. Mater. Research* 17 (2002), 1644.

[13] B.P. Gorman and H.U. Anderson, "Processing and characterization of yttrium-stabilized zirconia thin films on polyimide from aqueous polymeric precursors", *Thin Solid Films* 457 (2004), 258.

[14] C. A. Kodaira, H. F. Brito, O. L. Malta and O. A. Serra, "Luminescence and energy transfer of the europium (III) tungstate obtained via the Pechini method" , *J. Lumin.* 101 (2003), 11.

[15] C. B. Arnold, R. C. Wartena, K. E. Swider-Lyons and A. Pique, "Fabrication Of Mesoscale Energy Storage Systems By Laser Direct-Write", *Mat. Res. Soc. Symp. Proc.* 758 (2003), LL3.6.1.

[16] C. J. Gawlak and C. R. Aita, "Stress relief of basal orientaion zinc oxide thin films by isothermal annealing" , *J. Vac. Sci. Technol. A* 1 (1983), 415.

[17] C.-S. Kee, D.-K. Ko and J. Lee, “Photonic band gaps of two-dimensional ZnO nanorod photonic crystals”, *J. Phys. D: Appl. Phys.* 38 (2005), 3850.

[18] C. Shaoqiang, Z. Jian, F. Xiao, W. Xiaohua, L. laiqiang, S. Yanling, X. Qingsong, W. Chang, Z. Jianzhong and Z. Ziqiang, “Nanocrystalline ZnO thin films on porous silicon/silicon substrates obtained by sol–gel technique”, *Appl. Surf. Sci.* 241 (2005), 384.

[19] C X Xu, X W Sun, B J Chen, Z L Dong, M B Yu, X H Zhang and S J Chua, “Network array of zinc oxide whiskers”, *Nanotechnology* 16 (2005), 70.

[20] C. X. Xu and X. W. Sun , “Field emission from zinc oxide nanopins”, *Appl. Phys. Lett.* 83 (2003), 3806.

[21] D. B. Chrisey, “The power of direct writing”, *Science* 289 (2000), 879.

[22] D. Bao, H. Gu and A. Kuang, “Sol-gel-derived c-axis oriented ZnO thin films”, *Thin Solid Films* 312 (1998), 37.

[23] D. C. Look, D. C. Reynolds, C. W. Litton, R. L. Jones, D. B. Eason and G. Cantwell, “Characterization of homoepitaxial *p*-type ZnO grown by molecular beam epitaxy”, *Appl. Phys. Lett.* 81 (2002), 1830.

[24] D. E. Bornside, C. W. Macosko and L. E. Scriven, *J. Imaging Technol*. 13 (1987), 122.

[25] D. H. Zhang and D. E. Brodie, “Effects of annealing ZnO films prepared by ion-beam-assisted reactive deposition”, *Thin Solid Films* 238 (1994), 95.

[26] D. Schmid, M. Ruckh and H. W. Schock, “A comprehensive characterization of the interfaces in Mo/CIS/CdS/ZnO solar cell structures”, *Sol. Energy Mater. Sol. Cells* 41-42 (1996), 281.

[27] D. W. Hamby, D. A. Lucca, M. J. Klopfstein and G. Cantwell, “Temperature dependent exciton photoluminescence of bulk ZnO”, *J. Appl. Phys*. 93 (2003), 3214.

[28] D. Zhou, G. Huang, X. Chen, J. Xu and S. Gong, “Synthesis of $LaAlO_3$ via ethylenediaminetetraacetic acid precursor”, *Mater. Chem. Phys*. 84 (2004), 33.

[29] E. Fortunato, P. Barquinha, A. Pimentel, A. Gonçalves, A. Marques, L. Pereira and R. Martins, “Recent advances in ZnO transparent thin film transistors”, *Thin Solid Films* 487 (2005), 205.

[30] E. Fu, D. Zhuang, G. Zhang, Z. ming, W. Yang and J. Liu, *Properties of transparent conductive ZnO:Al thin films prepared by magnetron sputtering*, Microelectronics Journal 35 (2004), 383.

[31] E. J. Ibanga, C. Le Luyer and J. Mugnier, “Zinc oxide waveguide produced by thermal oxidation of chemical bath deposited zinc sulphide thin films”, *Mater. Chem. Phys.* 80 (2003), 490.

[32] E. M. Kaidashev, M. Lorenz, H. von Wenckstern, A. Rahm, H.-C. Semmelhack, K.-H. Han, G. Benndorf, C. Bundesmann, H. Hochmuth, and M. Grundmann, “High electron mobility of epitaxial ZnO thin films on *c*-plane sapphire grown by multistep pulsed-laser deposition”, *Appl. Phys. Lett.* 82 (2003), 3901.

[33] Eric W. Seelig, Betty Tang, Alexey Yamilov, Hui Cao and R. P. H. Chang, “Self-assembled 3D photonic crystals from ZnO colloidal spheres”, *Mater. Chem. Phys.* 80 (2003), 257.

[34] E.J. Luna-Arredondo, A. Maldonado, R. Asomoza, D.R. Acosta, M. A. Melé-

ndez-Lira and M. de la L. Olvera, “Indium-doped ZnO thin films deposited by the sol–gel technique”, *Thin Solid Films* 490 (2005), 132.

[35] E. M. Bachari, G. Baud, S. Ben Amor and M. Jacquet, “Structural and optical properties of sputtered ZnO films”, *Thin Solid Films* 348 (1999), 165.

[36] F.K. Shan, G.X. Liu, W.J. Lee, G.H. Lee, I.S. Kim, B.C. Shin and Y.C. Kim, “Transparent conductive ZnO thin films on glass substrates deposited by pulsed laser deposition”, *J. Cryst. Growth* 277 (2005), 284.

[37] F. M. Pontes, E. Longo, J. H. Rangel, M. I. Bernardi, E. R. Leite and J. A. Varela, “$Ba_{1-x}Sr_xTiO_3$ thin films by polymeric precursor method”, *Mater. lett*. 43 (2000), 249.

[38] G.-C. Yi, C. Wang and W. I. Park*, “*ZnO nanorods: synthesis, characterization and applications”*, Semicond. Sci. Technol.* 20 (2005), S22*.*

[39] G. Deng, A. Ding, X. Zheng, W. Cheng and P. Qiu, “Growth and optical property of zinc oxide thornballs”, *Mater. Res. Bull.* 40 (2005), 903.

[40] G. H. Gelinck, H. E. A. Huitema, E. van Veenedaal, E. Cantatore, L. Schrijnemakers, J. B. P. H. van der Putten, T. C. T. Geuns, M. Beenhakkers, J. B. Giesbers, B.-H. Huisman, E J. Meijer, E. M. Benito, F. J. Touwslager, A. W. Marsman, B. J. E. van Rens, and D. M. de Leeuw, “Flexible active-matrix displays and shift registers based on solution-processed organic transistors”, *Nat. Mater*. 3 (2004), 106.

[41] G. J. Marquez, M. J. Renn and W. D. Miller, “Aerosol-Based direct write of biological materials for biomedical applications”, *Mat. Res. Soc. Symp. Proc*. 698 (2002), Q5.2.1.

[42] H. Deng, J. J. Russell, R. N. Lamb, B. Jiang, Y. Li and X. Y. Zhou, "Microstructure control of ZnO thin films prepared by single source chemical vapor deposition", *Thin Solid Films* 458 (2004), 43.

[43] H. E. A. Huitema, G. H. Gelinck, J. B. P. H. van der Putten, K. E. Kuijk, C. M. Hart, E. Cantatore, P. T. Herwig, A. J. J. M. van Breemen and D. M. de Leeuw, "Plastic transistors in active-matrix displays", *Nature* 414 (2001), 599.

[44] H. Kato, M. Sano, K. Miyamoto and T. Yao, "Polarity control of ZnO on *c*-plane sapphire by plasma-assisted MBE", *J. Cryst. Growth* 275 (2005), e2459.

[45] H. Li, J. Wang, H. Liu, C. Yang, H. Xu, X. Li and H. Cui, "Sol–gel preparation of transparent zinc oxide films with highly preferential crystal orientation", *Vacuum* 77 (2004), 57.

[46] H. Ohta, K. Nomura, H. Hiramatsu, K. Ueda, T. Kamiya, M. Hirano and H. Hosono, "Frontier of transparent oxide semiconductors", *Solid-State Electronics* 47 (2003), 2261.

[47] H. U. Anderson, M. M. Nasrallah, C. C. Chen, *US Patent 5494700*, 1996.

[48] H. U. Anderson, M. M. Nasrallah, F. D. Blum and M. S. Smith, *Polymeric Synthesis of perovskite powders and films*, N. I. S. T. Special Publication 804, Chemistry of Electronic ceramic materials, 1990.

[49] H. X. Zhang, D. Lu, T. Liu, M. Mansuripur, and M. Fallahi, "Direct laser writing of electro-optic waveguide in chromophore-doped hybrid sol–gel", *Appl. Phys. Lett.* 85 (2004), 4275.

[50] H. Zhang, D. Yang, Y. Ji, X. Ma, J. Xu and D. Que, "Low Temperature Synthesis of of Flowerlike ZnO Nanostructures by Cetyltrimethylammonium

Bromide-Assisted Hydrothermal Process", *J. Phys. Chem. B* 108 (2004), 3955.

[51] H.W. Liang, Y.M. Lu, D.Z. Shen, J.F. Yan, B.H. Li, J.Y. Zhang, Y.C. Liu and X.W. Fan, "Investigation of growth mode in ZnO thin films prepared at different temperature by plasma-molecular beam epitaxy ", *J. Cryst. Growth* 278 (2005), 305.

[52] I.T. Weber, A. Rousseau, M. Guilloux-Viry, V. Bouquet and A. Perrin, "Microstructure comparison between $KNbO_3$ thin films grown by polymeric precursors and PLD methods", *Solid State Sci.* 7 (2005), 1317.

[53] J. A. Venables, G. D. T. Spiller and M. Hanbcken, "Nucleation and Growth of Thin Films", *Rep. Prog. Phys.* 47 (1984), 399.

[54] J. Du, Z. Liu, Y. Huang, Y. Gao, B. Han, W. Li and G. Yang, "Control of ZnO morphologies via surfactants assisted route in the subcritical water", *J. Cryst. Growth* 280 (2005), 126.

[55] J. F. Muth, R. M. Kolbas , A. K. Sharma, S. Oktyabrsky, and J. Narayan , "Excitonic structure and absorption coefficient measurements of ZnO single crystal epitaxial films deposited by pulsed laser deposition", *J. Appl. Phys*. 85 (1999), 7884.

[56] J. L. van Heerden and R. Swanepoel, "XRD analysis of ZnO thin films prepared by spray pyrolysis", *This Solid Films* 299 (1997), 72.

[57] J. Löffler, R. Groenen, J. L. Linden, M. C. M. van de Sanden and R. E. I. Schropp, "Amorphous silicon solar cells on natively textured ZnO grown by PECVD", *Thin Solid Films* 392 (2001), 315.

[58] J. Tersoff, A. W. Denier van der Gon and R. M. Tromp, "Critical island size

for layer-by-layer growth", *Phys. Rev. Lett.* 72 (1994), 266.

[59] J. Wang, V. Sallet, G. Amiri, J.-F. Rommeluère, A. Lusson, E. Rzepka, J. E. Lewis, P. Galtier, O. Gorochov, "Growth Parameters and Substrate Treatment for the MOCVD Growth of ZnO"**,** *Phys. Status Solidi A* 202 (2005), 1967.

[60] J. Xu, Q. Pan, Y. Shun and Z. Tian, "Grain size control and gas sensing properties of ZnO gas sensor", *Sens. Actuators, B* 66 (2000), 277.

[61] J.Y. Lao, J.Y. Huang, D.Z. Wang, Z.F. Ren, D. Steeves, B. Kimball and W. Porter, "ZnO nanowalls", *Appl. Phys. A: Mater. Sci. Process.* 78 (2004), 539.

[62] J. Yoo, J. Lee, S. Kim, K. Yoon, I. J. Park, S. K. Dhungel, B. Karunagaran, D. Mangalaraj and J. Yi, "High transmittance and low resistive ZnO:Al films for thin film solar cells", *Thin Solid Films* 480-481 (2005), 213.

[63] J. Zhang, L. Sun, J. Yin, H. Su, C. Liao and C. Yan, "Control of ZnO Morphology via a Simple Solution Route", *Chem. Mater.* 14 (2002), 4172.

[64] J. Zhao, L. Hu, Z. Wang, Z. Wang, H. Zhang, Y. Zhao and X. Liang, "Epitaxial growth of ZnO thin films on Si substrates by PLD technique", *J. Cryst. Growth* 280 (2005), 455.

[65] J. Zou, S. Zhou, C. Xia, X. Zhang, F. Su, G. Peng, X. Li and J. Xu, "Optical properties of ZnO thin film on γ-$LiAlO_2$ substrate grown by pulsed laser deposition", *Thin Solid Films* 496 (2006), 205.

[66] J. Zou, S. Zhou, C. Xia, Y. Hang, J. Xu, S. Gu and R. Zhang, "Structural, optical and electrical properties of ZnO films grown on *c*-plane sapphire and (1 0 0)*γ*-$LiAlO_2$ by pulse laser deposition", *J. Cryst. Growth* 280 (2005), 185.

[67] K. C. Ruthe, D. J. Cohen, and S. A. Barnett, "Low temperature epitaxy of

reactively sputtered ZnO on sapphire ", *J. Vac. Sci. Technol. A* 22 (2004), 2446.

[68] K. Ramamoorthy, C. Sanjeeviraja, M. Jayachandran, K. Sankaranarayanan, P. Misra and L.M. Kukreja, "Development of a novel high optical quality ZnO thin films by PLD for III–V opto-electronic devices ", *Curr. Appl. Phys*. 6 (2006) 103.

[69] K. Sakurai, M. Kanehiro, K. Nakahara, T. Tanabe, S. Fujita and S. Fujita, "Effects of oxygen plasma condition on MBE growth of ZnO", *J. Cryst. Growth* 209 (2000), 522.

[70] K. Vanheusden, W. L. Warren, C. H. Seager, D. R. Tallant, J. A. Voigt and B. E. Gnade, "Mechanisms behind green photoluminescence in ZnO phosphor powders", *J. Appl. Phys*. 79 (1996), 7983.

[71] K. Yu, Y. Zhang, R. Xu, S. Ouyang, D. Li, L. Luo, Z. Zhu, J. Ma, S. Xie, S. Han and H. Geng, "Efficient field emission from tetrapod-like zinc oxide nanoneedles", *Mater. Lett.* 59 (2005), 1866.

[72] L. Forró, "Display of flexibility", Nature 441 (2006), 414.

[73] L. Vayssieres, K. Keis, A. Hagfeldt and S. E. Lindquist, "Three-Dimensional Array of Highly Oriented Crystalline ZnO Microtubes", *Chem. Mater.* 13 (2001), 4395.

[74] David R. Lide (ed.), *CRC Handbook of Chemistry and Physics*, 86th ed., Taylor and Francis Group, Boca Raton, FL, 2005.

[75] M. Castonguay, B. Fernandez, F. Guillon, and J. D. N. Cheeke, "ZnO transducers on InSb for low-temperature ultrasonics", *J. Appl. Phys.* 61 (1987), 5199.

[76] M. H. Huang, S. Mao, H. Feick, H. Yan, Y.Wu, H. Kind, E.Webber, R. Russo

and P. Yang, “Room-Temperature Ultraviolet Nanowire Nanolasers”, *Science* 292 (2001), 1897.

[77] M. H. Huang, Y.Wu, H. Feick, N. Tran, E.Weber and P. Yang, “Catalytic Growth of Zinc Oxide Nanowires by Vapor Transport”, *Adv. Mater.* 13 (2001), 113.

[78] M. H. Sarvari and H. Sharghi, “Zinc oxide (ZnO) as a new, highly efficient, and reusable catalyst for acylation of alcohols, phenols and amines under solvent free conditions”, *Tetrahedron* 61 (2005), 10903.

[79] M. K. Puchert, P. Y. Timbrell and R. N. Lamb, “Postdeposition annealing of radio frequency magnetron sputtered ZnO films”, *J. Vac. Sci. Technol. A* 14 (1996), 2220.

[80] M. Kemell, F. Dartigues, M. Ritala and M. Leskel, “Electrochemical preparation of In and Al doped ZnO thin films for $CuInSe_2$ solar cells”, *Thin Solid Films* 434 (2003), 20.

[81] M. N. Kamalasanan and S. Chandra, “Sol-gel synthesis of ZnO thin films”, *Thin Solid Films* 288 (1996), 112.

[82] M. Ohyama, H. Kozuka and T. Yoko, “Sol-gel preparation of ZnO films with extremely preferred orientation along (002) plane from zinc acetate solution”, *Thin Solid Films* 306 (1997), 78.

[83] M. P. Pechini, US Patent No. 3,330,697, July 1967.

[84] M. Popa and M. Kakihana, “Synthesis of lanthanum cobaltite ($LaCoO_3$) by the polymerizable complex route”, *Solid State Ionics* 151 (2002), 251.

[85] M. Purica, E. Budianu, E. Rusu, M. Danila and R. Gavrila, “Optical and

structural investigation of ZnO thin films prepared by chemical vapor deposition (CVD)" , *Thin Solid Films* 403 - 404 (2002), 485.

[86] M. Zerdali, S. Hamzaoui, F.H. Teherani and D. Rogers, "Growth of ZnO thin film on SiO_2/Si substrate by pulsed laser deposition and study of their physical properties", *Mater. Lett.* 60 (2006), 504.

[87] N. Mais, J. P. Reithmaier, A. Forchel, M. Kohls, L. Spanhel and G. Mller , "Er doped nanocrystalline ZnO planar waveguide structures for 1.55 μm amplifier applications", *Appl. Phys. Lett.* 75 (1999), 2005.

[88] N. Mehan, M. Tomar, V. Gupta and A. Mansingh, "Optical waveguiding and birefringence properties of sputtered zinc oxide (ZnO) thin films on glass", *Opt. Mater.* 27 (2004), 241.

[89] N. Ohashi, K. Kataoka, T. Ohgaki, T. Miyagi, H. Haneda and K. Morinaga, "Synthesis of zinc oxide varistors with a breakdown voltage of three volts using an intergranular glass phase in the bismuth–boron–oxide system", Appl. Phys. Lett. 83 (2003), 4857.

[90] N. Saito, H. Haneda, W. S. Seo and K. Koumoto, "Selective Deposition of ZnF(OH) on Self-Assembled Monolayers in Zn-NH_4F Aqueous Solutions for Micropatterning of Zinc Oxide", *Langmuir* 17 (2001), 1461.

[91] N. W. Emanetoglu, J. Zhu, Y. Chen, J. Zhong, Y. Chen and Y. Lu, "Surface acoustic wave ultraviolet photodetectors using epitaxial ZnO multilayers grown on *r*-plane sapphire", *Appl. Phys. Lett.* 85 (2004), 3702.

[92] P. C. Rieke, B. J. Tarasevich, L. L. Wood, M. H. Engelhard, D. R. Baer, G. E. Fryxell, C. M. John, D. A. Laken and M. C. Jaehnig, "Spatially Resolved Mineral

Deposition on Patterned Self-Assembled Monolayers", *Langmuir* 10 (1994), 619.

[93] P. Durán, F. Capel, J. Tartaj, C. Moure, "Sintering Behavior and Electrical Properties of Nanosized Doped-ZnO Powders Produced by Metallorganic Polymeric Processing ", *J. Am. Ceram. Soc.* 84 (2001), 1661.

[94] P. Duran, J. Tartaj and C. Moure, "Fully Dense, Fine-Grained, Doped Zinc Oxide Varistors with Improved Nonlinear Properties by Thermal Processing Optimization *"*, *J. Am. Ceram. Soc.* 86 (2003), 1326.

[95] P. Jha, P.R. Arya and A.K. Ganguli, "Dielectric properties of lead zirconium titanates with nanometer size grains synthesized by the citrate precursor route", *Mater. Chem. Phys.* 82 (2003), 355.

[96] P. Sharma and K. Sreenivas, "Highly sensitive ultraviolet detector based on ZnO/$LiNbO_3$ hybrid surface acoustic wave filter", Appl. Phys. Lett. 83 (2003), 3617.

[97] P. X. Gao and Z. L.Wang, "Mesoporous Polyhedral Cages and Shells Formed by Textured Self-Assembly of ZnO Nanocrystals", *J. Am. Chem. Soc.* 125 (2003), 11299.

[98] R. Brenier and L. Ortega, "Structural properties and stress in ZnO films obtained from a nanocolloidal sol", *J. Sol-Gel Sc. Technol*. 29 (2004), 137.

[99] R. Ghosh, D. Basak and S. Fujihara, "Effect of substrate-induced strain on the structural, electrical, and optical properties of polycrystalline ZnO thin films", *J. Appl. Phys.* 96 (2004), 2689.

[100] R. J. Collins, H. Shin, M. R. DeGuire, A. H. Heuer and C. N. Sukenik, "Low temperature deposition of patterned TiO_2 thin films using photopatterned self-

assembled monolayers”*, Appl. Phys. Lett.* 69 (1996), 860.

[101] R. Lawrence, “Tracking own the thermal parameters of sapphire”, *LIGO Web Newsletter* (2001).

[102] Renn, M.J. et al., "Introduction to Direct-Write Technologies for Rapid Prototyping, In Direct-Write Technologies for Rapid Prototyping Applications: Sensors, Electronics, and Integrated Power Sources, Academic Press, San Diego, 2002.

[103] S.-H. Lim, D. Shindo, H.-B. Kang and K. Nakamura, “Defect structure of epitaxial ZnO films on (0001) sapphire studied by transmission electron microscopy*”, J. Vac. Sci. Technol. B* 19 (2001), 506.

[104] S. H. Seo, W. C. Shin and J. S. Park, “A novel method of fabricating ZnO/diamond/Si multilayers for surface acoustic wave (SAW) device applications ”, *Thin Solid Films* 416 (2002), 190.

[105] S. J. Pearton, D. P. Norton, K. Ip, Y. W. Heo and T. Steiner, “Recent progress in processing and properties of ZnO”, *Prog. Materials Science* 50 (2005), 293.

[106] S. Major, A. Banerjee and K. L. Chopra, “Annealing studies of undoped and indium-doped films of zinc oxide”, Thin Solid Films 122 (1984), 31.

[107] S. Major, A. Banerjee and K. L. Chopra*,* “Optical and electronic properties of zinc oxide films prepared by spray pyrolysis”, *Thin Solid Films* 125 (1985), 179.

[108] S. Monticone, R. Tufeu and A.V. Kanaev, “Complex Nature of the UV and Visible Fluorescence of Colloidal ZnO Nanoparticles”, *J. Phys. Chem. B.*102

(1998), 2854.

[109] S. Muthukumar, C. R. Gorla, N. W. Emanetoglu, S. Liang and Y. Lu, “Control of morphology and orientation of ZnO thin films grown on SiO_2/Si substrates”, *J. Cryst. Growth* 225 (2001), 197.

[110] S. T. Shishiyanu, T. S. Shishiyanu and O. I. Lupan, “Sensing characteristics of tin-doped ZnO thin films as NO_2 gas sensor”, *Sens. Actuators, B* 107 (2005), 379.

[111] S. Uthanna, T. K. Subramanyam, B. S. Naidu and G. M. Rao, “Structure-composition-property dependence in reactive magnetron sputtered ZnO thin films”, *Opt. Mater.* 19 (2002), 461.

[112] S. Vivekanandhan, M. Venkateswarlu and N. Satyanarayana, “Effect of different ethylene glycol precursors on the Pechini process for the synthesis of nano-crystalline $LiNi_{0.5}Co_{0.5}VO_4$ powders”, *Mater. Chem. Phys.* 91 (2005), 54.

[113] Y. Shapira, R. B. McQuistan, and D. Lichtman, “Relationship between photodesorption and surface conductivity in ZnO”, *Phys. Rev. B* 15 (1977), 2163.

[114] T. Andelman, Y. Gong, M. Polking, M. Yin, I. Kuskovsky, G. Neumark and S. OBrien, “Morphological Control and Photoluminescence of Zinc Oxide Nanocrystals”, *J. Phys. Chem. B* 109 (2005), 14314.

[115] T. E. Murphy, D. Y. Chen, E. Cagin and J. D. Phillips, “Electronic properties of ZnO epilayers grown on *c*-plane sapphire by plasma-assisted molecular beam epitaxy”, *J. Vac. Sci. Technol. B* 23 (2005), 1277.

[116] T. Gao and T. H. Wang, “Synthesis and properties of multipod-shaped ZnO nanorods for gas-sensor applications”, *Appl. Phys. A: Mater. Sci. Process*. 80

(2005), 1451.

[117] T. Suzuki, P. Jasinski, V. Petrovsky, X. D. Zhou and H. U. Anderson, "Optical and electrical properties of $Pr_{0.8}Sr_{0.2}MnO_3$ thin films", *J. Appl. Phys.* 93 (2003), 6223.

[118] T Szörényi, Zs Geretovszky, J Tóth, A Simon and Cs Cserháti, "Laser direct writing of tin oxide patterns", *Vacuum* 50 (1998), 327.

[119] U. Choppali and B. P. Gorman, "Controlling the Morphology of Polymeric Precursor derived ZnO Flower structures", accepted in *J. Am. Ceram. Soc.*

[120] U. Choppali and B. P. Gorman, "Nanocrystalline ZnO thin films derived using Glycerol and Ethylene Glycol as chelating agents in modified Pechini process", submitted to *Mater. Sci. Eng., B*

[121] U. Choppali and B. P. Gorman, "Polymeric precursor derived nanocrystalline ZnO thin films using EDTA as chelating agent", submitted to *Thin Solid Films*.

[122] U. Choppali and B. P. Gorman, "Synthesis and characterization of nanocrystalline ZnO thin films by citrate precursor route", submitted to J. Electroceramics.

[123] Ü. Özgür, Ya. I. Alivov, C. Liu, A. Teke, M. A. Reshchikov, S. Doğan , V. Avrutin, S.-J. Cho, and H. Morkoc, "A comprehensive review of ZnO materials and devices", *J. Appl. Phys.* 98 (2005), 041301.

[124] U. Pal and P. Santiago, "Controlling the Morphology of ZnO Nanostructures in a Low-Temperature Hydrothermal Process", J. Phys. Chem. B 109 (2005), 15317.

[125] Url of ImageJ http://rsb.info.nih.gov/ij/.

[126] V. Agarwal and M. Liu, “Preparation of barium cerate-based thin films using a modified Pechini process” *J. Mater. Sc.* 32 (1997), 619.

[127] V. Musat, B. Teixeira, E. Fortunato, R. C. C. Monteiro and P. Vilarinho, “Al-doped ZnO thin films by sol–gel method”, Surf. Coat. Technol. 180-181 (2004), 659.

[128] V. Srikant and D. R. Clarke, “Optical absorption edge of ZnO thin films: the effect of substrate”, *J. Appl. Phys.* 81 (1997), 6357.

[129] V. Vinothini, P. Singh and M. Balasubramanian, “Synthesis of barium titanate nanopowder using polymeric precursor method”, *Ceramics International* 32 (2006), 99.

[130] V.R. Shinde, T.P. Gujar, C.D. Lokhande, R.S. Mane, and Sung-Hwan Han, “Mn doped and undoped ZnO films: A comparative structural, optical and electrical properties study”, *Mater. Chem. Phys.* 96 (2006), 326.

[131] W. I. Park, G. C. Yi, M. Kim, and S. J. Pennycook, “ZnO Nanoneedles Grown Vertically on Si Substrates by Non-Catalytic Vapor-Phase Epitaxy”, *Adv. Mater.* 14 (2002), 1841.

[132] W. I. Park, G. C. Yia, J.-W. Kim, and S. M. Park, “Schottky nanocontacts on ZnO nanorod arrays”, *Appl. Phys. Lett.* 82 (2003), 4358.

[133] W.-J. Li, E.-W. Shi, W.-Z. Zhong, and Z.-W. Yin, “Growth mechanism and growth habit of oxide crystals”, *J. Cryst. Growth* 203 (1999), 186.

[134] W. Shan, W. Walukiewicz, J. W. Ager III , K. M. Yu, H. B. Yuan, H. P. Xin, G. Cantwell and J. J. Song, ““Nature of room-temperature photoluminescen-

ce in ZnO", *Appl. Phys. Lett.* 86 (2005), 191911.

[135] W. Voit, K.V. Rao, and W. Zapka, "Direct-Write Process for UV-Curable Epoxy Materials by Inkjet Technology", *Mat. Res. Soc. Symp. Proc.* 758 (2003), LL3.5.1.

[136] X. Yang, J. Zhang, Z. Bi, Y. He, Q. Xu, W. Hongbo, W. Zhang and X. Hou, "Glancing-incidence X-ray analysis of ZnO thin films and ZnO/ZnMgO heterostructures grown by laser-MBE", *J Cryst. Growth* 284 (2005), 123.

[137] X. D. Zhou, Q. Cai, J. Yang, M. Kim, W. B. Yelon, W. J. James, Y.-W. Shin, B. J. Scarfino, and H. U. Anderson, "Coupled electrical and magnetic properties in (La,Sr)$FeO_{3-\delta}$", *J. Appl. Phys.* 97 (2005), 10C314.

[138] X. Gao, X. Li, and W. Yu, "Flowerlike ZnO Nanostructures via Hexamethylenetetramine-Assisted Thermolysis of Zinc-Ethylenediamine Complex", *J. Phys. Chem. B* 109 (2005), 1155.

[139] X. Ma, "Comparison on the crystallization characteristics of sol–gel derived $(BiDy)_3Fe_5O_{12}$ garnet film and powder", *Mater. Lett.* 43 (2000), 170.

[140] X. W. Sun and H. S. Kwok, "Optical properties of epitaxially grown zinc oxide films on sapphire by pulsed laser deposition", *J. Appl. Phys.* 86 (1999), 408.

[141] X. Wei and D. Chen, "Synthesis and characterization of nanosized zinc aluminate spinel by sol–gel technique", *Mater. Lett.* 60 (2006), 823.

[142] X.Y. Kong, Y. Ding, R. Yang and Z. L. Wang, "Single-Crystal Nanorings Formed by Epitaxial Self-Coilingof Polar Nanobelts", *Science* 303 (2004), 1348.

[143] X.Y. Kong and Z. L. Wang, "Spontaneous Polarization-Induced Nanohelix-

es, Nanosprings, and Nanorings of Piezoelectric Nanobelts", *Nano Lett.* 3 (2003),1625.

[144] Y. Chen, D.M. Bagnall, Z. Zhu, T. Sekiuchi, K. Park, K. Hiraga, T. Yao, S. Koyama, M.Y. Shen, and T. Goto, "Growth of ZnO single crystal thin films on *c*-plane (0001) sapphire by plasma enhanced molecular beam epitaxy", *J. Cryst. Growth* 181 (1997), 165.

[145] Y. Ding, X. Y. Kong, and Z. L. Wang, "Doping and planar defects in the formation of single-crystal ZnO nanorings", *Phy. Rev. B.* 70 (2004), 235408.

[146] Y. Igasaki, T. Naito, K. Murakami, and W. Tomoda, "The effects of deposition conditions on the structural properties of ZnO sputtered films on sapphire substrates", *Appl. Surf. Sci.* 169-170 (2001), 512.

[147] Y. Kajikawa, "Texture development of non-epitaxial polycrystalline ZnO films", *J. Cryst. Growth* 289 (2006), 387.

[148] Y. Lao, J. Y. Huang, D.Z. Wang, and Z. F. Ren, "ZnO Nanobridges and Nanonails", *Nano Lett.* 3 (2003), 235.

[149] Y. Q. Huang, L. Meidong, Z. Yike, L. Churong, X. Donglin, and L. Shaobo, "Preparation and properties of ZnO-based ceramic films for low-voltage varistors by novel sol-gel process", *Mater. Sci. Eng., B* 86 (2001), 232.

[150] Y. Xu, X. Yuan, G. Huang, and H. Long, "Polymeric precursor synthesis of $Ba_2Ti_9O_{20}$", *Mater. Chem. Phys.* 90 (2005), 333.

[151] Y. Y. Villanueva, D.-R. Liu and P. T. Cheng, "Pulsed laser deposition of zinc oxide", *Thin Solid Films* 501 (2006), 366.

[152] Y.C. Liu, J.H. Hsieh, and S. K. Tung, "Extraction of optical constants of zinc

oxide thin films by ellipsometry with various models", *Thin Solid Films* 510 (2006), 32.

[153] Y.H. Leung, A.B. Djurišić, J. Gao, M.H. Xie, Z.F. Wei, S.J. Xu and W.K. Chan, "Zinc oxide ribbon and comb structures: synthesis and optical properties", *Chem. Phy. Lett.* 394 (2004), 452.

[154] Zhaoxia Bi, Rong Zhang, Xusheng Wang, Shulin Gu, Bo Shen, Yi Shi, Zhiguo Liu, Youdou Zheng, "Synthesis of Zinc Aluminate Spinel Film through the Solid-Phase Reaction between Zinc Oxide Film and α-Alumina Substrate", *J. Am. Ceram. Soc.* 86 (2003), 2059.

[155] Z. L. Wang, X. Y. Kong, Y. Ding, P. Gao, W. L. Hughes, R. Yang, Y. Zhang, "Semiconducting and Piezoelectric Oxide Nanostructures Induced by Polar Surfaces**"**, *Adv. Func. Mater.* 14 (2004), 943.

[156] Z. Wang, X. F. Qian, J. Yin and Z. K. Zhu, "Large-Scale Fabrication of Tower-like, Flower-like, and Tube-like ZnO Arrays by a Simple Chemical Solution Route", *Langmuir* 20 (2004), 3441.

[157] Z. Y. Xue, D. H. Zhang, Q. P. Wang and J. H. Wang, "The blue photoluminescence emitted from ZnO films deposited on glass substrate by rf magnetron sputtering", *Appl. Surf. Sci.* 195 (2002), 126.